

Novel Plasma Based Technology for Treatment of Emerging Contaminants in Water:
Understanding Physiochemical Processes and Applications

by

Amirreza Sohrabi

A thesis submitted in partial fulfillment of the requirements for the degree of

Doctor of Philosophy

in

Materials Engineering

Chemical and Materials Engineering
University of Alberta

© Amirreza Sohrabi, 2017

Abstract

Indiscriminate and widespread disposal of pharmaceutical compounds, dye molecules, and pesticides in to water resources pose a serious threat to the quality of drinking water. A critical need exists for developing novel practical, efficient, and cost effective water treatments for remediation of these emerging contaminants since conventional water treatment techniques are ineffective in treating these contaminants. In this research, a new class of water treatment technologies is proposed based on the application of non-thermal plasma. Creation of plasma by means of a helical resonator allows the use of low power for plasma generation (10-15 W, comparable to LED light bulbs). Furthermore, producing plasma by a single electrode significantly increases the flexibility of the method for real life applications. The most important feature that distinguishes this technology from other emerging methods is the presence of a post treatment stage in decontamination. Therefore, not only do the contaminants degrade in the presence of plasma (treatment stage), but decontamination also continues for a long period of time even after the plasma is switched off (post treatment stage). To gain deeper understanding of various physiochemical processes involved in the treatment mechanism, we have systematically investigated the effect of physical and chemical parameters such as the distance between the electrode and water surface (air gap distance), the input voltage to the helical resonator, pH and ion concentration of water. The results indicate that there is an optimum air gap distance (6 mm) at which maximum removal of contaminations can be achieved. Moreover, increasing the input voltage can enhance the removal of the contaminations. However, energy consumptions at higher input voltages render the method inefficient. Presence of various ionic species in water (chloride, phosphate, carbonate, etc.) and the initial pH of the solution can significantly alter the chemistry of the process. Special attention has been paid to the role of

chloride ions (Cl^-) in the solution. The reason was while some report that the presence of Cl^- deteriorates the efficiency, others suggest the enhancing role of these ions in removing contaminants. In this research, for the first time, we showed that during the treatment stage (presence of plasma) the scavenging behavior of Cl^- towards OH^\cdot decreases the removal%. On the other hand, due to the formation of singlet oxygen ($^1\text{O}_2$) from reaction of hypochlorous acid (HOCl) and hydrogen peroxide (H_2O_2) the removal% improves significantly during the post treatment stage (absence of plasma). The initial pH of the solution also affects the decontamination process. While highest removal% in the treatment stage was achieved with initial acidic conditions, both initial acidic and alkaline conditions deteriorate the post treatment stage. Furthermore, almost equal contributions from treatment and post treatment stages can be achieved for solutions with initial near neutral pH values. Finally, the application of the proposed system for degradation of four pharmaceutical contaminants (ampicillin, ibuprofen, fluoxetine and propranolol) has been investigated. We showed that after 3 hr of treatment, 100% of ampicillin, fluoxetine and propranolol and 90% of ibuprofen were removed from water. Moreover, the energy yield of the process (the amount of contaminant degraded for 1 kWh of energy consumption) was calculated to be in the range of 0.12-0.13 g/kWh. For each contaminant, degradation by-products were identified and a degradation pathway was suggested. For all contaminants, the degradation mechanism was mostly dominated by the action of hydroxyl radicals. However, formation of oxygenated by-products suggested the possible role of ozone in the process. Finally, for the first time, this research proposed the application of Excitation-Emission Matrix (EEM) analysis to track the degradation of each contaminant. Possible connections between the EEM analysis and identified degradation by-products were outlined. Not only can the results of this research enhance the understanding of the

physiochemical processes involved, but also open up new opportunities for the development of more advanced and efficient water treatment technologies.

Preface

This thesis is an original work of Amirreza Sohrabi. The literature review in this thesis was done by myself. The design and establishment of the experimental setups used throughout this work was done by myself, with the assistance of Ghazaleh Haghghat and Dr. Charles Van Neste. The concepts examined in Chapter 3 and Chapter 4 of this thesis and the experimental procedures were proposed by myself. The experiments were performed by myself, Ghazaleh Haghghat and Parmiss Mojir Shaibani. Data analysis and preparation of the final results were done by myself, with the assistance of Ghazaleh Haghghat and Dr. Selvaraj Naicker. Some of the information presented in Chapter 3 (marked by the footnote in the appropriate section) has been published in the journal of Environmental Science: Water Research & Technology as “Role of Chlorine Ions in Plasma-Activated Water Treatment Processes” by G. HAGHIGHAT, A. SOHRABI, P. M. SHAIBANI, C. W. VAN NESTE, S. NAICKER AND T.THUNDAT, Environ. Sci.: Water Res. Technol., 2017, 3, 156-168. The preparation of the manuscripts reflecting the outcome of this research has been done solely by myself. The results presented in Chapter 5 were obtained by the assistance of Shilpa Anthony and Mahtab Hassanpourfard.

Dedication

I would like to dedicate this work to my lovely and supportive wife, Parmiss Mojir Shaibani, and my wonderful family who offered their endless guidance and support throughout the period of this work. Also, I would like to dedicate this work to all the young researchers who believe that the outcome of their work should benefit society.

Acknowledgments

This work was supported by Canada Excellence Research Chairs (CERC) program.

I would like to offer my sincerest gratitude to Prof. Thomas Thundat who supported me and my work throughout the period of this work. His guidance not only has made me a better researcher, but also an individual thinker and a problem solver.

I also would like to thank Dr. Selvaraj Naicker who assisted me during every steps of planning, data analysis and data interpretation. Dr. Naicker has been a great source of inspiration in this work. His vast knowledge and practical point of view is of utmost appreciation.

I would like to offer my utmost appreciation to my supportive wife, Parmiss Mojir Shaibani who has helped me to be a better person. She has always offered her support to me and she has been inspiring.

I would like to offer my gratitude to Ghazaleh Haghghat and Dr. Charles Van Neste. Ghazaleh Haghghat has been a great assistance during the experimental steps of this work. Moreover, I would like to appreciate the openness of Dr. Van Neste to new ideas. He has been a great source of inspiration and positive thinking during this work. Especially, I would like to thank Dr. Van Neste for introducing the concept of helical resonators to me.

I would like to thank Oil Sands and Coal Interfacial Engineering Facility (OSCIEF) for characterization experiments. Moreover, I thank Stable Isotope Facility for Ecosystem Research (SIFER) and Mass Spectrometry Facility for ion chromatography and mass spectrometry analysis, respectively.

Finally, I would like to offer my sincerest gratitude to my colleagues and group members for providing me with their opinions. Discussions with Arindam Phani, Eric Hawk and Richard Hull have proven to be very helpful.

Table of Contents

Chapter 1: Introduction	1
1.1. Source of pharmaceutical compounds in water	2
1.2. Pharmaceutical classification and their adverse effects	4
1.3. Advanced Oxidation Processes (AOPs)	11
1.3.1. Ultraviolet/hydrogen peroxide oxidation (UV/H ₂ O ₂).....	11
1.3.2. Fenton and photo-Fenton Process	12
1.3.3. Semiconductor Photocatalysis	14
1.3.4. Electrolysis	16
1.3.5. Ozonation	19
1.3.6. Non-thermal plasma (NTP) treatment	21
1.3.7. Comparison of various AOPs	25
Chapter 2: Plasma-based water treatment processes	28
2.1. Introduction to gas discharge	28
2.1.1. Types of gas discharge	29
2.1.2 Plasma physics and chemistry	31
2.1.2.1. Electron avalanche -The Townsend mechanism of breakdown	32
2.1.2.2. Streamers in breakdown	36
2.1.2.3. Plasma chemistry	38
2.2. Plasma generation systems for water treatment	41
2.2.1. Dielectric Barrier Discharge (DBD).....	43
2.2.2. Floating Electrode Dielectric Barrier Discharge (FEDBD).....	46
2.2.3. Gliding Arc Discharge (GAD).....	48

2.2.4. Streamer Corona Discharge (SCD).....	50
2.2.5. Floating Electrode Streamer Corona Discharge (FESCD)	52
2.2.6. Plasma-based systems comparison matrix	53
2.2.6.1. Input waveform.....	55
2.2.6.2. Electrode configuration	56
2.2.6.3. Gas flow requirement	57
2.2.6.4. Power consumption	57
2.2.7. FESCD working principles	58
Chapter 3: Effect of physiochemical parameters	62
3.1. Introduction	62
3.2. Objectives	65
3.3. Experimental	66
3.3.1. Materials	66
3.3.2. Experimental setup and procedure	67
3.3.3. Analytical characterization	71
3.4. Role of physical parameters	72
3.4.1. Effect of air gap distance	73
3.4.2. Effect of input voltage of helical resonator	80
3.4.3. Effect of plasma injection period	83
3.5. Role of chemical parameters	90
3.5.1. Effect of Cl ⁻ concentration.....	90
3.5.2. Analytical characterization	96
3.5.2.1. Ion Chromatography (IC) analysis	96

3.5.2.1. High Performance Liquid Chromatography-Mass Spectrometry (HPLC-MS) analysis	97
3.5.3. Role of other ionic species	102
3.5.4. Effect of initial pH	109
3.5.5. Effect of initial MB concentration	113
Chapter 4: Degradation of pharmaceutical contaminants	116
4.1. Introduction	116
4.2. Objectives	118
4.3. Experimental	119
4.3.1. Materials	119
4.3.2. Experimental setup	119
4.3.3. Characterization	121
4.3.3.1. Total Organic Carbon-Inorganic Carbon (TOC-IC)	121
4.3.3.2. High Performance Liquid Chromatography-Mass Spectrometry (HPLC-MS) analysis	122
4.3.3.3. Excitation-Emission Matrix (EEM)	122
4.3.3.4. Measurement of ozone concentration	123
4.4. Removal% and energy yield	124
4.5. Degree of mineralization	128
4.6. Degradation by-products and pathway	134
4.6.1. Degradation of ampicillin	134
4.6.2. Degradation of ibuprofen	137
4.6.3. Degradation of fluoxetine	140
4.6.4. Degradation of propranolol	144

4.7. Excitation-Emission Matrix (EEM)	146
4.7.1. EEM analysis of ampicillin solution	147
4.7.2. EEM analysis of ibuprofen solution	150
4.7.2.1. Closer look into ibuprofen's EEM signal	152
4.7.3. EEM analysis of fluoxetine solution	158
4.7.4. EEM analysis of propranolol solution	160
4.8. Presence of ozone in the aqueous phase	163
Chapter 5: Conclusions and future directions	166
References	171

List of Tables

Table 1.1. Summary of application, detected concentration and negative effects of each pharmaceutical class (page 6-9).	6
Table 2.1. Comparison between various plasma generation techniques in terms of their main features.	54
Table 3.1. Summary of the parameters used in each study.	69
Table 3.2. Concentration of various inorganic ions detected by IC analysis.	97
Table 3.3. Chemical species detected by LC-MS due to the degradation of MB by plasma.	98
Table 4.1. Degradation time constant, removal% and energy yield of the plasma treatment process obtained for each of the pharmaceutical compounds in this study is summarized.	127
Table 4.2. The degree of mineralization of each compound in two different water matrices is summarized.	132
Table 4.3. Information on chemical species detected by HPLC-MS for ampicillin.	135
Table 4.4. Information on chemical species detected by HPLC-MS for ibuprofen.	138
Table 4.5. Information regarding the chemical species detected in fluoxetine containing solutions by HPLC-MS.	141
Table 4.6. Degradation by-products of propranolol detected by HPLC-MS.	144

List of Figures

Figure 1.1. Various pathways through which pharmaceutical compounds can be introduced into water [7]. As shown, the mechanism can be very complex and various sources such as household uses, animal farming and even the manufacturers can be involved.....	2
Figure 1.2. Pharmaceutical compounds most commonly found in the environment alongside their corresponding classifications [7]. These contaminants have been identified in the influent and effluent of WWTPs as well as surface water, ground water and even in the tap water.	5
Figure 1.3. The schematic illustration of the semiconductor photocatalysis shown for a BiFeO ₃ (BFO) nanowire. The involved processes including the generation of an electron-hole pair and hydroxyl radicals are shown [49].....	15
Figure 1.4. Various steps (a-f) involved in the direct electrochemical oxidation of organic compounds are shown [60]. “M” and “R” in the figure represent the surface of the anode and organic molecule, respectively.....	16
Figure 1.5. The change in the normalized publication regarding various AOPs used for degradation of pharmaceutical compounds is shown as a function of year. The fast increase in the number of publications corresponding to the application of non-thermal plasma in this area, especially in the last decade indicates the viability and versatility of this method.	25
Figure 2.1. Schematic illustration of voltage and current change during the course of a gas discharge process. Different types of discharge could be recognized distinctly based on the trend of the voltage and current [96].	30
Figure 2.2. Schematic representation of a discharge system in which a gaseous medium is placed between two planar electrodes is shown. When the applied electric field to the medium reaches a certain threshold, it can initiate the electron avalanche process.	33
Figure 2.3. The transition from the avalanche form to the streamer form is shown schematically. This transition occurs when the internal electric field created by the charge separation becomes comparable to the applied external electric field.	37
Figure 2.4. The schematic of a DBD system is shown. The dielectric barrier serves at the limiting factor for the current and hence avoiding the spark transition.	43
Figure 2.5. The structure of microdischarges in a DBD process [97].	44
Figure 2.6. The schematic of a FEDBD process is shown. The main difference between FEDBD and DBD processes is the ability to generate plasma by single electrode in FEDBD processes.	47
Figure 2.7. A GAD system is shown schematically. In this method, arcs are created between the two diverging electrodes. The plasma plum is blown on the surface of water with a gas flow.	48
Figure 2.8. A generic pin-to-plate SCD system is shown schematically.	50

Figure 2.9. Schematic illustration of the FESCD plasma generation system is shown. The main part of the FESCD system is the helical resonator. In this system, plasma is generated between the tip of the electrode and the surface of water.53

Figure 2.10. The versatility of the proposed technique for diverse applications is shown. Various hypothetical scenarios include (a) removal of pollutants from air (b) decontamination of water by injecting plasma from the surface (c) inactivation of microorganisms on the surfaces (coffee mug is used as a model surface) and (d) removal of contaminants from soil.59

Figure 3.1. The schematic of the experimental setup used in this study is illustrated. A sinusoidal wave is supplied to the power amplifier by the function generator. The output of the power amplifier is directly connected to the helical resonator. The input voltage and current to the resonator are monitored by an oscilloscope. The concentration of the MB in the solution is measured by a UV-Vis spectrophotometer equipped with an optic fiber probe for in-situ measurements. Magnetic stirring of the solution is used to ensure the homogeneity of the concentration during all experiments.68

Figure 3.2. (a) Optical spectrum of methylene blue obtained in this study. The peak absorbance at 667 nm is used as a measure for concentration of methylene blue in the solution. (b) Calibration curve achieved in this study, based on the optical absorption at 667 nm for various concentrations of methylene blue.70

Figure 3.3. The effect of air gap distance on the decontamination process is studied at constant rms value of input voltage of 68 V and plasma injection time of 10 min. (a) Variation in removal% as a function of time for different air gap distances is shown. As the distance increases, the effect of oxidizing agents created by plasma lasts for a shorter period of time. While the removal still occurs at 60 min for $d=2$ mm, it stops at 20 min for $d=10$ mm. This phenomenon could be attributed to the higher energy of particles in plasma at lower distances due to the higher electric field. (b) Final Removal% (at $t=60$ min) and energy yield are compared for the various air gap distances used in this study. As it is shown, removal% has a maximum at $d=6$ mm, which is probably due to a larger volume of the ionized air on top of water. Furthermore, as the air gap distance increases from 6 mm to 10 mm, the removal% decreases significantly. This may be due to the effect of ozone poisoning at high plasma powers and temperatures (c) The change in the normalized concentration as a function of time for different distances is used to study the kinetics of decontamination. (d) The temperature of the solution was monitored in the course of each experiment. The injection of plasma into the solution causes an increase in the temperature. As the distance was increased, the maximum temperature that the solution reached (approximately 47 °C for $d=10$ mm) also increased, due to a higher power of plasma.74

Figure 3.4. Images of plasma on top of the solution taken for various air gap distances of (a) 2 mm, (b) 6 mm and (c) 10 mm. When the air gap distance is increased to 6 mm, the volume of the plasma increased. Therefore, more ionized gas could reach the surface of water. This could be the reason behind the increased removal% when air gap distance was increased to 6 mm. Further increase in the distance resulted in a significant decrease in removal%. This could be partly due to lower injection probability of plasma to the surface of water, as shown by (c). At air gap distance of 10 mm, frequent injection of plasma to the surrounding air could be observed.77

Figure 3.5. The effect of temperature on the absorbance of the solution is studied. For both heating and cooling cycles, there is no significant change in the peak absorbance of methylene blue at 667 nm. This in turn proves that the change in the absorbance observed during the plasma treatment in this study is solely due to the removal of methylene blue.80

Figure 3.6. The effect of input voltage to the helical resonator on the water treatment process is investigated. The air gap distance and the plasma injection period were fixed at 2 mm and 10 min, respectively. (a) and (b) show the response of increasing input voltages on the removal of methylene blue. Moreover, as shown in (b), although final removal% increases with the increase in the input voltage, energy yield of the process does not increase accordingly. This means that the treatment process with 98 V as input voltage is not efficient in terms of energy consumption (power consumption of 3.1 ± 0.7 , 4.4 ± 0.8 , 5.1 ± 1.5 , 6 ± 0.9 and 7.4 ± 1 W for input voltages 38, 53, 68, 83 and 98 V, respectively). The kinetics of methylene blue removal is illustrated in (c). Regardless of the input voltage, an exponentially decaying kinetics could be observed. (d) shows the change in the solution temperature for various input voltages. A higher degree of change in temperature could be observed for higher input voltages. Based on the data presented, it could be concluded that at the air gap distance of 2 mm and plasma injection time of 10 min, the input voltage between 68 V and 83 V is optimum when considering removal%, energy yield and temperature change relative to room temperature ($20\text{ }^{\circ}\text{C}$).82

Figure 3.7. (a) The effect of time in which plasma is present on the surface of the solution is studied (rms value of the voltage and the air gap distance were kept at 83 V and 2 mm, respectively). As the plasma injection time increases, final removal% increases; however, the variation of removal% with injection time is more significant at periods lower than 15 min. This is probably due to the increasing rate of ozone concentration decay at higher temperatures. Maximum energy yield is obtained at 15 min. In smaller time periods, low removal% decreases the yield. On the other hand, at time periods greater than 15 min, high energy consumption, alongside a slow increase of removal%, lowers the overall energy yield. (b) As the period in which plasma is present increases, more energy dissipates in the form of heat; therefore, higher temperatures in the solution were reached. (c) and (d) illustrate the change in the removal% and normalized concentration as a function of time for various plasma injection periods used in this study. It could be seen that at high injection periods (20 min and 25 min), changes in removal% become insignificant when the process duration approached 60 min.85

Figure 3.8. Formation of new features in the optical spectrum of (a) solution with no methylene blue and (b) solution in the presence of methylene blue in the wavelength region of 300-400 nm is shown. The fact that these features appear in both of these cases is a qualitative indication of the generation of new plasma-activated species in the solution. Moreover, as shown in (a), the presence of these features in the optical spectrum even after 360 min proves the long lifetime of these species, even though plasma was absent from $t=15$ min. (c)-(f) depicts the change in the absorbance of each of the dominant peaks shown in (a) and (b) as a function of time. It is evident that the presence of methylene blue in the solution causes a lower amount of absorption in each case, when the plasma is removed from the surface. Therefore, it could be concluded that these new features in the spectrum are indeed related to plasma-activated species.89

Figure 3.9. The effect of NaCl concentration on the decontamination of MB is studied. (a) The change in the overall removal% and conductivity of the solution as a function of NaCl concentration is shown. The overall removal% has a maximum in the range of 10-50 mg/l in NaCl concentration. In order to understand this behavior, removal% during the treatment and post treatment stages as a function of NaCl concentration were compared separately, as shown in (b). The removal% during the treatment stage is maximum when no NaCl is added to the solution. The addition of the salt to the solution reduced the removal% during this stage. This can be explained by the scavenging behavior of Cl^- towards OH^\cdot . It has been shown that when Cl^- scavenges OH^\cdot , amongst various Cl-based by-products, Cl_2^\cdot is dominant [141]. Although Cl_2^\cdot can oxidize MB, its oxidation potential is much lower than OH^\cdot . As a result, removal% during the treatment stage decreases when NaCl concentration increases. On the other hand, removal% during the post treatment stage enhanced significantly when NaCl was introduced to the solution. This can be explained by the formation of singlet oxygen ($^1\text{O}_2$) from reaction of HOCl and H_2O_2 ; both of which are produced due to the action of plasma and are stable enough to induce MB degradation after plasma is extinguished. It can be hypothesized that upon the addition of NaCl, an optimum NaCl concentration (around 50 mg/l) exists where the negative effect of Cl^- (scavenging properties) and its positive role (production of $^1\text{O}_2$) are balanced. This reflects itself in the energy yield of the system, as shown in (c). Finally, the change in overall removal% as a function of time is shown in (d). The significant continuation of MB removal during the post treatment stage only exists when NaCl is present in the solution.91

Figure 3.10. As a control experiment, various concentrations of H_2O_2 were added to the MB containing solutions. (a) shows the removal% of MB as a function of time. Only minute removal of MB can be achieved (about 5%) when high concentrations of H_2O_2 (120 mM) are added to the solution. These high concentrations of H_2O_2 significantly exceeds the concentrations measured in our experiments, as shown in (b). In our experiments, the concentration of H_2O_2 was evaluated by means of fluorescence probe, Amplex red, according to previously published methods. Moreover, (b) shows that H_2O_2 can stay in the solution for a long period of time in the post treatment stage. As a result, they can react with HOCl to produce $^1\text{O}_2$ in the solution and continue the removal of MB in this stage.93

Figure 3.11. A degradation pathway for MB was suggested based on the species detected by HPLC-MS. The major pathway for degradation of MB molecules is believed to be the action of OH^\cdot . Moreover, the by-products can be categorized into three groups based on their formation in specific water matrices. These categories from left to right in the figure are: 1) Only in MilliQ 2) common by-products and 3) only in NaCl added to MilliQ water. The formation of sulfones (P11) and sulfinic acids (P5 and P8) in only samples with NaCl added to MilliQ water confirms the formation of $^1\text{O}_2$ as an oxidizing agent in these samples. Moreover, the presence of small organic molecules (such as P10) in both water matrices suggests the complete destruction of the aromatic ring and formation of aliphatic molecules. This is possibly due to the action of ozone molecules on aromatic compounds such as P9. This process proceeds first with the formation of ozonide compounds which are unstable and turn into aliphatic molecules.100

Figure 3.12. The competition between Fenton processes and $^1\text{O}_2$ production in Cl-mediated reactions was investigated. For this purpose, removal% of MB was calculated as a function of time for various electrolytes. This is shown in (a). There are two major differences between the removal% in different electrolytes. Firstly, removal of MB in solutions containing Fe^{2+} ions is higher and faster compared to the other electrolytes, regardless of the anion present in the solution. This is probably due to the homogenous formation of hydroxyl radicals in the solution from Fenton processes. Secondly, only solutions containing NaCl show appreciable degradation of MB during the post treatment stage (15 to 60 min). This is also shown in (b) where the removal% during the treatment and post treatment stages were plotted separately for each electrolyte.103

Figure 3.13. (a) The removal% of MB as a function of time is shown for solutions containing various concentrations of FeCl_2 . The results indicate that as the concentration of FeCl_2 is increased, higher MB removal could be obtained in the plasma treatment process. To evaluate the obtained results in a more detailed manner, the removal% during the treatment and post treatment stages were plotted separately as a function of the concentration of FeCl_2 , as shown in (b). The removal% during the treatment stage enhanced as the concentration of the salt increased. However, the rate of the increase in the removal% in this stage (the slope of the black curve in (b)) as a function of the concentration gradually decreased. This can be due to the fact that at high concentrations of FeCl_2 , the concentration of H_2O_2 measured in our system (Figure 3.10) becomes comparable to the concentration of Fe^{2+} in the solution. However, not all of the H_2O_2 molecules can be used by Fe^{2+} ions since there are many other side reactions that can remove H_2O_2 from solution. As a result, a plateau is expected in the removal% during the treatment stage as the concentration of Fe^{2+} is increased. Moreover, higher concentrations of FeCl_2 in the solution decreased the removal% during the post treatment stage.105

Figure 3.14. The effect of the presence of various ionic species in water on the removal% of MB is investigated. (a) The change in the overall removal% as a function of time is shown for various electrolytes. The highest removal% was obtained for solutions containing NaCl. On the other hand, the overall removal of MB is insignificant for solutions containing PO_4^{3-} and CO_3^{2-} ions. This is due to the fact that these ions are very well known for their scavenging behavior towards hydroxyl radicals. (b) illustrates the removal% during the treatment and post treatment stages for each electrolyte. Highest removal% during the treatment stage was obtained from MilliQ water. This can be justified by considering the fact that any ionic species in the solution can act as a scavenger of hydroxyl radicals. As a result, the concentration of hydroxyl radicals available for reaction with MB molecules is lowered. The highest removal% during the post treatment stage was achieved from solutions containing Cl⁻. This can be attributed to the production of $^1\text{O}_2$, as described in section 3.5.1.107

Figure 3.15. The effect of the initial pH of the solution on the decontamination of MB is investigated. (a) Overall removal%, removal% during the treatment stage (light gray) and removal% during the post treatment stage (dark gray) are shown as a function of the initial pH of the solution. The highest removal% during the treatment stage was achieved by using solutions with initial acidic pH values. This can be explained by various phenomena including the pH dependency of the oxidation potential of OH^\cdot , the acid-base equilibrium of the dye molecules, etc. The removal% during the post treatment stage is insignificant for solutions with either initial acidic or alkaline conditions (pH values of 2.8 and 10.12). This can be justified by considering

the pH dependency of the Cl-based reactions involved in the production of $^1\text{O}_2$ (Equations (3.17) and (3.19)). As discussed in section 3.5.1, when Cl^- is present in the solution, it can possibly scavenge OH^- . This reaction path eventually produces $^1\text{O}_2$ from two stable compounds, i.e. HOCl and H_2O_2 , which can degrade MB in the post treatment stage. Significantly high concentrations of OH^- or H^+ , when initial alkaline or acidic conditions are used respectively, can cause Equations (3.17) or (3.19) to occur with a faster rate in the reverse direction. As a result, lower concentration of $^1\text{O}_2$ is created and removal% in the post treatment stage reduces. This can be seen in (b) which illustrates the change in the removal% as a function of time for three different initial pH values. Initial near neutral pH values represent the most balanced condition for production of $^1\text{O}_2$. As a result, removal of MB continues significantly after the plasma is extinguished. The overall change in the pH of the solutions with various initial pH is shown in (c) (pH of the solution decreases). The acidification of the solutions is a direct consequence of formation of nitrite and nitrate ions in the solution, as discussed in section 2.1.2.3. The highest acidification happens for the solutions with initial alkaline condition. This is understandable since these solutions are depleted from H^+ . Finally, the pH change as a function of time is shown in (d).110

Figure 3.16. The efficiency of the plasma treatment system is evaluated against the increasing concentration of MB. (a) shows the change in the removal% and energy yield of the system as a function of MB concentration. Although removal% shows a slight decrease, the energy yield increases significantly as MB concentration increases. This is due to the fact that when higher concentrations of MB are present in the solution, the collision frequency between MB molecules and oxidizing agents is higher. For OH^- , this is very critical since their lifetime is very short. This also reflects itself in the reaction rate of the MB degradation during both treatment and post treatment stages, as shown in (b). In (b), k_1 and k_2 represent the reaction rates of MB degradation during the treatment and post treatment stages, respectively. These rates were obtained by fitting the data to a pseudo-first-order kinetics equation (Equation (3.8)), separately for each stage. As shown by (b), regardless of the MB concentration, k_1 (reaction rate during the treatment stage) is always higher. This is due to the action of more powerful oxidizing agents (such as OH^-) on MB molecules during the treatment stage. Moreover, higher reaction rates during treatment stage can be achieved if higher concentrations of MB are present in the solution. This reflects the importance of the collision frequency between MB molecules and OH^- during this stage. On the other hand, the reaction rate during the post treatment stage (k_2) is significantly less sensitive to the concentration of MB. This is probably due to the fact that removal of MB during this stage is not only dependent on the collision frequency between MB molecule and oxidizing agents (such as $^1\text{O}_2$), but also it is limited by reactions that create $^1\text{O}_2$. The negative sign of the reaction rates only shows the decrease in the concentration of MB during the degradation process.114

Figure 4.1. The schematic representation of the experimental setup is shown. Single electrode plasma in air at atmospheric pressure is created using a helical resonator. A sinusoidal wave at the resonance frequency of the resonator is fed to a power amplifier by a function generator. The input voltage and current to the helical resonator is measured to calculate the power consumption. A Pt/Ir electrode is used to generate the plasma due to its stability at high temperatures. The water samples are stirred by a magnetic stirrer to assure the homogeneity of the oxidation reactions.120

Figure 4.2. A calibration curve for indigo dye was obtained to correlate the concentration of the dye in the solution to its absorbance (UV/Vis spectroscopy at 600 nm). Based on the indigo method for measurement of ozone concentration in the solution [185], at low pH values, amino groups in the indigo dye molecules are protonated and they do not participate in any oxidation process. That is why the stock solution of the indigo trisulfonate is prepared in 20 mM solution of phosphoric acid. As a result, the only C=C double bond in the center of the molecule is expected to react with an ozone molecule. Thus, it can be assumed that one molecule of indigo trisulfonate reacts with one molecule of ozone. Using the calibration curve presented here, the absorbance of the indigo solution can be converted to the concentration of the indigo dye. Finally, the change in the concentration of the indigo dye represents the concentration of ozone in the solution.124

Figure 4.3. The change in the area underneath the curve in the chromatogram of (a) ampicillin, (b) ibuprofen, (c) fluoxetine and (d) propranolol as a function of time is shown. The insets show the Extracted Ion Chromatograms (EIC) at retention time of (a) 4.4 min, (b) 5.6 min, (c) 3.8 min and (d) 3.1 min corresponding to ampicillin (m/z of 350.11), ibuprofen (m/z of 206.13), fluoxetine (m/z of 310.14) and propranolol (m/z of 2601.6) molecules, respectively. The dash line in the graphs resulted from the fitting of the data to an exponential decay kinetics equation.125

Figure 4.4. The change in the relative TOC (TOC/TOC_0) and IC (IC/IC_0) of the solutions is shown for (a) ampicillin in tap water (b) ampicillin in MilliQ water (c) ibuprofen in tap water and (d) ibuprofen in MilliQ water. Approximately, 20% and 25% mineralization was obtained for ampicillin in tap water and MilliQ water, respectively (as shown by TOC/TOC_0 in (a) and (b)). On the other hand, significantly higher mineralization was achieved for ibuprofen solutions (56% and 61% in tap water and MilliQ water, respectively). This shows that although the degradation rate was higher for ampicillin molecules (as discussed in Figure 4.3), the degradation by-products of ampicillin are more recalcitrant compared to those of ibuprofen. In both cases, the lower mineralization in tap water can be explained by the presence of variety of ionic species (especially carbonate and bicarbonate) in tap water that can interfere with the oxidation of the target molecules. It is worth-mentioning that regardless of the nature of the pharmaceutical contamination, the inorganic content (IC/IC_0) of the tap water solutions decreased. Ionic species such as (CO_3^{2-} , HCO_3^- , etc.) are the main contributors to the IC of tap water. During the plasma treatment process, the pH of the solution decreases significantly. This acidification of the solution transforms these ionic species to gaseous CO_2 , which leaves the solution. As a result, IC of tap water solutions decreases. Moreover, in both cases, the IC of MilliQ water solutions showed a slight increase followed by a decline. Since the initial IC of the MilliQ water is low (<1 mg/l-C), the increase in IC can be related to the formation of carbonate and bicarbonate ions from oxidized organic molecule. The subsequent decrease is possibly due to the acidification of the solutions, as discussed earlier.129

Figure 4.5. The change in the normalized TOC and IC as a function of the treatment time for solution containing fluoxetine in tap water and MilliQ water are shown in (a) and (b), respectively. 60% and 65% mineralization was obtained in tap water and MilliQ water, respectively, for water samples spiked by 25 mg/l of fluoxetine. (c) and (d) illustrate the change in the normalized TOC and IC for propranolol containing samples in tap water and MilliQ water, respectively. Approximately, 17% and 20% of the organic content of the solution was

mineralized in tap water and MilliQ water. In both cases, the higher degree of mineralization for MilliQ water samples is due to the presence of various hydroxyl radical scavengers in tap water. Moreover, the difference between the changes in the normalized IC in both compounds is similar to the case of ampicillin and ibuprofen. As a result, the above-mentioned rationales hold in this case.131

Figure 4.6. The change in the solution pH and conductivity are shown as a function of treatment time for (a) ampicillin in tap water (b) ampicillin in MilliQ water (c) ibuprofen in tap water (d) ibuprofen in MilliQ water, (e) fluoxetine in tap water (f) fluoxetine in MilliQ water (g) propranolol in tap water and (h) propranolol in MilliQ water.133

Figure 4.7. A degradation pathway is suggested for ampicillin in MilliQ water. Three major reactions have been identified, based on the species detected by HPLC-MS. The first reaction is the hydrolysis of the ampicillin molecules (formation of ampicilloic acid). This occurs as a result of the dissolution of ampicillin sodium salt in water and it is independent of the degradation processes. The other two chemical reactions are reaction of organic molecules with hydroxyl radicals and ozone molecules. By-products such as P1, P2, P4 and P7 were formed by addition of one or multiple oxygen atoms to the organic molecules. This may be explained by the action of ozone. On the other hand, by-products such as P3, P5, P6, etc. were formed due to the cleavage of chemical bonds (shown by red dash line). This phenomenon is probably due to the degradation of organic molecules by hydroxyl radicals. Small portion (20-25%) of the by-products shown here were eventually mineralized as suggested by the TOC data (Figure 4.4(b)). Moreover, a larger portion (75-80%) of the by-products was further broken down to small organic molecules. These molecules were not detected by HPLC-MS, as suggested by Table 4.3 for treatment times of 2 hr and 3 hr.136

Figure 4.8. A degradation pathway is proposed for ibuprofen molecules. The two main reaction pathways include the reaction with hydroxyl radicals and ozone molecules. The reaction by-products such as B2 suggest that ozone molecules possibly cleave the aromatic ring and create carboxylic acid functional groups. Hydroxyl radicals react with organic molecules in two ways. The first pathway is the hydroxylation of ibuprofen molecules (formation of B1). Since hydroxyl functional group is an electron-donating group (EDG), it increases the electron density of the neighboring bonds through the inductive effect. As a result, the bonds near the hydroxyl group become stronger. That is probably why the further degradation of B1 starts from the opposite side of the molecule (formation of B12), until the aliphatic chain is completely cleaved (B11). The second pathway in which hydroxyl radicals react with the parent compound and its by-products is through the direct cleavage of bonds (by-products such as B4, B7 and B8). A comparison between the results presented here and TOC measurements (Figure 4.4(d)) indicates that although the smallest by-product (detected by HPLC-MS) is B5 (m/z of 134.11), further degradation by plasma treatment resulted in approximately 60% mineralization of organic compounds.139

Figure 4.9. A degradation pathway was proposed for fluoxetine based on the specie detected by HPLC-MS analysis. The only mechanism involved in the degradation of fluoxetine and its by-products is through hydroxyl radicals. Hydroxyl radicals can react with organic molecules in two ways. The first process is known as the hydroxylation of the molecules where a hydroxyl functional group is added to the structure. This is evident in the formation of by-products such as F1, F7 and F10. In the other hand, hydroxyl radicals can cause the cleavage of the chemical bonds in the structure. This can be seen in transformation of F1 to F5, F6 to F8, F8 to F9, etc.

.....142

Figure 4.10. A degradation pathway was suggested for propranolol during the plasma treatment process. The main degradation process is through the action of hydroxyl radicals. This process shows itself in two ways. The first pathway is by hydroxylation of the organic molecules. This in turn can occur in two different positions. The first position is the hydroxylation of the methyl groups (CH₃) at the end of the chain to form CH₂OH at this position. This can be seen in the formation of P1 and subsequently P2 from propranolol and the formation of P5. The second position for hydroxylation is in the aromatic ring (P5 and P6). This process is known to be the most common oxidative degradation of organic compounds [186]. The second process involving hydroxyl radicals is the direct cleavage of the bonds. This can be seen in the formation the transient by-product (in the bracket) and transformation of P5 to P6.145

Figure 4.11. Excitation-Emission Matrix (EEM) was utilized to follow the degradation of ampicillin molecule and its by-products in tap water. (a) represents the fluorescence signal of the blank sample (only tap water). The fluorescence signal of the solutions containing ampicillin and its by-products are shown in (b)-(f), corresponding to different periods of plasma treatment. The fluorescence signal shows an initial increase (at treatment time of 30 min) followed by a significant decrease at treatment times of 1 hr, 2 hr and 3 hr. After treating the solution for 3 hr, the fluorescence signal almost disappeared, as shown in (f). In conjunction with the results obtained by HPLC-MS analysis (Table 1 and Figure 4), one can conclude that the initial increase in the fluorescence signal is possibly due to the formation of oxygenated by-products (P1, P2, P4 and P7). It is well-known that the presence of oxygen or nitrogen in organic molecules can enhance the fluorescence properties of the molecules due to the lone electron spin of these elements [189]. The subsequent decrease in the fluorescence signal at longer treatment periods can be attributed to the combined effect of mineralization and breakdown of larger molecules to smaller organic molecules.148

Figure 4.12. The degradation of ibuprofen and its by-products in tap water was monitored through the application of Excitation-Emission Matrix (EEM). (a) The background fluorescence of the samples was measured by conducting EEM on tap water (as the control sample). The fluorescence signal of ibuprofen is shown in (b) which corresponds to 0 hr of plasma treatment. (c)-(f) illustrate the change in the fluorescence signal of the solutions treated by plasma for different periods of time. Unlike the results obtained for ampicillin (Figure 4.11), the fluorescence signal of the solutions containing ibuprofen did not increase at the beginning of the treatment process. This can be explained by the chemical species formed from ibuprofen. Although oxygenated by-products were formed during the plasma treatment from ibuprofen (B2, B6 and B7), similar to the case of ampicillin, this oxygenation occurred at the expense of the cleavage in the aromatic ring structure. It is known that the most important structural feature in organic compounds that induce the fluorescence properties is the presence of conjugated double

or triple bonds [189]. Subsequently, this cleavage in the aromatic ring (i.e. interference with the conjugated double bond structure) causes the fluorescence intensity to decrease. Moreover, further degradation and mineralization of the organic compounds resulted in the loss of the fluorescence signal.151

Figure 4.13. Fluorescence signal of solutions containing ibuprofen is shown with smaller intensity ranges. For these solutions, the main fluorescence signals are located in regions I and IV. As the plasma treatment time increased, the fluorescence signal decreased. This decrease can be attributed to the cleavage of the aromatic ring structure (discussed in Figures 4.12). More interestingly, a new fluorescence signal was developed as the solutions were treated for a longer period of time. The presence of this newly formed feature in region V of the EEMs can be clearly seen for treatment times of 2 hr and 3 hr, shown by (e) and (f), respectively. This new signal can be due to the formation of new by-products from ibuprofen at longer treatment times.153

Figure 4.14. FRI analysis was performed on the EEM signals of solutions containing ibuprofen. The results of this analysis are shown in the form of $\Phi_{S,n}$ (fluorescence volume) and $P_{S,n}$ (contribution percentage) as a function of treatment time. Two main points can be concluded from this analysis. Firstly, the fluorescence volume ($\Phi_{S,n}$) in regions I and IV (major EEM peaks) decreased significantly, representing the mineralization and breakdown of the organic molecules in the solution. The second conclusion can be drawn from the FRI analysis of region V, shown in (d). The fluorescence volume ($\Phi_{S,n}$) declined after 30 min of treatment, however, higher values of volume were obtained for longer treatment times. Moreover, $P_{S,n}$ (contribution percentage) increased gradually. These changes in $\Phi_{S,n}$ and $P_{S,n}$ of region V show the formation of new fluorescence features, as discussed in Figure 4.13.155

Figure 4.15. Two-dimensional (2D) fluorescence signals were obtained from EEMs of ibuprofen containing solutions by plotting the fluorescence intensity as a function of the excitation wavelength, at fixed emission wavelength values (vertical lines in EEMs). (a), (b) and (c) show the 2D analysis of the fluorescence signal of ibuprofen solutions at fixed emission wavelengths of 290, 425 and 570 nm, respectively. 2D analysis at emission wavelengths of 290 nm and 570 nm ((a) and (c)) represent the change in the fluorescence intensity of the two main peaks in EEMs of ibuprofen containing solutions. As shown in (a) and (c), the intensity of both peaks decreased. This is probably due to the mineralization and breakdown of the organic molecules. (b) depicts the change in the fluorescence intensity at the emission wavelength of 425 nm. At the beginning (treatment time of 0 min, black curve), no fluorescence signal was obtained. As the plasma treatment time increased, higher fluorescence intensities were obtained. This also points to the formation of new features in the EEM of the solutions at longer treatment periods.157

Figure 4.16. The evolution of the fluorescence signal of solutions containing ibuprofen as a function of the treatment time is shown. The fluorescence signal decreased significantly as the treatment time increased. It is interesting to note that the fluorescence signal faded away after a shorter period of time compared to other pharmaceutical compounds studied in this work. For instance, the fluorescence intensity became insignificant after treating the solutions containing fluoxetine for only 30 min. This significant decrease in the fluorescence signal was achieved after 3 hr and 1 hr of treatment for ampicillin and ibuprofen, respectively. This is understandable if we consider the degradation time constant of fluoxetine (5.44 hr^{-1} , Table 4.1) and the degree of

mineralization of fluoxetine solutions (60%, Table 4.2). These values were the highest amongst all the compounds in this study. Moreover, unlike the case of ampicillin, the fluorescence intensity did not show any increase. This can be either due to the lack of oxygenation or the destruction of the aromatic ring during the oxygenation (similar to ibuprofen). A comparison with the degradation pathway proposed for fluoxetine (Figure 4.9) reveals that indeed the lack of increase in the fluorescence intensity is due to the fact that no oxygenated by-products were formed.159

Figure 4.17. EEM analysis was used to investigate the change in the fluorescence properties of the solutions containing propranolol as a function of the treatment time. (a) shows the EEM signal of the blank solution, i.e. tap water. (b)-(f) illustrate the change in EEM signal of the solution as the treatment time increases from 0 hr to 3 hr. The EEM signal decreased as the treatment time increased. Similar to the case of fluoxetine, the lack of increase in the signal is due to the absence of oxygenated by-products, as proved by HPLC-MS analysis (Figure 4.10). After 3 hr of plasma treatment, the EEM signal was almost disappeared. This is partially due to the mineralization of the organic compounds (degree of mineralization of 20%, Figure 4.5(c)) and partially due to the breakdown of the molecules in the solution.161

Figure 4.18. (a) The presence of ozone in the aqueous phase was investigated using the Indigo method [185]. The measurements were done for one cycle of the plasma treatment process, i.e. 15 min of treatment followed by 15 min of post treatment. The change in the absorbance of the indigo dye was converted into the concentration of ozone by means of a previously obtained calibration curve (Figure 4.2). The concentration of ozone was measured in the presence (100 mg/l) and also absence of ampicillin in the solution. In both cases, the concentration of ozone in the solution increased during the treatment stage. This is understandable since during this stage (i.e. presence of plasma), ozone is created continuously in the gas phase and introduced to the solution from the gas/liquid interface. On the other hand, the concentration of ozone declined during the post treatment stage. In this stage, since plasma is not present, the continuous production of ozone in the gas phase does not occur. As a result, the change in the concentration of ozone is controlled by ozone decomposition processes such as direct reaction of ozone and water molecules [152]. In the presence of ampicillin in the solution as a model pharmaceutical contaminant, lower concentrations of ozone were measured. This shows that ampicillin molecules compete with indigo dye molecules to consume ozone. The difference between the concentration of ozone measured in the presence and absence of ampicillin can show the amount of ozone consumed by ampicillin molecules, as shown in (b).164

Figure 5.1. The FESCD system was used to assess the pathogen disinfection capability of the method. (a) Water samples contaminated by *E. coli* were treated directly with plasma. (b) Water samples were first treated by plasma and then spiked by bacterial. In this configuration, the efficiency of the post treatment stage can be evaluated.170

List of Abbreviations

2D	Two-dimensional
AC	Alternating current
ACN	Acetonitrile
AOP	Advanced oxidation process
ATCC	American type culture collection
BFO	Bismuth ferrite oxide
BOD	Biochemical oxygen demand
CA	Canada
CA	California
COD	Chemical oxygen demand
DBD	Dielectric barrier discharge
DC	Direct current
DMA	Dimethylantracene
DMSO	Dimethylsulfoxide
<i>E. coli</i>	<i>Escherichia coli</i>
EDG	Electron-donating group
EEM	Excitation emission matrix
EWG	Electron withdrawing group
FEDBD	Floating electrode dielectric barrier discharge
FESCD	Floating electrode streamer corona discharge
FRI	Fluorescence regional integration
G	Gram
GAD	Gliding arc discharge
HPLC-MS	High resolution liquid chromatography-mass spectrometry
Hr	Hour
HV	High voltage
IC	Ion chromatography
IC	Inorganic carbon
kWh	Kilowatt hour
MB	Methylene blue
MF	Modification factor
Min	Minute
MO	Metal oxide
MP	Medium pressure
MRSA	Methicillin-resistant <i>Staphylococcus aureus</i>
MS	Mass spectrometry
MW	Mega watt
NCHS	National Center for Health Statistics
NTP	Non-thermal plasma
NY	New york
OR	Oregon
RF	Radio frequency
SCD	Streamer corona discharge

TC	Total carbon
TOC	Total organic carbon
TOF	Time of flight
UK	United kingdom
USA	United states of America
UV	Ultraviolet
UV/Vis	Ultraviolet/Visible
VOC	Volatile organic compound
WHO	World health organization
WWTP	Wastewater treatment plant

Chapter 1: Introduction

The presence of pharmaceutical compounds in various water bodies has received the attention of societies due to their increasing usage worldwide and their possible adverse effects on humans and wildlife [1]. This problem becomes more acute considering the rate of population growth, the discovery of new drugs and the realization of new applications for existing drugs [2]. Moreover, most of the pharmaceutical compounds are designed to be very stable. Therefore, they can withstand conventional water treatment processes such as biological treatments [3–5]. As a result, if they are introduced to wastewater they can by-pass conventional wastewater treatment plants and find their way into various water sources (surface water, drinking water, etc.). The presence of certain pharmaceutical compounds in the effluent of wastewater treatment facilities, some even detected in tap water, indicates that current treatment technologies are not designed to handle pharmaceutical contaminations [2,6]. As a result, many studies have devoted to find new and effective water treatment processes to replace the orthodox methods. Amongst various studied approaches, Advanced Oxidation Processes (AOPs) are considered to be the most suitable methods for degradation of pharmaceutical compounds in water. The purpose of this chapter is to:

- 1) Introduce various pathways that pharmaceutical compounds can be introduced to water.
- 2) Explain briefly different categories of drugs used worldwide and their possible adverse impacts on environment, human and wildlife and;
- 3) Explain why we chose a plasma-based treatment system by introducing and comparing various AOPs used for degradation of pharmaceutical contaminants in water.

1.1. Source of pharmaceutical compounds in water

As mentioned in the previous section, the consumption of various drugs around the world has increased significantly during the last few decades. This is probably due to the rapid rise in the population, the exploration of new drugs for new diseases and the realization of new applications for existing drugs [2]. As a result, there is a very complex and interconnected mechanism with which pharmaceutical compounds and their metabolites can be introduced to various water sources. This mechanism with its interconnected routes is shown in Figure 1.1 [7].

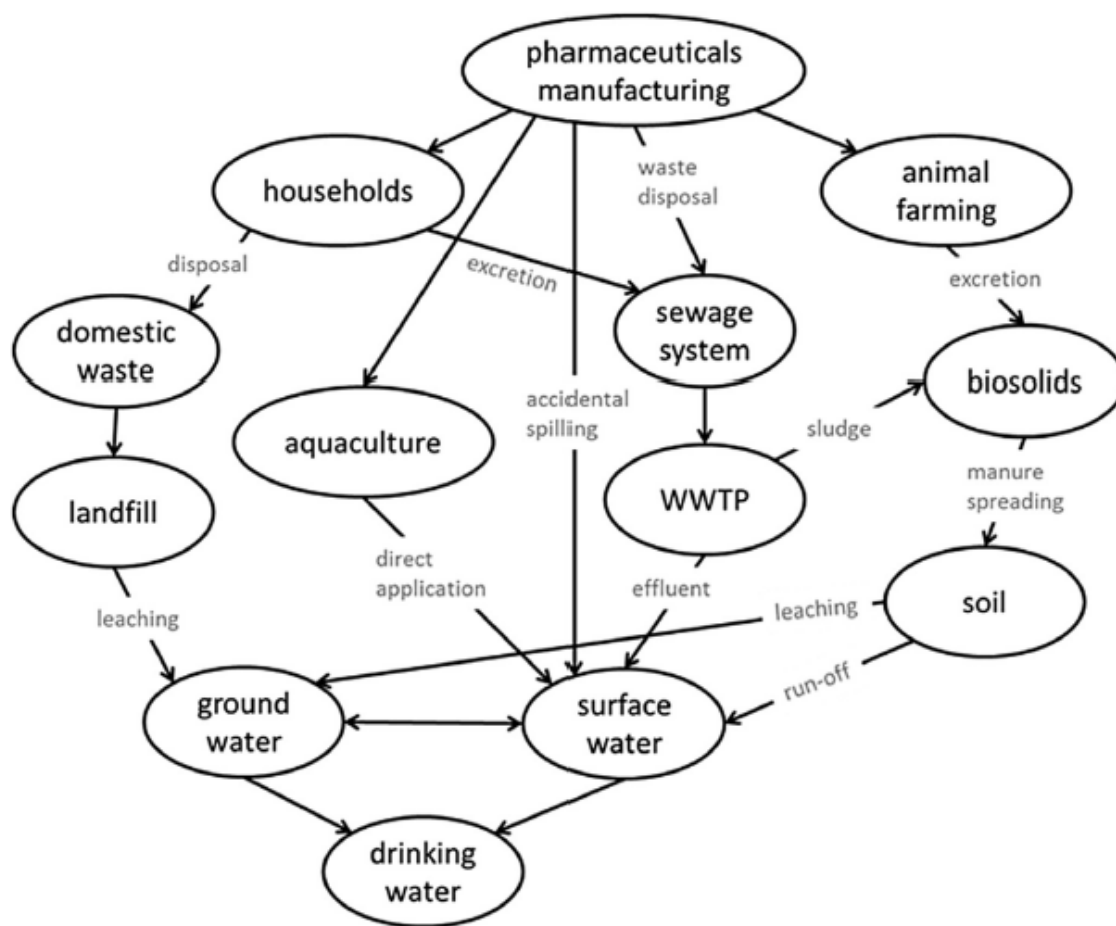


Figure 1.1. Various pathways through which pharmaceutical compounds can be introduced into water [7]. As shown, the mechanism can be very complex and various sources such as household uses, animal farming and even the manufacturers can be involved.

It is believed that one of the main sources of pharmaceutical compounds in water is through excretion, both from humans and animals. It is very well-known that complete metabolic absorption of drugs in the body is not possible; 25-70% of the drug concentration (depending on the drug formulation, the method of administration, the patient physical health, etc.) is excreted as unmetabolized compounds [8,9]. These unmetabolized drugs are normally disposed into the sewage system and find their way to the wastewater treatment plants (WWTPs). As described previously, since current available technologies used in the wastewater treatment plants are not designed to eliminate these compounds, pharmaceutical compounds eventually find their route to surface water through the effluent of WWTPs, as shown in Figure 1.1. Moreover, in some countries, the effluent of WWTPs is “recycled” and used to water plants and support vegetation. A recent news report indicated that in Israel, elevated concentrations of an anticonvulsant (carbamazepine) was detected in the urine of people who consumed vegetables grown by reclaimed wastewater [10]. Another by-product of a WWTP is normally the sludge or biosolid that can contain various pharmaceutical compounds. This sludge is normally used as fertilizer. Therefore, the soil can be contaminated and increase the risk of ground water contamination by leaching. On the other hand, veterinary medicines used in animal farming share almost the same fate. Since the metabolism of the veterinary drugs in animals is also not complete, they end up in the soil through the animal excretion. Further leaching of these compounds from the soil causes the introduction of pharmaceutical compounds to ground water sources. Also, the contact of the contaminated soil with surface water can result in the contamination of surface water [7]. Improper disposal of household unwanted medicines has turned out to be a significant problem for many societies. A 2009 report published by British Columbia Pharmacy Association shows that although rigorous medicine take-back programs have been established throughout the

province, only 20% of the population returned their unwanted/expired medicines to their pharmacies [11]. This means the rest of the 80% either keep their expired drugs, which can impose serious health risks in case of use, or dispose them through improper ways such as disposal in the trash or flushing down the toilet. While disposal in the trash increases the risk of soil contamination, discarding the unwanted medicines in the toilet directly introduces these compounds to the sewage and eventually surface water, as described above. Finally, improper disposal of the manufacturing waste or accidental spills during production or distribution can be counted as other sources of water contamination. These contaminations in surface water or ground water sources may reach drinking water treatment plants (DWTPs); however, some of these contaminations can end up in the tap water. The above-mentioned discussion alongside the flow chart presented in Figure 1.1 indicates that the introduction of pharmaceutical contaminants into various water bodies can happen through a many complex pathways. However, the bottom line is clear. When these compounds enter water, many of them survive our current treatment strategies and they tend to have negative impacts on the environment. These effects will be explored further in the next section.

1.2. Pharmaceutical classification and their adverse effects

The ever growing population and the advancement of technology has resulted in the production of a wide variety of medicines. However, seven categories can be identified for medicines that have a higher consumption rate worldwide. These medicines are more frequently found in the environment. Some of these compounds are known to be persistent in the environment such as carbamazepine, erythromycin, etc. [12]. These compounds tend to accumulate in water. The other group includes drugs known to be “pseudo-persistent”, i.e. although their lifetime is short in the environment; they enter our water sources continuously due to persistent use.

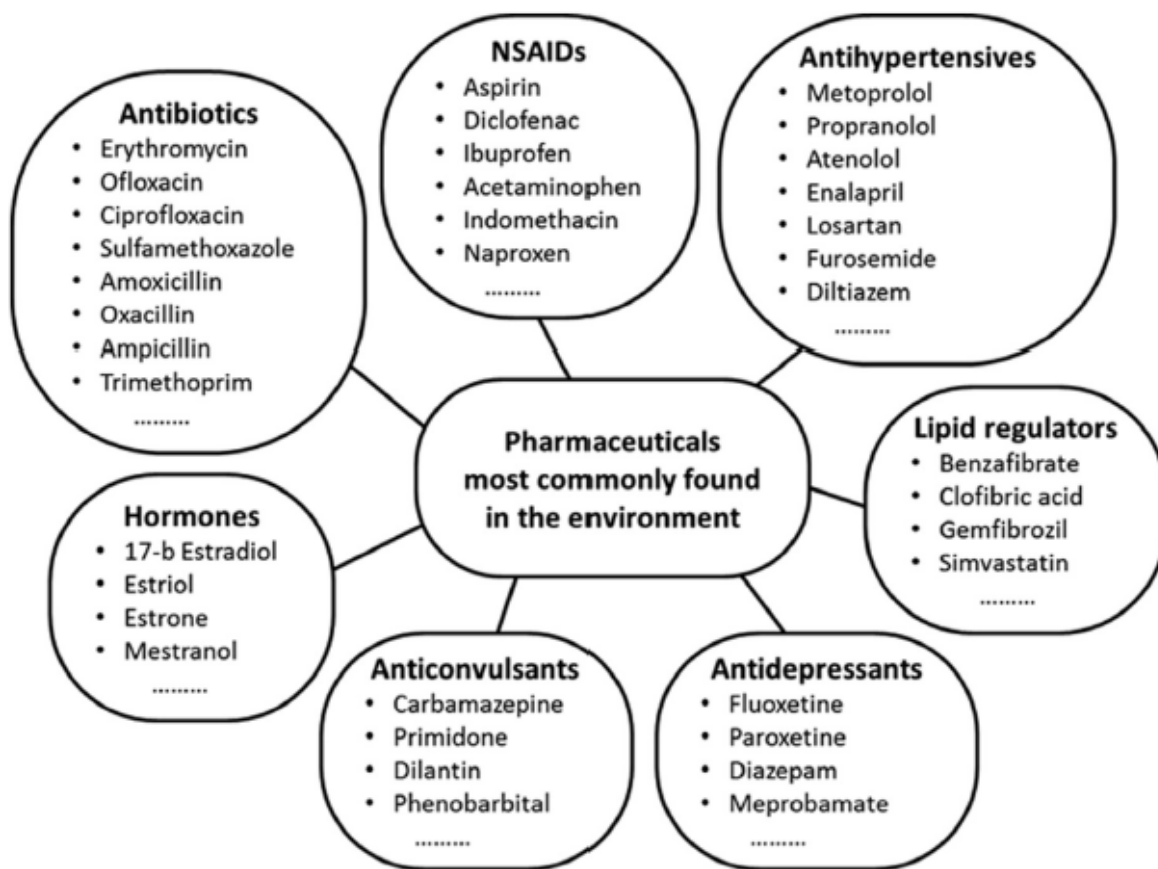


Figure 1.2. Pharmaceutical compounds most commonly found in the environment alongside their corresponding classifications [7]. These contaminants have been identified in the influent and effluent of WWTPs as well as surface water, ground water and even in the tap water.

This creates an almost constant background concentration level of these compounds. The most well known medicine that belongs to this group is diclofenac [2]. Figure 1.2 illustrates the most commonly found pharmaceuticals in the environment alongside their classifications. These compounds have been detected in the influent and effluent of WWTPs and also in various water bodies such as surface water, ground water, etc. [7]. Table 1.1 summarizes the application, the detected concentration in water and the negative impacts of each the above-mentioned classifications.

Table 1.1. Summary of application, detected concentration and negative effects of each pharmaceutical class (page 6-9).

Class	Application	Detected Concentration	Negative Effect
Antibiotic [4,5,13,14]	Antibiotic	-Higher $\mu\text{g/l}$ range in hospital effluent -Lower $\mu\text{g/l}$ in municipal wastewater -ng/l in surface, groundwater and tap water	-Emergence of antibiotic resistant bacteria (e.g. in the case of sulfonamides, fluoroquinolones) -Toxicity to aquatic organisms - Phytotoxicity
Lipid Regulator [15–17]	Blood lipid controller	-Tens of $\mu\text{g/l}$ in WWTPs influent and effluent (clofibrilic acid)	-Possible lower survival rate in aquatic life (little data available)

<p>Antihypertensive [15,18–20]</p>	<p>Lowers blood pressure</p>	<p>-Tens of ng/l surface water</p> <p>-Found in ground water and drinking water (beta blockers such as metoprolol, atenolol and propranolol)</p>	<p>-May pose a threat to freshwater and salt water biota (organisms)</p> <p>-Lack of toxicity data for some drugs</p>
<p>Anticonvulsant [18,21,22]</p>	<p>Treatment of epilepsy</p>	<p>-Tens of ng/l in rivers and lakes</p> <p>-ng/l range in ground water and drinking water</p> <p>-Few µg/l in WWTPs and drinking water (metabolites of carbamazepine)</p>	<p>-Affect marine life</p>

<p>Non-Steroidal Anti- Inflammatory (NSAIDs) [15,18,23,24]</p>	<p>-Analgesic (Pain killer) -Antipyretic (Reduces Fever) -Anti- inflammatory effect</p>	<p>-Tens of $\mu\text{g/l}$ in WWTPs influent and effluent -Tens to hundreds of ng/l in surface water -Found in drinking water (e.g. diclofenac, acetaminophen)</p>	<p>-Toxicity in the case of some NSAIDs -Influence on the growth of aquatic Phototrophs (ibuprofen) -High sensitivity in phytoplankton (ibuprofen) -Inhibition in reproduction (e.g. in snails after exposure to ibuprofen) -Lower fish survival (after 120 days, ibuprofen) -Liver and kidney damage with the Presence of aminophenols (paracetamol) -Increase in drug half life in the environment (paracetamol) - Inhibition of the tumor stopping human antibody: topoisomerase $\text{I}\alpha$ (paracetamol)</p>
---	---	--	--

Hormones [20,25]	-Hormone replacement therapy -Oral contraceptives -Veterinary medicine for growth enhancement	-Few ng/l in river water (17β-estradiol, 17α-ethinylestradiol) -Found in ground water and drinking water	-Intensively active even at very low concentration -Endocrine disrupting (aquatic species)
Antidepressant [26,27]	- Treatment of depression, anxiety and bipolar disorder	-100 ng/l to few μg/l in WWTPs influent and effluent and also surface water	- Alter mobility in snails - Alter memory and cognitive function in cuttlefish - Alter reproduction in fish

The most important conclusions that can be drawn from the summary of the literature presented in Table 1.1 are as follows:

1) The contamination of various water sources is not limited to a few pharmaceutical compounds. The presence of a large number of pharmaceuticals in the environment has been documented in the literature.

2) These compounds are present in the environment with a variety of concentrations. It has to be mentioned that although the detected concentration of some of these pharmaceuticals such as hormones are very low, they can pose serious risks to the environment due to their extreme activity.

3) Until the present day, the hazardous impact of these compounds has only been recorded for animals (fishes, snails, birds, etc.) and plants. However, a report published by the World Health Organization (WHO) in 2011 acknowledged that the effect of long-term exposure to these compounds on humans, even at low concentrations, is unknown and can be catastrophic. Moreover, the same report indicated that specific studies have to be designed to evaluate the effect of these compounds on special groups of the population such as pregnant women, elderlies, patients with compromised immune system, etc. [28].

4) The presence of the pharmaceutical contaminants in water is not limited to one or two countries. Reports from United States [12], Europe (Danube river) [20] and China [13] show that the problem of water contamination with pharmaceutical contaminants is a worldwide issue.

These conclusions explicitly express that the current water treatment processes are not capable of eliminating pharmaceutical compounds from water. As mentioned previously, AOPs have been proposed as one of the most suitable candidates for replacement of current water treatment strategies. In the next section, an introduction to various types of AOPs will be given.

Afterwards, a comparison will be made between these AOPs and the reason behind our interests in plasma-based technologies will be discussed.

1.3. Advanced Oxidation Processes (AOPs)

As described previously, due to the inability of the conventional water treatment processes such as chlorination and biodegradation to eliminate pharmaceutical compounds, various types of AOPs have been investigated for this purpose. In general, the basis of all AOPs is the in-situ generation of highly reactive transient oxidizing agents, such as hydroxyl radicals (OH[•]) in the aqueous phase [29]. These oxidizing agents can breakdown contaminants within the liquid, and are proven to be very effective in water treatment [30,31]. Here in this section we will explore some of the most used AOPs in the literature for degradation of pharmaceutical contaminants.

1.3.1. Ultraviolet/hydrogen peroxide oxidation (UV/H₂O₂)

The UV/H₂O₂ process is an AOP method in which the production of hydroxyl radicals is achieved through the decomposition of H₂O₂ by UV irradiation, as described by Equation 1.1. This process is normally categorized under the homogenous AOPs since the main component, i.e. hydrogen peroxide, is in the same phase as the reactants [32].

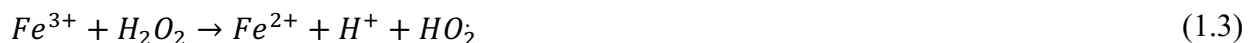


It has to be mentioned that the direct degradation of the pharmaceutical compounds by UV irradiation is also possible. This process is called “photolysis”. However, normally the rate of photolysis for pharmaceuticals in water is not very high and the process is not cost effective [33]. The rate of hydroxyl radical production in this process is directly related to the power of the incident light.

Kim et al. investigated the efficacy of both UV and UV/H₂O₂ processes for treatment of secondary effluents contaminated by pharmaceutical compounds [34]. Their initial analysis of the effluent showed that 41 types of pharmaceutical contaminants including 10 analgesics and 12 antibiotics were present in water. The results indicated that even at very high doses of UV irradiation, acceptable removal could only be achieved for few of the contaminants such as diclofenac. However, the addition of H₂O₂ to water and using an UV/H₂O₂ process resulted in 90% removal for 39 of the contaminants, at much lower UV dosages. This was attributed to the direct action of hydroxyl radicals, as the most powerful oxidizing agents, on the pharmaceutical contaminants. Elimination by means of the UV/H₂O₂ process has been reported for pharmaceuticals such as clofibrac acid [35], penicillin [36], metronidazole [37], naproxen and carbamazepine [38], 17 α -ethinylestradiol and 17 β -estradiol [39], etc. The advantage of treatment processes based on UV/H₂O₂ is the homogenous destruction of organic compounds in water. However, the concentration of the added H₂O₂ should be closely controlled since extra concentrations of H₂O₂ can participate in a side reaction with hydroxyl radicals and act as radical scavenger [32].

1.3.2. Fenton and photo-Fenton Process

Fenton processes, as a homogenous AOP, produce hydroxyl radicals in the solution based on the reaction of ferrous ions (Fe²⁺) with hydrogen peroxide molecules (H₂O₂). When ferrous ions and hydrogen peroxide are added to the solution, the following fundamental reactions can occur [40,41]:



Equation (1.2) describes the main reaction of Fenton processes in which the reaction of a ferrous ion (Fe^{2+}) and a hydrogen peroxide molecule creates one hydroxyl radical. The reaction rate for this process has been reported to be $76 \text{ M}^{-1}\text{s}^{-1}$ [42]. One of the by-products of Equation (1.2) is ferric ion (Fe^{3+}). Ferric ions cannot participate directly in the production of hydroxyl radicals. However, they can react with hydrogen peroxide to produce ferrous ions again, as shown by Equation (1.3). The reaction to produce ferrous ions happens with the rate of $0.01 \text{ M}^{-1}\text{s}^{-1}$ [42]. One of the main drawbacks of Fenton processes is rooted from this significant difference between the reaction rates of Equations (1.2) and (1.3). Ferrous ions are the main component of Fenton processes. The reaction (Equation (1.2)) to consume ferrous ions happens at a much faster rate compared to the reaction (Equation (1.3)) that reproduces ferrous ions. As a result, generation of hydroxyl radicals in a Fenton process happens quickly at the beginning but slows down significantly as it proceeds. Moreover, this inequality in the reaction rates results in a large production of iron sludge [43]. The application of light irradiation in photo-Fenton processes has been suggested to address these drawbacks. In acidic solutions (pH near 3), the main photoactive species that is created from ferric ions is $[Fe(OH)]_{aq}^{2+}$. Under UV-visible illumination, hydroxyl radical can be created from this species, as described by Equation (1.4).



Consequently, in a photo-Fenton process, not only are hydroxyl radicals created from ferrous ions (Fe^{2+}), but ferric ions (Fe^{+3}) also participate in the process. Another possible advantage of photo-Fenton processes, in case of UV irradiation, is the direct generation of hydroxyl radicals from hydrogen peroxide molecules. This phenomenon has already been discussed in section 1.3.1.

Shemer et al. evaluated the application of Fenton and photo-Fenton processes for degradation of metronidazole in di-ionized water. Their results showed that by using 29.4 μM of hydrogen peroxide and 5.9 μM of ferrous ion, 70% of metronidazole could be removed effectively from water in a period of 300 s. More importantly, using a medium pressure (MP) UV light in a photo-Fenton process and similar concentrations of hydrogen peroxide and ferrous ion, 90% of the contaminant could be degraded in the same period of time [37]. This was attributed to the additional production of hydroxyl radicals from ferric ions when UV irradiation is utilized. Using Fenton and/or photo-Fenton processes, successful degradation of various pharmaceutical compounds such as diclofenac [44,45], penicillin [36], sulfamethoxazole [46], azathioprine and thiotepa [47], etc. has been demonstrated.

1.3.3. Semiconductor Photocatalysis

Semiconductor photocatalysis is a process in which energetic oxidizing agents are produced through the application of a catalyst that absorbs photons. The catalyst in this process is a semiconductor such as TiO_2 , ZnO , etc. [48]. When a semiconductor is irradiated with a photon with energies higher than the band gap of the semiconductor, electron-hole pairs are created. By absorbing such a photon, an electron will be excited to the conduction band (e_{CB}^-) and leaves a hole in the valance band (h_{VB}^+). The holes in the valance band are powerful oxidizing agents that can react with organic compounds and cause their degradation [49]. Moreover, the holes can also react with water molecules at the semiconductor/water interface to create hydroxyl radicals [48]. The application of various semiconductors in the form of nanoparticles [50,51] and nanowires [49] have been demonstrated. Figure 1.3 illustrates the above-mentioned process for a BiFeO_3 (BFO) nanowire irradiated by photons with sufficient energy.

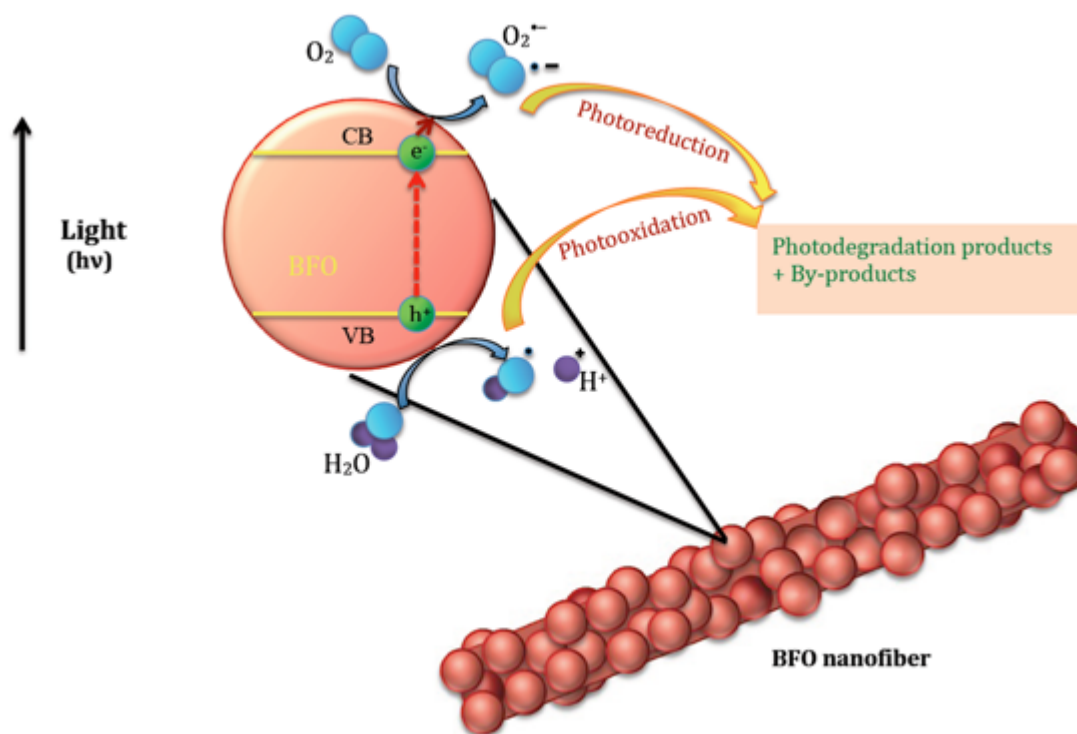


Figure 1.3. The schematic illustration of the semiconductor photocatalysis shown for a BiFeO_3 (BFO) nanowire. The involved processes including the generation of an electron-hole pair and hydroxyl radicals are shown [49].

The advantage of using homogeneously dispersed nanoparticles for a semiconductor photocatalysis process is the occurrence of oxidation reactions through the volume of the solution. However, special measures should be considered to remove nanoparticles from the solution, after the treatment process is done. This problem can be overcome by utilizing nanowire mats; however, in this case, oxidation reactions only happen at the semiconductor/water interface. This can limit the efficiency of such a method.

Perhaps, the most widely used semiconductor photocatalysis process for degradation of pharmaceutical compounds is the TiO_2 nanoparticles/UV system. Utilizing such a method, Reyes et al. demonstrated the removal of tetracycline in water. Their results indicated that when 0.5 g/l of TiO_2 nanoparticles are suspended in the water containing 40 mg/l of the contaminant, 50%

removal could be achieved in 10 min if UV lamp was used [52]. The degradation of a variety of pharmaceuticals such as 17 β -estradiol [53], triclosan [54], lincomycin [55], sulfamethazine [56] and many more has been explored.

1.3.4. Electrolysis

Electrolysis and electrochemical methods for water treatment have gained the attention of many researchers during the past few decades. The high number of companies around the world that offer electrochemical-based technologies is a testament to the versatility and effectiveness of these methods [57]. Electrochemical oxidation of organic compounds can be achieved either through direct or indirect pathways [58]. In the direct method, the oxidation of organic molecules happens at the anode of the electrochemical setup. At the anode, oxidation progresses by physisorbed hydroxyl radical (OH^\bullet) or chemisorbed oxygen in the lattice of the metal anode (MO_{x+1}) [59,60].

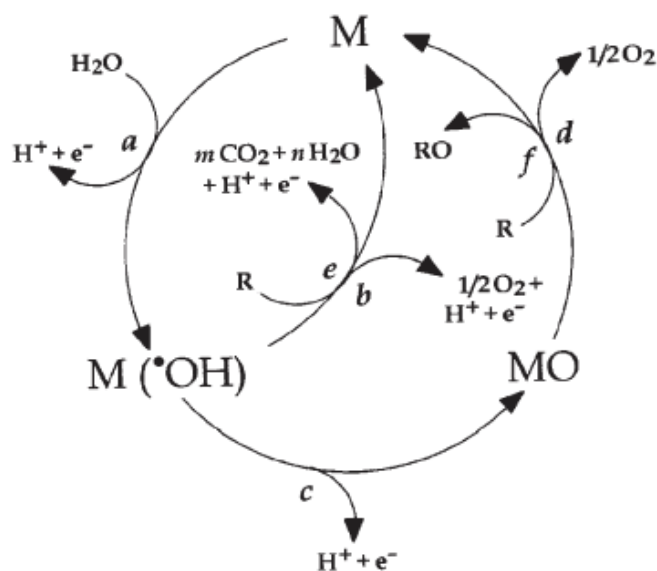


Figure 1.4. Various steps (a-f) involved in the direct electrochemical oxidation of organic compounds are shown [60]. “M” and “R” in the figure represent the surface of the anode and organic molecule, respectively.

The complete oxidation of organic pollutants or their oxidation conversion by means of direct electrochemical method is described by Comninellis et al. [60], schematically shown by Figure 1.4. The process starts with the electrolysis of water molecules at the anode surface (a). The direct consequence of the water electrolysis process is the production of hydroxyl radicals at the surface. These radicals participate in the subsequent reactions in two pathways. The first pathway is the direct reaction of hydroxyl radicals with organic molecules (e), which eventually results in the formation of water and carbon dioxide (complete mineralization). The second pathway (c and f) stems from the chemisorption of hydroxyl radicals on the anode surface ($M(OH)\cdot$). Since $M(OH)\cdot$ is unstable, it forms a higher metal oxide (MO) which can react with organic compounds on the surface and oxidize these molecules. It has to be mentioned that in both pathways mentioned above, competing reactions are present that prohibit the oxidation of organic compounds. One of the most important competing reactions is the evolution of oxygen molecules from the anode surface (b and d in Figure 1.4). Comninellis proposed that the role of each of these reactions (b and d) depends strongly on the nature of the anode electrode. Based on the results obtained by Comninellis et al., two types of electrodes were introduced, i.e. active and non-active anodes [60]. In active anodes, the interaction between the anode material (M) and hydroxyl radicals ($OH\cdot$) is strong. As a result, the adsorbed hydroxyl radical can react with the anode material and form higher oxide metal (MO). In this case, the oxidation of organic compounds in the solution can occur by this higher oxide metal (reaction f). On the other hand, in non-active anodes, the interaction between the anode and hydroxyl radicals is weak. Consequently, hydroxyl radicals can involve in the oxidation of organic compounds (reaction e) [60].

Beside direct pathways, the electrolytic degradation of organic compounds can happen through indirect pathways. In this method, secondary oxidizing agents such as chlorine gas molecules (Cl_2), hypochlorite (ClO^-) and peroxodisulfate ($\text{S}_2\text{O}_8^{2-}$) can be formed. Perhaps, the most studied secondary oxidizing agent is chlorine and its by-products, possibly due to the presence of various concentrations of Cl^- in different wastewaters [58]. Further analysis and identification of these Cl-based oxidation agents in electrolytic systems has been performed by Comninellis et al. [60] and Bonfatti et al. [61]. These studies proposed that depending on the concentration of Cl^- , the pH of the solution and other factors, oxidizing agents such as Cl_2 , ClO^- , HClO , etc. could be involved in degradation of organic compounds.

Pauwels et al. studied the electrolytic removal of ethinylestradiol, one of the most powerful synthetic estrogens, in water [62]. In this study, two different water matrices were treated, i.e. the effluent of a membrane bioreactor used for treating hospital sewage and drinking water spiked with 1 mg/l of ethinylestradiol. The results indicated that for both water matrices, when optimum parameters, such as the input current, were used, 98% removal of the contaminant could be achieved. Further investigation revealed that the removal of ethinylestradiol was increased as higher concentration of sodium chloride (NaCl) was added to the water. This was attributed to the possible role of free chlorine species such as ClO^- and Cl radicals [62]. Utilizing electrolytic cells with various designs, successful degradation of pharmaceutical compounds such as epirubicin hydrochloride [63], clofibrac acid [64], 17β -estradiol [65] and piroxicam [66] has been achieved.

1.3.5. Ozonation

The application of ozone for treatment of a variety of contaminants in water has been the subject of many researches during the past few decades. This is due to the high oxidation capability of ozone molecules. The oxidation potential of ozone molecules has been reported to be 2.07 V which is slightly lower than the oxidation potential of the most powerful oxidizing agent, i.e. hydroxyl radicals (2.8 V) [67]. Moreover, due to its structure, ozone molecules can react as an electrophile, a nucleophile or a dipole. As a result, a wide range of applications such as oxidation of organic pollutants, control of taste, color and odor in water and also disinfection of water contaminated by microorganisms have been proposed for ozonation [68]. Although the high reactivity of ozone molecules can be used for effective degradation of contaminants, it also promotes the degradation of ozone in water. This decomposition proceeds through the following five reactions [69]:



Even though the decomposition mechanism of ozone molecules in water can be complex, Equations (1.5) to (1.9) show that these mechanisms can be divided into two classes, i.e. instructive and destructive. Equations (1.5) and (1.8) describe two instructive reactions in which ozone molecules are decomposed into hydroxyl radicals. As a result, more powerful oxidizing

agents are produced. On the other hand, reactions such as Equation (1.6) consume ozone molecules in water to produce less powerful radicals such as hydroperoxyl radical ($\text{HO}_2\cdot$, oxidation potential of 1.7 V [70]). These reactions can be classified as destructive reactions since they reduce the overall oxidizing power of the ozonation process. It has to be mentioned that although the generation of hydroxyl radicals from ozone molecules (Equations (1.5) and (1.8)) can be considered instructive, hydroxyl radicals can further react with ozone molecules to produce less active species, as described by Equation (1.7). Moreover, the entire process of ozone decomposition depends on many parameters such as solution pH, presence of hydroxyl radical scavengers, etc. Based on these parameters, the lifetime of ozone molecules in water can span from few seconds to few tens of minutes [67]. Due to this rather short lifetime, normally high ozonation efficiencies can be achieved only at very high costs of operation. To further improve the efficiency of ozonation processes, the combinatory methods involving ozonation and other AOPs have been investigated. These methods include $\text{O}_3/\text{H}_2\text{O}_2$ [71] and O_3/UV [72] with the aim to generate higher concentrations of hydroxyl radicals. More detailed description of these combinatory methods is not the focus of this work and can be found in the literature [71,72].

Li et al. compared the efficiency of the ozonation process and $\text{O}_3/\text{H}_2\text{O}_2$ method for degradation of hydrocortisone in water [71]. The results indicated that for the ozonation process, at pH level of 5.7 and O_3 dosage of 217.5 mg/l, only 45% decrease in chemical oxygen demand (COD) could be achieved after 90 min of treatment. On the other hand, when $\text{H}_2\text{O}_2/\text{O}_3$ ratio of 0.3 and pH level of 3 was used, 67% decrease in COD could be obtained only after 15 min of treatment. This faster degradation during $\text{O}_3/\text{H}_2\text{O}_2$ process was attributed to the higher concentrations of hydroxyl radicals produced in this process compared to the ozonation process [71]. The

application of the ozonation process or its combinatory techniques was investigated for the degradation of various pharmaceuticals such as penicillin [73], lincomycin and spectinomycin [74], carbamazepine [75,76], acebutolol, atenolol and metoprolol [77].

1.3.6. Non-thermal plasma (NTP) treatment

The application of non-thermal plasma (NTP) for the degradation of various contaminants including pharmaceutical compounds has gained the attention of many researchers during the past few years. In general, plasma is known as the fourth state of matter. In this state, gaseous media is present in the ionized form. In other words, ionic species (positive and negative ions) and electrons are present in the gaseous phase in equilibrium. When a sufficiently high voltage is applied to a gas contained between two electrodes at atmospheric pressure, an electrical discharge occurs. In this process, the collision of energetic electrons with neutral gas molecules produces ionization. The result of this process is a medium in which ions, electrons, neutrals, radicals, UV photons, etc. coexist. The plasma is called non-thermal plasma since the gas is not fully ionized and the temperature of the electrons is much higher than that of ions and neutrals [78]. While more detailed description of physical and chemical processes will be given in the next chapter, it suffices to mention that one of the main pathways of generation of hydroxyl radicals in this type of AOP is the dissociation of water molecules. In plasma channels, since electric field is high, charged particles and in particular electrons are accelerated. Electrons are the most important feature of this process due to their smaller mass and higher kinetic energies they can obtain from the electric field. The dissociation of water molecules through inelastic collisions with energetic electrons is shown by Equation (1.10).



The generated hydroxyl radicals (OH \cdot) in this process are known as one of the most powerful oxidizing agents (oxidation potential of 2.8 V) [67]. In order to degrade contaminants in water, plasma can be generated either in the gas phase above the solution [79,80] or directly in the solution [81,82]. Creation of plasma in the bulk of the liquid is more energy intensive. This is probably due to the fact that the mean free path of electrons, as the main components of the plasma generation process, is much smaller in water than in the gas phase [70]. This is due to the higher density of water compared to air (1 g/cm 3 for water versus 0.001 g/cm 3 for air at 15 °C and sea level). The energy that an electron can acquire between two successive collisions is directly related to the amount of the electric field present and the mean free path. Since electrons need to reach a certain energy threshold to ionize neutral molecules, lower mean free path in water means higher electric fields are needed to compensate for the shorter path that electrons travel between two collisions. As a result, more energy is required to sustain plasma in the bulk of the liquid. Therefore, the rest of this work focuses on plasma generation technologies in the gas phase. When plasma is created in the gas phase, the collision of energetic electrons with moisture in the air can create hydroxyl radicals. However, since the lifetime of hydroxyl radicals is very short (few microseconds [83]), effective introduction of these agents from gas phase to the solution is improbable. On the other hand, at the interface of the plasma and solution, energetic electrons can collide with water molecules at the surface of the solution. This can provide a high concentration of hydroxyl radicals at the surface of the solution. If the treatment system is designed in a way that it can provide a sufficient mass transfer from bulk of the solution to the interface, significant degradation of the contaminants by hydroxyl radicals can be expected. However, this is not the only mechanism in which the decontamination process occurs.

Previous studies indicated that during a plasma treatment process, ozone (O₃) and hydrogen peroxide (H₂O₂) can be produced in the gas phase [84,85].



Equation (1.11) describes the molecular dissociation of oxygen molecules by energetic electrons in the gas phase. The product of this reaction is oxygen radical. These oxygen radicals take part in a three-body collision process to form ozone molecules, as shown by Equation (1.12). “M” represents the third collision partner that can be any of oxygen, nitrogen or argon molecules (if present). Hydrogen peroxide also forms from the recombination of two hydroxyl radicals, as described by Equation (1.13). These molecules have a much longer lifetime compared to hydroxyl radicals. As a result, they can diffuse through the gas/liquid interface and reach the bulk of the solution for further decontamination. Moreover, dissolved ozone and hydrogen peroxide molecules in the solution can be involved in many other reactions. Three of these reactions are shown below [81,84,85]:



The reactions shown by Equation (1.14) to (1.16) indicate that oxidizing agents created by plasma not only do involve in the degradation of contaminants, but also they interact with each

other to create either more powerful agents (Equation (1.15)) or new agents ($\text{HO}_2\cdot$ in Equation (1.16)). It has to be mentioned that the chemical reactions discussed in this section are only a small number of reactions that might happen by the action of plasma. More comprehensive studies and discussions can be found in the literature [85]. Furthermore, other chemical reactions containing other chemical elements (beside oxygen and hydrogen) can occur. Reactions involving nitrogen molecules and its by-products are of significant importance, especially in the post treatment stage. This topic will be more discussed in Chapter 3, where the effect of ionic constituents in the solution will be studied.

Zeng et al. studied the application of non-thermal plasma for degradation of ibuprofen in water [86]. Their results indicated that plasma treatment process could be considered as a suitable method for elimination of pharmaceuticals contaminants in water. After treating water contaminated by 60 mg/l of ibuprofen for 80 min, about 92% of ibuprofen molecules were degraded and 35% mineralization was obtained. Moreover, the significant increase in the biodegradability index (the ratio of Biochemical Oxygen Demand after 5 days to Chemical Oxygen Demand, BOD_5/COD) showed that further mineralization of the remaining organic content could be achieved by biological treatments. Degradation of many pharmaceutical compounds such as sulfadiazine [87], pentoxifylline [88], enalapril [89], amoxicillin, ampicillin and oxacillin [90], paracetamol and β -oestradiol [3], etc. has been shown. These studies have been performed using various plasma generation technologies such as Dielectric Barrier Discharge (DBD), corona discharge, etc. A detailed description of these techniques will be given in Chapter 2.

1.3.7. Comparison of various AOPs

A brief description regarding various AOPs and their application in elimination of various pharmaceutical compounds was given in section 1.3.1 to section 1.3.6. In this section, we will compare these methods briefly and outline our motivation behind choosing plasma-based technologies.

Figure 1.5 illustrates the change in the normalized publication regarding each of the above-mentioned AOPs over the last few decades. The data in Figure 1.5 was obtained in the following manner. Google Scholar© was used as the main database. In order to find the number of publications in each decade, advanced search was done by typing the AOP method name and the term “degradation of pharmaceuticals” in the “with the exact phrase” box. The resultant numbers of publication were then tabulated and the data in each decade was normalized to the total number of publications in each AOP category.

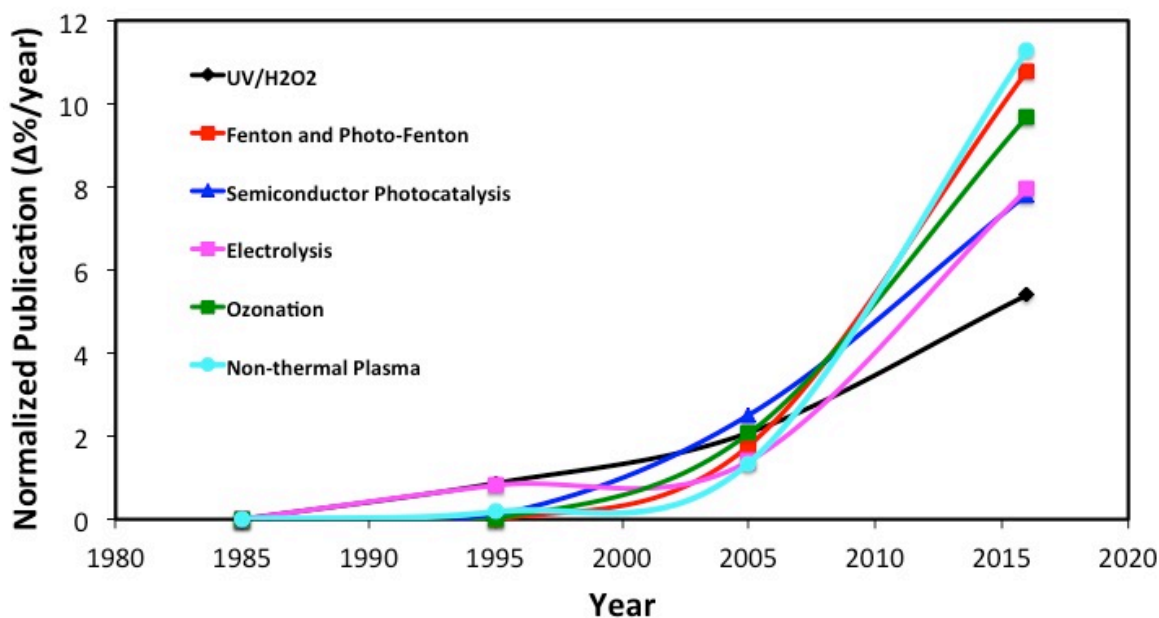


Figure 1.5. The change in the normalized publication regarding various AOPs used for degradation of pharmaceutical compounds is shown as a function of year. The fast increase in the number of publications corresponding to the application of non-thermal plasma in this area, especially in the last decade indicates the viability and versatility of this method.

Finally, the %change in the normalized number of publications was divided by the number of years passed. The calculated normalized publication ($\Delta\%/year$) was plotted as a function of year.

The trends shown by Figure 1.5 indicate that:

1) The number of publications regarding the application of all AOPs discussed above in degradation of pharmaceutical compounds has grown in the last decade. This is probably due to the fact that the number of studies proving the presence of pharmaceuticals in our water sources and their subsequent negative impacts has increased. Table 1.1 in section 1.2 described these effects.

2) The highest growth in the publication in the last few years (2010-2016) is in the area of non-thermal plasma and Fenton and photo-Fenton processes. The rise in the number of publications in the area of Fenton and photo-Fenton processes is probably due to the homogenous nature of this process. In Fenton and photo-Fenton processes, the generation of hydroxyl radicals occurs throughout the volume of the solution. This is in contradiction with electrolysis that hydroxyl radicals are only created at the surface of anodes. On the other hand, photocatalysis can be homogenous (in case of homogeneously dispersed catalysts); however, there is a need to remove the catalyst from the solution. The high number of publications in the area of non-thermal plasma is probably due to the simultaneous production of reactive chemical agents such as hydroxyl radicals, ozone, hydrogen peroxide (H_2O_2), peroxyxynitrite, etc. [42,80,91–94].

3) The sharpest growth in the publication (the slope of curves in Figure 1.5) in the last 10 years corresponds to the application of non-thermal plasma in pharmaceutical decontamination. As mentioned before, the variety of oxidizing agents created in this process can be a reason. Moreover, a significant post treatment stage can only be achieved through plasma-based

methods. In this stage, the degradation continues while plasma is turned off, i.e. no energy is used. Further discussions on the nature of this stage will be given in Chapter 2 and Chapter 3.

4) Finally, in most of the above-mentioned AOP techniques, addition of one or more constituents of the process is necessary. The necessity for adding hydrogen peroxide in the UV/H₂O₂ process as well as Fenton and photo-Fenton processes, the need for using additional UV sources for UV/H₂O₂ process and TiO₂ photocatalysis and the requirement for using separate ozone generators in ozonation implies the complex and costly nature of these processes for real life applications. On the other hand, in a plasma-based treatment system, hydrogen peroxide, UV light and ozone is automatically created by the action of plasma. This means that synergistic occurrence of many of the above-mentioned AOPs can be naturally expected along with the plasma process. This fact along with the presence of the post treatment stage presents a very crucial advantage for plasma-based technologies.

These four discussions in this section form the basis of our motivation to choose plasma-based technologies for treatment of water contaminated by pharmaceutical compounds. However, there are many variations to plasma-based technologies and these techniques and their comparison will be the subject of our next chapter.

Chapter 2: Plasma-based water treatment processes

In Chapter 1, we reviewed the negative impacts of the presence of the pharmaceutical compounds in our water bodies and various AOPs proposed for elimination of these compounds. The final section of Chapter 1 compared these methods and outlined the rationale behind our choice for using plasma-based technologies. The main aim of this chapter is to describe different variations made to plasma-based technologies, particularly the plasma generation method. However, the fundamental phenomena involved in all plasma-based methods are similar. As a result, the first section of this chapter gives a brief introduction to plasma in general and the phenomena associated with it. The second section outlines the main variations to plasma generation methods. At the end of this chapter, a comparison will be made between these methods and the motivation for inventing another variation in this study will be discussed.

2.1. Introduction to gas discharge¹

The formation of plasma in the gas phase starts with the ionization of neutral molecules, i.e. gas discharge phenomena [95]. Perhaps the first indication of the gas discharge in history dates back to 17th century. During the course of various electrostatic studies, researchers observed that when a charged piece of metal is left in a gaseous environment, with no connection to any other metal, it would gradually lose its charge. More interestingly, experiments in this area revealed that the rate of the charge loss depends on the gaseous environment surrounding the metallic piece. By mid-18th century, not only was the charge dissipation of a conductor to the gas proven experimentally, but studies of researchers such as Franklin also illustrated the formation of bright sparks between two conductors held close to each other and also lightening. From that period of

¹ Most of the materials in this section are adapted from “*An introduction to gas discharge*” by Howatson A. M. [95]. Additional references will be used if necessary and cited accordingly.

time to mid-19th century, the electric arc became a popular area of research, owing to the advent of continuous current sources. Investigations led by researchers such as Faraday on the nature of the discharge at pressures lower than atmospheric pressure resulted in the invention of gas discharge tubes and cathode rays. Finally, during the second half of the 19th century, gas discharge tubes were used in a variety of electronic applications such as high voltage switches, computing tubes, surge protectors, etc. However, the emergence of the semiconductor industry and especially silicon industry, has limited the application of these tubes to only very high voltages in our era.

One of the most important topics in the subject of the gas discharge is different types of discharge that could happen upon the application of high voltages to a gaseous medium. Therefore, a brief discussion on this topic would be delivered in the next section. Moreover, this brief discussion would serve as the introduction to plasma physics and various phenomena in plasma.

2.1.1. Types of gas discharge

Generally, gas discharge is described as a process in which the flow of electric current happens in a gas medium. This current is the direct result of the movement of charged species in the electric field. According to the current that is carried through the gas during the discharge, three distinct types of discharge are categorized for a low-pressure tube with two planar electrodes, attached to a direct current (DC) voltage source:

- 1- The **Townsend or dark discharge**, which could carry currents up to 10^{-6} A.
- 2- The **glow discharge** with currents ranging from 10^{-6} A to 0.1A.

3- The **arc discharge** which could have currents about 0.1A and higher.

The trend showed in Figure 2.1 is a general illustration of the change in the current in the gaseous medium as the voltage is increased [96].

A Townsend gas discharge is normally characterized with a number of features. These features are: 1) the current that passes in the gas phase is low, 2) the discharge is invisible, hence the name dark glow. This is mainly due to the fact that the number of excited particles with the ability to emit visible light is very small, 3) the discharge is not self-sustained, i.e. it cannot support its ionization entirely. This means that external sources such as ultraviolet (UV) or X-ray irradiation are required to produce primary electrons from either the body of the gas or the negative electrode.

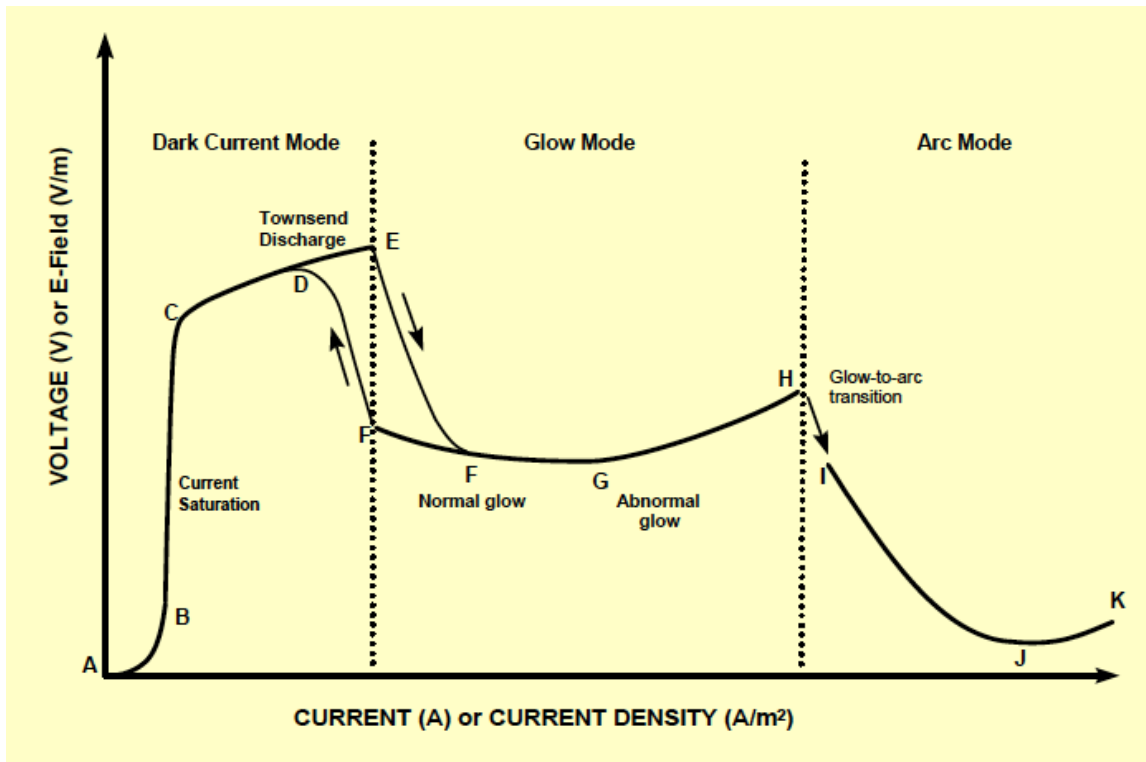


Figure 2.1. Schematic illustration of voltage and current change during the course of a gas discharge process. Different types of discharge could be recognized distinctly based on the trend of the voltage and current [96].

The early observations of the researchers on the charge dissipation of an isolated charged conductor are examples of the Townsend discharge. If the voltage across a gaseous medium that contains a Townsend discharge increases, at a threshold value the current increases sharply by orders of magnitude. This is the point known as the breakdown of the gas which could have voltages ranging from few hundreds of volts and upward, depending on the nature of the gas, pressure of the gas and the separation distance of the electrodes. At this point, the discharge is able to support its ionization since electrons are formed as a result of the breakdown. This discharge is luminous and it could take the form of the glow discharge or arc discharge depending on a number of parameters. Although glow discharges could be mainly observed in the pressures much lower than atmospheric pressure (few mmhg), but depending on the shape and the distance of the electrodes, they could be obtained at atmospheric pressure and upward. Generation of plasma (glow discharge) at atmospheric pressure is the subject of section 2.2. Finally, arc discharges are associated with random ionizations of gas molecules in narrow channels when high voltages are applied. The formation of lightening in the sky is an example of the arc discharge.

2.1.2 Plasma physics and chemistry

Traditionally, all plasma-based technologies are divided into two general categories, i.e. thermal plasma and non-thermal plasma [97]. Thermal plasma (such as arc) is known for its capability for delivering high powers. Each unit of a thermal plasma generator is able to produce up to 50 MW of power. However, because of the Joules heating and thermal ionization, extensive considerations should be made for cooling the system and also protecting the electrodes. That is the main reason why the application of thermal plasmas has been very limited. On the other hand, in non-thermal plasmas, the temperature of neutrals and ionic species is much lower than

the electrons temperature. As a result, the gas temperature does not rise significantly and the energy efficiency is high. Hence, no measures are required to cool the reactor [97]. As a result, non-thermal plasmas have found their way in many applications, especially for abatement of contaminants.

Regardless of the non-thermal plasma generation method, the fundamental basis of the plasma generation is similar. The majority of the energy given to the gas in the reactor is spent to accelerate electrons instead of heating the gas molecules. These energetic electrons in turn can collide with gas molecules and produce a wide range of species such as radicals, excited species and also more electrons. In the first part of this section, we deal with the production of electrons from the collision of accelerated primary electrons with gas molecules. This phenomenon is known as electron avalanche. In the second part, the production of other species, especially radicals, and their interactions with each other is discussed briefly. This area is known as plasma chemistry.

2.1.2.1. Electron avalanche -The Townsend mechanism of breakdown

Electrical breakdown of gases is known to happen when the electric field applied to the gas reaches a certain critical value. At this point, conductive gas channels will be created in the volume of the gas. Although this process can be very complicated and many forms of discharge (plasma) can be created, all of these forms start with the phenomenon called electron avalanche. Here we only restrict our discussions to a simple case of a gas medium between two planar electrodes with distance d and DC voltage of V applied between the electrodes. Detailed discussions regarding more complex discharge systems is not the scope of this work and can be found in the literature.

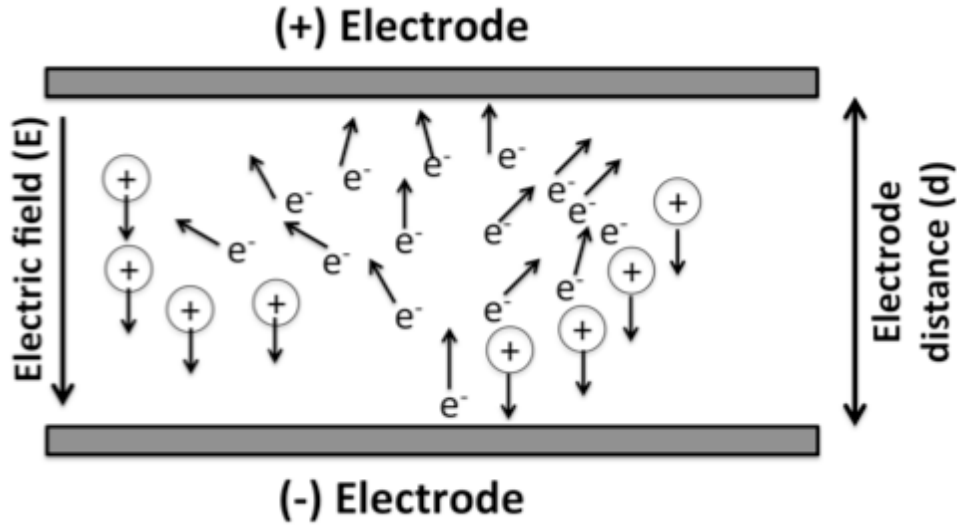


Figure 2.2. Schematic representation of a discharge system in which a gaseous medium is placed between two planar electrodes is shown. When the applied electric field to the medium reaches a certain threshold, it can initiate the electron avalanche process.

Figure 2.2 illustrates a simple discharge system with planar electrode configuration. One can imagine occasional formation of primary electrons near the negative electrode by cosmic or X-ray radiations. When a DC voltage is applied between the electrodes, an electric field will be created. In such a planar system, this uniform electric field can be calculated by Equation (2.1):

$$E = \frac{V}{d} \quad (2.1)$$

In Equation (2.1), V and d represent the applied DC voltage and the distance between the electrodes, respectively. The created electric field causes the movement of the primary electrons from the negative electrode towards the positive electrode. This gives rise to a low initial current of i_0 . If the voltage and hence the electric field is increased to a certain threshold (depending on the ionization energy of the gas phase molecules), the accelerated electrons can ionize neutral molecules during their travel towards the positive electrode. The subsequent secondary electrons

can also accelerate in the electric field and ionize more gas molecules. This multiplication of electrons is known as the electron avalanche, as schematically illustrated by Figure 2.2. This process is normally described by the Townsend ionization coefficient (α) that expresses the electron multiplication per unit length. As a result, by assuming that the avalanche only develops in one direction (x-direction), one can simply conclude that [97]:

$$\frac{dn_e}{dx} = \alpha n_e \quad (2.2)$$

In Equation (2.2), n_e defines the electron density present in the gas volume. Equation (2.2) is equivalent to:

$$n_e(x) = n_{e0} \exp(\alpha x) \quad (2.3)$$

in which $n_e(x)$ and n_{e0} represent the electron density in space along the x-direction and the initial electron density, respectively. Equation (2.3) indicates that the density of electrons during the avalanche process increases exponentially as they move from the negative electrode towards the positive electrode. The Townsend ionization coefficient depends on the electron mobility and the electric field since they define the energy gained by the electrons between two successive collisions. This dependency is shown by Equation (2.4) [82,97].

$$\alpha = \frac{1}{\mu_e} \frac{k(E/n_0)}{E/n_0} \quad (2.4)$$

In Equation (2.4), $k_i(E/n_0)$ denotes ionization rate coefficient. μ_e and E/n_0 are the electron mobility and reduced electric field, respectively.

As mentioned previously, during the electron avalanche, not only are electron created, but positive charges are also produced which travel towards the negative electrode. Using Equation

(2.3), one can infer that when one primary electron travels the distance between the electrodes (d), the number of positive charges created per one initial electron can be expressed by:

$$n_+(d) = \exp(\alpha d) - 1 \quad (2.5)$$

These positive charges move towards the negative electrode and create electrons from the negative electrode through the process of secondary electron emission. The number of electrons created by this process can be estimated by Equation (2.6).

$$n_{se} = \gamma[\exp(\alpha d) - 1] \quad (2.6)$$

in which γ expresses the secondary emission coefficient, defined as the probability of the secondary electron generation on the negative electrode by ion impact. This coefficient depends on the electrode material, the nature of the gas (positive ions), the state of the surface and the reduced electric field [97]. These secondary electrons can move in the electric field and they can contribute to further avalanche processes. It has to be mentioned that not all of the electrons created through the avalanche process are involved in ionization of further neutral molecules. A portion of the produced electrons is lost due to the recombination and attachment to electronegative molecule processes. These processes become significant when the gap distance is large ($d > 5$ mm) and the concentration of electronegative molecules such as oxygen is high. The inclusion of these processes in the general explanation of the phenomena intended in this work deviates us from the main focus. As a result, we will not explore these subjects.

As mentioned previously, the main contributor to the current that develops in the electrode gap is the movement of the electrons in the electric field. The current is non-self-sustained (dark current mode in Figure 2.1) if the positive ions reaching the negative electrode cannot produce at least one secondary electron. The discharge mode will make the transition from the dark mode to the

glow mode (Figure 2.1) when the electric field reaches a certain threshold. At this point the discharge current is self-sustained, i.e. the positive ions reaching the negative electrode can produce at least one secondary electron that can continue the electron avalanche process. This is generally known as the gas breakdown. Therefore, the simplest breakdown criterion is:

$$\gamma[\exp(\alpha d) - 1] = 1 \quad \text{or} \quad \alpha d = \ln\left(\frac{1}{\gamma} + 1\right) \quad (2.7)$$

2.1.2.2. Streamers in breakdown

Streamers are thin ionized channels that grow very fast in the gap between electrodes. The original concept of streamer formation during the electron avalanche process was developed by researchers such as Loeb [98], Meek and Craggs [99]. It is hypothesized that streamers are formed when the initial primary avalanche is very intense, i.e. the electron multiplication factor (αd) is large enough. If the space charge created in this intense avalanche is large enough, it can create an internal electric field comparable in magnitude to the external field. This results in the elongation of each previously formed avalanche in a specific direction. This transition from the avalanche form to the streamer form is shown schematically by Figure 2.3. The avalanche-to-streamer transition happens when the internal electric field becomes comparable in magnitude to the external applied electric field. This internal electric field is the direct result of the charge separation (electrons and positive ions) and can be visualized in three main positions. These positions are at the center of the streamer (in the charge separation zone), at the head (where electrons are moving) and at the tail (where ions are located) of the streamer.

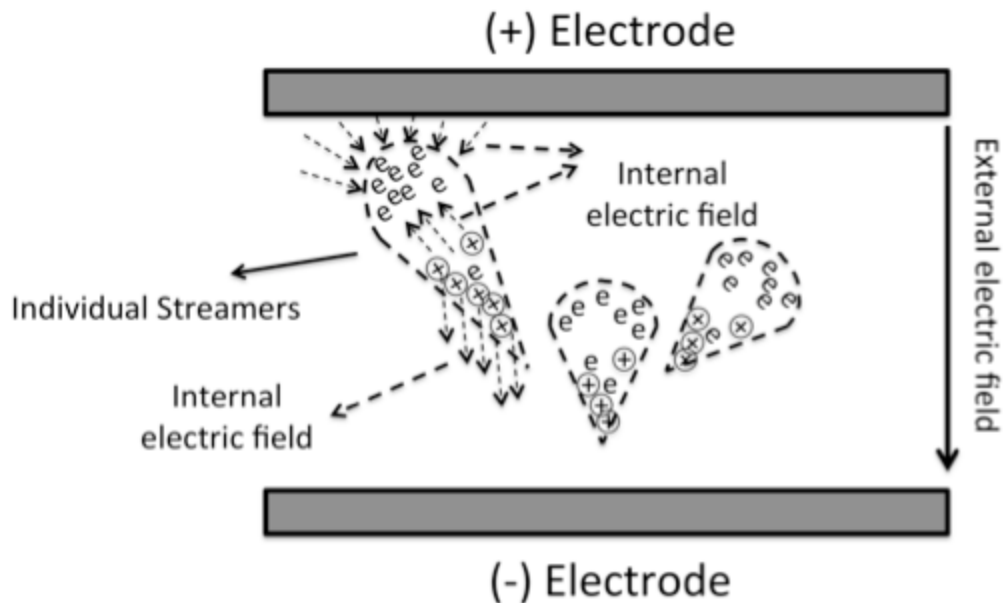


Figure 2.3. The transition from the avalanche form to the streamer form is shown schematically. This transition occurs when the internal electric field created by the charge separation becomes comparable to the applied external electric field.

The direction of the internal electric field located at the center of the streamer is opposite to the direction of the external electric field. As a result, the central internal electric field is weakened. This electric field is responsible for recombining the ionized molecules and electron in the streamer. Therefore, the weakening of this field means that the force to bring the charged particles back together is lowered. On the other hand, the two internal electric fields developed at the head and tail of the streamer have the same direction as the external electric field. This means that these two internal electric fields are intensified. The combined effect of the lowered central electric field and the intensified fields at both ends of the streamer causes the streamer to be stretched. This is why streamers are normally observed as elongated thin channels of ionized gas. This condition, i.e. the generation of a comparable internal electric field to the external applied

electric field by the charge separation in the avalanche is known as the Meek condition [99]. Detailed descriptions regarding the mathematical modeling and expression of the Meek condition is not the focus of this work and can be found in literature [97,99]. However, one criterion that is relevant in our discussions is the transition of the streamer discharge to the spark discharge mode. It has been proven that when the external electric field is large enough, the avalanche-to-streamer transition can occur far away from the positive electrode. In this case, the streamer propagates towards both electrodes. If the streamer channel stretches sufficiently to connect the electrodes, a significant current can pass through the gas medium and a transition from the streamer mode to spark mode can occur. This transition from the glow discharge to the spark discharge along side the sudden increase in the current is shown in Figure 2.1. This transition forms an important basis for designing various plasma-based treatment systems discussed in section 2.2.

2.1.2.3. Plasma chemistry

The description given in sections 2.1.2.1 and 2.1.2.2 regarding the electron avalanche and streamer formation only expresses one interaction of energetic electrons and neutral molecules, i.e. ionization. The direct result of this interaction is the production of electrons and positive ions, as described above. However, depending on the energy of the electrons and also the nature of the gas molecules, a variety of other species can be present in the plasma. These species include radicals, excited species, metastable species and a variety of newly generated molecules. In order to avoid any deviation from the main path of this work, we will focus our discussions to only species created in non-thermal plasmas generated in the air and in contact with the surface of water.

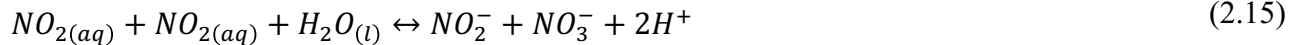
When plasma is generated in air, different molecular species in the air can interact with accelerated electrons. The most important species are oxygen (O₂), nitrogen (N₂) and water (H₂O, both moisture in the air and water molecules at the surface). The collision of energetic electrons with these molecules creates:



Reactions shown by Equations (2.8) to (2.10) indicate dissociation reactions that can occur in the plasma. The direct result of these reactions is the production of various radical species. It has to be mentioned that these reactions are the simplest reactions that can serve as an initial description of the process. Since plasma is a complex medium and the energy of all of the electrons is not similar, a variety of reactions is possible for each of the molecules mentioned above. For instance, a review done by Joshi et al. on the chemistry aspect of discharges includes more than twenty possible reactions for only water molecules [85]. Some of these possible reactions describe momentum transfer to water molecules and vibrational and rotational excitation of the water molecules. Further description of these processes are not the scope of this work.

Hydroxyl radicals (OH \cdot) created during the dissociation of water molecules (Equation (2.9)) are one of the most powerful oxidizing agents. As mentioned previously, since the lifetime of these radicals is very short (few microseconds [83]), effective introduction of hydroxyl radicals created in the bulk of the gas to the water is nearly impossible. However, hydroxyl radicals produced in a thin air layer close to the air/water interface alongside the radicals created by the collision of

electrons with water interface can diffuse to the surface of water. These radicals can effectively degrade contaminants that come to the surface. On the other hand, the combination of the radicals created in the air by plasma (Equations (2.8) to (2.10)) can create oxidizing agents that despite being less powerful than hydroxyl radicals, they generally remain in the solution for a much longer time and can diffuse to the bulk of the solution. These agents can be created by [94,100–104]:



Equation (2.11) represents a three-body reaction in which ozone molecules are formed from the reaction of oxygen molecules with oxygen radicals. In this reaction “M” is the third body that can be either oxygen or nitrogen molecules. Equation (2.12) describes the recombination of two hydroxyl radicals to form one hydrogen peroxide molecule. Both ozone (2.07 V) and hydrogen peroxide (1.77 V) are oxidizing agents with longer lifetime than hydroxyl radical [67,105]. Equations (2.13) to (2.17) show reactions in which nitrogen and oxygen radicals participate to create nitrogen monoxide (NO) and nitrogen dioxide (NO₂). These newly generated molecules

diffuse into the solution from the air/water interface and react with water molecules as shown by Equations (2.15) and (2.16). The most important reaction in this chain reaction is the formation of peroxyntrous acid (ONOOH) and its conjugate peroxyntrite (ONOO⁻), with the involvement of hydrogen peroxide. Various studies have concluded that the oxidizing properties of water treated with air plasma in the post treatment stage (towards various organic and biological contaminations) can be attributed to the action of peroxyntrite in the solution [100–103]. Other examples of further reactions of these secondary oxidizing agents with each other are shown by Equation (2.18) and (2.19) [81,84,85].



These reactions are responsible for reproduction of hydroxyl radicals and creation of other radicals from hydrogen peroxide and ozone molecules. The reactions discussed in this section under the topic of plasma chemistry show that in a plasma treatment system, a large variety of oxidizing agents with different lifetimes can be present to degrade contaminants in water. That is why plasma treatment systems have attracted the attention of many researchers in the past decade, as explained in section 1.3.7.

2.2. Plasma generation systems for water treatment

As described in section 2.1.2.2, one of the main processes that happen during the formation of non-thermal plasma at atmospheric pressure is the development of the streamers in the gas phase. Section 2.1.2.2 also briefly described that when the streamer channel elongates sufficiently to create a connection between two electrodes, a transition from the streamer discharge to spark

discharge occurs. Based on the above-mentioned discussion, there are three steps for the transition of a discharge to a spark. These steps are the avalanche to streamer transition, the streamer growth between two electrodes and the triggering of the return intense ionization wave. Previous studies indicate that by considering the streamer velocity in the order of 10^8 cm/s and a gap distance of 0.5-2 cm, the overall time for the initiation of electron avalanches, the transition to streamer discharge and the propagation of streamers is about 100-300 ns [106]. Since the transition to the spark mode is accompanied by the flow of a massive current through the gas medium, its formation has been deemed undesirable since it can damage the electronic and also increases the energy consumption.

It is rational to conclude that in order to sustain stable plasma, without transition to spark mode, two fundamental approaches can be used. One approach is to limit the growth of the streamer channel. The other technique is to completely eliminate the connection between the electrodes even when the streamer channel is able to grow to the size of the inter-electrode distance. Based on this rationale, four major methods have been used in literature in order to create plasma for water decontamination purposes. These techniques are:

- Dielectric Barrier Discharge (DBD)
- Floating Electrode Dielectric Barrier Discharge (FEDBD)
- Gliding Arc Discharge (GAD)
- Streamer Corona Discharge (SCD)

DBD and FEDBD systems are based on the application of one or two thin layers of dielectric materials such as quartz on one or both electrodes. In this manner, even in the case of the complete growth of the streamer channel, the two electrodes cannot be connected to each other

and streamer-to-spark transition can be avoided. In GAD method, unlike the others, the formation of sparks or arcs is desirable and a fast flow of a gas is used to blow the plasma plume on the surface of water. SCD systems use high voltage pulses with short durations. The duration of the pulse is normally shorter than the duration of the streamer formation and propagation (100-300 ns). In this way, the connection between the two electrodes can be avoided. In the following sections, each of the above-mentioned methods along with their applications in degradation of pharmaceutical compounds will be discussed.

2.2.1. Dielectric Barrier Discharge (DBD)

As mentioned in the previous section, one approach to avoid the streamer-to-spark transition is to eliminate the possibility of the connection of two electrodes. In practice, a thin layer of a dielectric barrier such as quartz or glass is used. In this manner, the streamer channel cannot physically connect the two electrodes and the current that passes through the gas is controlled.

Figure 2.4 illustrates a schematic of a simple DBD system.

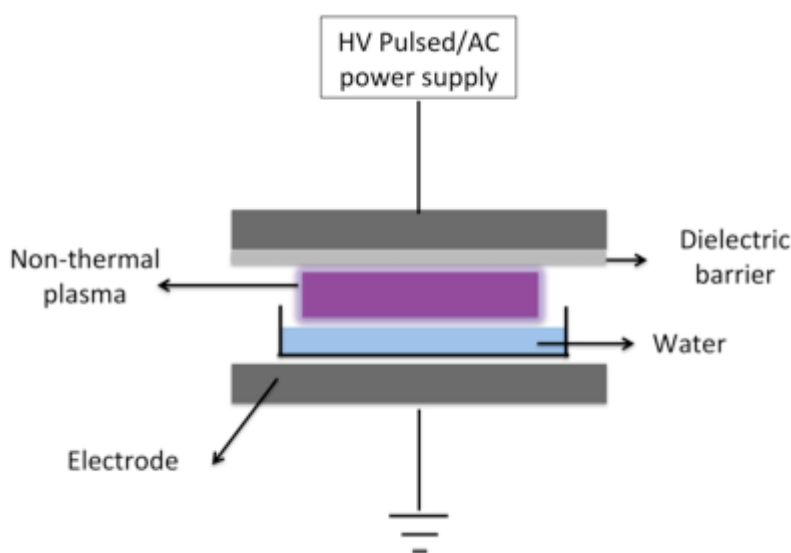


Figure 2.4. The schematic of a DBD system is shown. The dielectric barrier serves at the limiting factor for the current and hence avoiding the spark transition.

In order to generate plasma, a high voltage pulsed or alternating current (AC) power supply is used. The use of AC power supplies is more common since the presence of a pulsed power supply is not a necessity, as opposed to plasma system based on SCD (more explanation will be given in section 2.2.3). The use of pulsed power supplies can be a disadvantage since the circuitry of such a system can be complicated and upscaling is an issue due to high demands on the electronics of large pulsed power supplies [78]. Normally, for the air gap distances of a few millimeters, AC waveforms with the frequency in the range of 500 Hz-500 kHz and amplitude of approximately 10 kV are sufficient to create plasma in the gap. Two major configurations of DBD technology have been used extensively in literature, i.e. planar and cylindrical [107]. A planar configuration consists of two flat metallic electrodes as shown by Figure 2.4. On the other hand, in a cylindrical configuration, one metallic rod and another metallic hollow pipe can be used. In this configuration, water normally flows on the inner side of the hollow pipe. In most DBD processes, although the plasma in the electrode gap seems uniform, under magnification, it consists of numerous microdischarges propagated in the space between electrodes [97]. These microdischarges are shown in Figure 2.5.

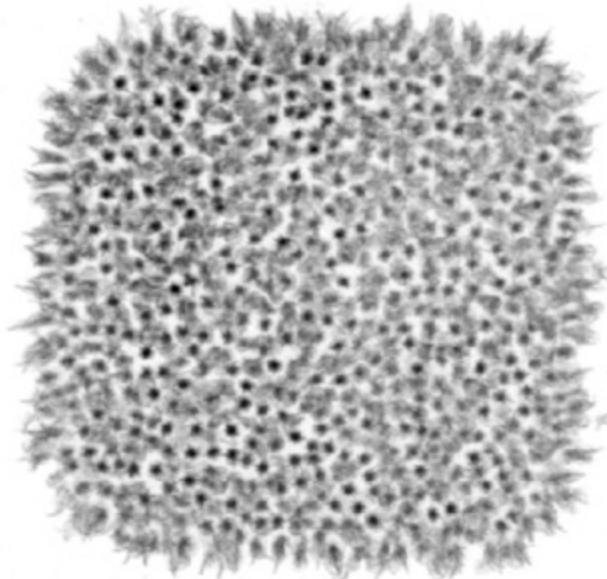


Figure 2.5. The structure of microdischarges in a DBD process [97].

The formation of microdischarges in a DBD process is a complex phenomenon; however, it can be simply explained by the action of the streamer channels. When streamer channels are formed in the gap, a charge separation occurs as described in section 2.1.2.2. In this process, electrons move towards the positive electrode and positive ions travel to the negative electrode (assuming that there is only positive ions in the gap). Electrons travel much faster than positive ions by virtue of their smaller size. In a gap of few millimeters, it takes about 40 ns for electrons to travel the gap and reach the positive electrode. As a result, the movement of electrons is normally used to explain various phenomena in plasma while ions are assumed to be stationary. When electrons reach the dielectric barrier of the positive electrode, they accumulate on the surface. This deposition and accumulation of electrons on the dielectric barrier prevents the formation and propagation of new avalanches and subsequently streamers nearby. This prevention from new streamer formation continues until the polarity of the applied voltage reverses. At this moment, electrons deposited on the dielectric barrier are repelled by the new negative electrode and start their travel to the opposite electrode [97]. This means that generation of new streamers starts from exactly the same position that electrons were deposited in the previous cycle. In other words, the formation of new streamer channels is not random. This phenomenon repeats itself during each cycle of the AC waveform. As a result, microdischarges are observed in a DBD process and plasma is not uniform.

The application of various forms of DBD systems for degradation of pharmaceutical compounds in water has been investigated. Magureanu et al. developed a DBD reactor with falling liquid film to investigate the degradation of three antibiotics (amoxicillin, ampicillin and oxacillin) in water [108]. The reactor in their study consisted of a coaxial configuration in which the contaminated water was flown as a thin layer of liquid on the surface of the inner electrode. The

solution was collected at the bottom of the reactor and it was pumped back to the reservoir containing the solution. In this manner, secondary oxidizing agents such as ozone and peroxyxynitrite were efficiently introduced to the bulk of the solution. Moreover, the gaseous environment surrounding the plasma was collected and pumped to the reservoir to introduce oxidizing agents present in the gas phase (such as ozone) to the bulk of the contaminated water. The results indicated that for water contaminated with 100 mg/l of the contaminants, 100% removal of amoxicillin was achieved in only 10 min. For the other two compounds, 30 min treatment was required to achieve complete degradation. Using similar reactors, degradation of other pharmaceutical compounds such as sulfadiazine [87], carbamazepine [109], pentoxifylline [88], enalapril [89] has been investigated. Another variation to the DBD technology is called rotating drum reactor. In this configuration, plasma is created between a plate covered with a layer of dielectric barrier and a rotating drum. The rotating drum is normally placed on top of the water reservoir. In each rotation, the drum partially enters the solution and carries a thin layer of the solution to the plasma zone. Using this method, the degradation of pharmaceuticals such as carbamazepine, clofibrac acid and iopromide [110] has been shown.

2.2.2. Floating Electrode Dielectric Barrier Discharge (FEDBD)

The concept of FEDBD was first introduced by Fridman et al. in 2006 [111]. FEDBD is a variation to DBD technology in which electrodes are covered by a layer of a dielectric barrier such as quartz. As a result, it is expected that the physics governing the plasma generation in a DBD process (discussed in section 2.2.1) is applicable in a FEDBD process. The main difference between FEDBD processes and DBD processes is the generation of plasma by only a single electrode in FEDBD processes. Figure 2.6 shows the schematic of such a process.

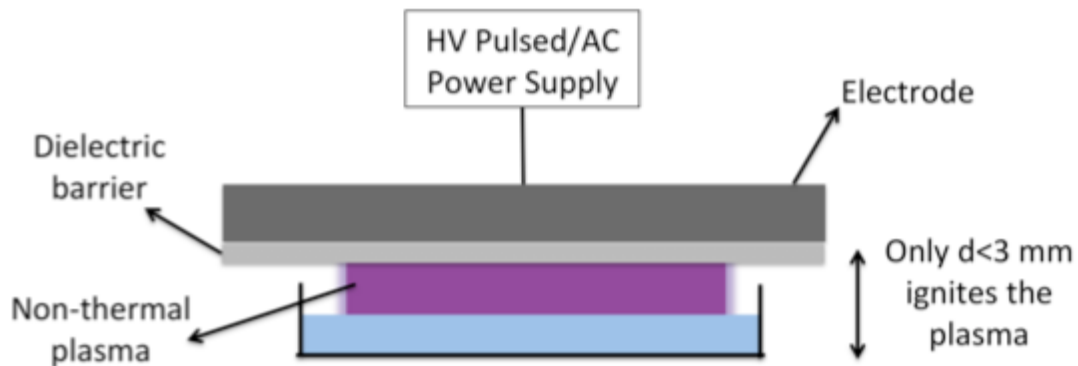


Figure 2.6. The schematic of a FEDBD process is shown. The main difference between FEDBD and DBD processes is the ability to generate plasma by single electrode in FEDBD processes.

Similar to DBD processes, a pulsed or AC high voltage power supply can be used to generate plasma. Fridman and his colleagues have used this technology in many applications. The focus of their studies was to develop a plasma-based technology that can be used in a variety of medical and biological applications. For instance, fast blood coagulation and living tissue sterilization [111], apoptosis of Melanoma skin cancer cell line [112] and elimination of bacteria [113] from surfaces have been investigated. In these studies, the subject to be treated acts as the second electrode in the process of the plasma generation. The advantage of FEDBD for these applications is the fact that since plasma can be generated from a single electrode; the system can be designed in a way that the plasma moves on the surface of the subject. Despite these applications, the use of FEDBD systems for degradation of pharmaceutical compounds in water has never been explored. This might be due to the fact that in FEDBD, plasma can be only generated when the distance between the electrode and the surface of the subject to be treated is less than 3 mm [111]. This limitation is not present in DBD systems where plasma can be generated over a larger ranager of gap distances.

2.2.3. Gliding Arc Discharge (GAD)

The application of GAD for abatement of contaminations in air was first proposed by Czernichowski et al. [114]. The schematic representation of a GAD system is shown by Figure 2.7. As shown in Figure 2.7, a GAD system consists of two diverging electrodes in the gas phase. One of the electrodes is connected to a pulsed or AC or DC high voltage power supply while the other is grounded. When the high voltage is applied, an arc forms in the narrowest gap, i.e. at the top of the electrodes. This arc by itself is thermal plasma. This means that the temperature of gas molecules is very high. However, a flow of a gas is used to move the formed arc along the length of the two electrodes.

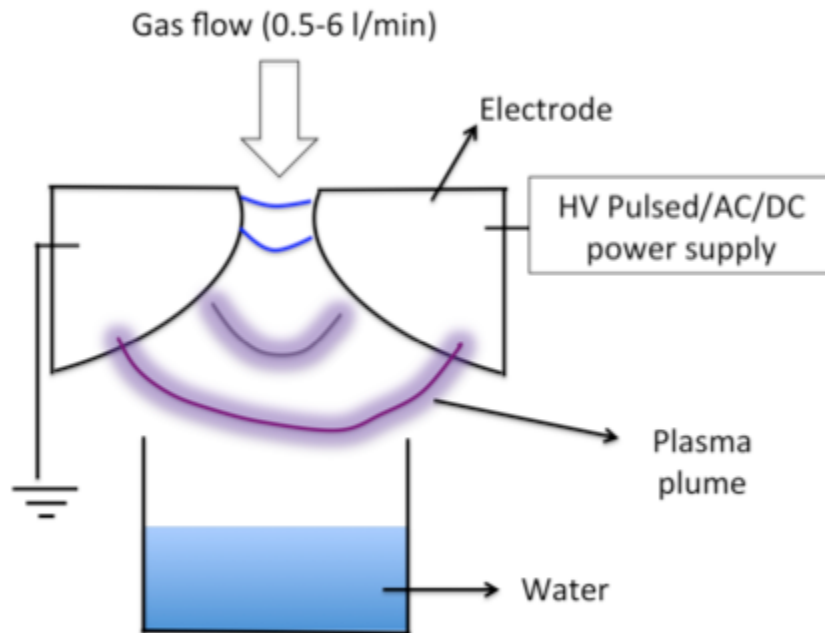


Figure 2.7. A GAD system is shown schematically. In this method, arcs are created between the two diverging electrodes. The plasma plume is blown on the surface of water with a gas flow.

As the arc moves down, its size increases since the two electrodes are diverging. This results in the formation of a new arc at the top. The formation of the new arc causes the old arc to break and turn into a plasma plume. As the size of the arc increases, the temperature of the gas molecules decreases. As a result, the plasma present in the plume is a non-thermal plasma upon breaking [94]. The main advantage of GAD compared to other plasma generation technologies is that it possesses advantages offered by both thermal and non-thermal plasma. In thermal plasmas, a much higher concentration of energetic electrons can be produced compared to non-thermal plasmas. As a result, higher concentrations of radicals and oxidizing agents should be anticipated. However, thermal plasmas never meet this expectation since the temperature of ions and neutrals is also very high and the energy supplied to the plasma is not selectively used for generation of radicals (as discussed in section 2.1.2.3). In non-thermal plasmas, although the electron density and energy are lower, the chemical processes created by the collision of electrons with neutrals are much more selective. This is due to the high degree of non-equilibrium between electron and neutrals in non-thermal plasmas. In a GAD system, the entire process of plasma generation starts with thermal plasmas in the form of arcs and finishes with non-thermal plasmas in the form of plasma plumes. Consequently, high density of energetic electrons and high degree of non-equilibrium can be achieved [97].

Studies investigating the application of GAD technology for degradation of pharmaceutical compounds in water are very few. For instance, Krishna et al. investigated the degradation of verapamil chloride in water by a GAD reactor [115]. Verapamil is a medicine normally prescribed for controlling hypertension and cardiac arrhythmia in patients. The results indicated that by treating the solution contaminated by 50 μM of verapamil chloride, more than 95% of removal could be achieved in 80 min.

2.2.4. Streamer Corona Discharge (SCD)

The application of corona/streamer discharge for removal of a variety of contaminants has been studied extensively during the past decade. In general, corona is formed when an intense electric field inhomogeneity is present, due to an asymmetrical electrode structure. It is in the form of a small luminous region around the electrode with the highest radius of curvature. The application of wire-to-plate [116], wire-to-cylinder [117] and pin-to-plate [118] electrode configurations has been shown. A schematic of a pin-to-plate SCD system is shown by Figure 2.8. In order for a corona discharge to be effective for contamination removal, activated species created in the corona region should reach the contaminated body. The use of an external gas flow [118] and natural ion wind created in the discharge [119] for inactivation of *E. coli* and removal of organic contaminations from water has been investigated, respectively. The simplest method to create corona is to use a high voltage DC power supply with an asymmetric electrode configuration. However, there are two main issues regarding the application of DC corona discharges for contamination removal.

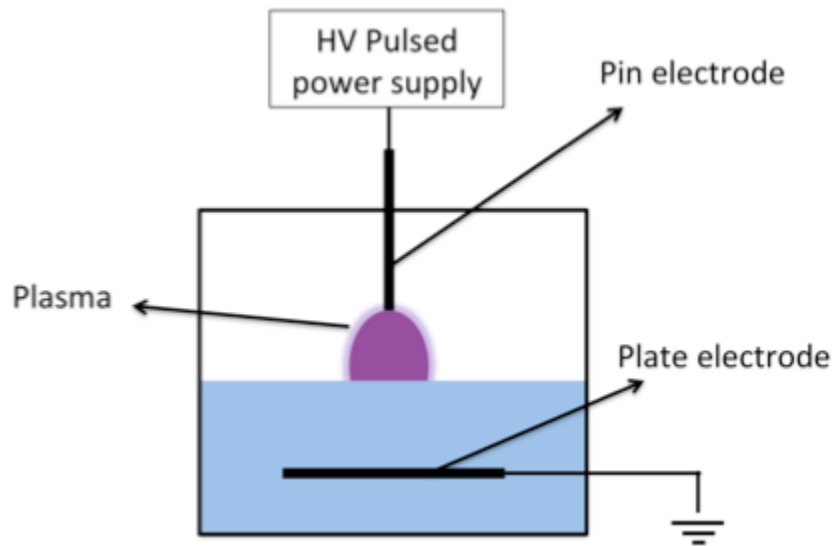


Figure 2.8. A generic pin-to-plate SCD system is shown schematically.

First, this type of discharge is only operable at very low power inputs, impractical for real life applications. An increase in the power results in the transformation of the discharge to streamer discharge. At high DC powers, sustaining a stable streamer discharge is impossible and transformation to spark discharge is inevitable. The occurrence of sparks is mostly undesirable since it can damage the electronics and it consumes a significant amount of energy. Second, during a corona discharge, active species are only created in the corona region, a small region around the sharp electrode, far from the contaminated body. Since hydroxyl radicals (as the most active species in AOPs) have a very short lifetime, they cannot interact with the contaminations; hence, the decontamination efficiency is low [82,106]. In order to solve these problems, the use of high voltage pulses with very short durations has been suggested [106,120]. The rationale behind the application of high voltage pulses can be briefly explained based on the theory of streamer development in the gas, as explained in section 2.1.2.2 [106]. As discussed previously, there are three steps for the transition of a discharge to a spark. These steps are the avalanche to streamer transition, the streamer growth between two electrodes and the triggering of the return intense ionization wave. Previous studies indicate that by considering the streamer velocity in the order of 10^8 cm/s and a gap distance of 0.5-2 cm, the overall time for the initiation of electron avalanches, the transition to streamer discharge and the propagation of streamers is about 100-300 ns. This means that by using high voltage pulses with durations in the above-mentioned range, sustaining non-thermal plasma in the streamer mode with high power is possible. This means that the gas only experiences a sufficiently high electric field for a very short period of time. As a result, the electric field is eliminated before the streamer channel can connect the electrodes to each other.

Zeng et al. utilized a wire-to-cylinder SCD reactor to investigate the degradation of ibuprofen in water. In this system, a wire connected to the high voltage is inserted into the center of a grounded hollow cylinder. A voltage pulse with the amplitude of 32 kV and duration of approximately 200 ns was used to generate streamer corona discharges between the wire and inner surface of the cylinder. Water solutions contaminated with ibuprofen with concentrations in the range of 10-60 mg/l were pumped from a reservoir. The solution flowed as a thin layer on the inner surface of the cylinder where it came into contact with the plasma. The results indicated that for the highest concentration of ibuprofen used, 91.7% degradation could be achieved in 80 min. This type of SCD reactors is known as wetted-wall corona reactor. Using a similar reactor design, successful degradation of sulfadiazine was also achieved [87]. Simple pin-to-plate type SCD reactors have also been used to degrade various pharmaceuticals such as tetracycline [50], diclofenac [121] and methylparaben [122]. Another improvement to the corona discharge reactor is to shower the solution in the plasma region. Using this type of reactors, treatment of water contaminated by paracetamol, indomethacin and β -oestradiol [3] has been investigated.

2.2.5. Floating Electrode Streamer Corona Discharge (FESCD)

The concept of plasma generation by FESCD method and its application for degradation of pharmaceutical compounds in water is the main objective of this research. Here in this section, we will give a brief overview regarding the FESCD method. In the next section, we will outline the rationale behind inventing this technique by making a comparison between all the plasma generation methods discussed in this chapter. Moreover, the working principles will be discussed. The use of a FESCD reactor for elimination of pharmaceuticals from water will be discussed in Chapter 4.

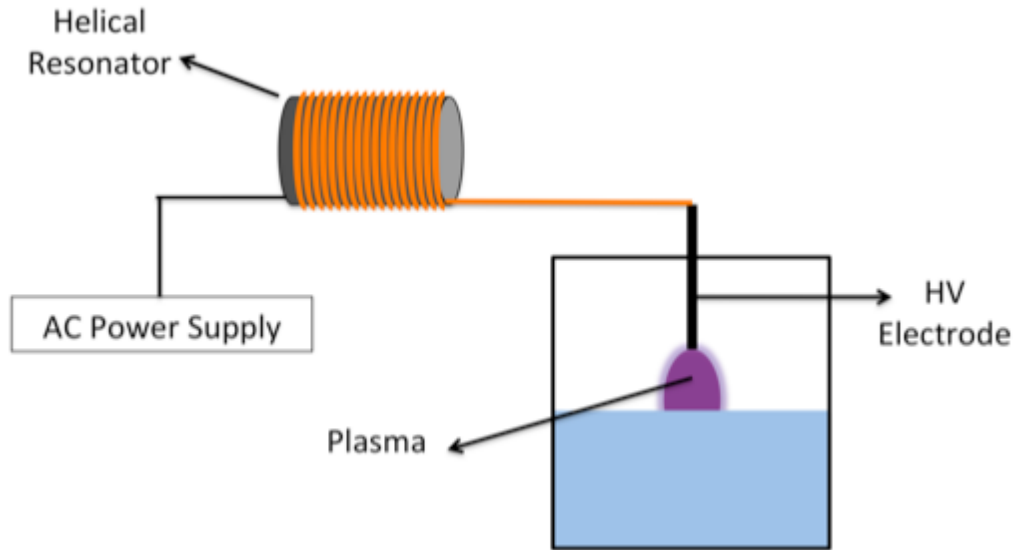


Figure 2.9. Schematic illustration of the FESCD plasma generation system is shown. The main part of the FESCD system is the helical resonator. In this system, plasma is generated between the tip of the electrode and the surface of water.

Similar to the improvements done by Fridman et al. to create plasma in a DBD system by a single electrode (FEDBD) [111], the main enhancement in the FESCD is to generate a streamer discharge from a single electrode. Figure 2.9 illustrates the general form of the FESCD system schematically. The main component of the FESCD system is the application of the helical resonator. Before discussing the working principles of the FESCD method, we will compare the above-mentioned plasma generation technique. Especial comparison will be made between FESCD and SCD to outline the advantages of the FESCD method.

2.2.6. Plasma-based systems comparison matrix

In order to compare the plasma generation techniques discussed in the chapter, all of the main characteristics of each setup is summarized in the Table 2.1.

Table 2.1. Comparison between various plasma generation techniques in terms of their main features.

	Input Waveform	Electrode Configuration	Treatment Substrate	Treatment Mode	Gas Flow Requirement	Power Consumption
Floating Electrode Streamer Corona Discharge	AC	Single Electrode	Gas, Liquid, Solid (soil, non-metallic, etc.)	Direct	NO Flow	10-15 W
Streamer Corona Discharge	Pulse	Two Electrodes	Gas, Liquid	Indirect	NO Flow	Liquid Discharge: 60-120W Gas Discharge: 20-30 W
Dielectric Barrier Discharge	Pulse/AC	Two Electrodes	Gas, Liquid	Indirect	NO Flow	>30 W
Floating Electrode Dielectric Barrier Discharge	Pulse/AC	Single Electrode	Gas, Liquid, Solid (soil, non-metallic, etc.)	Direct	NO Flow	5-10 W
Gliding Arc Discharge	DC/AC/ Pulse	Two Electrodes	Gas, Liquid, Solid (soil, non-metallic, etc.)	Direct	0.5-6 l/min	500-900 W

Based on the information given by Table 2.1, five main factors can be used to compare various plasma generation techniques. These factors are discussed in the next four sections.

2.2.6.1. Input waveform

In general, three waveforms can be used to create plasma, depending on the plasma generation technique. These are direct current (DC), alternating current (AC) and pulsed. The use of pulsed voltages for the creation of plasma in SCD is inevitable. This is due to the quick transition of the discharge type from streamer mode to arc mode, if pulsed voltages are not used. In general, arcing is not desirable in almost all of the industrial applications since it can damage the electrical components of the system heavily. One desirable application of the arcs is in GAD, as discussed in the section 2.2.3; however, there are disadvantages associated with this technique, which will be addressed in the sections 2.2.6.4 and 2.2.6.5. In the case of DBD, FEDBD and GAD, although pulsed voltages have been used in most of the proposed systems, the use of AC waveform and DC voltages (in the case of GAD) has been proposed. In order to create plasma with a pulsed waveform, these requirements should be considered:

- a) A high voltage pulse with amplitude of 10-20 kV is required.
- b) The duration of the pulse should be very short (100-300 ns).
- c) The pulse rise rate should be very high (0.5-3 kV/ns).

This means that complex circuitry should be used to satisfy all of the above-mentioned requirements. Although these circuitries are available, upscaling of the treatment system is an issue due to the high demand of electronics of large pulse power supplies. This means that the

application of simple waveforms such as AC and DC is favorable. From this point of view, generation of plasma by SCD is inferior to other methods in which AC waveform is used.

2.2.6.2. Electrode configuration

The only two techniques that do not require the use of two electrodes (one HV electrode and one ground electrode) are FESCD and FEDBD. These techniques use the treatment substrate as the floating electrode to create the plasma. The advantage of using only one electrode is the significant increase in the flexibility and feasibility of the treatment system. The effect of this flexibility will be further discussed later.

A more specific comparison can be made between FESCD and SCD where the former can be considered as the improvement to the latter. The use of the two-electrode system in SCD means that the ground electrode is always placed in the liquid (when water treatment is the goal). This raises the concern regarding the corrosion of the ground electrode in real life applications. Furthermore, previous studies showed that in the case of SCD, the distance between the HV electrode and ground electrode should be controlled precisely. This is due to the fact that the type of the discharge is dependent on the inter-electrode distance and it can change from a streamer discharge type to an arc discharge type [123,124]. As mentioned before, this transformation to arc discharge is mostly undesirable.

Based on the above-mentioned discussions, FESCD and FEDBD are superior to other methods in terms of the advantages resulting from the single electrode configuration.

2.2.6.3. Gas flow requirement

Except for GAD, none of the techniques discussed require gas flow for treatment. As mentioned in section 2.2.3, GAD works based on the formation of arc discharge between two diverging electrode. The discharge is then blown to the surface of the substrate to be treated (flow rates of 0.5-6 l/min have been used). This creates extra complexity in the treatment system since extra instrumentations are needed for controlling the flow of the gas. This is one of the main disadvantages of GAD in comparison with other above-mentioned methods.

2.2.6.4. Power consumption

As shown in the comparison Table 2.1, FESCD consumes 10-15 W of power, which is similar if not lower compared to the power consumption of SCD, DBD and FEDBD. The power consumption of the GAD technique is much higher than the others since it works based on the creation of arcs, which only occurs at high input voltages and currents, i.e. high power consumptions. This is another main drawback of GAD technique for treatment purposes. Before drawing a conclusion, one point should be addressed; the power consumptions mentioned in the comparison table only include systems from literature in which the contaminated water is stationary. More complex systems can be found in literature in which water is circulated between the reaction chamber and a reservoir, water is flown on the surface of the electrode in the shape of a thin layer (such as DBD with falling liquid film or wetted-wall corona), the gaseous media around the discharge is bubbled into the liquid, etc. Although these complexities can increase the efficiency, they require additional power consumption for controlling the flow of water or gas. These power consumptions may or may not be included in the values found in literature. As a result, we excluded these studies from our considerations.

Based on the discussions provided, one can conclude that Floating Electrode Streamer Corona Discharge (FESCD) is a superior technique for treatment of various substrates. It combines the flexibility and feasibility for real life applications, low electronic demand due to the use of a simple AC waveform, direct treatment of substrates (especially solid substrates such as contaminated soils and surfaces) and low power consumption. The only current drawback is the low contact area of plasma with substrate and therefore the low treatable volume in case of liquid substrates. Strategies to increase the number of HV electrodes can be used to increase the plasma contact area and subsequently the treatable liquid volume.

2.2.7. FESCD working principles

As described in section 2.2.6.1 to section 2.2.6.5, the FESCD system has three important advantages, i.e. single electrode plasma generation, low power consumption and the ability to use AC waveform (when compared to the SCD method). These advantages stem from the working principles of the FESCD technique.

One of the main advantages of the technique proposed in this research when compared to its previous counterpart methods [42,120,123,125,126] is the capability of generating plasma (streamer discharge) by using only one electrode. This ability not only solves challenges regarding the role of the submerged grounded electrode in water (as discussed in section 2.2.6.2), but also opens up new opportunities for diverse applications. As discussed explicitly in the previous study by Van Neste et al. [127], the helical resonator completes its circuit with the stray capacitance of its surrounding environment. This eliminates the need for a physical return cable (or a ground electrode in this case).

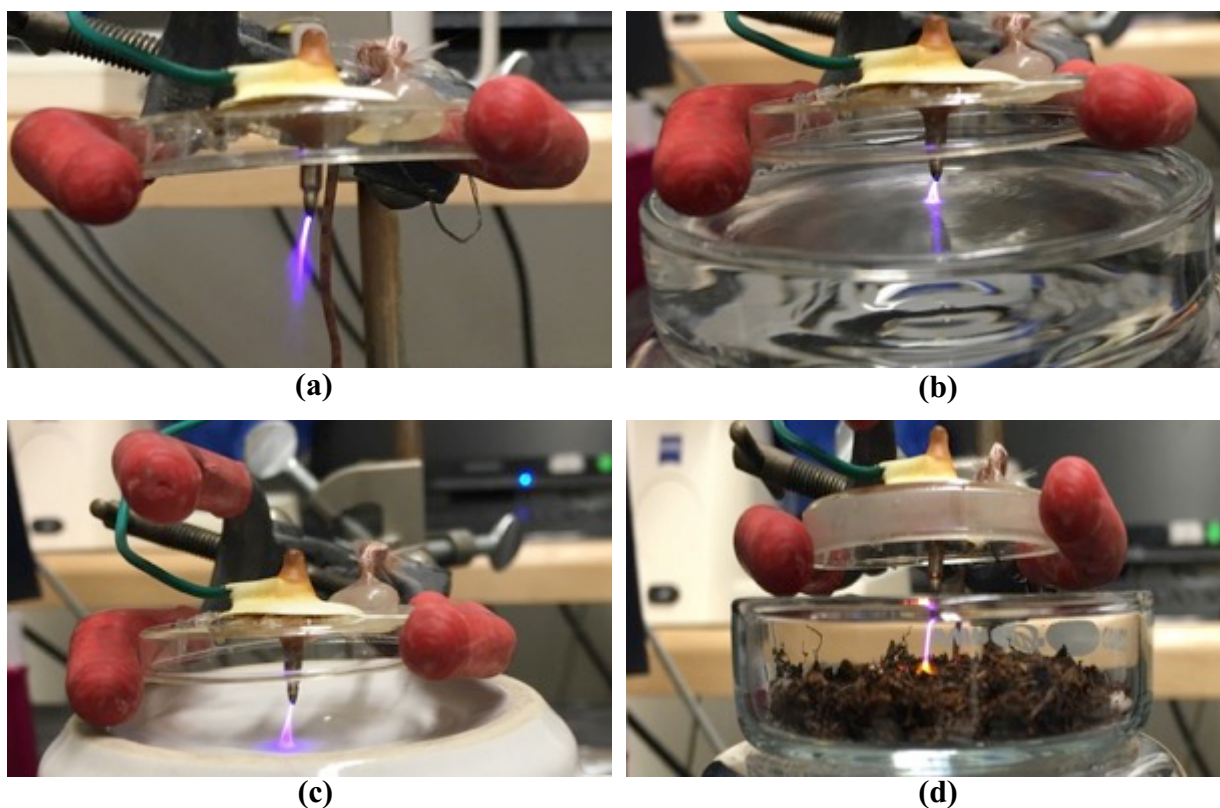


Figure 2.10. The versatility of the proposed technique for diverse applications is shown. Various hypothetical scenarios include (a) removal of pollutants from air (b) decontamination of water by injecting plasma from the surface (c) inactivation of microorganisms on the surfaces (coffee mug is used as a model surface) and (d) removal of contaminants from soil.

This also means that when a high enough voltage is applied to the Pt/Ir electrode, it uses the air around it as a virtual secondary electrode (held at a floating potential) and creates plasma in this space. Using such a technique, one can create plasma with appreciable size in air (Figure 2.10(a)). This can possibly be used for removal of pollutants from air (for instance VOC abatement). If a dielectric object such as water, ceramic tile or soil is kept close enough to the electrode with a sufficient driving waveform to the resonator, plasma will be created between the tip of the electrode and the surface of the object (Figure 2.10(b), (c) and (d)). This can be used for the removal of contaminants from water, inactivating organisms such as bacteria on the

surfaces and decontaminating soil. Similarly, plasma jets [128] and GAD method (as described in section 2.2.3) [79,101] have been developed to eliminate the need for a submerged electrode in water. These technologies are also able to create plasma in the gas phase; however, a flow of gas (1-4 l/min) is required to direct the plasma to the surface being treated. This requirement is not necessary in the technology proposed in this study.

The second important feature that should be discussed is the ability to use low input voltages (less than 100 V). In the previous study, Van Neste et al. elaborated the fundamental working principles of the helical resonators [127]. In general, in a normal transmission line, the output electric field as a function of the position on the line (d) can be expressed by:

$$E_{out} = E_{in} \exp [j(\gamma d + \omega t)] \quad (2.19)$$

in which γ denotes the propagation constant and can be defined as $\gamma = \alpha + j\beta$. α and β are known as the attenuation factor and the phase constant, respectively. Moreover, ω is the angular frequency of the wave being propagated. However, in the special case of the standing wave propagating along a helical resonator, the phase constant (β) is a function of the position (d), as discussed explicitly by Van Neste et al [127]. This means that γ is not constant anymore. As a result, the electric field build-up along the length of the helical resonator is governed by:

$$|E_i| = (|E_{i-1}| + E_0 e^{j|\alpha_i + j\beta_i|d_i}) \cdot e^{j\omega t}, \quad \forall i = [1, N] \quad (2.20)$$

in which N represents the total number of the turns in the helical resonator. The direct consequence of this electric field build-up in a helical resonator (Equation (2.19) vs. Equation (2.20)) is the achievable field amplification factor. In a traditional transmission line a maximum field amplification of 2 or 2.5092 can be achieved (assuming the perfect reflection of the wave from the terminal end); however, the field (or voltage) amplification of 100 times can be

obtained at the terminal end of a helical resonator [127]. More detailed discussions and analysis can be found in the work of Van Neste et al. [127].

The final feature of the proposed method is the capability of plasma generation (streamer discharge) using a simple AC waveform instead of commonly used pulsed waveforms (in SCD). It has to be mentioned that the resonance frequency of the helical resonator used in this study is about 2 MHz. The equivalent of this value in the time domain (inverse of frequency) is 500 ns, which is the duration in which both polarities (negative and positive) of the AC voltage are applied to the electrode. In each half cycle (250 ns), electron avalanches and the subsequent streamers propagate in the opposite direction of the electric field. As the polarity changes, the direction of streamer propagation changes as well. It takes about 100-300 ns for the initiation of electron avalanches, the transition to streamer discharge and the propagation of streamers (i.e. prior to transition to spark), depending on the velocity of the streamers. Since the AC waveform used in this study has a half cycle of 250 ns, it can be qualitatively concluded that the use of a helical resonator with a resonance frequency of approximately 2 MHz can create stable plasma without any transitioning from streamer discharge to spark discharge.

Chapter 3: Effect of physiochemical parameters

In Chapter 2, various physical and chemical phenomena that are involved in the plasma treatment of contaminated water were introduced. In this chapter, the effects of these processes on the efficiency of our plasma treatment method are explained experimentally. Before providing the discussions regarding the obtained results, an introduction will be given and the goals of this chapter will be outlined. Afterwards, the detailed experimental procedure will be discussed. Finally the obtained results and their correlation to the fundamental physical and chemical phenomena will be explored.

3.1. Introduction

As discussed in Chapter 2, the plasma treatment process introduced in this work involves the production of plasma in air and its subsequent injection to the surface of water. In such a process, both physical aspects of the plasma generation and chemical aspects of various oxidizing agents created in the plasma are important. These parameters can alter the efficiency of the degradation of contaminants in water. The most important physical phenomenon that initiates the plasma formation is the electron avalanche. This phenomenon is described by the Townsend mechanism of breakdown, as explained in section 2.1.2.1. An examination of the governing equations (Equations (2.1) to (2.7)) reveals that the two most crucial parameters that can control the breakdown process are the applied voltage between the electrodes and the inter-electrode distance (air gap distance). This is due to the fact that both parameters are involved in defining the electric field present in the gap (Equation (2.1)). This electric field determines the energy acquired by the electrons between two successive collisions. Moreover, the number of electrons multiplied in the gap between two electrodes depends on the gap distance and the Townsend

ionization coefficient (α). This coefficient by itself depends on the electric field. These correlations will be explained in details in section 3.4. The investigations into the effect of the applied voltage and the gap distance not only do provide fundamental understandings of the process, but also set the operational parameters for the rest of the experiments that follow.

The chemistry of plasma produced in air was discussed in section 2.1.2.3; various oxidizing agents produced either in air or at the air/water interface were introduced. Many researchers have studied the role of the atmosphere in which the plasma is generated [88,90,124,129,130]. Atmospheres containing pure oxygen, nitrogen and argon or the mixtures of these gases have been used. The main goals of this type of experiments are to understand the role of different oxidizing agents created in various atmospheres and also to realize the optimum atmosphere in which the degradation of contaminants is at its maximum. Although this type of studies can bear valuable information, the use of other atmospheres other than air for practical water treatment processes is not feasible. The other aspect of plasma chemistry that can be more crucial is various chemical phenomena occur in water due to different ionic species present. In general, different ionic species with various concentrations can be present in wastewater [131]. Chloride (Cl^-), sulfate (SO_4^{2-}), carbonate (CO_3^{2-}), phosphate (PO_4^{3-}), ferrous (Fe^{2+}) and ferric (Fe^{3+}) ions are amongst the most important ionic constituents in water that can influence the outcome of a plasma-based treatment process. Moreover, the initial pH of the solution under treatment can play a crucial role.

Perhaps, one of the most studied ionic constituents in the area of AOPs is chloride ion (Cl^-). The effect of chloride ion (Cl^-) on the removal efficiency of various AOP treatment systems, including plasma-based methods [132–137] and UV and UV/ H_2O_2 based treatments [138,139] has been investigated previously. In general, the scavenging properties of Cl^- towards OH^\cdot is well

accepted [138–143]. However, conflicting results regarding the effect of Cl^- on the contamination removal efficiency have been reported. Researchers such as Pignatello et al. and Kiwi et al. point towards the inhibitory role of Cl^- [40,144–146]. In other words, the presence of Cl^- reduces the degradation capability of the AOP system studied. This phenomenon is attributed to the scavenging properties of Cl^- towards OH^\cdot . As a result, various chlorine-based active species including chlorine radical anions ($\text{Cl}_2^{\cdot-}$) are formed. These newly formed species are less active and are not as powerful as OH^\cdot . On the other hand, Liang et al. observed that the presence of Cl^- in the solution can promote the degradation of contaminants [147]. This discrepancy can be associated with the nature of the contaminations and the concentration of Cl^- . As described by Yang et al., halogen radicals such as $\text{Cl}_2^{\cdot-}$ are more selective than OH^\cdot in reacting with electron-rich organic molecules. Moreover, during the degradation of a textile azo dyestuff (R3BS), Ramjaun et al. observed that removal efficiency depends on the concentration of Cl^- . For $[\text{Cl}^-] < 0.01 \text{ M}$, removal efficiency of the dye decreased; however, higher concentrations of Cl^- helped the decontamination process [135].

Similar to the case of Cl^- ions, the presence of any other ionic species in water can act as hydroxyl scavengers. Phosphate (PO_4^{3-}) and carbonate (CO_3^{2-}) ions are known as the most efficient hydroxyl radical scavengers. The presence of these ions in water can reduce the efficiency of the treatment process to degrade contaminants [147]. Since in a plasma treatment process in air, hydrogen peroxide can be introduced to the solution, Fenton reactions are expected to occur if water contains ferrous and ferric ions [42,44,148]. Finally, sulfate ions (SO_4^{2-}) can scavenge hydroxyl radicals in the aqueous phase and form sulfate radicals ($\text{SO}_4^{\cdot-}$). These radicals can also cause the oxidation of organic contaminants but they are less active than

hydroxyl radicals [149]. The role of these ions in our plasma treatment system will be experimentally studied in section 3.5.

The effect of pH on the contamination degradation is also dependent on the nature of the contamination [85]. While the removal of contaminants such as methylene blue is promoted in acidic conditions [150], removal of phenol is faster in alkaline conditions [81,85]. Various lines of reasoning have been used to justify the effect of the pH of the solution. These include the acid-based equilibrium of dye molecules [81,85], the effect of alkaline conditions on OH⁻, etc. [85,123,125,135]. The effect of the solution initial pH will be experimentally discussed in section 3.5.

3.2. Objectives

Based on the introduction given in section 3.1, the following goals were set for understanding various physical phenomena governing the process:

- 1) Investigate the effect of the operational parameters, i.e. the air gap distance, the applied voltage and the plasma injection period
- 2) Outline the physical phenomenon connecting the obtained results to the above-mentioned operational parameters
- 3) Realize the optimum operational parameters to be used in the next parts of this study

The following aims were set to understand the fundamental chemistry involved in the treatment process:

- 1) Examine the role of Cl⁻ in the treatment stage (presence of plasma) and post treatment stage (absence of plasma) separately

- 2) Propose a chemical mechanism by which Cl^- ions are involved in the process and prove it by means of analytical methods
- 3) Investigate the role of other ionic species on the treatment process
- 4) Study the effect of the solution initial pH
- 5) Examine the effect of various concentrations of the contaminant in water

3.3. Experimental

3.3.1. Materials

Methylene blue (MB) (obtained from Sigma Aldrich Ontario, Canada) was the target contaminant used throughout this study due to its ease of quantification through optical methods. During the examination of operational parameter, water samples created for treatment were prepared by dissolving 100 mg/l of NaCl and 0.75 mg/l of MB in MilliQ water. This resulted in an initial solution conductivity of 1.87 ± 0.02 mS/cm.

In order to study the effect of Cl^- concentration, sodium chloride (NaCl, certified ACS crystalline supplied by Fisher Scientific of Ontario, Canada) was added to MilliQ water. Various concentrations of Cl^- used in this study include 0, 10, 50, 100, 150 and 250 mg/l. The above-mentioned chemicals were applied without further purification. The water samples created for treatment were prepared by dissolving the above-mentioned concentrations of NaCl and 0.75 mg/l of MB in MilliQ water. To examine the effect of other ionic species on the treatment process, 0.85 mM of sodium chloride (NaCl), sodium phosphate (Na_3PO_4), sodium carbonate (Na_2CO_3), sodium thiosulfate ($\text{Na}_2\text{S}_2\text{O}_3$) and sodium sulfate (Na_2SO_4) were added to MilliQ

water in separate experiments. All of the above-mentioned chemicals were supplied by Fisher Scientific (Ontario, Canada).

In order to investigate the effect of the initial pH of the solution, the concentration of NaCl and MB were fixed at 50 mg/l and 0.75 mg/l, respectively. The initial pH of the solution was adjusted by adding sufficient amount of HCl or NaOH (0.1 M). Three initial pH values of 2.8, 6.4 and 10.12 were used in this study, representing the initial acidic, near neutral and alkaline conditions, respectively.

Finally, to investigate the effect of the initial MB concentration, five concentrations of 0.75, 1.25, 2, 3 and 3.75 mg/l were tested; the concentration of NaCl and the initial pH of the solution were fixed at 50 mg/l and 6.4, respectively. It has to be mentioned that higher concentrations of MB create highly opaque solutions where accurate in-situ optical measurement (see section 3.3.2) of the concentration is not possible.

3.3.2. Experimental setup and procedure

Figure 3.1 shows the schematic illustration of the experimental setup. To generate plasma from a single electrode, a sinusoidal wave at the resonance frequency of the helical resonator (1.7-1.8 MHz) is supplied by the function generator (Agilent 33522A, CA, USA) and fed to a power amplifier (2100L RF power amplifier, E&I Inc., NY, USA). More information on the working principles of the helical resonator is given section 2.2.7 and can be found in the previous publication [127]. The output of the power amplifier is used as the input for the helical resonator. The input voltage and current to the helical resonator are measured by means of an oscilloscope (TDS 2024C, Tektronix, OR, USA) and a current probe (CT2, Tektronix, OR, USA) connected to the oscilloscope, respectively (as shown in Figure 3.1).

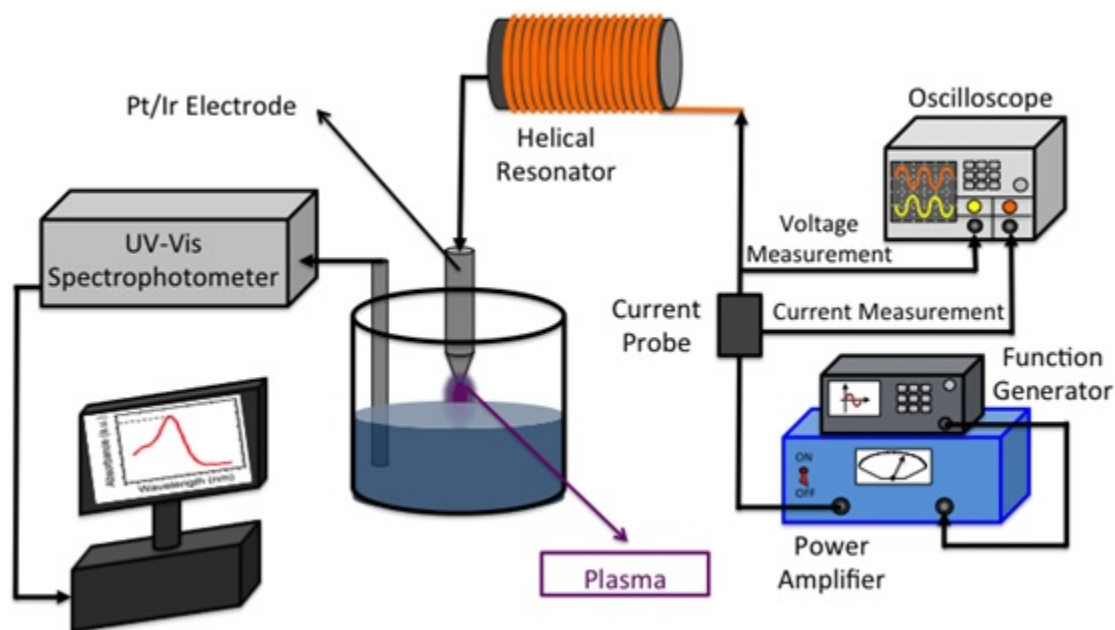


Figure 3.1. The schematic of the experimental setup used in this study is illustrated. A sinusoidal wave is supplied to the power amplifier by the function generator. The output of the power amplifier is directly connected to the helical resonator. The input voltage and current to the resonator are monitored by an oscilloscope. The concentration of the MB in the solution is measured by a UV-Vis spectrophotometer equipped with an optic fiber probe for in-situ measurements. Magnetic stirring of the solution is used to ensure the homogeneity of the concentration during all experiments.

The power input to the helical resonator was calculated using the multiplication of V_{rms} and I_{rms} (rms values of input voltage and current) with their corresponding phase angle (which was zero degrees when tuned to resonance [127] and producing plasma). 45±1 ml of the solution was poured into a glass beaker (50 ml, Fisher Scientific, Ontario, Canada) in each test. Table 3.1 summarizes the parameters used in each study.

Table 3.1. Summary of the parameters used in each study.

	Studied parameter	variable parameter	Fixed parameters
Physical	Air gap distance	Air gap distances of 2, 6 and 10 mm	[NaCl]=100 mg/l, [MB]=0.75 mg/l, plasma injection period of 10 min, input voltage of 68 V
	Input voltage of helical resonator	Input voltages of 38, 53, 68, 83 and 98 V	[NaCl]=100 mg/l, [MB]=0.75 mg/l, plasma injection period of 10 min, air gap distance of 2 mm
	Plasma injection period	Periods of 5, 10, 15, 20 and 25 min	[NaCl]=100 mg/l, [MB]=0.75 mg/l, input voltage of 83 V, air gap distance of 2 mm
Chemical	Chloride ions (Cl ⁻)	[Cl ⁻]=0, 10, 50, 100, 150 and 250 mg/l	[MB]=0.75 mg/l, input voltage of 70 V, air gap distance of 2 mm, plasma injection period of 15 min
	Other ionic species	0.85 mM of various ions	
	Initial pH	pH= 2.8, 6.4 and 10.12	
	Initial concentration of MB	[MB]=0.75, 1.25, 2, 3 and 3.75 mg/l	

The optical spectrum of MB at the beginning of experiments is shown in Figure 3.2(a) with a wavelength range of 200-800 nm. Normally, the peak absorbance (at 667 nm) is used as an indication for the concentration of MB. To obtain a calibration curve for MB (Figure 3.2(b)), different solutions containing various concentrations of MB were made and the change in the absorbance as a function of MB concentration was monitored. The linear relation between absorbance at 667 nm and MB concentration obtained by this calibration curve is used

throughout this study, to calculate the changing concentration of MB (during and after treatment stages). Moreover, removal percentage (removal%) is calculated by Equation (3.1) as follows:

$$\text{Removal\%} = \left(1 - \frac{C}{C_0}\right) \times 100 \quad (3.1)$$

In Equation (3.1), C and C_0 denote the concentration of MB at any point in time during the experiment, and the initial concentration of MB, respectively. From Removal%, one may calculate the energy yield of the process, as shown by Equation (3.2) [7].

$$\text{EnergyYield} = \frac{C_0 \times V \times R}{P \times t} \times 0.01 \quad (3.2)$$

in which C_0 is the initial concentration of MB (in g/l), V is the volume of the treated solution (in l), R is the final value of removal% (in percentage) obtained in each experiment at 60 min, P is the power supplied to the system in (kW) and t is the duration in which power is used (in hr).

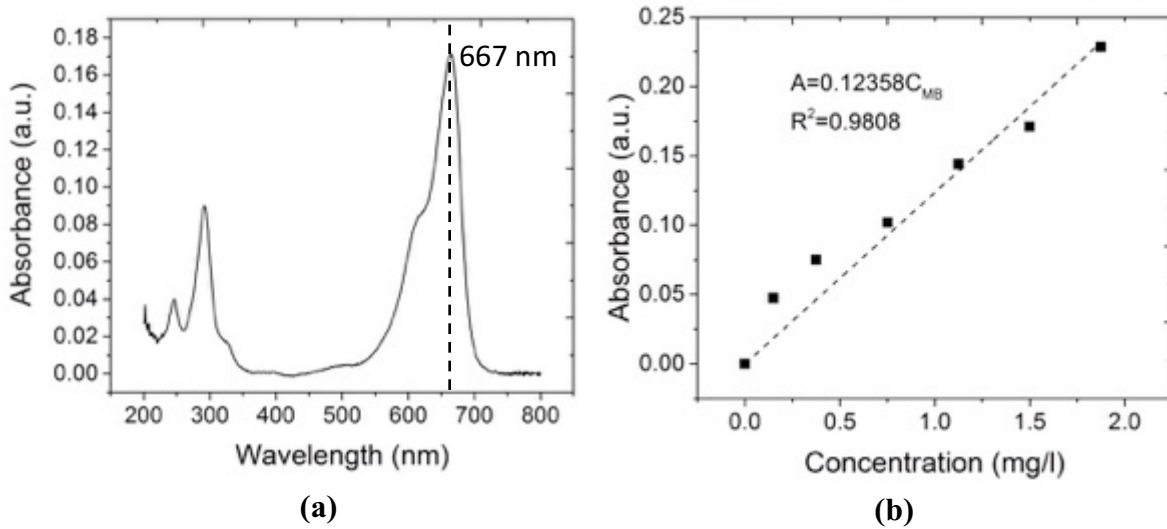


Figure 3.2. (a) Optical spectrum of methylene blue obtained in this study. The peak absorbance at 667 nm is used as a measure for concentration of methylene blue in the solution. (b) Calibration curve achieved in this study, based on the optical absorption at 667 nm for various concentrations of methylene blue.

The energy yield estimates the amount of the contamination removed from the solution (in grams) per unit of energy consumed during the treatment (in kWh). Calculated values of removal% and energy yield form the basis of the comparison between different parameters investigated in this study. Magnetic stirring of the solution was employed to assure the homogeneity of the solution and correct measurement of the optical spectrum. Each experiment was done in triplicate to ensure the repeatability of the treatment process. Conductivity and pH values of the solutions were measured using a Fisher Scientific Accumet® Excel conductivity meter (XL60, Ontario, Canada) and a Mettler Toledo FiveEasy® pH meter equipped with InLab® Expert Pro-ISM probe (Ohio, US), respectively.

3.3.3. Analytical characterization

In order to characterize the treated and untreated solutions in terms of their inorganic and organic constituents, Ion Chromatography (IC) and Mass Spectrometry (MS) analysis were used, respectively. In each analysis, two sets of samples were prepared. In the first set, MilliQ water was used as the water matrix. The second set of samples was prepared by adding NaCl (50 mg/l) to MilliQ water as the water matrix. In both sets, the concentration of MB was fixed at 0.75 mg/l. IC analysis was performed using Dionex Ion Chromatography (DX 600, CA, USA) instrument with an injection loop volume of 25 µl. Sodium carbonate (Na₂CO₃) solution with a concentration of 9 mM was used as the eluent. Calibration standards were prepared in-house, and the calibration was verified using an external reference solution purchased from SCP Science (Quebec, Canada).

RP-HPLC-MS was performed using an Agilent 1200 SL HPLC system. Chromatographic separation was obtained using a Kinetex EVO C18 column with guard (Phenomenex, 2.1 mm

internal diameter, 50 mm length, 1.6 μm particle size) at 40 °C. The buffer gradient system composed of 0.1% formic acid in water as mobile phase A and 0.1% formic acid in acetonitrile (ACN) as mobile phase B. Samples were loaded onto the column at a flow rate of 0.5 ml/min and an initial buffer composition of 98% mobile phase A and 2% mobile phase B. After injection, the column was washed using the initial loading conditions for 1 min followed by elution of the analytes by using a linear gradient in the form of: 2% to 40% mobile phase B over a period of 6 min, 40% to 98% mobile phase B over a period of 3 min, held at 98% mobile phase B for 4 min to remove all analytes from the column and back to 2% mobile phase B over 1 min. Mass spectra were acquired in positive mode of ionization using an Agilent 6220 Accurate-Mass TOF HPLC-MS system (Santa Clara, CA, USA) equipped with a dual sprayer electrospray ionization source with the second sprayer providing a reference mass solution. Mass spectrometric conditions were: drying gas 9 l/min at 300 °C, nebulizer pressure 20 psi, mass range 100-1000 Da, acquisition rate of ~ 1.03 spectra/s, fragmentor voltage of 175 V, skimmer voltage of 65 V and capillary voltage of 3500V. Mass correction was performed for every individual spectrum using peaks at m/z 121.0509 and 922.0098 from the reference solution. Data acquisition was performed using the Mass Hunter software package (ver. B.04.00.). Analysis of the HPLC-MS data was done using the Agilent Mass Hunter Qualitative Analysis software (ver. B.07.00).

3.4. Role of physical parameters

As discussed in section 3.1, three physical (operational) parameters are very important in any plasma-based water treatment process. These parameters are the air gap distance, the input voltage and the plasma injection period. In this section, the effect of these parameters on the degradation of MB in water will be examined.

3.4.1. Effect of air gap distance

As mentioned in section 2.2.7, the technique described here uses only a single electrode to generate plasma (with water playing the role of a floating electrode). The distance between the tip of the electrode and surface of the water plays an important role, as it defines the electric field present in the air gap between the two. In this investigation, three distances of 2 mm, 6 mm and 10 mm were employed and their effect on removal%, energy yield, and solution temperature were studied. This is shown in Figure 3.3. The rms value of the input voltage and the plasma injection period (the time during which plasma was in contact with the solution) were kept constant at 68 V and 10 min, respectively. In each experiment, plasma was present during the first 10 min (treatment stage in Figure 3.3(a)) followed by a post treatment stage (for 50 min) in which plasma was extinguished. Three major points should be discussed, as reflected by Figure 3.3. These are:

- 1) Maximum overall removal% (at $t=60$ min) can be achieved with the air gap distance of 6 mm, as illustrated by Figure 3.3(a) and (b). Moreover, Figure 3.3(a) indicates that the highest contribution from the treatment stage can be achieved with the air gap distance of 6 mm.
- 2) As shown by Figure 3.3(a), when the air gap distance is fixed at its minimum (2 mm), the removal% continues to increase, even 50 min after the point that plasma is turned off. Moreover, as the air gap distance is increased to 6 mm and 10 mm, the change in the removal% during the post treatment stage becomes slower. At a distance of 10 mm, the change in removal% ends at $t=20$ min. In other words, the contribution of the post treatment stage is more significant at smaller air gap distances.

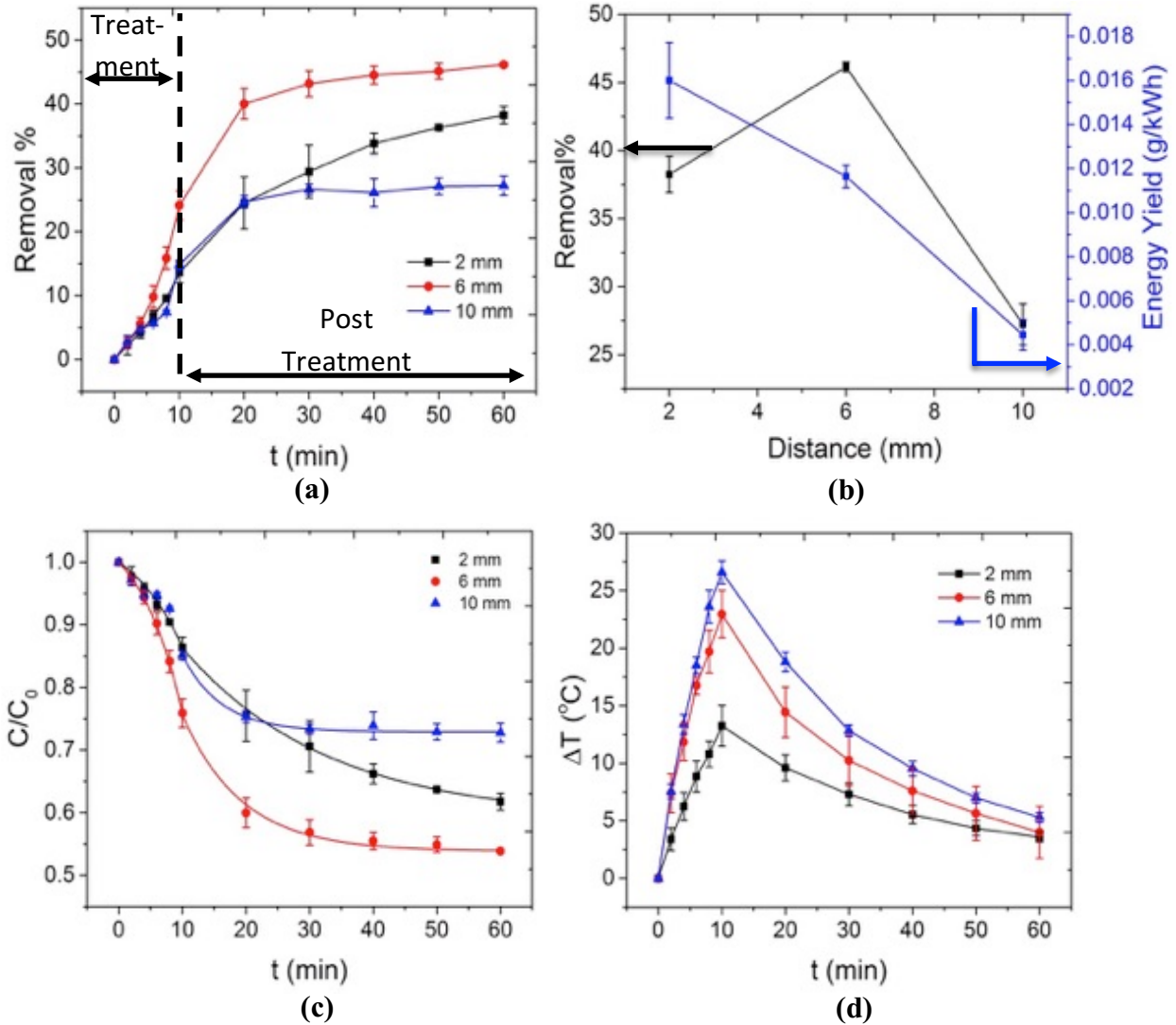


Figure 3.3. The effect of air gap distance on the decontamination process is studied at constant rms value of input voltage of 68 V and plasma injection time of 10 min. (a) Variation in removal% as a function of time for different air gap distances is shown. As the distance increases, the effect of oxidizing agents created by plasma lasts for a shorter period of time. While the removal still occurs at 60 min for $d=2$ mm, it stops at 20 min for $d=10$ mm. This phenomenon could be attributed to the higher energy of particles in plasma at lower distances due to the higher electric field. (b) Final Removal% (at $t=60$ min) and energy yield are compared for the various air gap distances used in this study. As it is shown, removal% has a maximum at $d=6$ mm, which is probably due to a larger volume of the ionized air on top of water. Furthermore, as the air gap distance increases from 6 mm to 10 mm, the removal% decreases significantly. This may be due to the instability of ozone molecules at high plasma powers and temperatures (c) The change in the normalized concentration as a function of time for different distances is used to study the kinetics of decontamination. (d) The temperature of the solution was monitored in the course of each experiment. The injection of plasma into the solution causes an increase in the temperature. As the distance was increased, the maximum temperature that the solution reached (approximately 47 °C for $d=10$ mm) also increased, due to a higher power of plasma.

3) Although the air gap distance of 6 mm results in the highest removal%, the energy yield of the system (calculated by Equation (3.2)) decreases with the increase in the air gap distance.

The dependency of the removal% during the treatment stage to the air gap distance can be explained by the underlying phenomena of plasma generation, i.e. electron avalanche. Electron avalanches are the building blocks of any plasma generation system. In general, in the presence of an intense electric field, primary electrons are accelerated. These energetic electrons can ionize gas molecules by means of inelastic collisions and create new electrons. Although the process of ionization by inelastic collisions is sophisticated, it can be expressed by Townsend mechanism of electrical breakdown, as described in section 2.1.2.1 [106].

$$n_e(x) = n_{e0} \exp [(\alpha_T - \beta_T)x] \quad (3.3)$$

In Equation (3.3), $n_e(x)$ and n_{e0} denote the density of electrons as a function of distance from the electrode and the initial density of primary electrons, respectively. α_T is the Townsend ionization coefficient and it shows the multiplication of electrons per unit length. It is expressed by [106]:

$$\frac{\alpha_T}{p} = A \exp\left(-\frac{B}{E/p}\right) \quad (3.4)$$

In Equation (3.4), A and B are constants that can be calculated numerically. Moreover, p refers to the gas pressure in which the discharge happens. Finally, the term β_T in Equation (3.3) is defined as the second Townsend coefficient; it describes the number of electrons lost to attachment processes (due to electronegative molecules such as oxygen) per unit length. The second Townsend coefficient becomes crucial at large gaps ($d > 5$ cm) and can be ignored here [106]. As the air gap increases, $n_e(d)$ (number of electron at a distance “d” from the electrode) also increases. This is due to the fact that the number of electrons generated due to the electron

avalanches has an exponential dependency to the distance, as shown by Equation (3.3). On the other hand, at a fixed applied voltage, the electric field reduces as the air gap increases. This can reflect itself in the Townsend ionization coefficient (α_T), as described by Equation (3.4). The reduction in the electric field can possibly lower the ionization coefficient. It can be hypothesized that when the air gap distance increases from 2 mm to 6 mm, the direct influence of parameter “d” on the $n_e(d)$ compensates for the effect of decreased electric field in α_T . As a result, the number of energetic particles, more specifically electrons that hit the surface of the water, increases. One of the most important consequences of the collision between electrons and water molecules is the formation of hydroxyl radicals. Hydroxyl radicals are one of the most powerful oxidizing agents (oxidation potential of 2.8 V) [85]. Their ability to degrade organic compounds such as dye molecules is well known [150,151]. Therefore, the removal% enhanced when the air gap distance was changed from 2 mm to 6 mm. The decrease in the removal% at d=10 mm is probably due to the dominant role of the lowered electric field in determination of $n_e(d)$. More importantly, our experiments show that while at d=2 mm the plasma is highly focused on the surface of water, at d=10 mm it barely reaches the surface and spreads in the air. This is shown in Figure 3.4. This lowers the probability of the injection of the energetic particles into the water surface. As a result, the lowest overall removal% was obtained for the air gap distance of 10 mm, as shown by Figure 3.3(b).

The effect of the air gap distance on the removal% during the post treatment stage also shows an interesting trend. As shown in Figure 3.3(a), as the air gap distance increases, the ability of the treatment system to remove MB during the post treatment stage is lowered. In other words, the change in the removal% as a function of time becomes less significant for d=6 mm and d=10 mm.

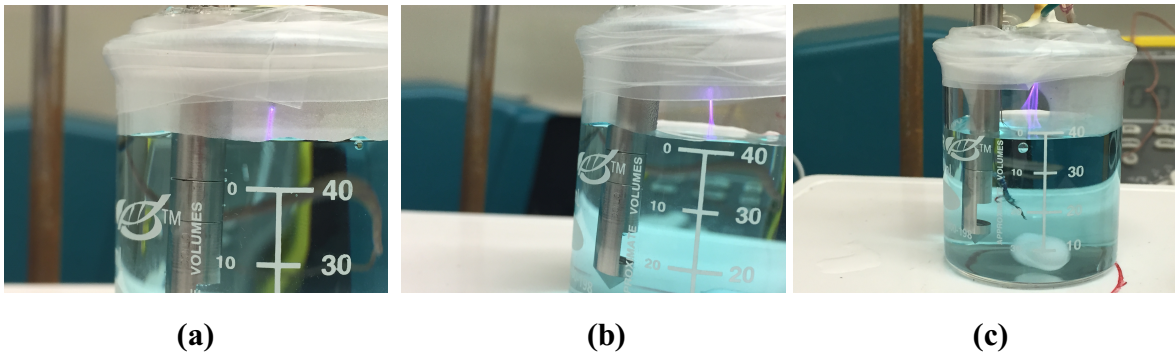


Figure 3.4. Images of plasma on top of the solution taken for various air gap distances of (a) 2 mm, (b) 6 mm and (c) 10 mm. When the air gap distance is increased to 6 mm, the volume of the plasma increased. Therefore, more ionized gas could reach the surface of water. This could be the reason behind the increased removal% when air gap distance was increased to 6 mm. Further increase in the distance resulted in a significant decrease in removal%. This could be partly due to lower injection probability of plasma to the surface of water, as shown by (c). At air gap distance of 10 mm, frequent injection of plasma to the surrounding air could be observed.

As mentioned in section 2.1.2.3, the role of nitrogen-based compounds such as peroxyxynitrite in the post treatment stage, for air plasma, has been established [94,100–103,113]. Moreover, generation of ozone, as a strong oxidizing agent (oxidation potential of 2.07 V) [85], in the plasma has been studied [84,104]. The effect of the air gap distance on the post treatment behavior of the system can be explained based on the presence of ozone in the solution. Any possible reason that lowers the concentration of ozone in the liquid phase can affect the removal% during the post treatment stage. There are three major factors that can alter the concentration of ozone in water. These are:

1) As shown in Figure 3.3(d), the increase in the solution temperature for air gap distances of 6 and 10 mm is more significant than the air gap distance of 2 mm. While the solution temperature reached a maximum of 32 °C for $d=2$ mm, maximum temperatures of 42 °C and 47 °C were obtained for $d=6$ mm and $d=10$ mm, respectively. Previous studies have been performed to understand the kinetic of ozone decomposition, under various conditions [152–155]. Although different decomposition rates have been proposed for ozone, possibly due to the different

parameters involved in these studies, one key feature emerges. This is the fact that the decomposition rate is inversely and exponentially related to the solution temperature. In other words, the thermal decomposition of ozone occurs faster when the solution temperature increases. The effective application of ozone for decontamination purposes in water is not possible for solution temperatures higher than 40-45 °C. This is due to the very short half-life of ozone in these temperatures [156,157].

2) Another consequence of the increase in the solution temperature is lower solubility of ozone in water [158]. Therefore, it is expected that as the maximum solution temperature increases (due to the higher air gap distance), lower concentration of ozone can dissolve in the solution.

3) Finally, the presence of water molecules in the gas environment can be detrimental to the produced ozone by plasma. The dissociation of water molecules in the gas phase by collision with energetic electrons yields OH· and H· radicals, as explained in section 2.1.2.3. These radicals can react with ozone molecules (Equations (3.5) to (3.7)) in the gas phase and prevent their sufficient introduction to the solution [84].



As mentioned previously, the increase in the air gap distance can enhance the electron avalanche processes (Equation (3.3)). This means that the probability of formation of OH· and H· radicals in the gas phase increases. As a result, it can be expected that the concentration of ozone in the gas phase decrease as larger air gap distances are used.

The combination of the all of the above-mentioned rationales can possibly explain the lower removal% during the post treatment stage for $d= 6$ mm and $d= 10$ mm. Finally, as shown by Figure 3.3(b), the energy yield of the system deteriorates with increase in the air gap distance. This is due to the fact that more power is consumed by the plasma at higher distances (power consumption of 5.1 ± 1.5 , 9 ± 2 and 14.8 ± 1.9 W for air gap distances of 2, 6 and 10 mm, respectively). As shown by Equation (3.2), the energy yield changes inversely with respect to the input power. As the air gap increases, the flow of charged particles experiences less resistance, due to the greater probability of electron avalanches. Consequently, input current supplied by the power amplifier increases because of the perceived reduction in the total system load resistance.

The kinetics of decontamination were investigated as shown in Figure 3.3(c). Regardless of the air gap distance, the whole decontamination process followed the pseudo-first-order kinetics in the form of:

$$\ln\left(\frac{C}{C_0}\right) = -kt \quad (3.8)$$

in which k signifies the reaction rate (in min^{-1}). The minus sign in Equation (3.8) shows the decrease in the contamination concentration as a function of time.

Based on the above-mentioned arguments, the air gap distance of 2 mm was chosen for the rest of the experiments since not only does it provide a longer decontamination period during the post treatment stage, but also consumes the lowest energy while having the highest energy yield. Additionally, the increase in the solution temperature from room temperature (20°C) is minimal (increase of $10\text{-}15^\circ\text{C}$).

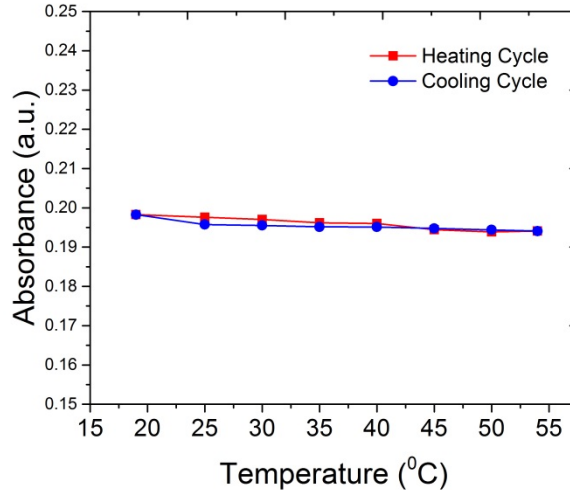


Figure 3.5. The effect of temperature on the absorbance of the solution is studied. For both heating and cooling cycles, there is no significant change in the peak absorbance of methylene blue at 667 nm. This in turn proves that the change in the absorbance observed during the plasma treatment in this study is solely due to the removal of methylene blue.

As a control experiment, the solution was heated to various temperatures using a hot plate and the peak absorbance of MB at 667 nm was monitored (Figure 3.5). It was revealed that the increase in the solution temperature has no effect in the peak absorbance of MB. We can conclude that the variation of this absorbance during non-thermal plasma treatment of the solution was solely due to the decontamination process and not thermal degradation.

3.4.2. Effect of input voltage of helical resonator

As mentioned in section 3.3.2, the main component of the treatment process is the helical resonator that generates atmospheric pressure plasma in air. As a result, the input voltage to the helical resonator may be crucial in optimizing the decontamination process in terms of removal% and energy yield. In this study, five input voltages (with rms values of 38, 53, 68, 83 and 98 V)

were applied to the helical resonator. The air gap distance of 2 mm and the plasma injection period of 10 minutes were kept constant throughout each experiment. Based on the mentioned input voltages, it could be readily deduced that using the helical resonator for the generation of plasma requires much lower voltages when compared to traditional plasma generators, which need voltages in the range of 1-20 kV [29,150]. Since the helical resonator could act as a passive amplifier by itself (as discussed in section 2.2.7), low input voltages of less than 100 V are sufficient for plasma generation. Figure 3.6 shows the effect of various input voltages on the decontamination process. As indicated in Figure 3.6(a) and 3.6(b), increasing the input voltage increases the removal%; however, energy yield of the process does not increase accordingly for an input voltage higher than 83 V. The increase in the removal% can be explained based on the effect of the electric field on the electron avalanches. As indicated by Equation (3.4), the Townsend ionization coefficient (α_T) depends on the electric field present in the air gap. The increase in the applied voltage results in the higher electric field in the gap and subsequently higher ionization coefficient (α_T). Therefore, the density of electrons generated due to the electron avalanches increase, as expressed by Equation (3.3). This higher density of energetic electrons can increase the probability of the formation of active species such as hydroxyl radicals as they hit the water surface. Hence, removal% increases. On the other hand, higher density of energetic electrons (due to higher input voltage) in the air gap can cause faster destruction of ozone by production of more OH \cdot and H \cdot radicals in the gas phase (according to reactions (3.5)-(3.7)). However, our results show that regardless of the input voltage used, the effect of continued decontamination from activated species with a long lifetime (e.g. ozone) is still present in the post treatment stage (Figure 3.6(a)).

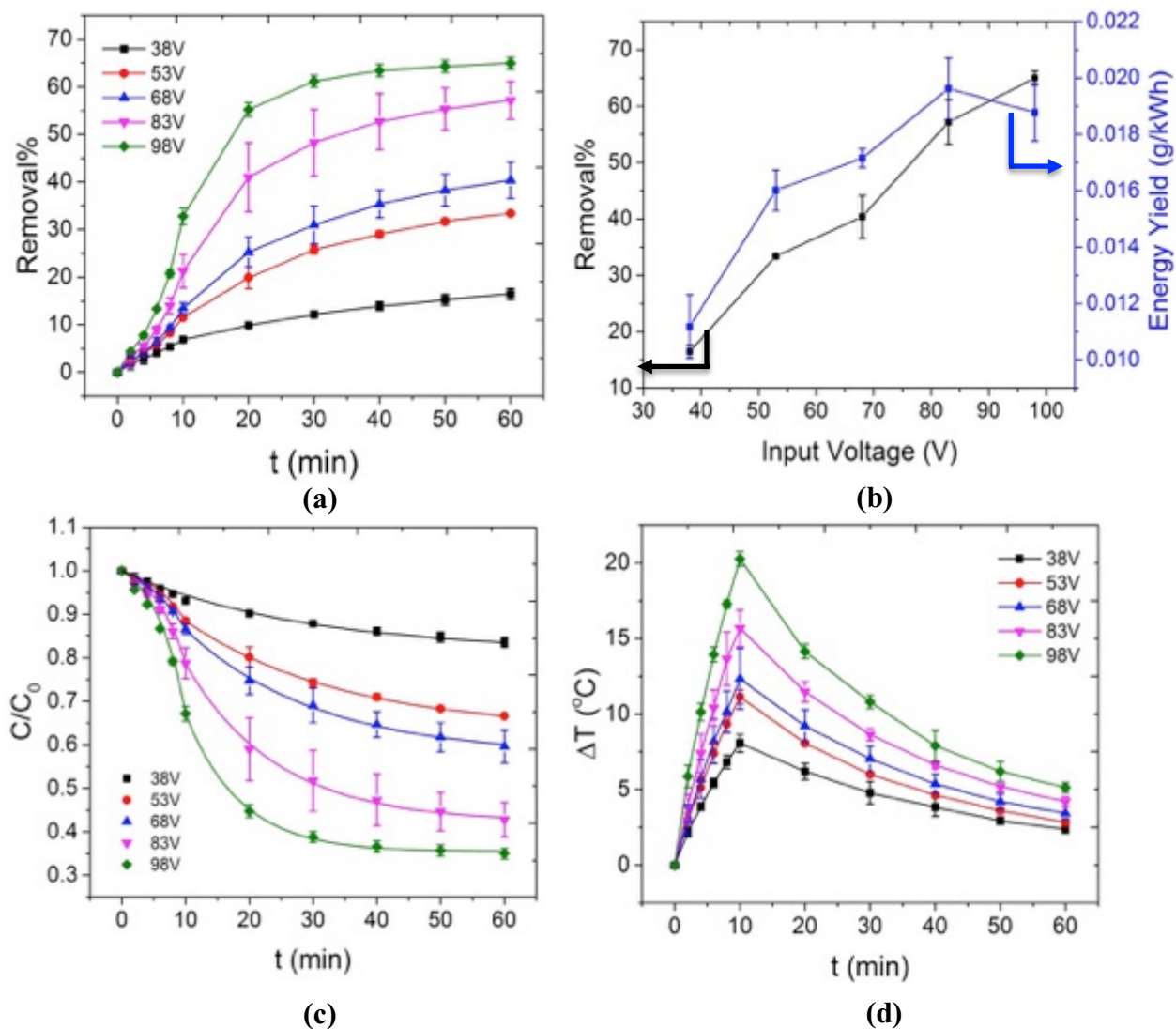


Figure 3.6. The effect of input voltage to the helical resonator on the water treatment process is investigated. The air gap distance and the plasma injection period were fixed at 2 mm and 10 min, respectively. (a) and (b) show the response of increasing input voltages on the removal of methylene blue. Moreover, as shown in (b), although final removal% increases with the increase in the input voltage, energy yield of the process does not increase accordingly. This means that the treatment process with 98 V as input voltage is not efficient in terms of energy consumption (power consumption of 3.1 ± 0.7 , 4.4 ± 0.8 , 5.1 ± 1.5 , 6 ± 0.9 and 7.4 ± 1 W for input voltages 38, 53, 68, 83 and 98 V, respectively). The kinetics of methylene blue removal is illustrated in (c). Regardless of the input voltage, an exponentially decaying kinetics could be observed. (d) shows the change in the solution temperature for various input voltages. A higher degree of change in temperature could be observed for higher input voltages. Based on the data presented, it could be concluded that at the air gap distance of 2 mm and plasma injection time of 10 min, the input voltage between 68 V and 83 V is optimum when considering removal%, energy yield and temperature change relative to room temperature (20 °C).

This means that the effect of the air gap distance (as discussed in section 3.4.1) on ozone concentration and removal% during the post treatment stage is more pronounced than the effect of the applied voltage. As shown by Figure 3.6(b), the energy yield does not increase continuously with higher input voltages. This is probably because when the input voltage increases more power is used. At input voltages higher than 83 V, the role of power consumption becomes dominant in determining the energy yield; therefore, no increase in energy yield is observed. The kinetics of decontamination (Figure 3.6(c)) follows the same exponential decay (as indicated by Equation (3.8)), regardless of the input voltage. Figure 3.6(d) plots the change of the solution temperature with increasing input voltage. The increase in the solution temperature (maximum temperature of 40 °C at input voltage of 98 V) could be attributed to the increase in the plasma power as the input voltage increases. Based on the results presented here, one could conclude that the application of moderate voltages (around 83 V) is most beneficial since not only is maximum energy yield reached, but also lower temperature elevations occurred. This diminishes the possibility of ozone poisoning and its concentration decay at high plasma powers and temperatures. Unlike the air gap distance, which can affect the shape of the plasma and hence the contact area with water surface (discussed in section 3.4.1 and Figure 3.4), no significant change is observed in the shape of the plasma as the input voltage varies.

3.4.3. Effect of plasma injection period

In this study, the plasma injection period is defined as a period of time in which plasma is in contact with the solution surface. As indicated in sections 3.4.1 and 3.4.2, the kinetics of the decontamination always follow an exponential trend in the treatment stage, when the plasma is present. It is expected that longer plasma injection periods increase the removal% significantly, since higher concentrations of activated species can be supplied for the decontamination process.

In this study, the effect of five plasma injection periods, namely 5, 10, 15, 20 and 25 min, at a fixed air gap distance of 2 mm and a rms value of input voltage of 83 V, was investigated (power consumption 6 ± 0.9 W). As shown in Figure 3.7(a), although increasing the injection period could enhance the removal%, the rate of increase in removal% as a function of plasma injection period (the slope of the removal% curve in Figure 3.7(a)) becomes slower (the slope became smaller) at periods higher than 15 min. One possible explanation for this behavior could be provided based on the sensitivity of ozone concentration in the solution to temperature. As indicated by Figure 3.7(b), an increase in the plasma injection period from 5 min to 25 min results in a net change in temperature elevation from 5 °C to 25 °C. As a consequence of these high temperatures (maximum of 45 °C for the injection period of 25 min) at high injection periods ($t > 15$ min), thermal degradation of ozone, as one of the main oxidizing agents in any non-thermal plasma treatment system, could occur faster [159]. Therefore, the removal% alters with a higher rate at $t \leq 15$ min compared to $t > 15$ min. This effect is also reflected in the energy yield of the process, as shown by Figure 3.7(a). Finally, the energy yield of the process reached a maximum value at $t = 15$ min. This is because in smaller time periods, low removal% decreases the yield. On the other hand, at time periods greater than 15 min, high energy consumption, alongside a slow increase of removal%, lowers the overall energy yield.

It has to be mentioned that using the optimized parameters investigated in this study ($d = 2$ mm, $V = 83$ V and $t = 15$ min), the value of pH and conductivity of the solution were measured before and after the treatment. The pH of the solution decreases from 6.4 ± 0.07 to 3.15 ± 0.01 . This acidification of the solution could be associated with the formation of species such as NO_3^- in water [100,150].

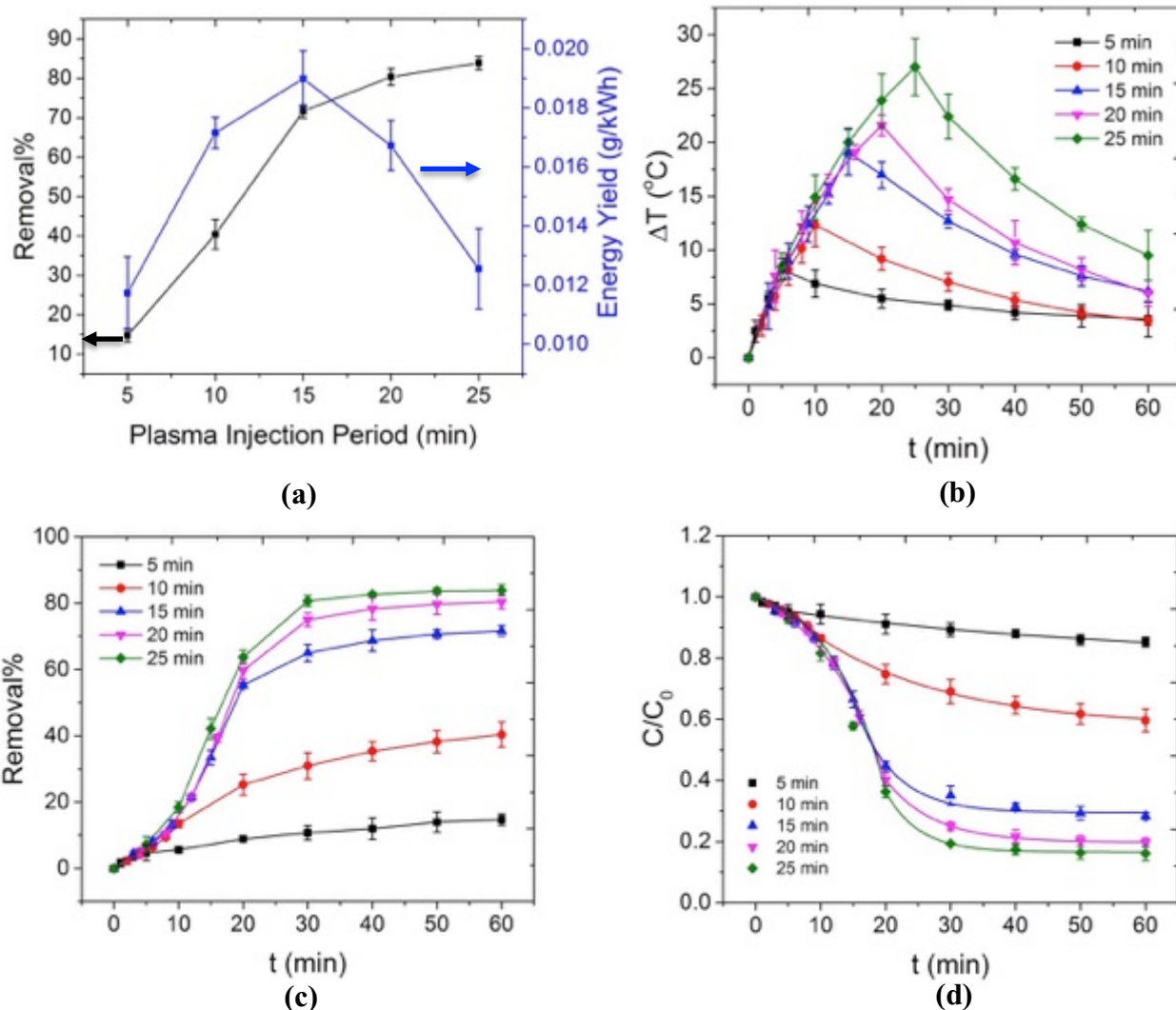


Figure 3.7. (a) The effect of time in which plasma is present on the surface of the solution is studied (rms value of the voltage and the air gap distance were kept at 83 V and 2 mm, respectively). As the plasma injection time increases, final removal% increases; however, the variation of removal% with injection time is more significant at periods lower than 15 min. This is probably due to the increasing rate of ozone concentration decay at higher temperatures. Maximum energy yield is obtained at 15 min. In smaller time periods, low removal% decreases the yield. On the other hand, at time periods greater than 15 min, high energy consumption, alongside a slow increase of removal%, lowers the overall energy yield. (b) As the period in which plasma is present increases, more energy dissipates in the form of heat; therefore, higher temperatures in the solution were reached. (c) and (d) illustrate the change in the removal% and normalized concentration as a function of time for various plasma injection periods used in this study. It could be seen that at high injection periods (20 min and 25 min), changes in removal% become insignificant when the process duration approached 60 min.

Furthermore, the conductivity of the solution changes from an initial value of 1.87 ± 0.02 mS/cm to 3.39 ± 0.11 mS/Cm. This could be due to the formation of ionic species such as H_3O^+ , NO_3^- , etc. [151]. Preliminary characterization by Ion Chromatography (IC) of the treated solutions shows that on average, 11.8 ± 0.1 mg/l of nitrate ions (NO_3^-) and 4.1 ± 0.1 mg/l of nitrite ions (NO_2^-) are formed in the solution. This confirms the acidification and also the increase in the conductivity of the solution. Using the optimized parameters, the maximum obtainable energy yield in this system is approximately 0.02 g/kWh (for removal% of 70%). This value of energy yield is comparable to the values calculated in previous studies (a list of which can be found in the study by Magureanu et al. [7]). Although unlike previous studies, no significant measures were taken to design the reactor in the current study. Therefore, with a few modifications (such as pumping the gas around plasma to the water for the efficient introduction of active species such as O_3 , modification of the applied waveform to the helical resonator, water circulation between the reaction chamber and a reservoir, etc.), higher energy yields could be expected from our proposed technique. Moreover, we calculated the electrical energy efficiency (based on power consumption) of our plasma generating system (power amplifier and helical resonator) as follows [127]:

$$\eta = \frac{P_{\text{WithPlasma}} - P_{\text{WithoutPlasma}}}{P_{\text{WithPlasma}}} \times 100 \quad (3.9)$$

Basically, in the presence of the plasma, the equivalent circuit of the helical resonator and plasma can be estimated with two resistances in series. The first resistance represents the resistance of the wire in the helical resonator. The other resistance is related to the resistance of the plasma since it is an ionic medium with flow of charges. It has to be mentioned that the helical resonator also has capacitance and inductance components; however, in any RLC system

at resonance, the contributions of capacitance and inductance components cancel out in determination of the total impedance. In Equation (3.9), $P_{\text{WithPlasma}}$ denotes the power consumed by the helical resonator when plasma is present. On the other hand, $P_{\text{WithoutPlasma}}$ is the power consumption of the resonator in the absence of plasma (i.e. the power dissipated in the wire only). The subtraction of $P_{\text{WithPlasma}}$ with $P_{\text{WithoutPlasma}}$ yields the estimated power dissipated in the plasma. The electrical efficiency is thus the power of the plasma divided by the total power (plasma plus wire). Furthermore, the measurements were done at a constant input current to the resonator. In other words, $P_{\text{WithPlasma}}$ and $P_{\text{WithoutPlasma}}$ show the difference between the input voltages, in the presence and absence of plasma, respectively. In order to avoid the formation of plasma (for calculation of $P_{\text{WithoutPlasma}}$), an aluminum ball (approximately 5 mm in diameter) was attached to the tip of the Pt/Ir electrode. This eliminates the formation of plasma by increasing the radius of the curvature of the electrode. As a result, the electrical energy efficiency calculated by Equation (3.9) refers to the amount of energy transferred to the plasma for the treatment process, compared to the total energy input to the electrical system. The energy yield was found to be 93%. This means that only 7% of the energy supplied to the system is lost (the main loss occurring in the wire resistance of the resonator) and 93% of the input electrical energy is available for the treatment process. We believe that this number is significant, alongside the removal% and energy yield, when real life applications of plasma-based water treatment systems are considered. In addition, the energy yield (Equation (3.2)) and the electrical energy efficiency of the system (Equation (3.9)) refer to two different but important parameters. Electrical energy efficiency shows the efficiency of the system in transferring the input energy to the plasma. The extent of the efficiency of the plasma in removing the contaminations (MB in this study) is shown by the energy yield of the system.

Our preliminary investigation on the nature of these long-lived, activated species indicates that when the optimized process parameters are applied to a blank solution (MilliQ water + 100 mg/l of NaCl), new features are formed in the optical spectrum of the solution (Figure 3.8). These features are created during the injection of plasma and are found in the wavelength range of 300-400 nm, which can be attributed to nitrites and nitrates. A comparison between the absorbance of these newly formed peaks in the presence and absence of MB (Figure 3.8 (c)-(f)), reveals that during the treatment stage the absorbance of all peaks increases almost equally in both cases; however, the absorbance values in the presence of MB decay much faster during the post treatment stage. This could be a qualitative indication of the consumption of these activated species or their reaction products such as peroxyxynitrite[94,100–103,113] by MB molecules. More importantly, as shown in Figure 3.8 (a), for the blank solution exposed to plasma, the absorbance in this wavelength region persists for as long as 6 hr after the plasma is extinguished. This is a clear indication of the generation of activated species with a long lifetime. A better understanding towards the nature of these activated species and their effect in the degradation pathways of MB could be achieved through the application of standard chemical analysis such as High Performance Liquid Chromatography (HPLC). The result of this analysis will be presented in section 3.5.1.

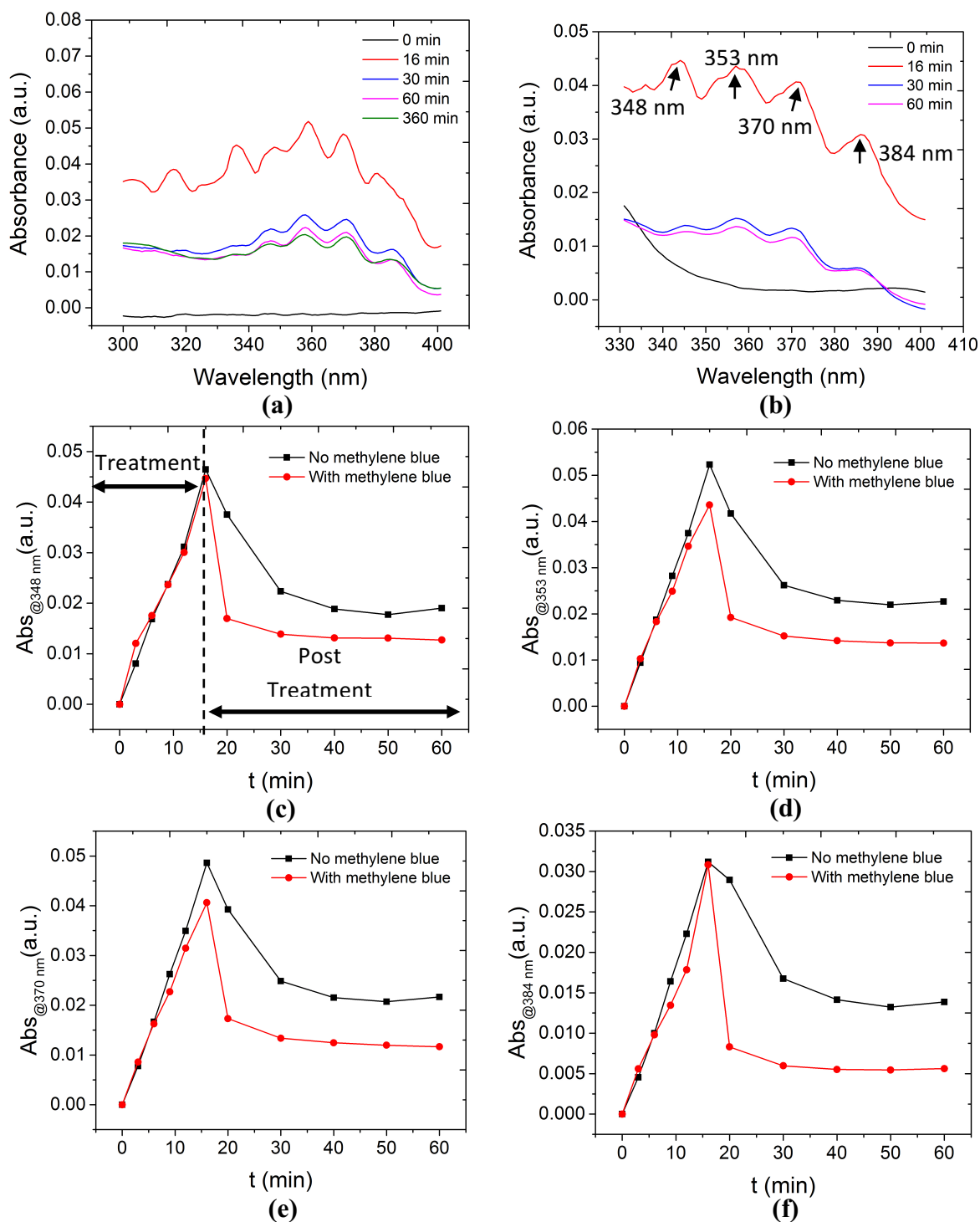


Figure 3.8. Formation of new features in the optical spectrum of (a) solution with no methylene blue and (b) solution in the presence of methylene blue in the wavelength region of 300-400 nm is shown. The fact that these features appear in both of these cases is a qualitative indication of the generation of new plasma-activated species in the solution. Moreover, as shown in (a), the presence of these features in the optical spectrum even after 360 min proves the long lifetime of these species, even though plasma was absent from $t=15$ min. (c)-(f) depicts the change in the absorbance of each of the dominant peaks shown in (a) and (b) as a function of time. It is evident that the presence of methylene blue in the solution causes a lower amount of absorption in each case, when the plasma is removed from the surface. Therefore, it could be concluded that these new features in the spectrum are indeed related to plasma-activated species.

3.5. Role of chemical parameters²

As discussed in Chapter 2 and section 3.1, chemical phenomena that affect the plasma treatment process of contaminants in water can occur both in the gas phase and the aqueous phase. While processes in the gas phase can be of importance, in this section, we will focus our attention on the phenomena that are crucial in the aqueous phase. These phenomena can be due to the presence of various ionic species, pH of the solution, etc. Amongst the possible ionic species, the role of Cl^- has been controversial and conflicting results have been obtained. As a result, the first section in this part of the research will be allocated to systematically study the role of Cl^- in the treatment process experimentally. Afterwards, the effect of other ionic constituents such as PO_4^{3-} , CO_3^{2-} , Fe^{2+} , etc. will be examined. The effect of the initial pH of the solution and the initial concentration of the contaminant form the rest of the sections of this chapter.

3.5.1. Effect of Cl^- concentration

The effect of variation in the electrolyte concentration (NaCl) is investigated on methylene blue removal efficiency. In all experiments, the duration of the treatment stage (when plasma is present) and post treatment stage (in the absence of plasma) are 15 min and 45 min, respectively ($t=0$ min to $t=15$ min for treatment stage and $t=15$ min to $t=60$ min for post treatment stage). The initial pH of the solutions was set to be near neutral (6.4-6.7). Figure 3.9(a) illustrates the overall removal% and changes in the conductivity of the solution as a function of NaCl concentration. A local maximum in removal% at NaCl concentration of 10-50 mg/l could be observed. Moreover, in the absence of NaCl (0 mg/l), the overall removal% is significantly lower.

² Parts of this section have been published in the journal of Environmental Science: Water Research & Technology, 2017, 3, 156-168.

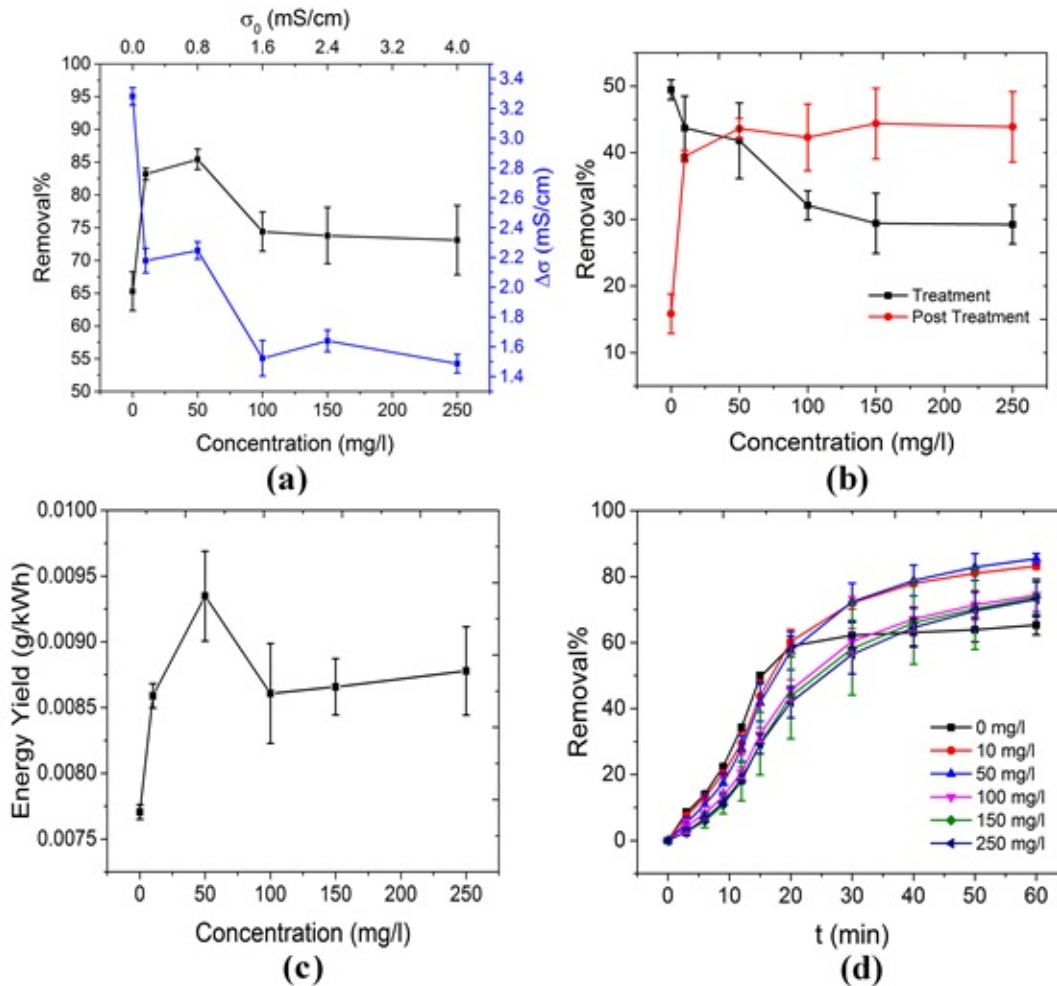


Figure 3.9. The effect of NaCl concentration on the decontamination of MB is studied. (a) The change in the overall removal% and conductivity of the solution as a function of NaCl concentration is shown. The overall removal% has a maximum in the range of 10-50 mg/l in NaCl concentration. In order to understand this behavior, removal% during the treatment and post treatment stages as a function of NaCl concentration were compared separately, as shown in (b). The removal% during the treatment stage is maximum when no NaCl is added to the solution. The addition of the salt to the solution reduced the removal% during this stage. This can be explained by the scavenging behavior of Cl^- towards OH^\cdot . It has been shown that when Cl^- scavenges OH^\cdot , amongst various Cl^- -based by-products, $\text{Cl}_2^{\cdot-}$ is dominant [141]. Although $\text{Cl}_2^{\cdot-}$ can oxidize MB, its oxidation potential is much lower than OH^\cdot . As a result, removal% during the treatment stage decreases when NaCl concentration increases. On the other hand, removal% during the post treatment stage enhanced significantly when NaCl was introduced to the solution. This can be explained by the formation of singlet oxygen ($^1\text{O}_2$) from reaction of HOCl and H_2O_2 ; both of which are produced due to the action of plasma and are stable enough to induce MB degradation after plasma is extinguished. It can be hypothesized that upon the addition of NaCl, an optimum NaCl concentration (around 50 mg/l) exists where the negative effect of Cl^- (scavenging properties) and its positive role (production of $^1\text{O}_2$) are balanced. This reflects itself in the energy yield of the system, as shown in (c). Finally, the change in overall removal% as a function of time is shown in (d). The significant continuation of MB removal during the post treatment stage only exists when NaCl is present in the solution.

Removal of MB in the treatment stage and in the absence of NaCl (about 50% removal) can be attributed to the action of hydroxyl radicals (OH·) on the MB molecules. These radicals are the most powerful oxidizing agents and they are formed due to the collision of energetic electrons with water molecules [85].

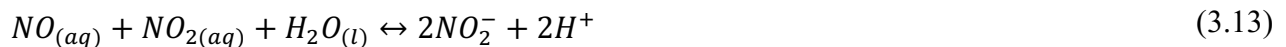
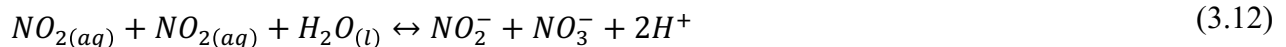


One of the by-products of reaction (3.10) is the formation of hydrogen peroxide (H₂O₂)[85]:



Hydrogen peroxide is also an oxidizing agent (oxidation potential of 1.78 V); however, our results show that even at very high concentrations of H₂O₂ (120 mM), MB shows little discoloration (about 5%), as illustrated by Figure 3.10(a). These high concentrations of H₂O₂ significantly exceed the values we measured in our experiments (approximately 1.2 mM), as shown in Figure 3.10(b). The concentration of H₂O₂ was measured using previously published methods based on the application of the fluorescence probe, Amplex Red [160,161]. Figure 3.10(b) also shows that the produced H₂O₂ remains in the solution for a long time after plasma is extinguished.

The removal of MB during the post treatment stage in the absence of NaCl, can be explained by the introduction of nitrogen-based compounds to the solution from plasma. The overall chemical reactions involved have been studied by Lukes et al, Brisset et al, Fridman et al, etc. [94,100–103]. The reactions can be expressed as follows:



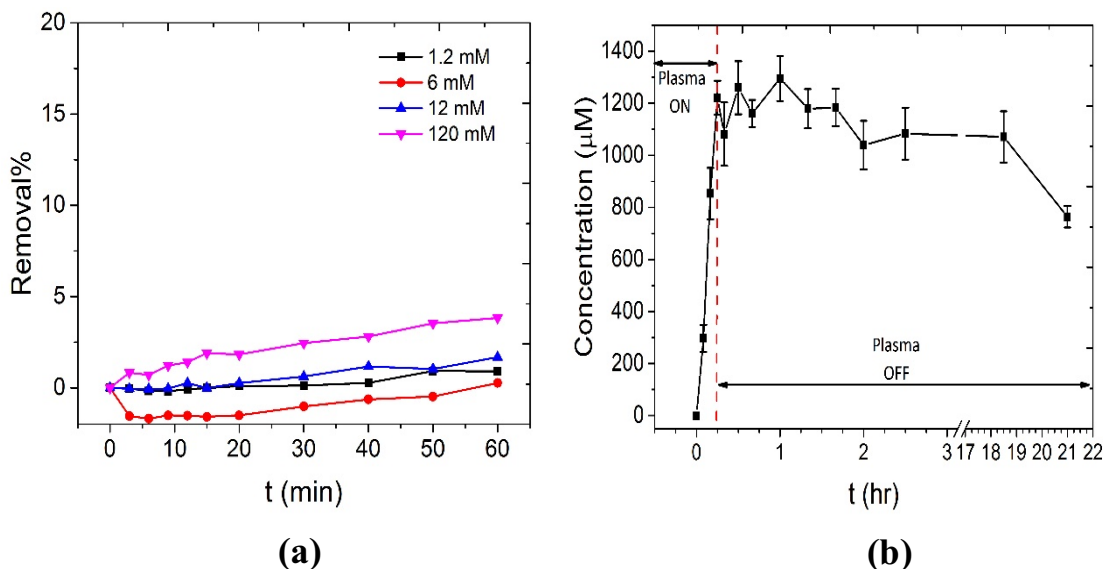


Figure 3.10. As a control experiment, various concentrations of H₂O₂ were added to the MB containing solutions. (a) shows the removal% of MB as a function of time. Only minute removal of MB can be achieved (about 5%) when high concentrations of H₂O₂ (120 mM) are added to the solution. These high concentrations of H₂O₂ significantly exceeds the concentrations measured in our experiments, as shown in (b). In our experiments, the concentration of H₂O₂ was evaluated by means of fluorescence probe, Amplex red, according to previously published methods. Moreover, (b) shows that H₂O₂ can stay in the solution for a long period of time in the post treatment stage. As a result, they can react with HOCl to produce ¹O₂ in the solution and continue the removal of MB in this stage.

In reactions (3.12) and (3.13), NO_(aq) and NO_{2(aq)} are introduced after the dissociation of N₂ and O₂ in air by collisions with electrons in plasma, as discussed in section 2.1.2.3. The direct consequence of these phenomena are the introduction of nitrite and nitrate ions to the solution as shown by reactions (3.12) and (3.13). In addition, formation of H⁺ in the solution means that the conductivity of the solution exposed to air plasma increases and its pH decreases, as shown in Figure 3.9(a) and Figure 3.10(d), respectively. Amongst the various suggested reaction paths that nitrite and nitrate ions can follow, the most important one is the formation of peroxyxynitrite (ONOOH) in the following manner:



Various studies have concluded that the oxidizing properties of water treated with air plasma in the post treatment stage (towards various organic and biological contaminations) can be attributed to the action of peroxyntirite in the solution [100–103]. The results presented in Figure 3.9(b) clearly shows that in the absence of NaCl in the solution, 15% of MB removal occurs during the post treatment stage which can possibly be due to the action of peroxyntirite. However, it has to be mentioned that in acidic conditions ($\text{pH} < 6.8$), H^+ -catalyzed decomposition of peroxyntirite can happen [100], according to Equation (3.15).



This can limit the effect of peroxyntirite in the post treatment stage considering the fact that the pH of the solution decreases quickly as it is treated with air plasma (see section 3.5.4 for further discussion). On the other hand, decomposition products of peroxyntirite in acidic conditions (as shown by Equation (3.15)) are powerful oxidizing agents, but with short lifetime, that can help the MB removal process (possibly during the treatment stage).

As shown in Figure 3.9(b), increase in the concentration of NaCl in the solution resulted in a gradual decrease in the removal% during the treatment stage. However, a significant increase in the removal% during the post treatment stage occurred. The gradual decline of removal% during the treatment stage can be explained by the scavenging properties of Cl^- towards $\text{OH}\cdot$ [137,141], as shown by Equation 3.16. According to the kinetic modeling performed by Yuan et al., chlorine radical anions ($\text{Cl}_2^{\cdot-}$) are the most dominant in terms of concentration amongst many possible chlorine-based by-products [141]. The role of $\text{Cl}_2^{\cdot-}$ in degradation of organic pollutants has been also suggested [137].





As shown by Equations (3.16) and (3.17), Cl^- can scavenge OH^{\cdot} and $Cl_2^{\cdot -}$ is eventually formed in the solution. Chlorine radical anion is an oxidizing agent; however, its oxidation potential is lower than the oxidation potential of hydroxyl radicals (1.57 V for $Cl_2^{\cdot -}$ versus 2.8 V for OH^{\cdot}) [70]. This means that the presence of Cl^- in the solution can reduce the decontamination ability of the plasma treatment process, especially in the treatment stage. This is due to the fact that during the treatment stage the action of OH^{\cdot} towards MB molecules is the most important decontamination pathway (see section 3.5.2 for further discussion). This is in accordance with the trend observed for removal% in the treatment stage illustrated by Figure 3.9(b). On the other hand, for Cl^- to be able to contribute to the increase in the removal% during the post treatment stage, stable chemicals should be produced in the solution. Only then the prolonged decontamination in the post treatment stage can be expected, as shown by Figure 3.9(d) for Cl^- -containing solutions. One pathway (reactions (3.18) and (3.19)) that can justify the role of Cl^- in the post treatment stage, is the production of singlet oxygen (1O_2) [132,134–136].



According to reaction (3.19), the formation of the singlet oxygen depends on the presence of hydrogen peroxide (H_2O_2) and hypochlorous acid ($HOCl$) in the solution formed by reactions (3.11) and (3.18), respectively. These chemicals are stable in the solution (as shown in Figure 3.10(b) for H_2O_2) to induce prolonged decontamination in the post treatment stage. It is worth-mentioning that we attempted to detect 1O_2 in the solution using the fluorescence probe, 9,10-dimethylanthracene (DMA), as described in literature [160,162]. DMA is a fluorescent molecule

in nature and it loses its fluorescence properties when it reacts with $^1\text{O}_2$. However, DMA is not soluble in water and our experiments show that upon dissolution in acetonitrile and subsequent mixture with the untreated aqueous phase, it loses its fluorescent properties. As a result, distinguishing between the effect of $^1\text{O}_2$ and mixture with aqueous phase on the fluorescence properties of DMA proved to be a challenge. The application of the HPLC-MS and identification of the degradation by-products provided indirect proofs for the presence of $^1\text{O}_2$ in the solution. The results of this study will be presented in section 3.5.2.

Finally, the calculated energy yield of the process for various concentrations of NaCl is shown in Figure 3.9(c). A local maximum at 50 mg/l is due to the higher removal% at this concentration. This local maximum in the overall removal% is probably due to the balanced role of OH^\cdot during the treatment stage and $^1\text{O}_2$ during the post treatment stage. The variation of the overall removal% as a function of time is shown in Figure 3.9(d) for various concentrations of NaCl. It clearly shows the role of Cl^- ions in the solution for continuation of decontamination in the post treatment stage (from $t=15$ min to $t=60$ min).

3.5.2. Analytical characterization

As described in section 3.3.3, IC and HPLC-MS analysis was used to characterize solution with and without Cl^- . The results of these studies are discussed in the next two sections.

3.5.2.1. Ion Chromatography (IC) analysis

IC analysis was used to measure the concentration of inorganic species in water, both before and after treatment. Table 1 summarizes the results obtained from IC analysis.

Table 3.2. Concentration of various inorganic ions detected by IC analysis.

Sample	Treatment stage	Concentration (mg/l)		
		Cl ⁻	NO ₃ ⁻	NO ₂ ⁻
MilliQ Water	Before	--	--	--
	After	--	14.4±0.026	5.1±0.036
MilliQ Water+NaCl	Before	50±0.09	--	--
	After	50.36±0.35	11.08±0.07	4.1±0.032

The results indicate that regardless of the nature of the water matrix, nitrate (NO₃⁻) and nitrite (NO₂⁻) ions are formed in the solution. This is due to the direct action of plasma on water, as discussed in section 3.5.1 (Equation (3.12) and (3.13)). The results in Table 3.2 also show that for solutions containing NaCl, the concentration of Cl⁻ is similar before and after the plasma treatment. This can be explained based on the Equations (3.16)-(3.19), mentioned in section 3.5.1. These reactions describe a chemical path in which Cl⁻ is a reactant in reaction (3.16) and a product in reaction (3.19). In other words, Cl⁻ acts as a catalyst in the formation of ¹O₂. As a result, the concentration of Cl⁻ before and after the plasma treatment is same.

3.5.2.2. High Performance Liquid Chromatography-Mass Spectrometry (HPLC-MS) analysis

HPLC-MS was used to determine the degradation by-products of MB and to suggest a pathway in which plasma affects MB structure. The analysis was performed on both water matrices, i.e. only MilliQ water and MilliQ water with NaCl (50 mg/l). As discussed in section 3.5.1, the nature of MB degradation (especially in the post treatment stage) can be different in the presence and absence of Cl⁻.

Table 3.3. Chemical species detected by LC-MS due to the degradation of MB by plasma.

Sample	Detected m/z	Identification
MilliQ-Before	284.12	Methylene blue
MilliQ-After	166.06	P7
	101.02	P10
	107.07	P9
	180.07	P6
	256.09	P2
	270.11	P1
	284.12	Methylene blue
	244.07	P3
	228.06	P4
NaCl-Before	284.12	Methylene blue
NaCl-After	107.07	P9
	180.07	P6
	101.02	P10
	270.11	P1
	187.07	P5
	244.07	P3
	231.04	P11
	228.06	P4
	158.02	P8

While in the absence of Cl^- , peroxyxynitrite is possibly the main contributor to the degradation of MB during the post treatment stage, in the presence of Cl^- , the enhanced removal% can be attributed to the formation of $^1\text{O}_2$. Table 3.3 summarizes the compounds detected by HPLC-MS for each sample. In Table 3.3, terms “before” and “after” indicate the stage of the samples during

the process, i.e. before and after treatment. On the other hand, “MilliQ” and “NaCl” in the name of the samples reflect only MilliQ water and MilliQ with NaCl water matrices, respectively. The highlighted compounds in the table indicate the compounds detected in only one of the water matrices. Two conclusions can be readily made from the results summarized in Table 3.3 regarding the by-products formed by plasma treatment.

1) After treatment by plasma, residues of the parent compound (MB) are only present in the samples with MilliQ water matrix. However, HPLC-MS could not detect any MB in treated samples where NaCl was added to MilliQ water (NaCl-After). This is understandable considering the higher removal% obtained when 50 mg/l of NaCl was added to MilliQ water (85% versus 65%), as shown in Figure 3.9.

2) Although most of the degradation by-products are similar in both treated samples, there are few organic species formed only in one or another water matrix after plasma treatment. As shown by Table 3.3, besides MB, products P2 and P7 only formed when only MilliQ used as the water matrix. More importantly, products P5, P8 and P11 were only detected in treated samples with NaCl added to the water matrix. This possibly points to the hypothesis that the degradation mechanism is at least partially different in the two water matrices, as discussed in section 3.5.1.

Based on the species summarized in Table 3.3, a degradation pathway was suggested for MB, as shown by Figure 3.11. The identified by-products can be categorized into three groups based on their appearance in specific water matrix. These include only in MilliQ (P2 and P7), common by-products (P1, P3, P4, P6, P9 and P10) and only in NaCl added to MilliQ water (P5, P8, P11).

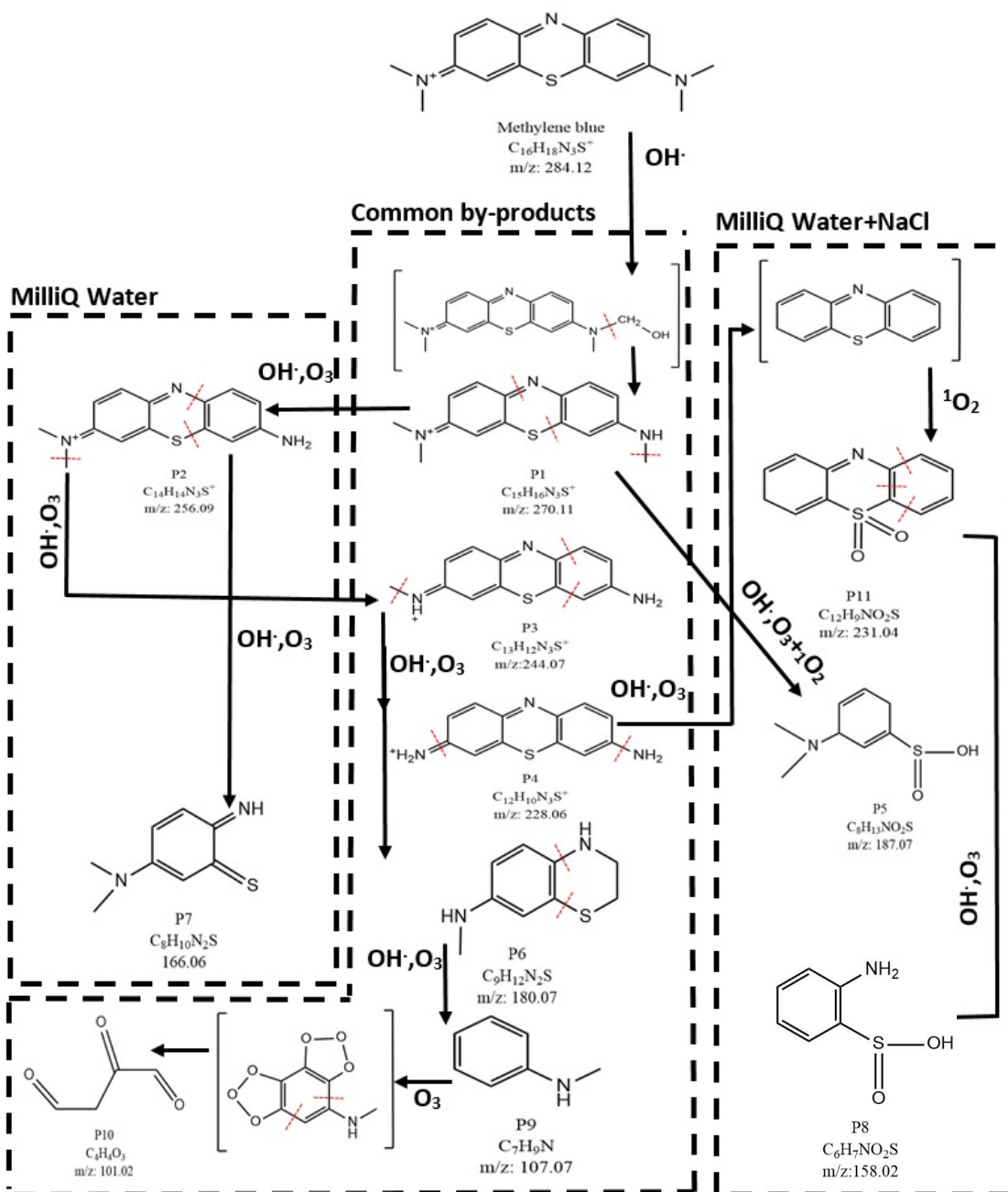


Figure 3.11. A degradation pathway for MB was suggested based on the species detected by HPLC-MS. The major pathway for degradation of MB molecules is believed to be the action of OH^\cdot . Moreover, the by-products can be categorized into three groups based on their formation in specific water matrices. These categories from left to right in the figure are: 1) Only in MilliQ 2) common by-products and 3) only in NaCl added to MilliQ water. The formation of sulfones (P11) and sulfinic acids (P5 and P8) in only samples with NaCl added to MilliQ water confirms the formation of 1O_2 as an oxidizing agent in these samples. Moreover, the presence of small organic molecules (such as P10) in both water matrices suggests the complete destruction of the aromatic ring and formation of aliphatic molecules. This is possibly due to the action of ozone molecules on aromatic compounds such as P9. This process proceeds first with the formation of ozonide compounds which are unstable and turn into aliphatic molecules.

In Figure 3.11, a chemical structure inside two brackets indicates an intermediate compound which although not detected by HPLC-MS, its inclusion in the degradation pathway increases the clarity of various steps involved in the degradation mechanism. The major pathway in degradation of MB is oxidation by OH^\cdot . The first step is the oxidation of a methyl group (CH_3) to a hydroxymethyl group ($\text{CH}_2\text{-OH}$). This structure is probably unstable (shown in the bracket in Figure 3.11) and results in the termination of the methyl group from MB molecule (P1). The remaining methyl groups can go through a similar process to yield P2, P3 and P4. It has to be mentioned that the same by-products can be achieved through the action of ozone (O_3) on MB molecules, as suggested by Huang et al. [150]. Product P4 can degrade further by losing its amine (-NH_2) groups to form an intermediate (top right corner of Figure 3.11). This intermediate is probably the substrate for oxidation by $^1\text{O}_2$, in the case of NaCl added to MilliQ water, to form sulfones (P11). P11 can be further oxidized by OH^\cdot or O_3 to create sulfinic acid by-products (P8). The presence of the sulfones (P11) and sulfinic acids (P5 and P8) can be explained by the action of $^1\text{O}_2$ on organic molecules. Due to the high electrophilicity, $^1\text{O}_2$ is capable of oxidizing phenols, sulfides and amines. Oxidation of sulfides by $^1\text{O}_2$ results in the formation of sulfoxides and sulfones [163,164]. The sulfone group is known to be an electron-withdrawing group (EWG), i.e. it draws the electron density from neighboring atoms. Subsequently, the strength of the bonds neighboring the sulfone group decreases. As a result, further degradation of the organic molecule containing sulfone group becomes easier. This confirms the hypothesis discussed in section 3.5.1 in which the increased removal% of MB (during the post treatment stage) in solutions containing Cl^- was attributed to the formation of $^1\text{O}_2$ through a series of reactions mediated by Cl-based compounds. HPLC-MS results presented in Figure 3.11 indicates that one major step in degradation of MB, regardless of the water matrix used, is the degradation

of the aromatic moieties. This is probably done by the attack of hydroxyl radicals and results in the formation of products such as P7 from P2, P6 from P3, etc. This aromatic ring destruction continues until the organic molecules turn into their simplest aromatic form (P9). Finally, P9 can lose its aromatic structure completely and form the aliphatic by-product P10. This is possible by formation of an ozonide intermediate, as suggested by Kim et al. [165]. Finally, the HPLC-MS results suggest that there are no chlorinated by-products present in the plasma treated solutions, in the case of NaCl added to MilliQ water matrix. These chlorinated by-products can be hazardous (if present) for wildlife due to bioaccumulation [135].

3.5.3. Role of other ionic species

In section 3.5.1, the role of Cl^- ions on the degradation of MB during the treatment and post treatment stages was elaborately explained. Moreover, chemical mechanisms involved in each stage were outlined. Beside Cl^- ions, various types of ionic species can be present in water. These ions can influence the decontamination process as well and their roles should be investigated. In this section, we start the examination by exploring the role of ferrous (Fe^{2+}) ions in water. As described in section 1.3.2, the catalytic role of Fe^{2+} ions in Fenton processes to produce hydroxyl radicals has been used extensively to eliminate various contaminants from water. The most important reactions involved in Fenton processes are:



A quick look at Equation (3.20) and (3.21) indicates that in Fenton processes, beside Fe^{2+} ions, the presence of H_2O_2 is necessary. Similar necessity was also observed in Equations (3.16) to (3.19), where the role of Cl^- in production of $^1\text{O}_2$ was discussed. As a result, it is interesting to

investigate the competition between Fenton processes and $^1\text{O}_2$ production in the solution when both Fe^{2+} and Cl^- ions are present simultaneously. In order to achieve this goal, sodium chloride (NaCl) and iron (II) chloride (FeCl_2) with a concentration of 0.85 mM were added to MilliQ water separately. For comparison purposes, solutions with similar concentration of iron (II) sulfate (FeSO_4) were also used. To investigate the degradation efficiency in each solution, 0.75 mg/l of MB was also added. The experimental setup was similar to the setup used for other experiments.

Figure 3.12(a) shows the change in the removal% as a function of time for various electrolytes used in this study. In addition, the extent of MB removal during the treatment (0 to 15 min) and post treatment (15 to 60 min) stages are plotted separately for each electrolyte in Figure 3.12(b).

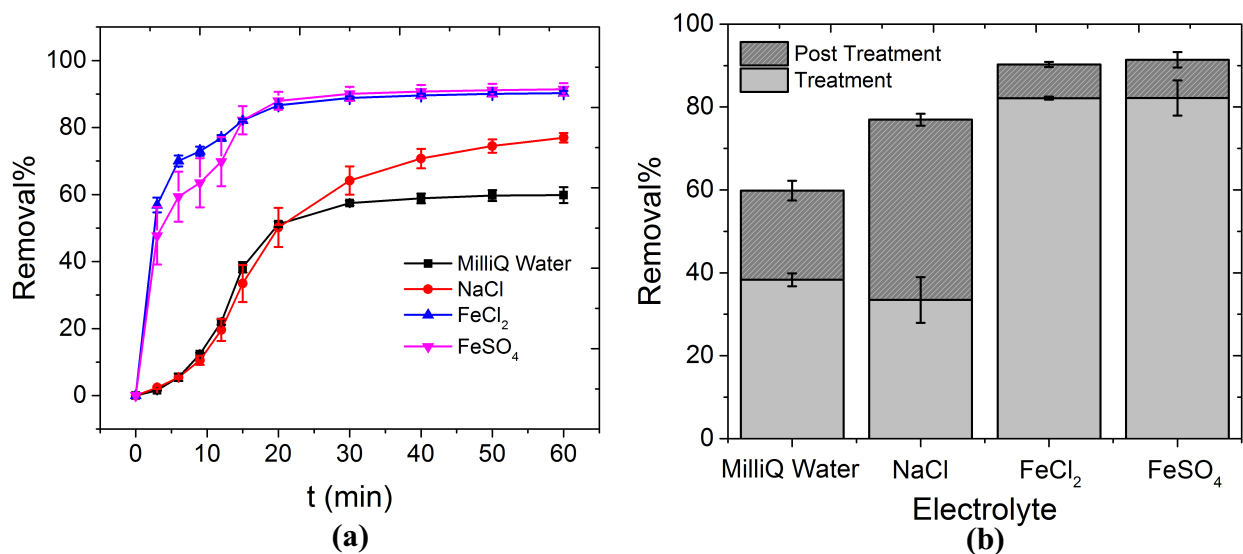


Figure 3.12. The competition between Fenton processes and $^1\text{O}_2$ production in Cl-mediated reactions was investigated. For this purpose, removal% of MB was calculated as a function of time for various electrolytes. This is shown in (a). There are two major differences between the removal% in different electrolytes. Firstly, removal of MB in solutions containing Fe^{2+} ions is higher and faster compared to the other electrolytes, regardless of the anion present in the solution. This is probably due to the homogenous formation of hydroxyl radicals in the solution from Fenton processes. Secondly, only solutions containing NaCl show appreciable degradation of MB during the post treatment stage (15 to 60 min). This is also shown in (b) where the removal% during the treatment and post treatment stages were plotted separately for each electrolyte.

There are two major differences between the removal% of MB in various electrolytes. Firstly, the degradation of MB in solutions containing Fe^{2+} ions occurred more and at a much faster rate, regardless of the anion (Cl^- or SO_4^{2-}) present in the solution. This is probably due to the fact that when Fe^{2+} ions are present in the solution, upon production of H_2O_2 by plasma, Fenton processes take place in the entire solution homogeneously. The direct result of this phenomenon is the homogeneous production of hydroxyl radicals (Equation (3.20)) throughout the solution. Subsequently, the degradation of MB molecules by hydroxyl radicals proceeds in the entire volume of the solution. This is in contradiction with the case of other electrolytes where hydroxyl radicals are mostly created at the interface of plasma and water. As a result, the degradation of MB in solutions containing Fe^{2+} ions is much faster. The second difference can be observed from the extent of MB removal during the treatment and post treatment stages of each electrolyte, as shown in Figure 3.12(b). Although the highest removal% during the treatment stage was obtained for Fe^{2+} containing solutions, these solutions showed a small removal% during the post treatment stage. On the other hand, the highest removal% during the post treatment stage could be achieved from solutions containing Cl^- . This becomes more interesting in the case of FeCl_2 where both Fe^{2+} and Cl^- ions are present in the solution. Moreover, the removal% during the post treatment stage was higher for MilliQ water than solutions containing Fe^{2+} ions. These results can be explained in this manner. In section 3.5.1, we explained that when MilliQ water is used as the electrolyte, the degradation of MB in the post treatment stage is probably caused by the action of peroxyxynitrite. In this process, H_2O_2 is required to produce peroxyxynitrite. On the other hand, we described the role of Cl^- ions in the solution in which $^1\text{O}_2$ is produced by the action of H_2O_2 . These statements show that the occurrence of appreciable post treatment stages in both cases requires the presence of H_2O_2 . When Fe^{2+} ions are present in the

solution, they tend to consume H_2O_2 molecules in Fenton processes to produce hydroxyl radicals. As a result, it can be hypothesized that due to the Fenton processes, a significant portion of the produced H_2O_2 molecules are used in the treatment stage. As a result, the removal% during the post treatment stage of the solutions containing Fe^{2+} is insignificant, although Cl^- ions coexisted in the solution.

To further investigate the competition between Fenton processes and Cl^- -mediated reactions, various concentrations of FeCl_2 (0, 0.05, 0.2, 0.425, 0.85 and 1.2 mM) were added to MilliQ water. The efficiency of the system in terms of the removal% of MB for each solution was studied.

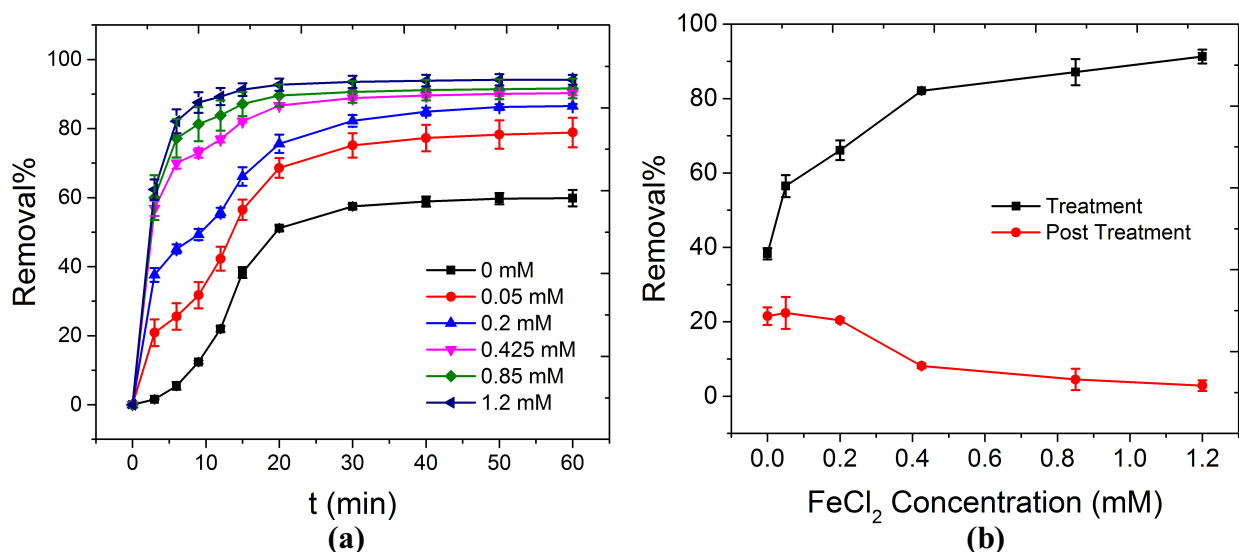


Figure 3.13. (a) The removal% of MB as a function of time is shown for solutions containing various concentrations of FeCl_2 . The results indicate that as the concentration of FeCl_2 is increased, higher MB removal could be obtained in the plasma treatment process. To evaluate the obtained results in a more detailed manner, the removal% during the treatment and post treatment stages were plotted separately as a function of the concentration of FeCl_2 , as shown in (b). The removal% during the treatment stage enhanced as the concentration of the salt increased. However, the rate of the increase in the removal% in this stage (the slope of the black curve in (b)) as a function of the concentration gradually decreased. This can be due to the fact that at high concentrations of FeCl_2 , the concentration of H_2O_2 measured in our system (Figure 3.10) becomes comparable to the concentration of Fe^{2+} in the solution. However, not all of the H_2O_2 molecules can be used by Fe^{2+} ions since there are many other side reactions that can remove H_2O_2 from solution. As a result, a plateau is expected in the removal% during the treatment stage as the concentration of Fe^{2+} is increased. Moreover, higher concentrations of FeCl_2 in the solution decreased the removal% during the post treatment stage.

Figure 3.13(a) illustrates the change in the overall removal% as a function of time for various concentrations of FeCl_2 in the solution. As the concentration of FeCl_2 is increased in the solution, the overall removal% of MB also was enhanced. To evaluate the obtained results in a more detailed manner, the removal% during the treatment and post treatment stages were plotted separately as a function of the concentration of FeCl_2 , as shown in (b). The removal% during the treatment stage enhanced as the concentration of the salt increased. However, the rate of the increase in the removal% in this stage (the slope of the black curve in (b)) as a function of the concentration gradually decreased. This can be due to the fact that at high concentrations of FeCl_2 , the concentration of H_2O_2 measured in our system (Figure 3.10) becomes comparable to the concentration of Fe^{2+} in the solution. However, not all of the H_2O_2 molecules can be used by Fe^{2+} ions since there are many other side reactions that can remove H_2O_2 from solution. As a result, a plateau is expected in the removal% during the treatment stage as the concentration of Fe^{2+} is increased. On the other hand, higher concentrations of FeCl_2 in the solution reduced the removal% during the post treatment stage. As described before, in order to expect a significant removal%, either through the action of peroxyxynitrite or $^1\text{O}_2$, H_2O_2 is required. As the concentration of Fe^{2+} is increased, higher concentrations of H_2O_2 are consumed in Fenton processes. As a result, reactions involved in the production of peroxyxynitrite or $^1\text{O}_2$ (Equations (3.14) and (3.20)) happen at slower rates. Subsequently, the removal% during the post treatment stage gradually decreased with the increase in the concentration of Fe^{2+} .

Beside Fe^{2+} ions that can influence the efficiency of the plasma treatment system by promoting Fenton processes, other ionic species can be present in wastewater. These ions are PO_4^{3-} , CO_3^{2-} and SO_4^{2-} . In order to show the difference between the effects of different ionic forms constituting similar elements, we also investigated the addition of thiosulfate to the solution

($S_2O_3^{2-}$). The results of this study are shown in Figure 3.14. Figure 3.14(a) illustrates the change in the overall removal% as a function of time for different electrolytes. The highest overall removal% was obtained from NaCl electrolyte. On the other hand, the lowest degradation of MB happened in solutions containing PO_4^{3-} and CO_3^{2-} ions. This is probably due to the fact that these ions scavenge hydroxyl radicals with a very high rate ($7 \times 10^6 \text{ M}^{-1}\text{S}^{-1}$ and $2.8 \times 10^8 \text{ M}^{-1}\text{S}^{-1}$ for reaction of hydroxyl radicals with PO_4^{3-} and CO_3^{2-} ions, respectively [166]). This high rate of reaction between hydroxyl radicals and the above-mentioned ions can possibly prevent the effective reaction of hydroxyl radicals with MB molecules.

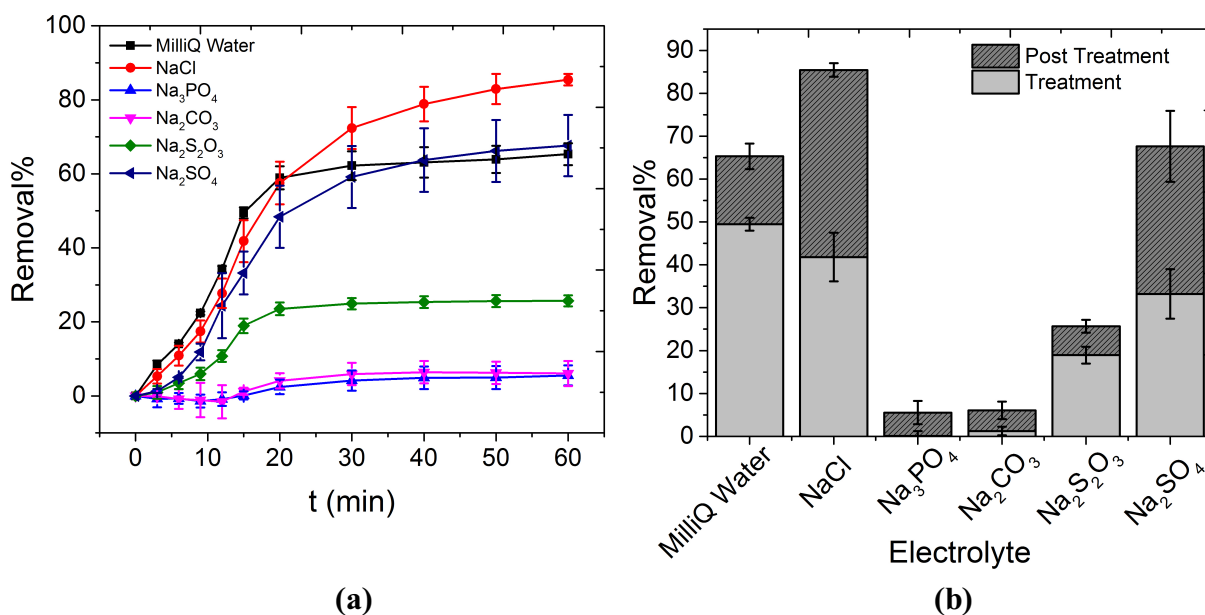


Figure 3.14. The effect of the presence of various ionic species in water on the removal% of MB is investigated. (a) The change in the overall removal% as a function of time is shown for various electrolytes. The highest removal% was obtained for solutions containing NaCl. On the other hand, the overall removal of MB is insignificant for solutions containing PO_4^{3-} and CO_3^{2-} ions. This is due to the fact that these ions are very well known for their scavenging behavior towards hydroxyl radicals. (b) illustrates the removal% during the treatment and post treatment stages for each electrolyte. Highest removal% during the treatment stage was obtained from MilliQ water. This can be justified by considering the fact that any ionic species in the solution can act as a scavenger of hydroxyl radicals. As a result, the concentration of hydroxyl radicals available for reaction with MB molecules is lowered. The highest removal% during the post treatment stage was achieved from solutions containing Cl⁻. This can be attributed to the production of 1O_2 , as described in section 3.5.1.

Similar explanation can be given for Cl^- ions. These ions are also capable of scavenging hydroxyl radicals. However, this reaction is the initial step for the production of $^1\text{O}_2$ in the solution that induces a significant removal% during the post treatment stage. As a result, it can be hypothesized that the reaction of hydroxyl radicals with PO_4^{3-} and CO_3^{2-} ions probably creates species that are not strong oxidizing agents. For instance, Balachandran et al. concluded that the reaction of hydroxyl radicals with CO_3^{2-} ions produces carbonate anion radicals ($\text{CO}_3^{\cdot-}$). These radicals react with organic molecules very slowly [167]. Figure 3.14(b) shows the removal% during the treatment and post treatment stages for various electrolytes. As mentioned previously, the maximum removal% during the treatment stage was obtained from MilliQ water. This is because any additional ions in the solution act as the scavenger of hydroxyl radicals. On the other hand, the highest removal% in the post treatment stage was obtained from NaCl containing solution, possibly to the production of $^1\text{O}_2$. The removal% in the treatment stage for solutions containing SO_4^{2-} is comparable to the case of NaCl solutions. This can be explained by the following chemical reactions [131]:



The sulfate anion radical formed in Equation (3.23) is an oxidizing agent that can degrade MB molecules. However, its oxidation strength is lower than the oxidation capability of hydroxyl radicals, but higher than that of $\text{CO}_3^{\cdot-}$ [149]. Finally, as shown by Figure 3.14(b), the removal% during the post treatment stage in solutions containing SO_4^{2-} is also comparable to the solutions containing NaCl. This can be explained based on the formation of peroxodisulfate in the solution [131].



The peroxodisulfate ions formed from the combination of sulfate anion radicals is an oxidizing agent [168] that can degrade MB molecules. It has to be mentioned that the reaction kinetics of peroxodisulfate ions towards many organic compounds is very slow at ambient temperature; however, at elevated temperatures achieved through the injection of plasma to the water surface (section 3.4), the degradation of organic compounds by this ion can be expected.

3.5.4. Effect of initial pH

The initial pH of the solution is another parameter that can affect the treatment process, as described in section 3.1. Since the chemistry involved in plasma treatment processes can be complicated in the presence of various ionic species in water, the effect of the solution initial pH will be only examined in the presence of Cl^- ions. In this study, the concentration of MB and NaCl was fixed at 0.75 mg/l and 50 mg/l, respectively. The initial pH of the solutions was adjusted by adding sufficient amount of 0.1 M solutions of HCl or NaOH to create acidic or alkaline conditions, respectively. Figure 3.15(a) shows the effect of the initial pH of the solution on the removal% during the treatment and post treatment stages. Maximum overall removal% can be achieved in either acidic and near neutral pH values (82-85%). However, decontamination process at pH=2.8 mostly occurred in the treatment stage (75%) and the role of the post treatment stage was insignificant (10%). On the other hand, when the initial pH was set to 6.4, the contribution of the treatment (40%) and post treatment stage (45%) to the overall decontamination was almost equal.

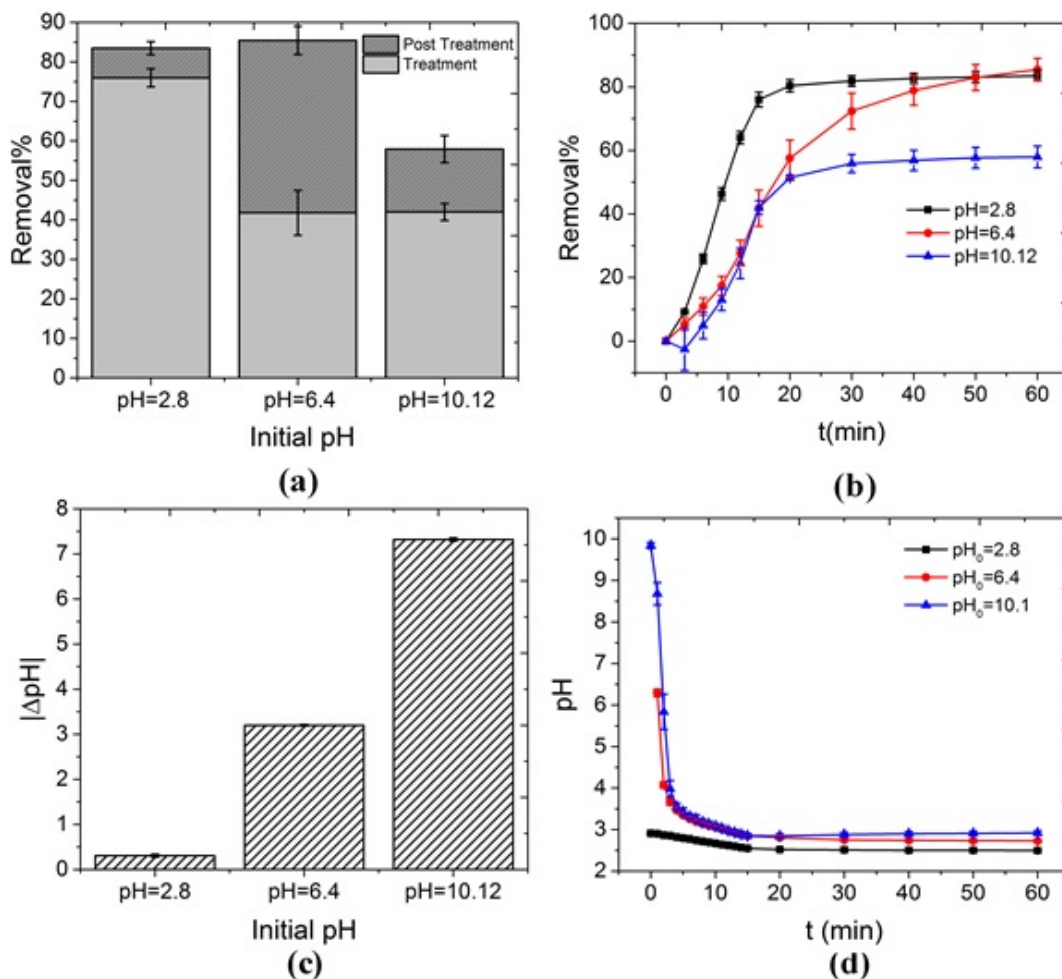


Figure 3.15. The effect of the initial pH of the solution on the decontamination of MB is investigated. (a) Overall removal%, removal% during the treatment stage (light gray) and removal% during the post treatment stage (dark gray) are shown as a function of the initial pH of the solution. The highest removal% during the treatment stage was achieved by using solutions with initial acidic pH values. This can be explained by various phenomena including the pH dependency of the oxidation potential of OH^\cdot , the acid-base equilibrium of the dye molecules, etc. The removal% during the post treatment stage is insignificant for solutions with either initial acidic or alkaline conditions (pH values of 2.8 and 10.12). This can be justified by considering the pH dependency of the Cl-based reactions involved in the production of $^1\text{O}_2$ (Equations (3.17) and (3.19)). As discussed in section 3.5.1, when Cl^- is present in the solution, it can possibly scavenge OH^\cdot . This reaction path eventually produces $^1\text{O}_2$ from two stable compounds, i.e. HOCl and H_2O_2 , which can degrade MB in the post treatment stage. Significantly high concentrations of OH^- or H^+ , when initial alkaline or acidic conditions are used respectively, can cause Equations (3.17) or (3.19) to occur with a faster rate in the reverse direction. As a result, lower concentration of $^1\text{O}_2$ is created and removal% in the post treatment stage reduces. This can be seen in (b) which illustrates the change in the removal% as a function of time for three different initial pH values. Initial near neutral pH values represent the most balanced condition for production of $^1\text{O}_2$. As a result, removal of MB continues significantly after the plasma is extinguished. The overall change in the pH of the solutions with various initial pH is shown in (c) (pH of the solution decreases). The acidification of the solutions is a direct consequence of formation of nitrite and nitrate ions in the solution, as discussed in section 2.1.2.3. The highest acidification happens for the solutions with initial alkaline condition. This is understandable since these solutions are depleted from H^+ . Finally, the pH change as a function of time is shown in (d).

As discussed in section 3.5.1, the most important oxidizing agent during the treatment stage is $\text{OH}\cdot$. In acidic solutions (initial pH of 2.8) significant removal% during the treatment stage, compared to initial pH values of 6.4 and 10.12 can be explained by multiple reasons. These are:

1) Oxidation potential of $\text{OH}\cdot$ (as the most powerful oxidizing agent) is known to be 2.8 V; however, this value only holds in acidic solutions. Previous studies show that in non-acidic conditions, the oxidation potential of $\text{OH}\cdot$ is reduced to 1.8 V [139,169]. This diminishes the oxidation ability of $\text{OH}\cdot$ towards organic contaminations significantly.

2) Previous studies suggested that for dye molecules and in general organic compounds, the acid-base equilibrium of the molecule can play a significant role in its decomposition at different pH values [85]. This rationale was used to explain the higher degradation rate of phenol molecules in alkaline conditions [81]. Moreover, higher removal% (during the treatment stage) of MB in solutions with initial acidic conditions is in accordance with previous studies [150]. However, the effect of the initial pH on removal% during the post treatment stage was not considered previously.

3) It has been suggested that in alkaline conditions ($\text{pH} > 7$), $\text{OH}\cdot$ reacts selectively with carbonate ions which are the by-products of organic molecules degradation [85,123,125,170]. This competition between MB molecules and carbonate ions to react with $\text{OH}\cdot$ can possibly reduce the removal% of MB during the treatment stage, at initial pH of 10.12.

4) At highly alkaline solutions, since the concentration of hydroxyl ions (OH^-) exceeds the concentration of MB significantly, $\text{OH}\cdot$ can participate in a side reaction (Equation (3.25)) which transforms $\text{OH}\cdot$ to its less reactive conjugate base, O^- [85,135,171,172].



This transformation of OH⁻ to a less reactive species can possibly lower the removal% during the treatment stage for highly alkaline solutions.

We have established in section 3.5.1 that Cl⁻ plays an important role in the removal of MB, especially during the post treatment stage. As a result, it is plausible that the pH dependency of the reactions involving Cl⁻ and its derivatives can explain the pH dependency of the removal% at this stage, as shown in Figure 3.15(a) and 3.15(b). A quick investigation into the reactions proposed in this study for the effect of Cl⁻ (Equations (3.16)-(3.19)) shows that reactions (3.17) and (3.19) are highly pH dependent. When alkaline solutions are used (initial pH of 10.12), the concentration of OH⁻ is high. As a result, reaction (3.17) occurs in the reverse direction at a faster rate. This becomes more crucial considering the rate constants of the forward and reverse reactions ($k_{\text{For}}=10^5 \text{ M}^{-1}\text{S}^{-1}$ and $k_{\text{Rev}}=4.5 \times 10^7 \text{ M}^{-1}\text{S}^{-1}$ [141]). This means that lower concentrations of Cl₂⁻ are available to produce HOCl and as a result ¹O₂. Therefore, the removal% during the post treatment stage for alkaline solutions is small, as shown in Figure 3.15(a). On the other hand, for solutions with initial acidic conditions (initial pH of 2.8), the post treatment removal% is also insignificant. This can be explained based on the pH dependency of reaction (3.19). In a similar manner discussed above, in highly acidic solutions, the concentration of H⁺ is high. As a result, reaction (3.19) happens at a faster rate in the reverse direction. This means that lower concentrations of ¹O₂ would be available for reaction with MB during the post treatment stage. Based on the above-mentioned rationale, it can be hypothesized that near neutral condition (pH=6.4) represents the most balanced condition for reactions (3.17) and (3.19). As a result, the highest concentration of ¹O₂ can possibly be achieved for solutions with initial pH values in the neutral region. Therefore, the highest removal% for post treatment stage was obtained for initial pH of 6.4.

Figure 3.15(c) and 3.15(d) shows the overall change in the solution pH as a function of the initial pH and pH variation as a function of the treatment time, respectively. The highest pH change occurred for the solutions with the initial pH of 10.12. This is understandable since alkaline solutions are inherently depleted of H^+ . This facilitates the production of H^+ by reactions (3.12) and (3.13). It is worth mentioning that based on the results presented by Figure 3.15, the initial pH of the solution is crucial in determining the decomposition ability of the system. However, solutions treated by air plasma become acidic quickly. In other words, all the treated solutions share almost the same pH value for most of the treatment time, regardless of the initial pH value (Figure 3.15(d)). This means that the initial pH has negative or positive effects on one or some of the components of the system at the beginning of the process. However, the chemistry of the water treated by plasma is quite complex and further analysis and kinetic modeling is required to understand this phenomenon completely.

3.5.5. Effect of initial MB concentration

The decontamination capability of the technique against increasing concentrations of MB is investigated. The electrolyte consists of NaCl (50 mg/l) dissolved in MiliQ water. The initial pH of the solutions was set to near neutral values (pH=6.4-6.7). Although removal% decreased slightly at higher concentrations of MB, energy yield of the system increased significantly (Figure 3.16(a)) due to the higher concentration of MB degraded (the average power consumption used for energy yield calculations by Equation (3.2) is 13.7 ± 0.2 W). This can possibly be explained by means of the collision theory of molecules. When plasma is injected to the surface of water, primary oxidizing agents such as OH^\cdot and secondary species such as 1O_2 are formed in the solution.

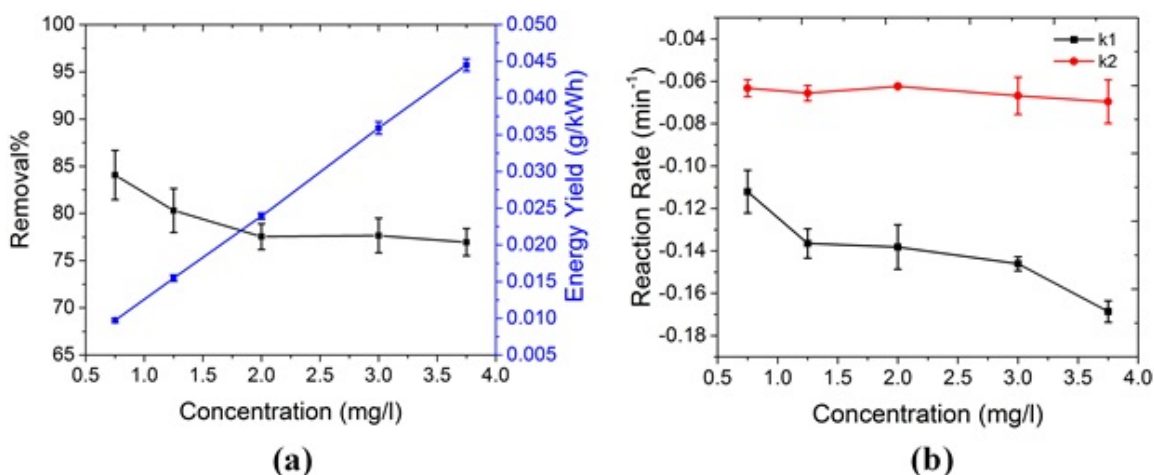


Figure 3.16. The efficiency of the plasma treatment system is evaluated against the increasing concentration of MB. (a) shows the change in the removal% and energy yield of the system as a function of MB concentration. Although removal% shows a slight decrease, the energy yield increases significantly as MB concentration increases. This is due to the fact that when higher concentrations of MB are present in the solution, the collision frequency between MB molecules and oxidizing agents is higher. For OH^\cdot , this is very critical since their lifetime is very short. This also reflects itself in the reaction rate of the MB degradation during both treatment and post treatment stages, as shown in (b). In (b), k_1 and k_2 represent the reaction rates of MB degradation during the treatment and post treatment stages, respectively. These rates were obtained by fitting the data to a pseudo-first-order kinetics equation (Equation (3.8)), separately for each stage. As shown by (b), regardless of the MB concentration, k_1 (reaction rate during the treatment stage) is always higher. This is due to the action of more powerful oxidizing agents (such as OH^\cdot) on MB molecules during the treatment stage. Moreover, higher reaction rates during treatment stage can be achieved if higher concentrations of MB are present in the solution. This reflects the importance of the collision frequency between MB molecules and OH^\cdot during this stage. On the other hand, the reaction rate during the post treatment stage (k_2) is significantly less sensitive to the concentration of MB. This is probably due to the fact that removal of MB during this stage is not only dependent on the collision frequency between MB molecule and oxidizing agents (such as $^1\text{O}_2$), but also it is limited by reactions that create $^1\text{O}_2$. The negative sign of the reaction rates only shows the decrease in the concentration of MB during the degradation process.

When number of MB molecules present in the solution is higher, the collision frequency between active species and MB is significantly higher. This has crucial impact on the process, especially in the case of OH^\cdot where the lifetime is very short. Therefore, the collision between MB molecules and active species can occur more efficiently. This also reflects itself in the reaction rate of the process, as shown in Figure 4(b). k_1 and k_2 show the decontamination reaction rates

during the treatment stage (with plasma present) and post treatment stage (without plasma), respectively. These rates were obtained by fitting the data with the pseudo-first-order kinetics equation (Equation (3.8)), separately for each stage. As shown in Figure 3.16(b), the reaction rate during the treatment stage is always higher than the post treatment stage, possibly due to the presence of stronger oxidizing agents such as OH^\cdot in this stage. Moreover, higher concentrations of MB resulted in higher reduction rates during the treatment stage. This can be explained by higher frequency of collisions between MB molecules and oxidizing agents, as discussed earlier. Finally, the reaction rate during the post treatment stage is almost constant, regardless of the concentration of MB. This indicates that the decontamination process during the post treatment stage mainly occurs by secondary active species, i.e. $^1\text{O}_2$. In the case of these secondary oxidizing species, the reaction rate with MB is not only dependent on the MB concentration, but also depends on the rate constants of reactions that produce $^1\text{O}_2$ (reactions (3.16)-(3.19)). This rational can possibly explain the lower sensitivity of k_2 to MB concentration.

Chapter 4: Degradation of pharmaceutical contaminants

4.1. Introduction

As described in Chapter 1, the presence of pharmaceutical compounds in various water bodies has received the attention of societies due to their increasing usage worldwide and their possible adverse effects on human and wildlife [1]. Previous studies have indicated that these compounds are present in the environment at very low concentrations (in the range of ng/l to µg/l) [173,174]. However, a report published by the World Health Organization (WHO) in 2011 acknowledged that the effect of long-term exposure to these compounds, even at low concentrations, is unknown and can be catastrophic [28]. This problem becomes more acute considering the rate of the population growth, the discovery of new drugs and the realization of new applications for existing drugs [2]. The introduction of pharmaceutical contaminants can occur through various pathways including human and animal excretion, improper disposal of unwanted drugs from houses and hospitals, incorrect waste disposal from pharmaceutical manufacturing, etc. [7]. Moreover, in Chapter 1, we introduced various classes of pharmaceutical compounds and discussed their negative effects on humans, wildlife and environment. This information can be found in Table 1.1. As mentioned previously, most of the pharmaceutical compounds can withstand conventional water treatment processes such as biological treatment [3–5]. Hence, they can by-pass conventional wastewater treatment plants and find their way into various water sources. As a result, the main goal of this chapter is to evaluate the efficiency of our novel plasma generation method for degradation of pharmaceutical compounds in water matrices that are relevant in real life situations. For this purpose, we chose to focus our attention on four popular compounds that belong to four different classes of pharmaceuticals. These compounds are: ampicillin (antibiotic), ibuprofen (NSAIDs), fluoxetine (antidepressant) and propranolol

(antihypertensive). The main water matrix used in this investigation is tap water due to its similarities to real life applications.

Amongst these pharmaceutical drugs, antibiotics and non-steroidal anti-inflammatory drugs (NSAIDs) are the most consumed drugs around the world. Reports indicated that more than 100,000 to 200,000 metric tons of antibiotics are used annually worldwide [175] ; amongst which the class of β -lactam antibiotics [176] (50-70% of all antibiotics) and more specifically the group of penicillin [177] (up to 44% of β -lactam class) form the largest consumption. The main concern regarding the presence of antibiotics in water is the emergence of antibiotic-resistant bacteria that can cause life-threatening infections such as methicillin-resistant *Staphylococcus aureus* (MRSA) [7,178]. Further negative impact of the presence of antibiotics in water includes disruption in metabolism of bacterial communities and interference with the photosynthesis of plants [50]. NSAIDs and in particular ibuprofen, an analgesic drug, are regarded as one of the most used drugs around the world [86]; annual production of ibuprofen exceeds 15,000 tons worldwide [179]. The hazardous effects of ibuprofen include interference with the growth of aquatic phototrophs, inhibition in reproduction (e.g. in snails) and lower fish survival [24]. Fluoxetine is normally prescribed to treat patients with major depressive disorder, eating disorder, panic disorder and obsessive-compulsive disorder. A report published by National Center for Health Statistics (NCHS) in 2011 revealed that between the years of 1988-1994 and 2005-2008, the rate of antidepressant consumption especially fluoxetine (known by its brand name Prozac®) amongst teens and adults (age 12 and older), increased by almost 400% in US [180]. The same statistics reported that between the years of 2005 and 2008, about 1 in every 10 Americans used some type of antidepressant medication, making this class of pharmaceuticals the third most prescribed medication in that year [180]. Similar type of studies in UK in 2013

indicated that the use of Prozac® has soared 500% during the past two decades [181]. Investigations performed by Bringolf et al. revealed that the presence of fluoxetine in freshwater can cause the bioaccumulation of this compounds in marine species. This bioaccumulation in turn resulted in the disruption of several aspects of reproduction in these species [182]. Propranolol is a beta-blocker used to treat chest pain, hypertension and heart rhythm disorder. A report published by WHO in 2012 indicated that approximately 75000-150000 tablets of propranolol are used annually in US [183]. Similar to fluoxetine, the presence of propranolol in freshwater can cause bioaccumulation in marine organisms [19].

4.2. Objectives

Based on the introduction given in section 4.1, the following objectives were defined for this chapter of the study:

- 1) Evaluate the feasibility of the Floating Electrode Streamer Corona Discharge (FESCD) setup for degradation of pharmaceutical compounds (ampicillin, ibuprofen, fluoxetine and propranolol) by means of standard water characterization methods such Total Organic Carbon (TOC).
- 2) Identify the degradation by-products using High Performance Liquid Chromatography-Mass Spectrometry (HPLC-MS) and,
- 3) Evaluate the application of Excitation-Emission Matrix (EEM) analysis for characterization of water and realizing possible connections between EEM and HPLC-MS analyses.

4.3. Experimental

4.3.1. Materials

Ampicillin sodium salt, ibuprofen, fluoxetine hydrochloride and propranolol hydrochloride (>98%, obtained from Sigma Aldrich Ontario, Canada) were the target contaminants used throughout this study. Potassium indigo trisulfonate (Sigma Aldrich Ontario, Canada) was used for detection of ozone in water. In order to prepare the solutions for plasma treatment, each contaminant was dissolved separately in tap water (100 mg/l) except for fluoxetine where a concentration of 25 mg/l was used. Tap water was used as the main water matrix due to its similarities to real life situations. The same concentration of the contaminants was also dissolved in MilliQ water (18.2 M Ω /cm) for comparison purposes.

4.3.2. Experimental setup

Figure 4.1 shows the schematic illustration of the experimental setup. To generate plasma from a single electrode, a sinusoidal wave at the resonance frequency of the helical resonator (1.65 MHz) is supplied by the function generator (Agilent 33522A, CA, USA) and fed to a power amplifier (2100L RF power amplifier, E&I Inc., NY, USA). More information on the working principles of the helical resonator is available in our previous publication [127]. The output of the power amplifier is used as the input for the helical resonator. The input voltage and current to the helical resonator are measured by means of an oscilloscope (TDS 2024C, Tektronix, OR, USA) and a current probe (CT2, Tektronix, OR, USA) connected to the oscilloscope, respectively (as shown in Figure 4.1).

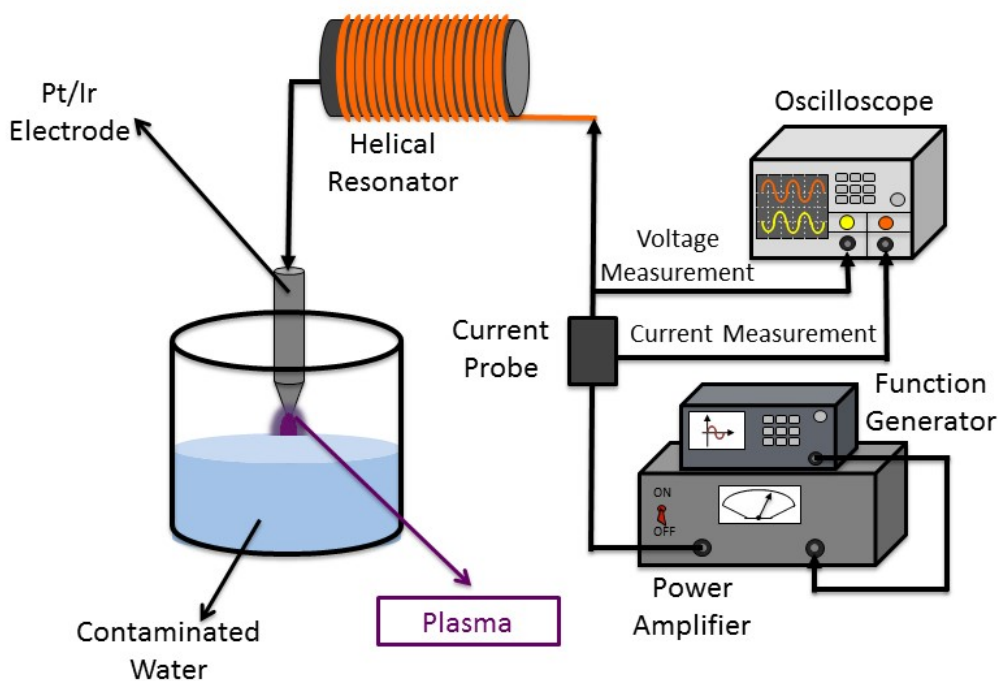


Figure 4.1. The schematic representation of the experimental setup is shown. Single electrode plasma in air at atmospheric pressure is created using a helical resonator. A sinusoidal wave at the resonance frequency of the resonator is fed to a power amplifier by a function generator. The input voltage and current to the helical resonator is measured to calculate the power consumption. A Pt/Ir electrode is used to generate the plasma due to its stability at high temperatures. The water samples are stirred by a magnetic stirrer to assure the homogeneity of the oxidation reactions.

The power input to the helical resonator was calculated using the multiplication of V_{rms} and I_{rms} (rms values of input voltage and current) with their corresponding phase angle (which was zero degrees when tuned to resonance [127] and producing plasma). Each solution (tap water or MilliQ water spiked by the desired concentration of each of the pharmaceutical compounds) was treated with plasma for various periods of 0, 0.5, 1, 2 and 3 hr. For each treatment time, 60 ± 1 ml of the desired solution was poured into a glass beaker (100 ml, Fisher Scientific, Ontario, Canada). To avoid over heating the plasma electrode, plasma was applied on top of the solution intermittently for 15 min, with 15 min off cycles in between. Therefore, treatment time of 1 hr, in

this study for instance consisted of 4 on-cycles (each 15 min) and 4 off-cycles (each 15 min) after each on-cycle. The distance between the electrode tip and water surface (air gap distance) and the input voltage to the resonator were kept constant at 2 mm and 71 V, respectively. *Pt/Ir* electrodes (conical shaped with the tip diameter of approximately 0.5 mm) were used for the generation of plasma, due to their stability at high temperatures. Magnetic stirring of the solution was employed to assure the homogeneity of the solution. The treatment chamber was open at the top during each experiment. Conductivity and pH values of the solutions were measured using a Fisher Scientific Accumet® Excel conductivity meter (XL60, Ontario, Canada) and a Mettler Toledo FiveEasy® pH meter equipped with InLab® Expert Pro-ISM probe (Ohio, US), respectively.

4.3.3. Characterization

To analyze the treated (0.5, 1, 2 and 3 hr) and untreated solutions (0 hr), three analysis methods were used, as described below.

4.3.3.1. Total Organic Carbon-Inorganic Carbon (TOC-IC)

To evaluate the degree of mineralization in each solution (both in tap water and MilliQ water), a TOC-IC analyzer (TOC-L, Shimadzu, Kyoto, Japan) was used. For each sample, the TOC was calculated by subtracting the value of the IC from the value of the Total Carbon (TC). TC and IC measurements were carried out based on the infrared absorption of carbon dioxide. Measurement of IC involves the acidification of the samples (by means of 0.1 M H_3PO_4) to convert HCO_3^- and CO_3^{2-} to CO_2 and subsequent quantification of the released CO_2 . TC was determined using the high temperature combustion method [184]. For each measurement, 40 ml of the desired solution was poured into a glass vial (Fisher Scientific, Ontario, Canada) and put in the analyzer auto

sampler (ASI-L, Auto Sampler, Shimadzu, Kyoto, Japan). To assure the accuracy of the measurements, each vial was thoroughly cleaned and preconditioned at 250 °C for 2 hr.

4.3.3.2. High Performance Liquid Chromatography-Mass Spectrometry (HPLC-MS)

The experimental procedure regarding the application of HPLC-MS was previously described in section 3.3.3. It is worth mentioning that due to the complexity of samples containing tap water, identification of unknown by-products in the solutions by HPLC-MS analysis was only performed only on samples with MilliQ water matrix.

4.3.3.3. Excitation-Emission Matrix (EEM)

Fluorescence EEM measurements were carried out using a Varian Cary Eclipse spectrophotometer (Agilent, USA). The spectrophotometer showed a maximum emission intensity of 1000 arbitrary units (a.u.). Xenon excitation source was used in this study and the excitation and emission slits were set to 5 nm. To obtain EEMs from samples, 4 ml of each sample was poured into a quartz cuvette. The excitation wavelength was incrementally increased from 200 nm to 400 nm, with steps of 5 nm. At each excitation wavelength, the emission was detected in the range of 200-650 nm, with 1 nm steps. In order to partially account for the Raleigh scattering, fluorescence signal of a blank sample (sample without the addition of ampicillin or ibuprofen, i.e. only tap water) was recorded and subsequently subtracted from the fluorescence spectra of the main samples. It has to be mentioned that EEM analysis was performed at room temperature using only samples with tap water matrix. pH of all samples was adjusted to 7 beforehand using 1 M solution of NaOH. EEMs were plotted using Origin 2015 software with 10 contour lines and emission intensities in the range of -10 to 1005 a.u. Keeping

the same intensity range for all the plots is very important since in this manner a clear change in the fluorescence signal can be observed as the treatment time increases.

4.3.3.4. Measurement of ozone concentration

In order to measure the concentration of ozone in the aqueous phase, Indigo dye method was used [185]. The stock solution of Indigo Reagent was prepared by dissolving 1 mM of potassium indigo trisulfonate salt in 20 mM phosphoric acid solution. A calibration curve for Indigo dye (shown by Figure 4.2) was obtained by diluting the stock solution with MilliQ water to various ratios and measuring the absorbance of the solution at 600 nm (UV/Vis spectrophotometer Varian Carey 50, Agilent, USA). The measurements were done during one cycle of the plasma treatment process, i.e. 15 min of treatment followed by 15 min of post treatment. Furthermore, to estimate the concentration of ozone consumed by one of the model pharmaceutical compound in this study, i.e. ampicillin, experiments were carried out in the absence and presence of ampicillin (100 mg/l) in MilliQ water. In each experiment, 60 ± 1 ml of the solution was poured into a glass beaker. At desired time intervals (either in the treatment or post treatment stage), 0.25 ml of the Indigo dye stock solution was added to the aqueous solution and the change in the absorbance was monitored in-situ by means of a fiber optic connected to the UV/Vis spectrophotometer. The difference between the ozone concentration measured in the presence and absence of ampicillin indicated the amount of ozone consumed by ampicillin molecules.

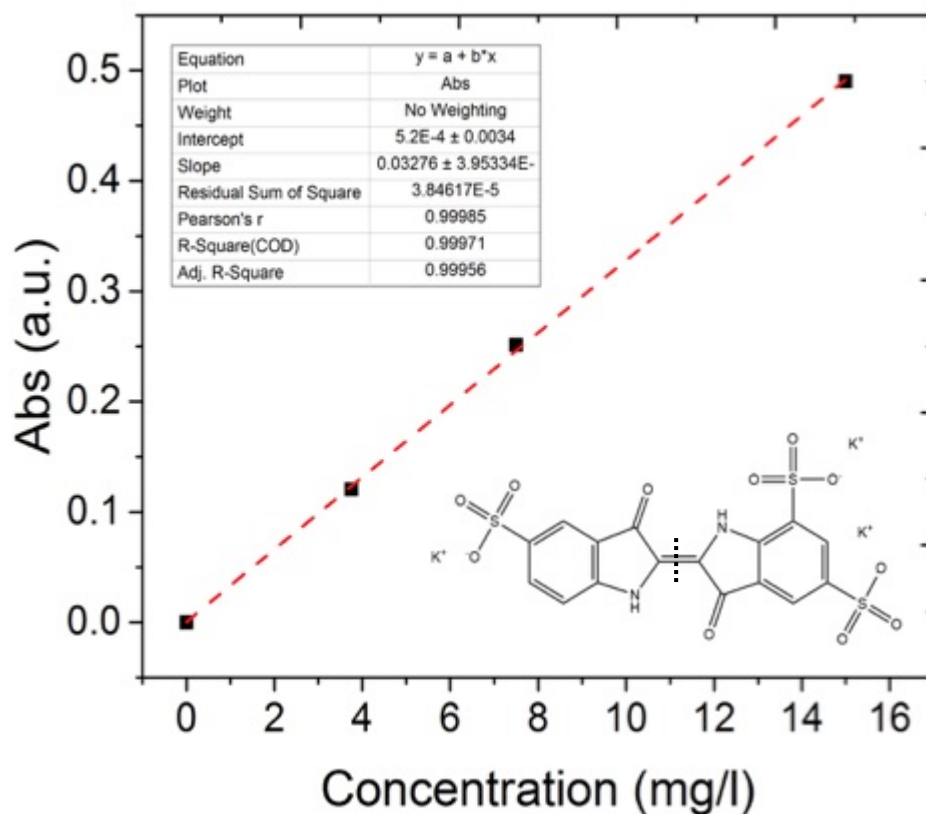


Figure 4.2. A calibration curve for indigo dye was obtained to correlate the concentration of the dye in the solution to its absorbance (UV/Vis spectroscopy at 600 nm). Based on the indigo method for measurement of ozone concentration in the solution [185], at low pH values, amino groups in the indigo dye molecules are protonated and they do not participate in any oxidation process. That is why the stock solution of the indigo trisulfonate is prepared in 20 mM solution of phosphoric acid. As a result, the only C=C double bond in the center of the molecule is expected to react with an ozone molecule. Thus, it can be assumed that one molecule of indigo trisulfonate reacts with one molecule of ozone. Using the calibration curve presented here, the absorbance of the indigo solution can be converted to the concentration of the indigo dye. Finally, the change in the concentration of the indigo dye represents the concentration of ozone in the solution.

4.4. Removal% and energy yield

In order to evaluate the treatment process in terms of the removal% and energy yield, chromatograms of each compound obtained during HPLC-MS analysis was used. The change in the chromatogram of ampicillin, ibuprofen, fluoxetine and propranolol as a function of the treatment time is shown in the insets of Figure 4.3(a), 4.3(b), 4.3(c) and 4.3(d), respectively. The

area under the curve for each compound was plotted as a function of the treatment time, as shown in Figure 4.3(a), 4.3(b), 4.3(c) and 4.3(d) for ampicillin, ibuprofen, fluoxetine and propranolol, respectively. It is clear that for all parent compounds the degradation follows an exponentially decaying behavior.

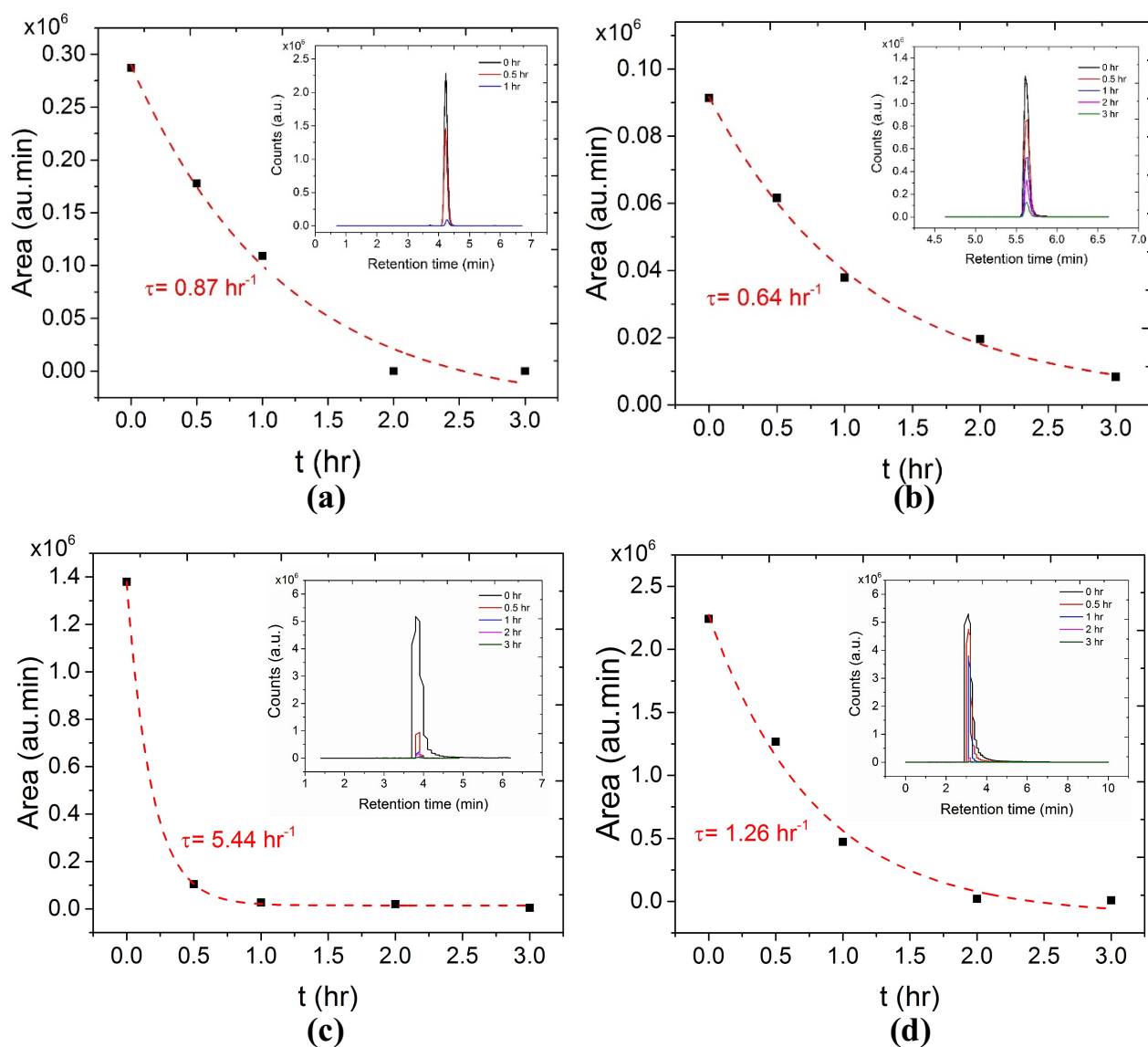


Figure 4.3. The change in the area underneath the curve in the chromatogram of (a) ampicillin, (b) ibuprofen, (c) fluoxetine and (d) propranolol as a function of time is shown. The insets show the Extracted Ion Chromatograms (EIC) at retention time of (a) 4.4 min, (b) 5.6 min, (c) 3.8 min and (d) 3.1 min corresponding to ampicillin (m/z of 350.11), ibuprofen (m/z of 206.13), fluoxetine (m/z of 310.14) and propranolol (m/z of 2601.6) molecules, respectively. The dash line in the graphs resulted from the fitting of the data to an exponential decay kinetics equation.

By fitting the data shown in Figure 4.3 with an exponentially decaying function ($R^2 > 0.99$), one can obtain the time constant for degradation of each compound. To calculate the removal%, Equation (4.1) is used for the case of each compound separately.

$$\text{Removal\%} = \left(1 - \frac{A}{A_0}\right) \times 100 \quad (4.1)$$

In Equation (4.1), A and A_0 show the area under the chromatogram's peak at any treatment time and before treatment (original peak area), respectively. Using the removal% obtained by Equation (4.1) in Equation (4.2), we can calculate the energy yield of the plasma treatment process.

$$\text{Energy Yield} = \frac{C_0 \times V \times R}{P \times t} \times 0.01 \quad (4.2)$$

In Equation (4.2), C_0 is the initial concentration of the parent compound in g/l, V is the volume of the treated sample, R is the final removal% after 3 hr, P is the power input to the helical resonator in kW and t is the duration of time in which power is consumed (in hr). The values of the degradation time constant, removal% and energy yield for each compound is summarized in Table 4.1. The results obtained in this study show that the lowest degradation time constant and hence removal% corresponds to ibuprofen molecules. This possibly shows that ibuprofen molecules are more recalcitrant towards reaction with various oxidizing agents (OH^\cdot , O_3 , etc.) created during the plasma treatment process.

Table 4.1. Degradation time constant, removal% and energy yield of the plasma treatment process obtained for each of the pharmaceutical compounds in this study is summarized.

Pharmaceutical Compound	Degradation time constant (hr ⁻¹)	Removal%	Energy Yield (g/kWh)
Ampicillin	0.87	100.00	0.13
Ibuprofen	0.64	90.91	0.12
Fluoxetine	5.44	99.66	0.03
Propranolol	1.26	99.64	0.13

The lowest energy yield was obtained for the case of fluoxetine (0.03 g/kWh), although the degradation of fluoxetine occurred with the fastest time constant (5.44 hr⁻¹). This is only due to the fact that the initial concentration of fluoxetine used in this study was 25 mg/l that is one fourth of the other compounds (100 mg/l). In general, the values of the energy yield obtained for various pharmaceutical compounds in this study are in the range of 0.12-0.13 g/kWh. We believe that improving the design of the treatment systems can further increase these values. For instance, the volume of the treated water can be significantly increased by using flow through systems in which water is circulated between a reservoir tank and a plasma treatment tank. It has to be mentioned that the degradation time constant, removal% and energy yield values calculated here are based on the chromatograms that obtained during HPLC-MS analysis. As mentioned in section 4.3.3.2, samples with MilliQ water were used for this analysis. As a result, values reported here for removal% and energy yield can be a slight overestimation of the values that may be obtained in real water matrices (such as tap water). This is due to the fact that in tap water, hydroxyl radical scavengers such as carbonate and bicarbonate ions can be present (as

discussed in section 3.5.3). These scavengers can interfere with the plasma treatment process and slow down the degradation process.

4.5. Degree of mineralization

The removal% calculated in section 4.4 only describes the degradation of the parent compounds, i.e. ampicillin, ibuprofen, fluoxetine and propranolol. However, the degradation of by-products and their evolution during a treatment process are of importance. A general idea about the evolution of the parent compounds and their by-products as an ensemble can be achieved by measuring TOC of the solutions. Figure 4.4 shows the change in the TOC of the solution containing ampicillin and ibuprofen. Figure 4.5 provides similar information for fluoxetine and propranolol. The change in the normalized TOC (TOC/TOC_0) and normalized IC (IC/IC_0) as a function of the treatment time are shown by Figure 4.4(a) and 4.4(b) for ampicillin in tap water and MilliQ water, respectively. While the degree of mineralization for ampicillin solutions in tap water is about 20%, this value for solutions made with MilliQ water is approximately 25% (TOC/TOC_0 of 0.8 versus TOC/TOC_0 of 0.75 at 3 hr). This again shows the inhibition role of scavengers such as CO_3^{2-} that might be present in tap water. As shown in Figure 4.4(a), the normalized IC of the ampicillin solutions in tap water decreased significantly. This behavior can be explained considering the initial IC of the tap water (about 23 mg/l-C) and the decrease in the pH of the solution treated by plasma (shown by Figure 4.6). As the treatment time increases, the pH of the solution decreases possibly due to the formation of species such as NO_3^- in water [100,150]. This acidification of the solution transforms the CO_3^{2-} and HCO_3^- , present initially in tap water, into CO_2 that eventually leaves the solution. As a result, normalized IC in tap water declines significantly.

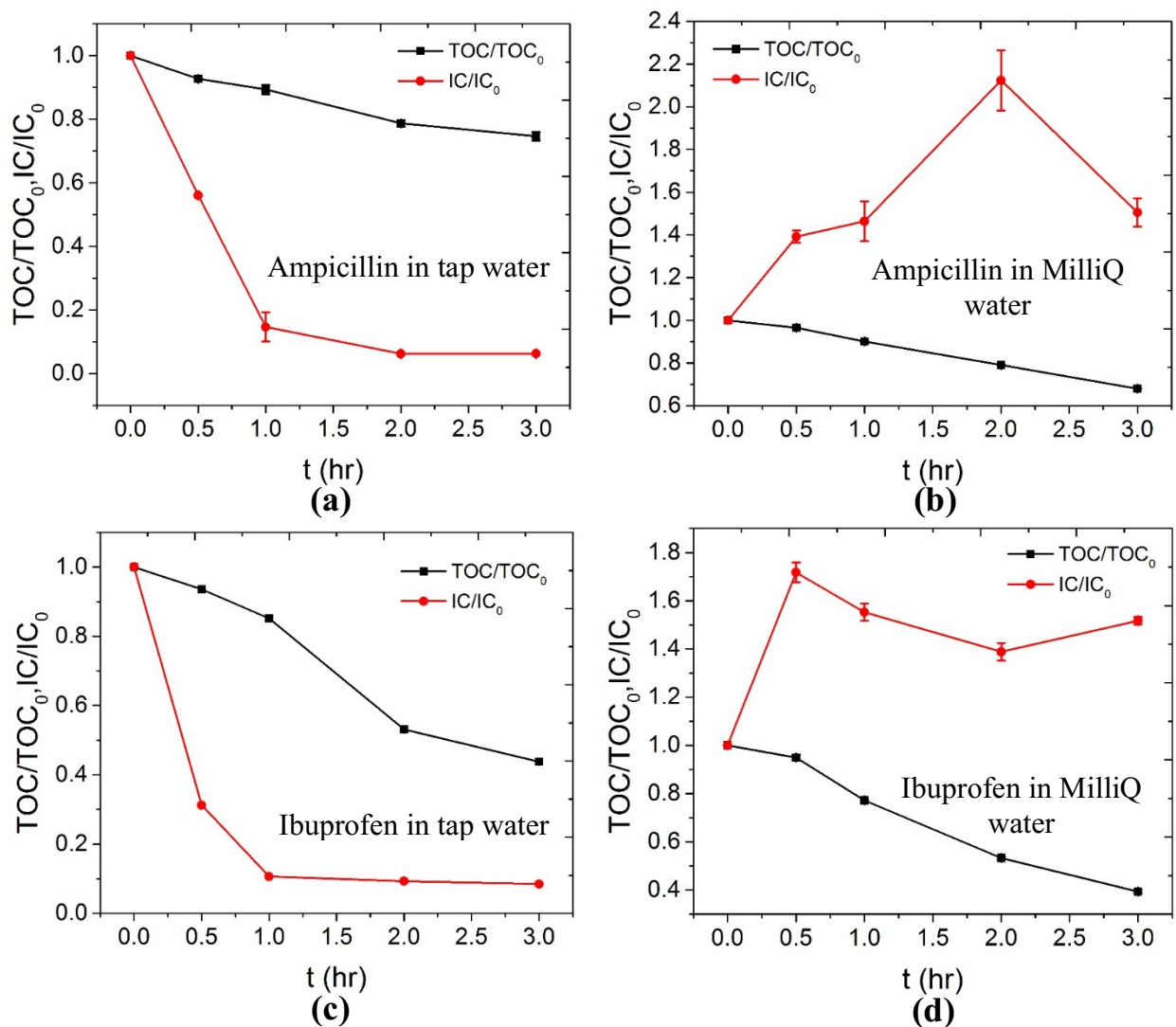


Figure 4.4. The change in the relative TOC (TOC/TOC_0) and IC (IC/IC_0) of the solutions is shown for (a) ampicillin in tap water (b) ampicillin in MilliQ water (c) ibuprofen in tap water and (d) ibuprofen in MilliQ water. Approximately, 20% and 25% mineralization was obtained for ampicillin in tap water and MilliQ water, respectively (as shown by TOC/TOC_0 in (a) and (b)). On the other hand, significantly higher mineralization was achieved for ibuprofen solutions (56% and 61% in tap water and MilliQ water, respectively). This shows that although the degradation rate was higher for ampicillin molecules (as discussed in Figure 4.3), the degradation by-products of ampicillin are more recalcitrant compared to those of ibuprofen. In both cases, the lower mineralization in tap water can be explained by the presence of variety of ionic species (especially carbonate and bicarbonate) in tap water that can interfere with the oxidation of the target molecules. It is worth-mentioning that regardless of the nature of the pharmaceutical contamination, the inorganic content (IC/IC_0) of the tap water solutions decreased. Ionic species such as (CO_3^{2-} , HCO_3^- , etc.) are the main contributors to the IC of tap water. During the plasma treatment process, the pH of the solution decreases significantly. This acidification of the solution transforms these ionic species to gaseous CO_2 , which leaves the solution. As a result, IC of tap water solutions decreases. Moreover, in both cases, the IC of MilliQ water solutions showed a slight increase followed by a decline. Since the initial IC of the MilliQ water is low (<1 mg/l-C), the increase in IC can be related to the formation of carbonate and bicarbonate ions from oxidized organic molecule. The subsequent decrease is possibly due to the acidification of the solutions, as discussed earlier.

The results shown in Figure 4.4(b) indicate that the normalized IC for ampicillin solutions in MilliQ water underwent an initial increase followed by a subsequent decrease. In explaining this behavior, it has to be mentioned that the initial IC of the solutions with MilliQ water is very low (<1 mg/l-C). The initial increase in IC/IC_0 in MilliQ water can possibly be attributed to the formation of carbonate ions from the degradation of ampicillin and its by-products [150]. The subsequent decline is probably due to the acidification of the solution due to the plasma treatment and transformation of carbonate ions into carbon dioxide, as described earlier. Figure 4.4(c) and 4.4(d) illustrates the change in TOC/TOC_0 and IC/IC_0 of solutions containing ibuprofen in tap water and MilliQ water, respectively. Similar to the case of ampicillin, the degree of mineralization in ibuprofen solutions is higher in MilliQ water compared to tap water. Moreover, the change in IC/IC_0 of solutions in tap water and MilliQ water is similar to the case of ampicillin. As a result, explanations given for the case of ampicillin hold for ibuprofen solutions.

Figure 4.5(a) and 4.5(b) show the change in the normalized TOC and IC of the solutions containing fluoxetine in tap water and MilliQ water, respectively. 60% and 65% mineralization was obtained in tap water and MilliQ water, respectively, for water samples spiked by 25 mg/l of fluoxetine. Figure 4.5(c) and 4.5(d) illustrate the change in the normalized TOC and IC for propranolol containing samples in tap water and MilliQ water, respectively. Approximately, 17% and 20% of the organic content of the solution was mineralized in tap water and MilliQ water. In both cases, the higher degree of mineralization for MilliQ water samples is due to the presence of various hydroxyl radical scavengers in tap water. Moreover, the difference between the changes in the normalized IC in both compounds is similar to the case of ampicillin and ibuprofen. As a result, the above-mentioned rationales hold in this case.

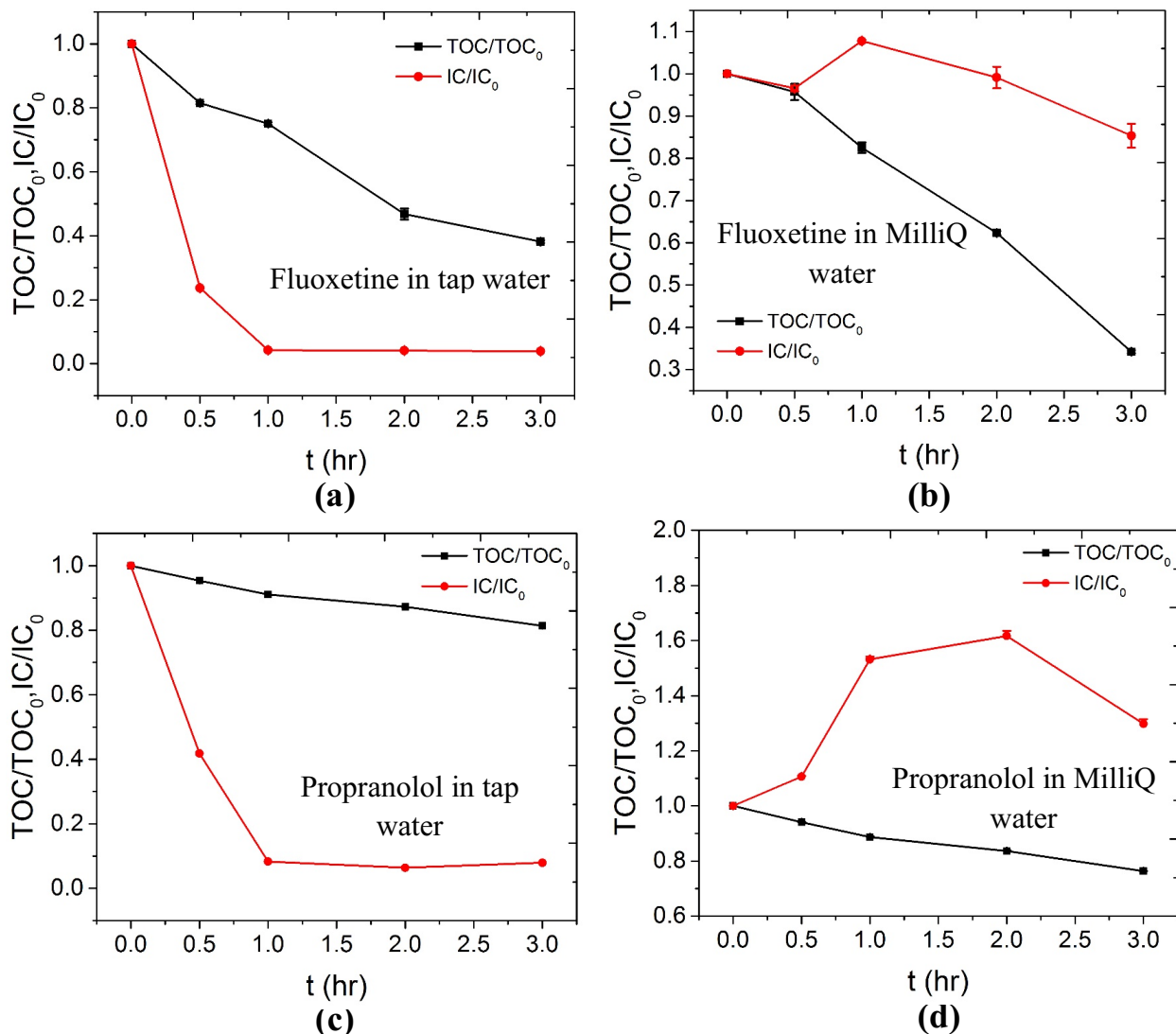


Figure 4.5. The change in the normalized TOC and IC as a function of the treatment time for solution containing fluoxetine in tap water and MilliQ water are shown in (a) and (b), respectively. 60% and 65% mineralization was obtained in tap water and MilliQ water, respectively, for water samples spiked by 25 mg/l of fluoxetine. (c) and (d) illustrate the change in the normalized TOC and IC for propranolol containing samples in tap water and MilliQ water, respectively. Approximately, 17% and 20% of the organic content of the solution was mineralized in tap water and MilliQ water. In both cases, the higher degree of mineralization for MilliQ water samples is due to the presence of various hydroxyl radical scavengers in tap water. Moreover, the difference between the changes in the normalized IC in both compounds is similar to the case of ampicillin and ibuprofen. As a result, the above-mentioned rationales hold in this case.

Table 4.2. The degree of mineralization of each compound in two different water matrices is summarized.

Pharmaceutical Compound	Degree of mineralization (%)	
	Tap water	MilliQ water
Ampicillin	20	25
Ibuprofen	56	61
Fluoxetine	60	65
Propranolol	17	20

Table 4.2 presents a summary of the degree of mineralization of each pharmaceutical compound studied in this work. It is interesting to note that the highest degree of mineralization was obtained from fluoxetine and ibuprofen containing solutions. These two compounds also showed the highest (5.44 hr^{-1} in the case of fluoxetine) and the lowest (0.64 hr^{-1}) degradation time constants, as shown in Table 4.1. This shows that the degradation of the parent compound and its by-products is fast in the case of fluoxetine. In the case of ibuprofen however, although ibuprofen itself is more recalcitrant compared to the other parent compounds, its degradation by-products as a whole are more prone to oxidation in the plasma treatment. The evolution of the degradation by-products and its pathway will be discussed in the next section (section 4.6).

Finally, as mentioned in the discussions regarding the change in the normalized IC of the solutions, the decrease in the pH plays an important role. As a result, we measured the pH and also conductivity of the solution made with tap water and MilliQ water, spiked with different pharmaceutical contaminants. These are shown in Figure 4.6. Regardless of the contaminant (ampicillin, ibuprofen, fluoxetine or propranolol) and the type of the water matrix (tap water or MilliQ water), the pH of the solutions decreased and the conductivity increased significantly.

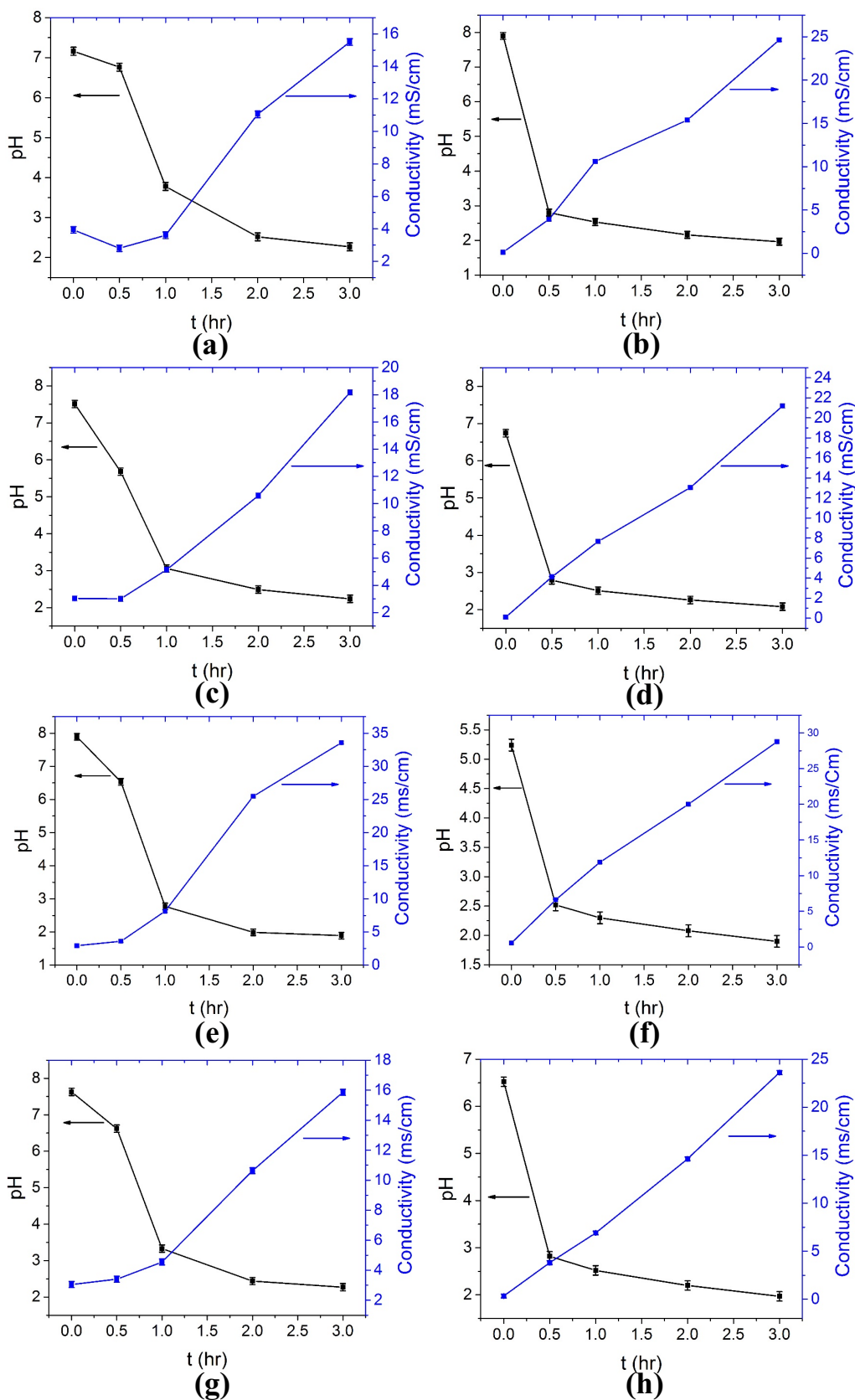


Figure 4.6. The change in the solution pH and conductivity are shown as a function of treatment time for (a) ampicillin in tap water (b) ampicillin in MilliQ water (c) ibuprofen in tap water (d) ibuprofen in MilliQ water, (e) fluoxetine in tap water (f) fluoxetine in MilliQ water (g) propranolol in tap water and (h) propranolol in MilliQ water.

This is probably due to the introduction of the nitrogen-based compounds to water ($\text{NO}_{(\text{aq})}$ and $\text{NO}_{2(\text{aq})}$) and subsequent formation of ionic species such as NO_2^- , NO_3^- and H^+ in the solutions [150]. One interesting observation is that the above-mentioned changes occurred faster when MilliQ water is used as the water matrix. This can be attributed to the presence of various ionic species in tap water such as carbonate and bicarbonate that can interact with the species created by plasma.

4.6. Degradation by-products and pathway

Sections 4.4 and 4.5 dealt with the degradation of the parent compounds (ampicillin, ibuprofen, fluoxetine and propranolol) and the combined evolution of the organic content in the solution, respectively. One important step in treatment of organic contaminants in water is the identification of the degradation by-products. For this means, we used HPLC-MS analysis on solutions with MilliQ water matrix.

4.6.1. Degradation of ampicillin

Table 4.3 shows a summary of the detected chemical species in ampicillin solutions treated for various periods. It is interesting to note HPLC-MS could not detect any compounds for treatment periods greater than 1 hr. Moreover, beside ampicillin, the only detected by-product with a known structure is ampicilloic acid. This compound was only present at the beginning of the treatment process (until 30 min treatment) and disappeared afterwards.

Table 4.3. Chemical species detected by HPLC-MS for ampicillin solutions.

Treatment Time (hr)	Detected m/z	Identification	Ratio
0	350.11	Ampicillin	1.000
	368.12	Ampicilloic acid	0.063
0.5	350.11	Ampicillin	0.625
	368.12	Ampicilloic acid	0.016
	366.11	P1	0.013
	382.1	P2	0.011
	259.07	P3	0.008
	349.09	P4	0.017
	333.09	P5	0.004
1	322.12	P6	0.004
	350.11	Ampicillin	0.031
	366.11	P1	0.003
	382.1	P2	0.016
	349.09	P4	0.006
2	398.1	P7	0.004
	-----	-----	0.000
3	-----	-----	0.000

*The ratio is calculated by dividing the peak intensity (count) of each compound by the peak intensity of the parent compound.

Based on the chemical species detected by HPLC-MS for ampicillin solution, a degradation pathway was proposed, as shown by Figure 4.7. Three major reaction pathways can be imagined for ampicillin solutions. The first reaction pathway is the hydrolysis of ampicillin molecules that results in the formation of ampicilloic acid. This reaction pathway is completely independent of the plasma treatment process and it is due to the dissolution of the ampicillin sodium salt in water. Based on the by-products detected by HPLC-MS, the other two reaction pathways that happened as a direct result of plasma treatment are reaction with hydroxyl radicals and with ozone molecules. By-products such as P1, P2, P4 and P7 were formed by addition of one or multiple oxygen atoms to the organic molecules.

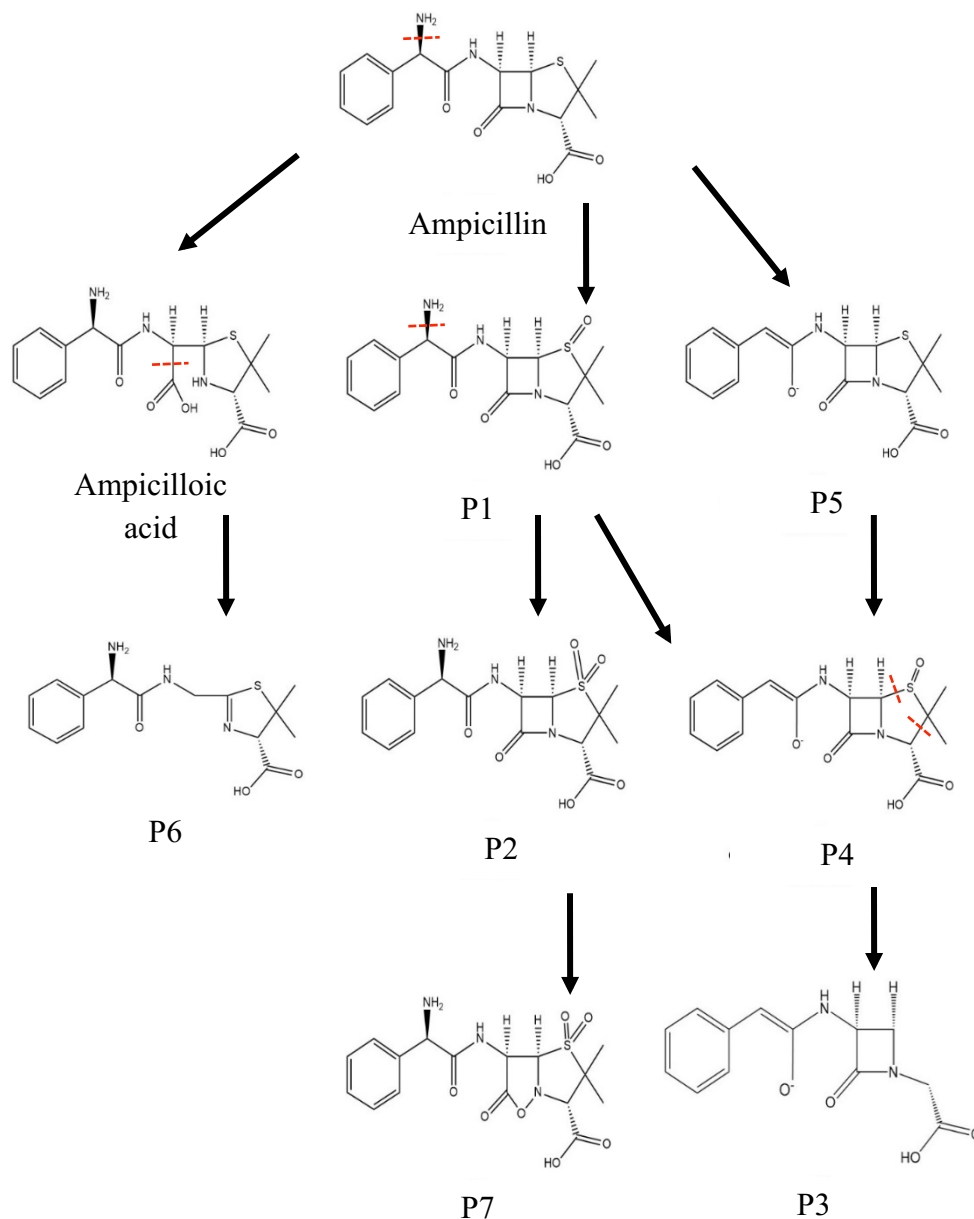


Figure 4.7. A degradation pathway is suggested for ampicillin in MilliQ water. Three major reactions have been identified, based on the species detected by HPLC-MS. The first reaction is the hydrolysis of the ampicillin molecules (formation of ampicilloic acid). This occurs as a result of the dissolution of ampicillin sodium salt in water and it is independent of the degradation processes. The other two chemical reactions are reaction of organic molecules with hydroxyl radicals and ozone molecules. By-products such as P1, P2, P4 and P7 were formed by addition of one or multiple oxygen atoms to the organic molecules. This may be explained by the action of ozone. On the other hand, by-products such as P3, P5, P6, etc. were formed due to the cleavage of chemical bonds (shown by red dash line). This phenomenon is probably due to the degradation of organic molecules by hydroxyl radicals. Small portion (20-25%) of the by-products shown here were eventually mineralized as suggested by the TOC data (Figure 4.4(b)). Moreover, a larger portion (75-80%) of the by-products was further broken down to small organic molecules. These molecules were not detected by HPLC-MS, as suggested by Table 4.3 for treatment times of 2 hr and 3 hr.

This may be explained by the action of ozone. Generally, during a plasma treatment process in ambient air, ozone is possibly created from oxygen and dissolves in the aqueous phase, as discussed in section 2.1.2.3. The presence of ozone in the solution will be further explored in section 4.8.

On the other hand, by-products such as P3, P5, P6, etc. were formed due to the cleavage of chemical bonds (shown by red dash line). This phenomenon is probably due to the degradation of organic molecules by hydroxyl radicals. It is worth noting that the degradation of the by-product P4 to P3 results in the detachment of one dimethyl sulfoxide (DMSO) molecule from one P4 molecule. The formation of a brownish color in the solution at initial steps of the plasma treatment observed during the experiments is probably due to the formation of DMSO in the solution during these stages. This brownish color faded away at later stages of the plasma treatment (2 hr and 3 hr treatment period), indicating that DMSO molecules were broken down further to form smaller molecules. Considering the results obtained by HPLC-MS and TOC analysis for solutions containing ampicillin, one can conclude that 20-25% of the organic molecules shown here were completely mineralized after 3 hr of plasma treatment. The rest of 70-75% of the organic content remained in the solution are possibly small organic molecules that could not be detected by HPLC-MS.

4.6.2. Degradation of ibuprofen

HPLC-MS was also used to determine the degradation by-products of plasma treated solutions containing ibuprofen, a summary of which is given in Table 4.4. Unlike the case of ampicillin, ibuprofen and its by-products were detected even after 3 hr of plasma treatment. However, the number of the detected by-products gradually decreased from treatment period of 1 hr to 3 hr.

Table 4.4. Information on the species detected by HPLC-MS for ibuprofen solutions.

Treatment Time (hr)	Detected m/z	Identification	Ratio*
0	206.13	Ibuprofen	1.000
	190.14	B4	0.020
0.5	134.11	B5	0.082
	270.11	B2	0.036
	178.14	B3	0.036
	222.13	B1	0.127
	206.13	Ibuprofen	0.682
	193.0514	B8	0.019
1	150.1	B11	0.041
	226.12	B6	0.016
	190.14	B4	0.018
	256.13	B7	0.028
	175.1137	B9	0.025
	222.13	B1	0.015
	178.14	B3	0.082
	206.13	Ibuprofen	0.409
	270.11	B2	0.027
2	134.11	B5	0.127
	270.11	B2	0.064
	206.13	Ibuprofen	0.209
	226.12	B6	0.015
	193.0514	B8	0.015
3	165.0565	B12	0.017
	150.1	B11	0.032
	175.1137	B9	0.026
	206.13	Ibuprofen	0.100

*The ratio is calculated by dividing the peak intensity (count) of each compound by the peak intensity of the parent compound.

Using the chemical species presented in Table 4.4, a degradation pathway was proposed for ibuprofen, as shown in Figure 4.8. Two major reaction pathways can be considered for the degradation of ibuprofen and its by-products. In the first pathway, ozone molecules can react with ibuprofen molecules.

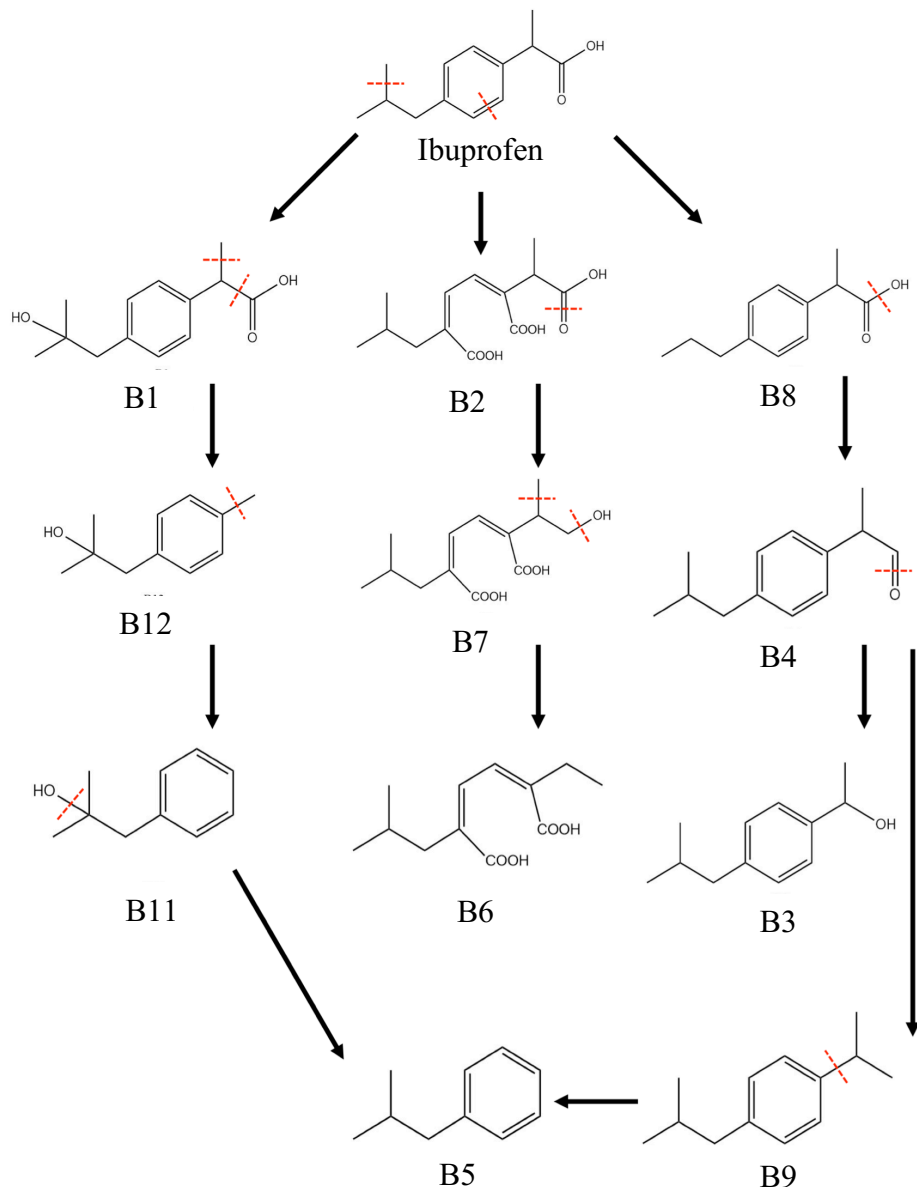


Figure 4.8. A degradation pathway is proposed for ibuprofen molecules. The two main reaction pathways include the reaction with hydroxyl radicals and ozone molecules. The reaction by-products such as B2 suggest that ozone molecules possibly cleave the aromatic ring and create carboxylic acid functional groups. Hydroxyl radicals react with organic molecules in two ways. The first pathway is the hydroxylation of ibuprofen molecules (formation of B1). Since hydroxyl functional group is an electron-donating group (EDG), it increases the electron density of the neighboring bonds through the inductive effect. As a result, the bonds near the hydroxyl group become stronger. That is probably why the further degradation of B1 starts from the opposite side of the molecule (formation of B12), until the aliphatic chain is completely cleaved (B11). The second pathway in which hydroxyl radicals react with the parent compound and its by-products is through the direct cleavage of bonds (by-products such as B4, B7 and B8). A comparison between the results presented here and TOC measurements (Figure 4.4(d)) indicates that although the smallest by-product (detected by HPLC-MS) is B5 (m/z of 134.11), further degradation by plasma treatment resulted in approximately 60% mineralization of organic compounds.

The reaction by-products such as B2 suggest that ozone molecules possibly cleave the aromatic ring in ibuprofen molecules and create carboxylic acid functional groups. A More important reaction pathway is through the reaction of hydroxyl radicals with organic molecules. Hydroxyl radicals react with organic molecules present in the ibuprofen containing solutions in two ways. The first pathway is the hydroxylation of ibuprofen molecules (formation of B1). Since the hydroxyl functional group is an electron-donating group (EDG), it increases the electron density of the neighboring bonds through the inductive effect. As a result, the bonds near the added hydroxyl group become stronger. That is probably why the further degradation of B1 starts from the opposite side of the molecule (formation of B12), until the aliphatic chain is completely cleaved (B11). The second pathway in which hydroxyl radicals react with the parent compound and its by-products is through the direct cleavage of bonds (by-products such as B4, B7 and B8). Results presented in Figure 4.8 indicate that the smallest detected by-product in ibuprofen solutions is B5 (m/z of 134.11). However, a comparison with TOC measurements (Figure 4.4(d)) shows that further degradation of this compound by plasma results in approximately 60% mineralization.

4.6.3. Degradation of fluoxetine

Table 4.5 summarizes the detected chemical species by HPLC-MS along with their m/z for water samples containing fluoxetine and treated for various periods of time. Similar to the case of ibuprofen, the parent compound (fluoxetine) was detected even in the samples treated for 3 hr by plasma. Based on the species summarized in Table 4.5, a degradation pathway was suggested for fluoxetine, as shown by Figure 4.9.

Table 4.5. Information regarding the chemical species detected in fluoxetine containing solutions by HPLC-MS.

Treatment Time (hr)	Detected m/z	Identification	Ratio*
0	310.14	Fluoxetine	1.000
0.5	326.13	F1	0.015
	310.14	Fluoxetine	0.267
1	326.13	F1	0.004
	310.14	Fluoxetine	0.080
	249.1	F5	0.003
	255.16	F2	0.002
	220.09	F6	0.006
2	326.13	F1	0.002
	310.14	Fluoxetine	0.067
	272.16	F7	0.003
	227.12	F3	0.003
	220.09	F6	0.005
3	170.11	F10	0.010
	213.12	F4	0.005
	310.14	Fluoxetine	0.013
	272.16	F7	0.003
	147.04	F9	0.006
	177.05	F8	0.010
	227.12	F3	0.003
	220.09	F6	0.005

*The ratio is calculated by dividing the peak intensity (count) of each compound by the peak intensity of the parent compound.

Unlike the case of ampicillin and ibuprofen where both mechanisms of interaction with hydroxyl radicals and ozone molecules were involved, the only degradation mechanism observed for fluoxetine and its by-products is reaction with hydroxyl radicals. Hydroxyl radicals can react with organic molecules in two ways. The first process is known as the hydroxylation of the molecules where a hydroxyl functional group is added to the structure. This is evident in the formation of by-products such as F1, F7 and F10.

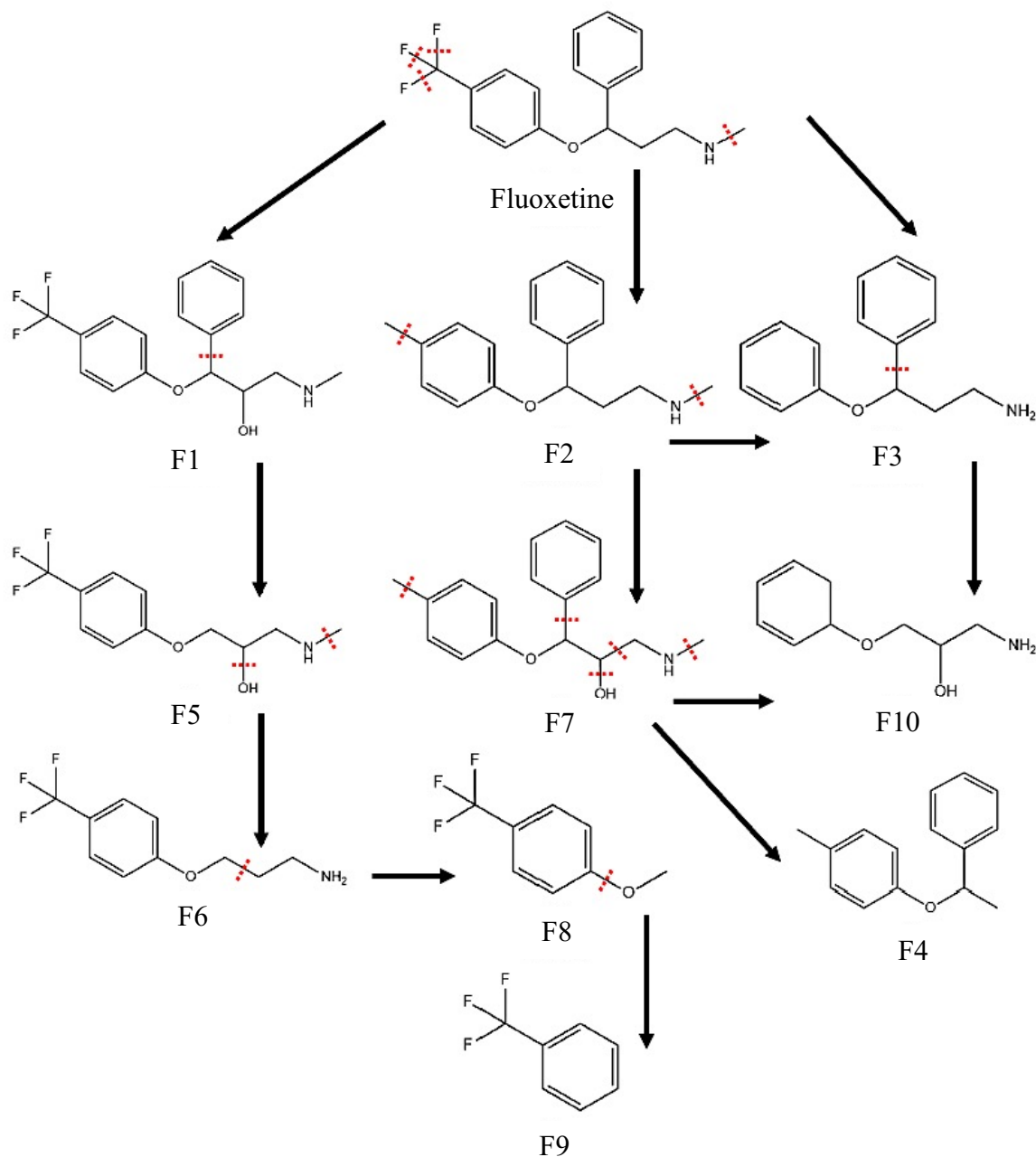


Figure 4.9. A degradation pathway was proposed for fluoxetine based on the specie detected by HPLC-MS analysis. The only mechanism involved in the degradation of fluoxetine and its by-products is through hydroxyl radicals. Hydroxyl radicals can react with organic molecules in two ways. The first process is known as the hydroxylation of the molecules where a hydroxyl functional group is added to the structure. This is evident in the formation of by-products such as F1, F7 and F10. In the other hand, hydroxyl radicals can cause the cleavage of the chemical bonds in the structure. This can be seen in transformation of F1 to F5, F6 to F8, F8 to F9, etc.

On the other hand, hydroxyl radicals can cause the cleavage of the chemical bonds in the structure. This can be seen in transformation of F1 to F5, F6 to F8, F8 to F9, etc. Another process that is involved in the degradation pathway, shown in Figure 4.9, is the reduction of organic molecules by hydrogen radicals ($H\cdot$). Hydrogen radicals are the direct result of the collision of energetic electrons by water molecules [85], as described by Equation (2.10) in section (2.1.2.3). The involvement of hydrogen radicals in the reduction of organic molecules can be seen in detachment of fluorine atoms from the structure (formation of F2 from fluoxetine). This process can be explained in this manner. Imagine the case where fluorine atoms are detached as fluoride ions (F^-). The detachment of three fluorine atoms from fluoxetine in the form of fluoride ions leaves the carbon atom in the structure as a carbon ion (C^{3+}). This means that for the formation of a methyl group (CH_3) at that end of the structure, hydrogen should be involved in the form of three negative ions (H^-), which is not rational. This process can be explained by the role of hydrogen radicals. In this process, fluorine atoms detach from the structure as radicals and leave the carbon radical behind. This carbon radical is terminated by hydrogen radicals to form the methyl group. Results presented in Figure 4.9 indicate that the smallest by-product that contains fluorine is F9. Moreover, F4 is the smallest by-product that does not possess fluorine atoms in its structure. A comparison with the TOC results obtained for fluoxetine containing solutions (Figure 4.5(b)) shows that further degradation of these by-products resulted in 65% mineralization of the organic compounds. The rest of the 35% of the organic content is in the form of the compounds shown in Table 4.5 at treatment time of 3 hr.

4.6.4. Degradation of propranolol

HPLC-MS analysis was used to determine the degradation by-products of propranolol during the plasma treatment process. Table 4.6 presents a summary of the species found by HPLC-MS analysis.

Table 4.6. Degradation by-products of propranolol detected by HPLC-MS.

Treatment Time (hr)	Detected m/z	Identification	Ratio*
0	260.16	Propranolol	1.000
	290.13	P4	0.073
	281.11	P5	0.027
	274.14	P3	0.043
	292.15	P2	0.050
	276.16	P1	0.233
	265.12	P6	0.070
	218.11	P7	0.027
	260.16	Propranolol	0.533
1	281.11	P5	0.053
	274.14	P3	0.023
	276.16	P1	0.030
	292.15	P2	0.040
	290.13	P4	0.058
	265.12	P6	0.040
	260.16	Propranolol	0.023
2	260.16	Propranolol	0.004
3	260.16	Propranolol	0.001

*The ratio is calculated by dividing the peak intensity (count) of each compound by the peak intensity of the parent compound.

It is interesting to note that HPLC-MS analysis could not detect any by-products for treatment times of 2 hr and 3 hr. The only species large enough to be detected at these treatment times is the parent compound, i.e. propranolol, although at very low concentrations considering the removal% (99.64%) discussed in section 4.4.

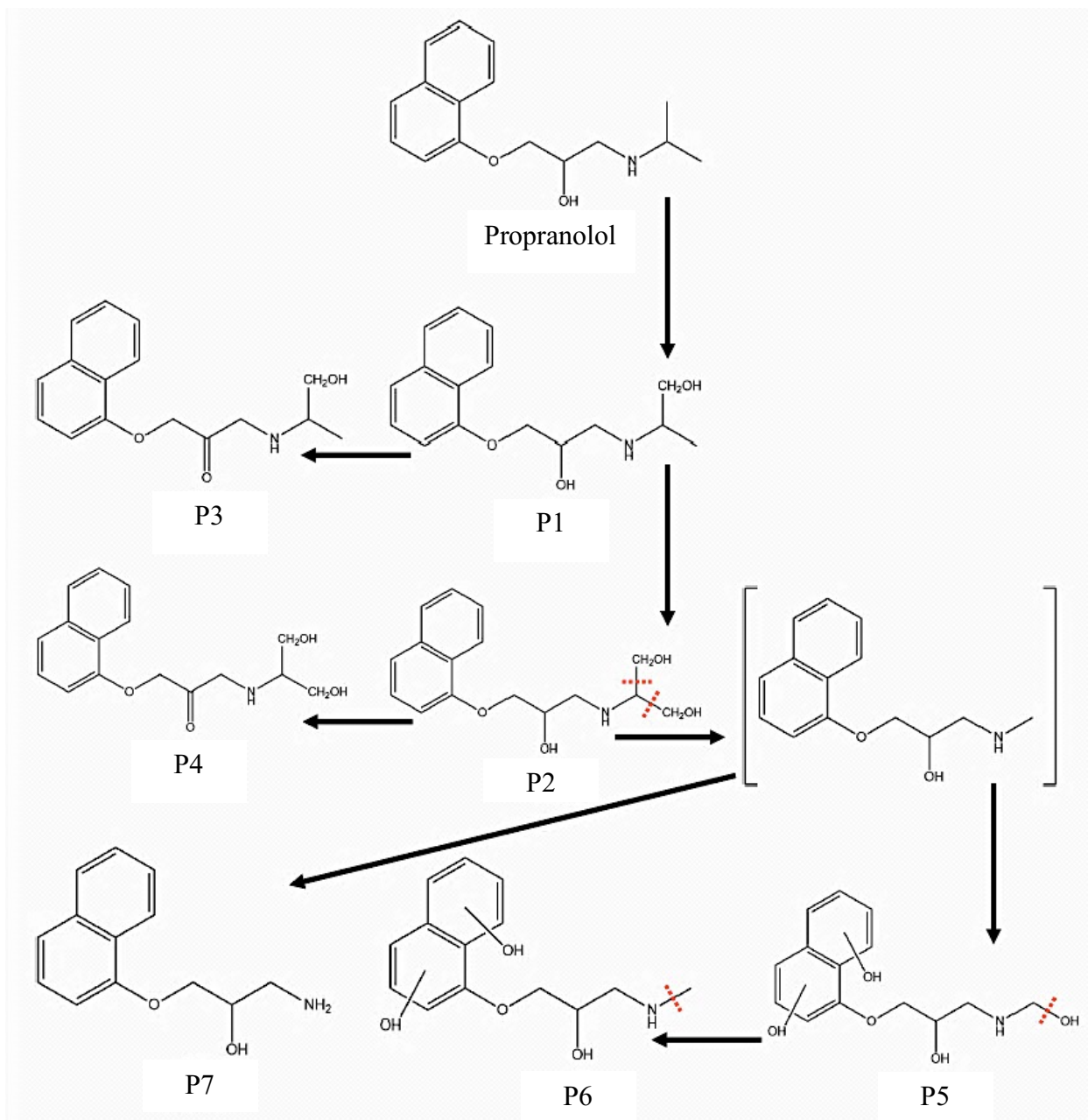


Figure 4.10. A degradation pathway was suggested for propranolol during the plasma treatment process. The main degradation process is through the action of hydroxyl radicals. This process shows itself in two ways. The first pathway is by hydroxylation of the organic molecules. This in turn can occur in two different positions. The first position is the hydroxylation of the methyl groups (CH_3) at the end of the chain to form CH_2OH at this position. This can be seen in the formation of P1 and subsequently P2 from propranolol and the formation of P5. The second position for hydroxylation is in the aromatic ring (P5 and P6). This process is known to be the most common oxidative degradation of organic compounds [186]. The second process involving hydroxyl radicals is the direct cleavage of the bonds. This can be seen in the formation the transient by-product (in the bracket) and transformation of P5 to P6.

This also implies that propranolol molecules are more recalcitrant towards oxidation by various oxidizing agents compared to their by-products. As discussed in section 4.5, the degree of mineralization for solutions containing propranolol was approximately 20%. One can hypothesize that 80% of the solution organic content treated for 3 hr by plasma consisted of propranolol itself and organic molecules that were too small to be detected by HPLC-MS. Figure 4.10 illustrates the degradation pathway proposed for propranolol based on the species detected by HPLC-MS. The main degradation process for propranolol molecules is through the action of hydroxyl radicals. This process shows itself in two ways. The first pathway is by hydroxylation of the organic molecules. This in turn can occur in two different positions. The first position is the hydroxylation of the methyl groups (CH_3) at the end of the chain to form hydroxymethyl functional groups (CH_2OH) at this position. This can be seen in the formation of P1 and subsequently P2 from propranolol and the formation of P5. The second position for hydroxylation is in the aromatic ring (P5 and P6). This process is known to be the most common oxidative degradation of organic compounds [186]. The second process involving hydroxyl radicals is the direct cleavage of the bonds. This can be seen in the formation the transient by-product (in the bracket) and transformation of P5 to P6. Another oxidation pathway that can be observed in the degradation pathway is the process known as the oxidation of secondary alcohols to ketones. This can be seen in the transformation of P3 from P1 and P4 from P2. P3 and P4 are both ketones that are resulted from the oxidation of alcohols (P1 and P2). This can be done through the action of ozone molecules on the above-mentioned alcohols [187].

4.7. Excitation-Emission Matrix (EEM)

As we discussed in section 4.6, HPLC-MS analysis was used to identify the degradation by-products of ampicillin, ibuprofen, fluoxetine and propranolol. Based on these by-products, a

degradation pathway was proposed for each contaminant. However, identification of unknown compounds by HPLC-MS is only possible for solutions with a simple water matrix, i.e. MilliQ water. Here in this section, we propose the application of EEM analysis to follow the degradation of the contaminants in more complex water matrices such as tap water. In general, EEM analysis is based on the fluorescence property of the organic molecules. The result of such a study is normally shown as contour maps with the excitation wavelength on the y-axis and the emission wavelength on the x-axis. The emission intensity of the compounds in the solution is shown as contour maps. Regarding the application of EEM analysis to characterize treated water containing pharmaceutical contaminants, one can conduct the experiment at various time intervals during the plasma treatment. Then the change in the fluorescence intensity or the position of the signal in the EEM map can be related to the possible by-products formed during the treatment.

4.7.1. EEM analysis of ampicillin solution

Figure 4.11 depicts the evolution of the fluorescence signal for solutions containing ampicillin as a function of the treatment time. Figure 4.11(a) illustrates the EEM signal for the blank solution (tap water without ampicillin) as the control. The change in the fluorescence signal of the solutions containing ampicillin and its by-products is shown in Figure 4.11(b) through Figure 4.11(f), corresponding to the treatment times of 0 hr to 3 hr, respectively. It is interesting to note that at the beginning of the plasma treatment process (30 min, Figure 4.11(b)), the emission intensity of the solution increased. This was followed by a decline in the intensity at longer treatment times until the fluorescence signal almost disappeared at treatment time of 3 hr (Figure 4.11(f)). To have an initial understanding of fluorescence signals and interpret their changes, few fundamental points should be taken into account.

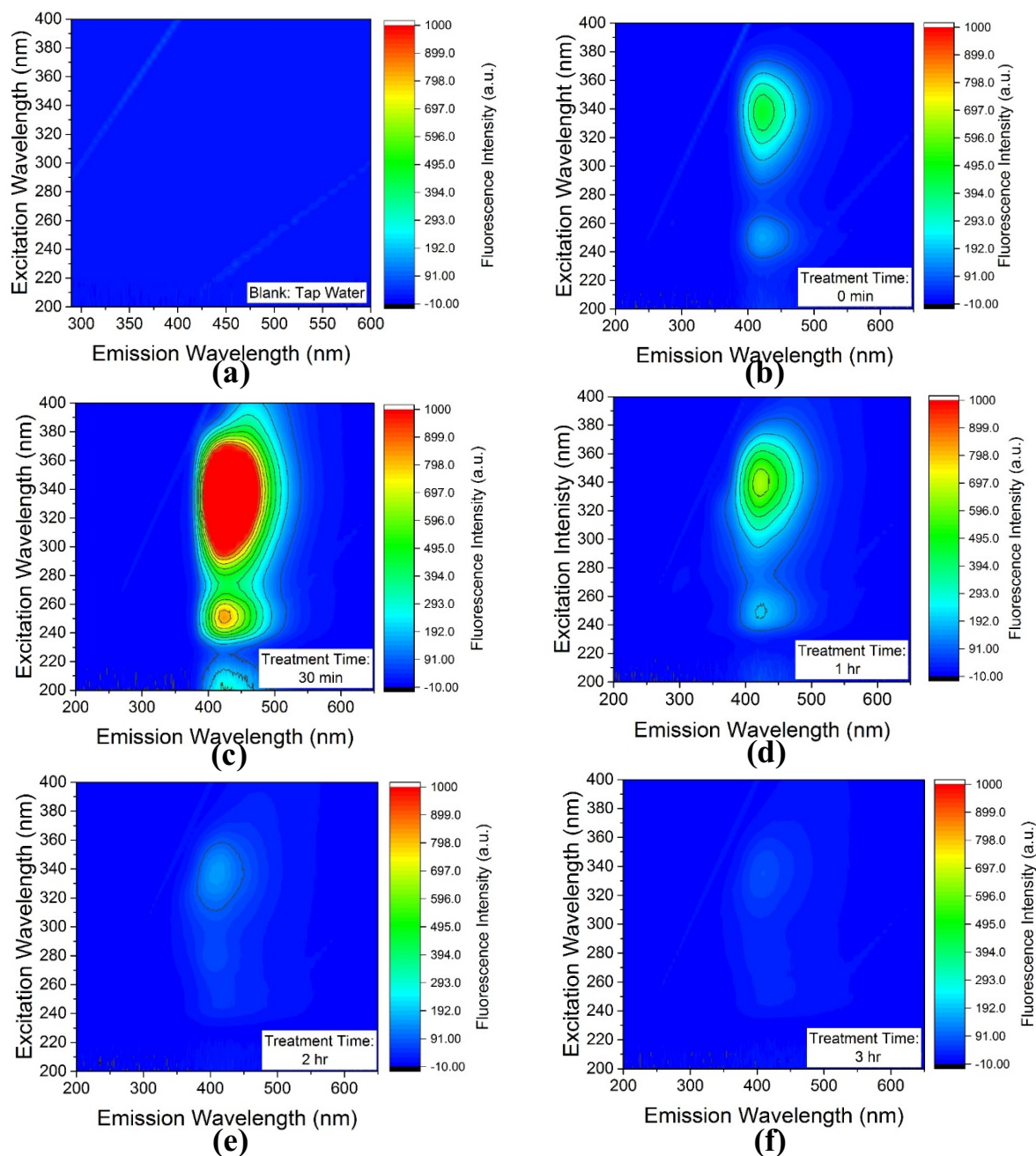


Figure 4.11. Excitation-Emission Matrix (EEM) was utilized to follow the degradation of ampicillin molecule and its by-products in tap water. (a) represents the fluorescence signal of the blank sample (only tap water). The fluorescence signal of the solutions containing ampicillin and its by-products are shown in (b)-(f), corresponding to different periods of plasma treatment. The fluorescence signal shows an initial increase (at treatment time of 30 min) followed by a significant decrease at treatment times of 1 hr, 2 hr and 3 hr. After treating the solution for 3 hr, the fluorescence signal almost disappeared, as shown in (f). In conjunction with the results obtained by HPLC-MS analysis (Table 1 and Figure 4), one can conclude that the initial increase in the fluorescence signal is possibly due to the formation of oxygenated by-products (P1, P2, P4 and P7). It is well-known that the presence of oxygen or nitrogen in organic molecules can enhance the fluorescence properties of the molecules due to the lone electron spin of these elements [189]. The subsequent decrease in the fluorescence signal at longer treatment periods can be attributed to the combined effect of mineralization and breakdown of larger molecules to smaller organic molecules.

Firstly, one structural feature common to all organic molecules that show significant fluorescence properties in visible and near ultra-violet (UV) wavelengths is the presence of conjugated double bond systems [188]. This is probably due to the fact that the delocalized π -electrons in these systems are less bound to the molecule and act in many ways similar to electrons in metals. As a result, the excitation of these electrons with visible and near UV wavelengths and their subsequent fluorescence emission is possible. The second important structural feature is related to the arrangement of these conjugated double bonds in a molecule. It is well known that the fluorescence behavior of molecules containing conjugated double bonds in a cyclic structure is different from those with conjugated double bonds in a chain structure. This is probably due to the difference in the degree of non-localization of π -electron in the two systems. In cyclic structures, electrons are completely delocalized and can circulate uniformly around the ring. On the other hand, in chain structures electrons are only free towards the center of the chain and are localized at the ends. For localized electrons, the probability of radiationless transfer from an excited state is significantly higher compared to delocalized electrons. In other words, the probability of a successful fluorescence emission is higher from an excited non-localized electron. This is probably why fluorescence emission is found more in molecules with cyclic structure compared to chain structures [188]. Finally, the presence of nitrogen or oxygen atoms in an organic molecule can enhance the fluorescence properties. This is probably due to the lone electron pairs in these atoms which enables them to resonance, similar to aromatic rings [189,190].

Considering the above-mentioned molecular structural features, the EEM results obtained for ampicillin solutions can be explained. One can imagine that not only does the presence of oxygen or nitrogen enhance the fluorescence signal, but also their possible addition to an organic

molecule can increase the fluorescence emission. As a result, the initial increase in the fluorescence emission of ampicillin containing solutions (at treatment time of 30 min) can be attributed to the oxygenation of ampicillin or its by-products. This hypothesis can be confirmed by HPLC-MS results that indicate the presence of oxygenated by-products (P1, P2, P4 and P7) in the solution, as discussed in section 4.6.1 (Figure 4.7). The subsequent decrease in the fluorescence intensity can be attributed to the breakdown of the organic molecules. After 3 hr of plasma treatment, this breakdown can either cause the complete mineralization of the organic compounds (about 20-25% based on TOC results in Figure 4.4(a) and Figure 4.4(b)) or result in transformation of larger molecules to much smaller molecules. These molecules were too small to be detected by HPLC-MS (Table 4.3, treatment time of 2 hr and 3 hr) and possibly lost most of their fluorescence properties.

4.7.2. EEM analysis of ibuprofen solution

EEM analysis was carried out on solutions of ibuprofen in tap water. The results of such an analysis is shown by Figure 4.12. Unlike the trend observed for ampicillin, the fluorescence intensity did not show any increase. From the fluorescence properties stand point, unlike the case of ampicillin, either no oxygenation should be expected for ibuprofen and its by-products, or oxygenation happened at the expense of the cleavage in the cyclic structure. This can be confirmed by means of HPLC-MS analysis. As shown by the degradation pathway proposed for ibuprofen in Figure 4.8, although oxygenated by-products were formed during the plasma treatment (B2, B6 and B7), similar to the case of ampicillin, this oxygenation occurred at the expense of the cleavage in the aromatic ring structure. As discussed previously, the probability of a successful fluorescence emission is much higher from π -electrons of a cyclic system [189].

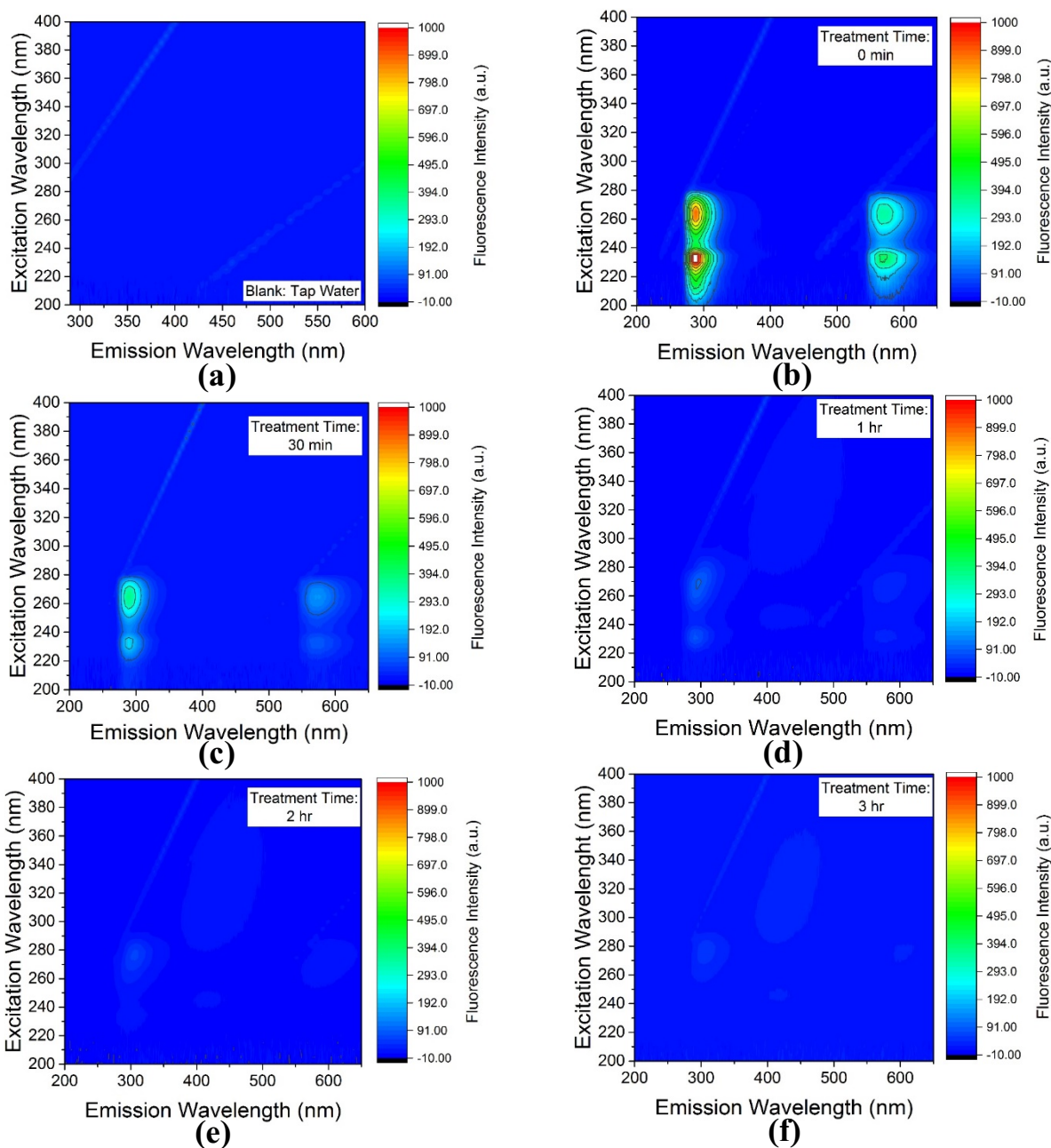


Figure 4.12. The degradation of ibuprofen and its by-products in tap water was monitored through the application of Excitation-Emission Matrix (EEM). (a) The background fluorescence of the samples was measured by conducting EEM on tap water (as the control sample). The fluorescence signal of ibuprofen is shown in (b) which corresponds to 0 hr of plasma treatment. (c)-(f) illustrate the change in the fluorescence signal of the solutions treated by plasma for different periods of time. Unlike the results obtained for ampicillin (Figure 4.11), the fluorescence signal of the solutions containing ibuprofen did not increase at the beginning of the treatment process. This can be explained by the chemical species formed from ibuprofen. Although oxygenated by-products were formed during the plasma treatment from ibuprofen (B2, B6 and B7), similar to the case of ampicillin, this oxygenation occurred at the expense of the cleavage in the aromatic ring structure. It is known that the most important structural feature in organic compounds that induce the fluorescence properties is the presence of conjugated double or triple bonds [189]. Subsequently, this cleavage in the aromatic ring (i.e. interference with the conjugated double bond structure) causes the fluorescence intensity to decrease. Moreover, further degradation and mineralization of the organic compounds resulted in the loss of the fluorescence signal.

Subsequently, this cleavage in the aromatic ring (i.e. interference with the cyclic conjugated double bond structure) causes the fluorescence intensity to decrease. Finally, the continuous decline in the fluorescence intensity can be attributed to two reasons. The first one is similar to the case of ampicillin, i.e. the mineralization (~60% based on the TOC results shown by Figure 4.4(c) and Figure 4.4(d)). More importantly, two notable structural changes in ibuprofen and its by-products can be accounted. The first one is the loss of the cyclic structure, as mentioned earlier. This becomes more crucial considering that this loss of cyclic structure was carried over to other ibuprofen by-products, namely B6 and B7, as shown in Figure 4.8. The other structural change that might be effective in lowering the fluorescence intensity is the loss of the oxygen atom that can be observed in oxidation of B2 to B7. These two structural changes alongside the degradation and mineralization of the organic molecules are probably responsible for the decrease in the fluorescence intensity in the solutions containing ibuprofen.

4.7.2.1. Closer look into ibuprofen's EEM signal

As mentioned in section 4.3.3.3, when analyzing the EEM signals, if the fluorescence intensity scale (the color bar) is kept similar for all the results, interesting comparisons regarding the change in the fluorescence intensity can be made. This type of analysis is shown in the manuscript. However, if the contour maps are plotted within a limited intensity range, new information can be revealed. This is illustrated by Figure 4.13 for ibuprofen solutions. As shown by Figure 4.13(b) to 4.13(f), for each treatment time, a limited range of intensity is chosen. The regions I-V marked on each map has been defined by Chen et al [190]. These regions are: I) Aromatic protein II) Aromatic proteinII III) Fulvic acid-like IV) Soluble microbial by-product-like and V) Humic acid-like.

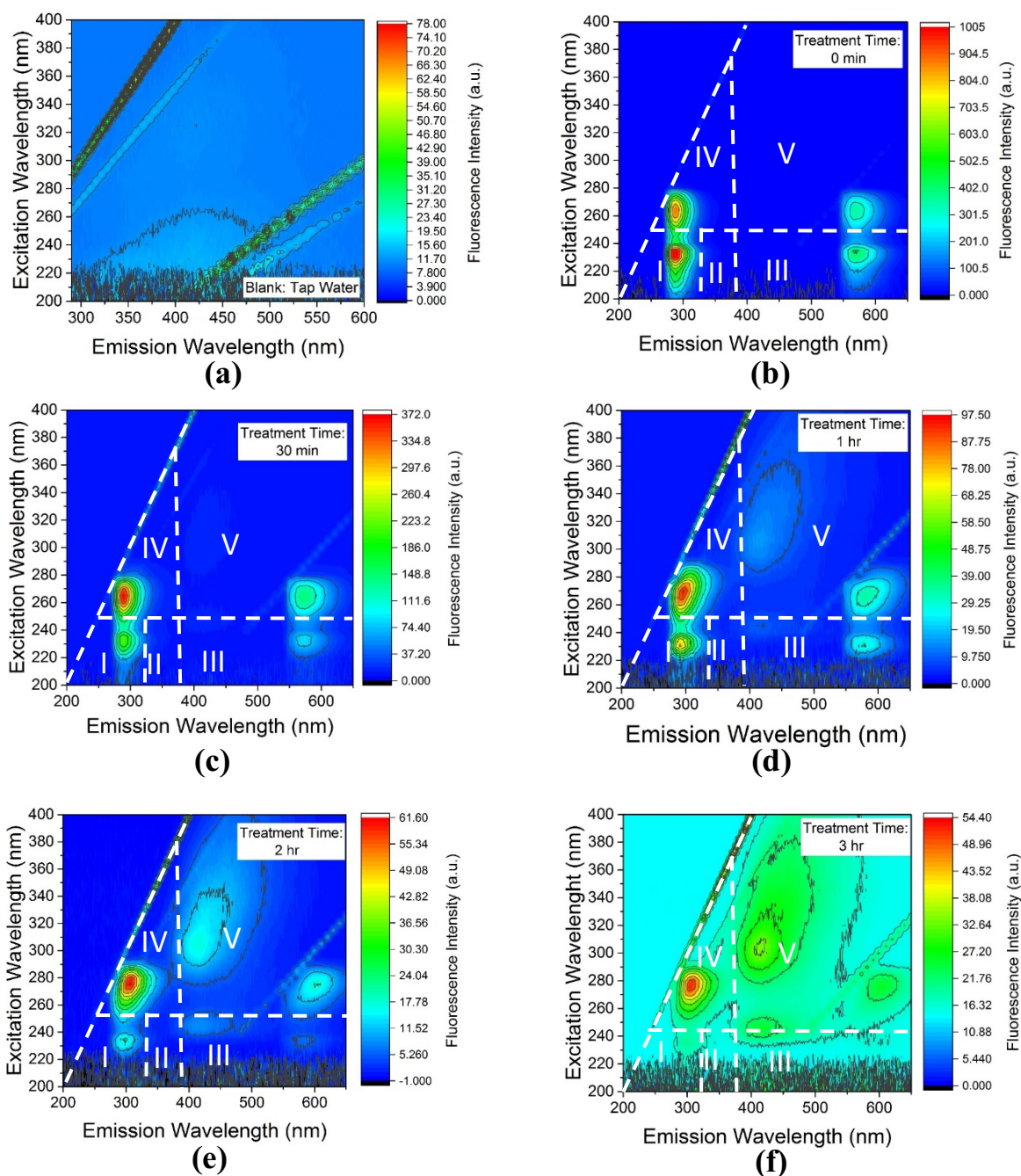


Figure 4.13. Fluorescence signal of solutions containing ibuprofen is shown with smaller intensity ranges. For these solutions, the main fluorescence signals are located in regions I and IV. As the plasma treatment time increased, the fluorescence signal decreased. This decrease can be attributed to the cleavage of the aromatic ring structure (discussed in Figures 4.12). More interestingly, a new fluorescence signal was developed as the solutions were treated for a longer period of time. The presence of this newly formed feature in region V of the EEMs can be clearly seen for treatment times of 2 hr and 3 hr, shown by (e) and (f), respectively. This new signal can be due to the formation of new by-products from ibuprofen at longer treatment times.

As shown by the EEM signals in Figure 4.13, not only did the original fluorescence signal fade away as the treatment time increased, but also a new fluorescence feature appeared in the EEM results. This newly formed feature is in Region V of the EEM signals, located in the excitation and emission wavelength regions of 280-380 nm and 400-500 nm, respectively. The formation of this new feature can be further explored using two methods, i.e. Fluorescence Regional Integration (FRI) and two-dimensional analysis (2D-EEM). FRI analysis was first introduced by Chen et al [190]. In this analysis, since the EEM maps are 3-dimensional, the volume under the fluorescence signal of each of the above-mentioned regions is calculated. To correct for possible non-zero fluorescence base levels in the signal, the EEM signal of the blank solution is subtracted from the signal of the solution at each treatment time. For region “i” of the EEM signal, the volume under the fluorescence signal can be approximately calculated by Equation (4.3) [190].

$$\Phi_i = \sum_{ex} \sum_{em} I(\lambda_{ex}\lambda_{em})\Delta\lambda_{ex}\Delta\lambda_{em} \quad (4.3)$$

In Equation (4.3), $I(\lambda_{ex}\lambda_{em})$ is the intensity of the emission fluorescence at a specific pair of excitation-emission wavelength, $\Delta\lambda_{ex}$ is the excitation wavelength interval (taken as 5 nm) and $\Delta\lambda_{em}$ is the emission wavelength interval (taken as 1 nm).

To correct for the unequal size of the different regions, a modification factor (MF) is defined equal to the inverse of the fractional projected excitation-emission area for each region. As a result, the corrected fluorescence volume of each region can be calculated as:

$$\Phi_{S,n} = MF_i\Phi_i \quad (4.4)$$

Another parameter that can be calculated for each region is the percentage contribution of each region to the total fluorescence volume. This is calculated as:

$$P_{S,n} = \frac{\Phi_{S,n}}{\Phi_{T,n}} \times 100 \quad (4.5)$$

In Equation (4.5), $\Phi_{T,n}$ is the total volume of the fluorescence signal obtained for one sample.

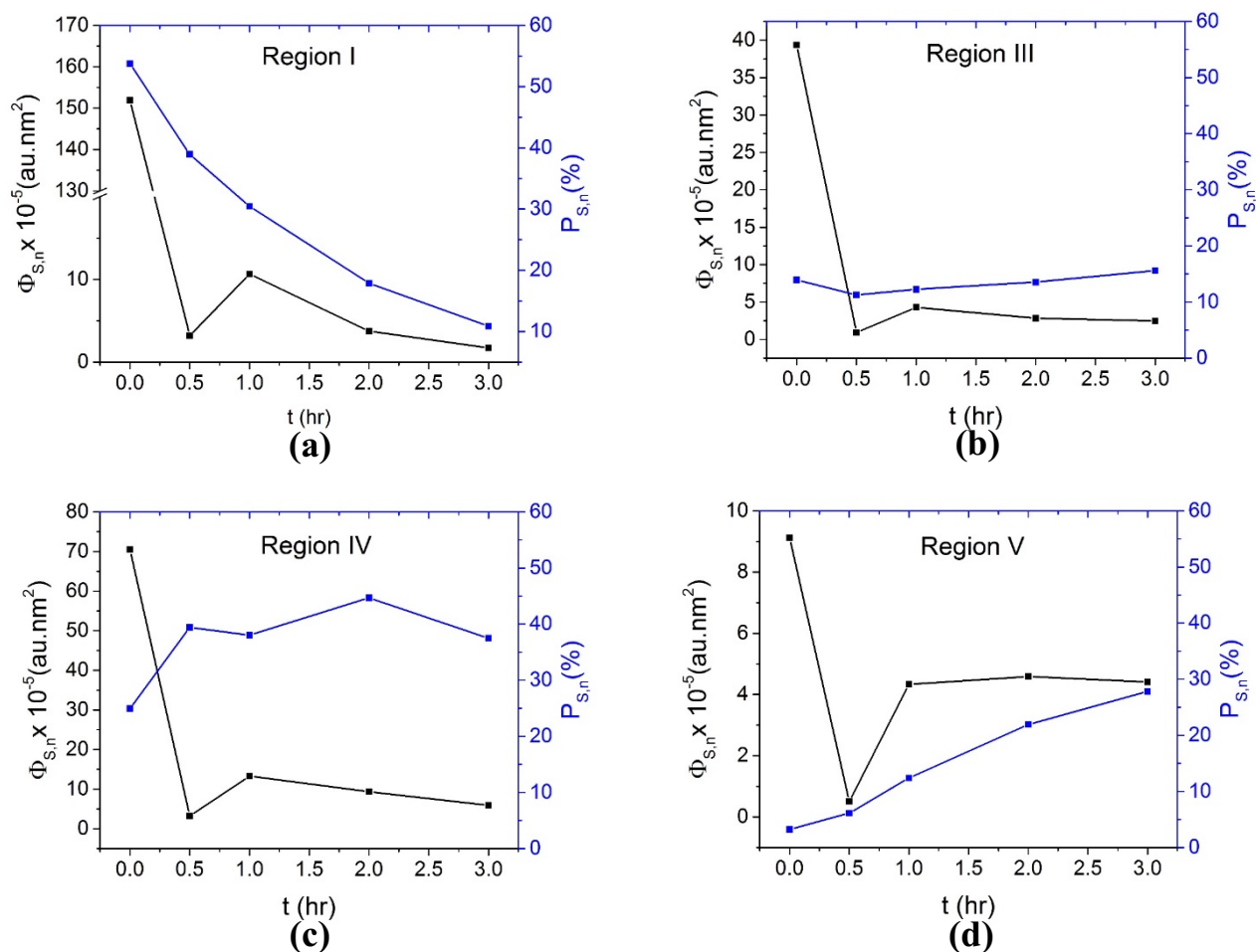


Figure 4.14. FRI analysis was performed on the EEM signals of solutions containing ibuprofen. The results of this analysis are shown in the form of $\Phi_{S,n}$ (fluorescence volume) and $P_{S,n}$ (contribution percentage) as a function of treatment time. Two main points can be concluded from this analysis. Firstly, the fluorescence volume ($\Phi_{S,n}$) in regions I and IV (major EEM peaks) decreased significantly, representing the mineralization and breakdown of the organic molecules in the solution. The second conclusion can be drawn from the FRI analysis of region V, shown in (d). The fluorescence volume ($\Phi_{S,n}$) declined after 30 min of treatment, however, higher values of volume were obtained for longer treatment times. Moreover, $P_{S,n}$ (contribution percentage) increased gradually. These changes in $\Phi_{S,n}$ and $P_{S,n}$ of region V show the formation of new fluorescence features, as discussed in Figure 4.13.

Figure 4.14 shows the calculated values of $\Phi_{S,n}$ and $P_{S,n}$ for various regions of fluorescence signal obtained for ibuprofen containing solutions. Two main points can be concluded from this analysis. Firstly, the fluorescence volume ($\Phi_{S,n}$) in regions I and IV (major EEM peaks) decreased significantly, representing the mineralization and breakdown of the organic molecules in the solution. The second conclusion can be drawn from the FRI analysis of region V, shown in Figure 4.14(d). The fluorescence volume ($\Phi_{S,n}$) declined after 30 min of treatment, however, higher values of volume were obtained for longer treatment times. Moreover, $P_{S,n}$ (contribution percentage) increased gradually. These changes in $\Phi_{S,n}$ and $P_{S,n}$ of region V can possibly indicate the formation of a new fluorescence feature, as discussed in Figure 4.13.

Another possible analysis on the obtained EEM results is two-dimensional analysis (2D-EEM). In this analysis, the fluorescence intensity of a solution is plotted as a function of the excitation wavelength, at a fixed emission wavelength. The 2D-EEM analysis of ibuprofen containing solutions is shown by Figure 4.15(a), 4.15(b) and 4.15(c), corresponding to three emission wavelengths of 290 nm, 425 nm and 570 nm, respectively.

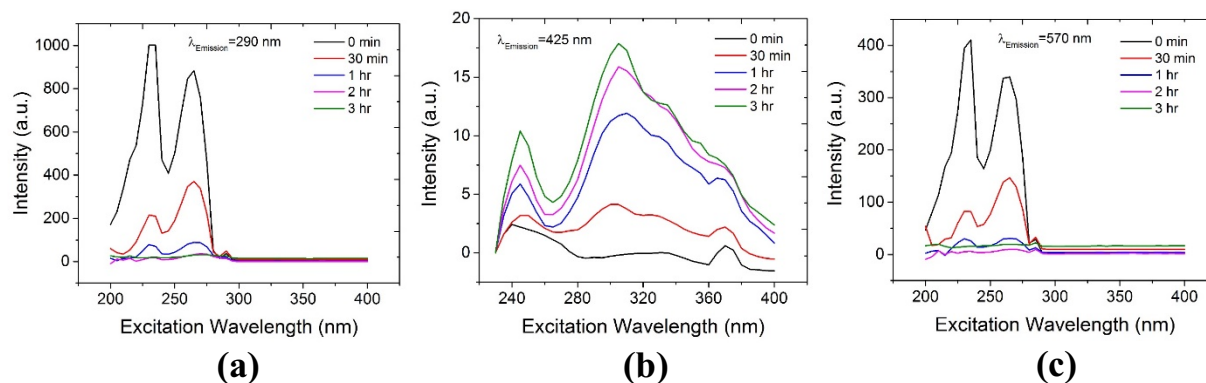


Figure 4.15. Two-dimensional (2D) fluorescence signals were obtained from EEMs of ibuprofen containing solutions by plotting the fluorescence intensity as a function of the excitation wavelength, at fixed emission wavelength values (vertical lines in EEMs). (a), (b) and (c) show the 2D analysis of the fluorescence signal of ibuprofen solutions at fixed emission wavelengths of 290, 425 and 570 nm, respectively. 2D analysis at emission wavelengths of 290 nm and 570 nm ((a) and (c)) represent the change in the fluorescence intensity of the two main peaks in EEMs of ibuprofen containing solutions. As shown in (a) and (c), the intensity of both peaks decreased. This is probably due to the mineralization and breakdown of the organic molecules. (b) depicts the change in the fluorescence intensity at the emission wavelength of 425 nm. At the beginning (treatment time of 0 min, black curve), no fluorescence signal was obtained. As the plasma treatment time increased, higher fluorescence intensities were obtained. This also points to the formation of new features in the EEM of the solutions at longer treatment periods.

The 2D-EEM analysis at emission wavelengths of 290 nm and 570 nm (Figure 4.15(a) and 4.15(c)) represent the change in the fluorescence intensity of the two main peaks in EEMs of ibuprofen containing solutions. The intensity of both peaks decreased. This is probably due to the mineralization and breakdown of the organic molecules. Figure 4.15(b) depicts the change in the fluorescence intensity at the emission wavelength of 425 nm. At the beginning (treatment time of 0 min, black curve), no fluorescence signal was obtained. As the plasma treatment time increased, higher fluorescence intensities were obtained. This also points to the formation of a new feature in the EEM of the solutions at longer treatment periods. We believe that further studies and improvements to this methodology can perhaps shed light on possible sources of this newly formed fluorescence feature.

4.7.3. EEM analysis of fluoxetine solution

EEM analysis was used to follow the degradation of fluoxetine in tap water. The results of this study are shown in Figure 4.16. The fluorescence signal decreased significantly as the treatment time increased. It is interesting to note that the fluorescence signal faded away after a shorter period of time compared to other pharmaceutical compounds studied in this work. For instance, the fluorescence intensity became insignificant after treating the solutions containing fluoxetine for only 30 min. This significant decrease in the fluorescence signal was achieved after 3 hr and 1 hr of treatment for ampicillin and ibuprofen solutions, respectively. This is understandable if we consider the degradation time constant of fluoxetine (5.44 hr^{-1} , Table 4.1) and the degree of mineralization of fluoxetine solutions (60%, Table 4.2). These values were the highest amongst all the compounds in this study.

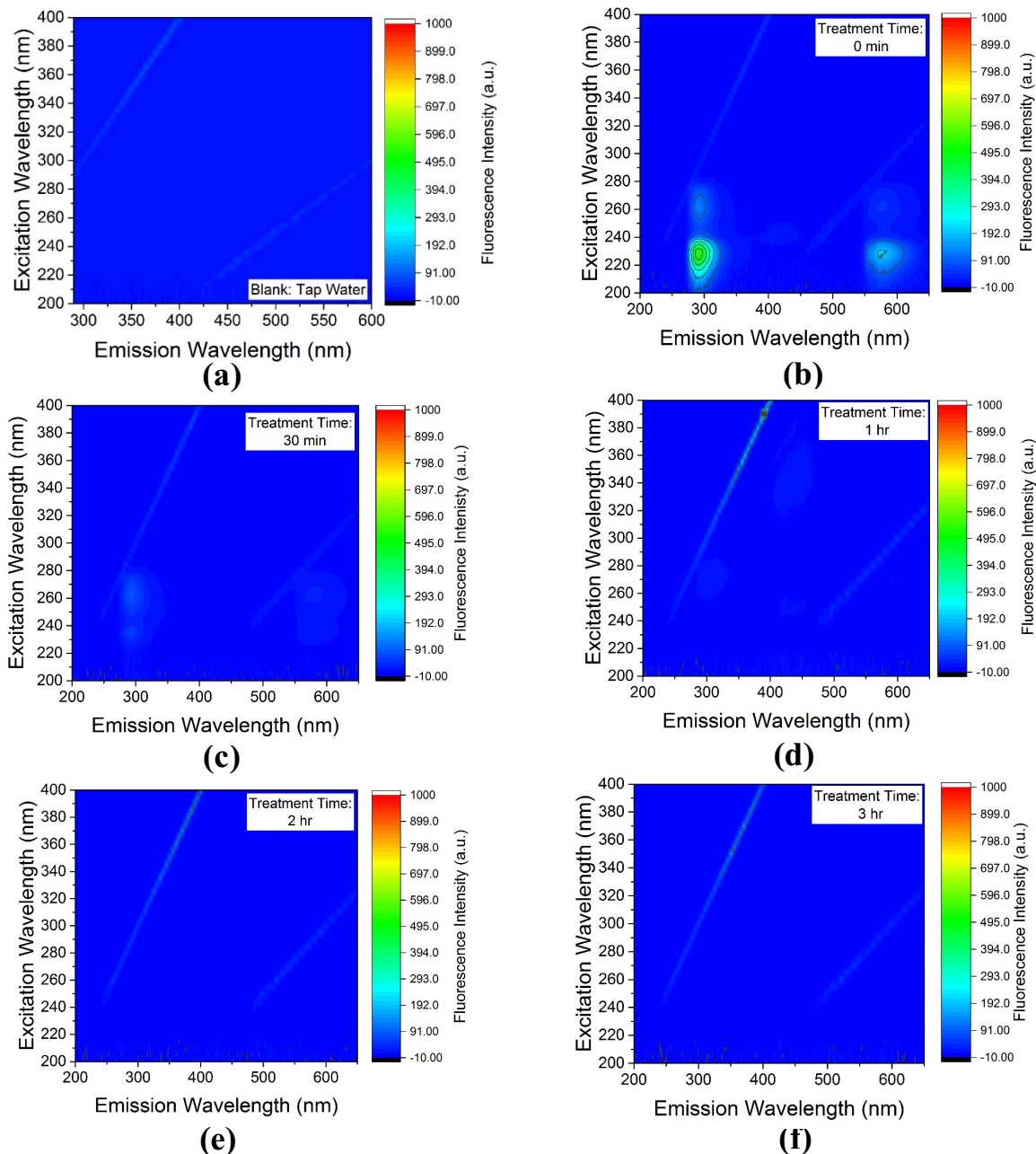


Figure 4.16. The evolution of the fluorescence signal of solutions containing ibuprofen as a function of the treatment time is shown. The fluorescence signal decreased significantly as the treatment time increased. It is interesting to note that the fluorescence signal faded away after a shorter period of time compared to other pharmaceutical compounds studied in this work. For instance, the fluorescence intensity became insignificant after treating the solutions containing fluoxetine for only 30 min. This significant decrease in the fluorescence signal was achieved after 3 hr and 1 hr of treatment for ampicillin and ibuprofen, respectively. This is understandable if we consider the degradation time constant of fluoxetine (5.44 hr^{-1} , Table 4.1) and the degree of mineralization of fluoxetine solutions (60%, Table 4.2). These values were the highest amongst all the compounds in this study. Moreover, unlike the case of ampicillin, the fluorescence intensity did not show any increase. This can be either due to the lack of oxygenation or the destruction of the aromatic ring during the oxygenation (similar to ibuprofen). A comparison with the degradation pathway proposed for fluoxetine (Figure 4.9) reveals that indeed the lack of increase in the fluorescence intensity is due to the fact that no oxygenated by-products were formed.

Also, the lower initial concentration of fluoxetine used in this study compared to other compounds (25 mg/l versus 100 mg/l for other compounds) can be a reason. In addition, unlike the case of ampicillin, the fluorescence intensity did not show any increase. This can be either due to the lack of oxygenation or the destruction of the aromatic ring during the oxygenation (similar to ibuprofen). A comparison with the degradation pathway proposed for fluoxetine (Figure 4.9) reveals that indeed the lack of increase in the fluorescence intensity is due to the fact that no oxygenated by-products were formed. Similar to the case of ibuprofen where a new feature was formed in the EEM signal of the solutions (section 4.7.2.1), a new fluorescence feature was also formed in the EEM signal of the solutions containing fluoxetine. Due to the similarities in the results, we will not show these results obtained from fluoxetine solutions. However, an interesting observation was made. The new fluorescence feature in the EEM signal of fluoxetine is formed exactly in the same position as in the EEM signal of ibuprofen. The only difference is, for ibuprofen, the fluorescence intensity of this feature increased gradually as the treatment time increased. However, in the case of fluoxetine, the intensity increased at the beginning and declined after treatment time of 1 hr. This possibly implies that this EEM feature corresponds to a similar group of organic compounds. Furthermore, these compounds underwent further degradation in the case of fluoxetine.

4.7.4. EEM analysis of propranolol solution

Figure 4.17 illustrates the EEM analysis of the solutions containing propranolol. Figure 4.17(a) shows the fluorescence signal of the blank solution (tap water), used as the background signal. Comparing the initial fluorescence signal (at 0 hr, Figure 4.17(b)) with the initial signal of the fluoxetine and ibuprofen solutions (Figure 4.16(b) and Figure 4.12(b), respectively) shows that the main fluorescence signal of propranolol is red-shifted along the emission wavelength axis.

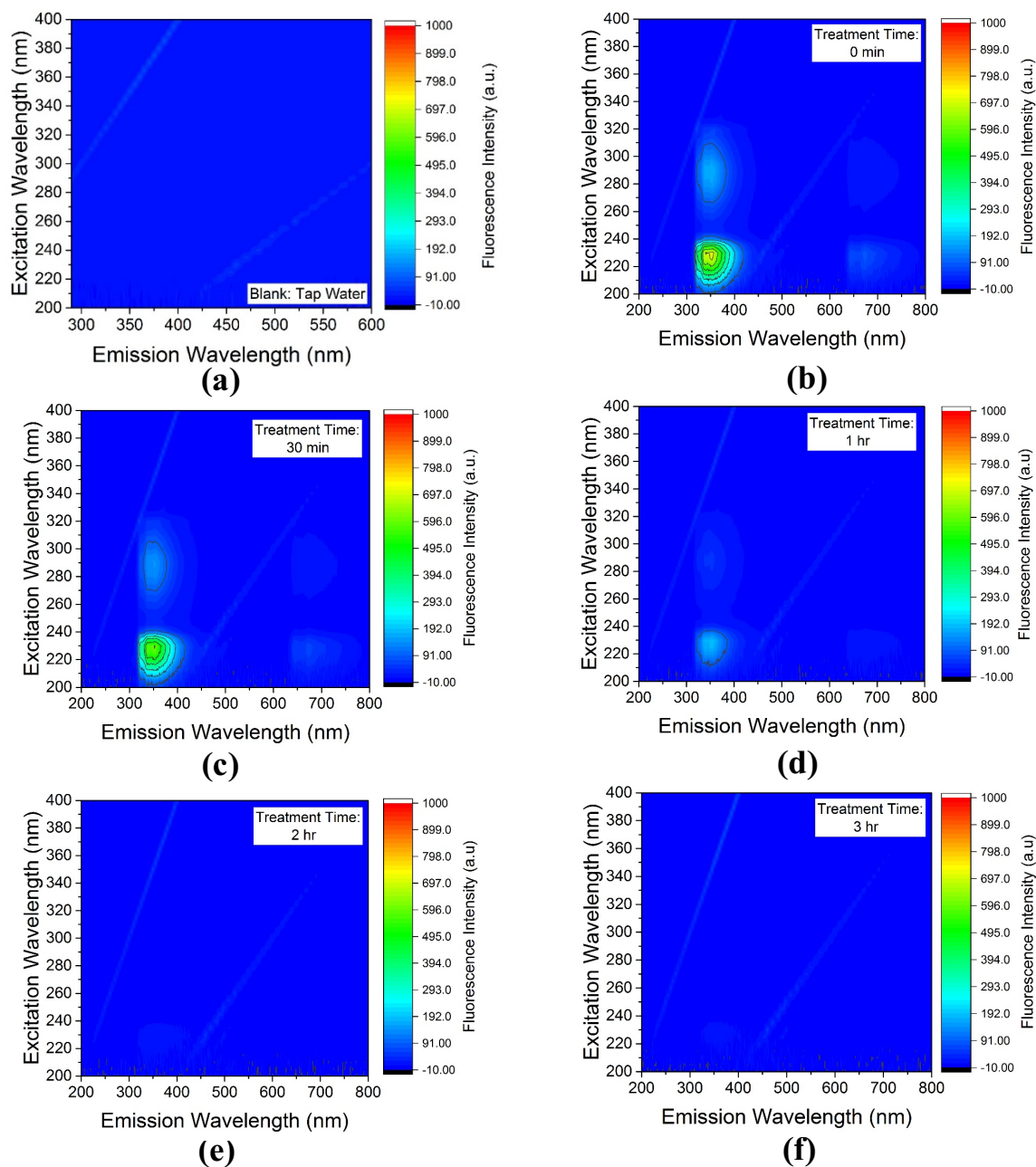


Figure 4.17. EEM analysis was used to investigate the change in the fluorescence properties of the solutions containing propranolol as a function of the treatment time. (a) shows the EEM signal of the blank solution, i.e. tap water. (b)-(f) illustrate the change in EEM signal of the solution as the treatment time increases from 0 hr to 3 hr. The EEM signal decreased as the treatment time increased. Similar to the case of fluoxetine, the lack of increase in the signal is due to the absence of oxygenated by-products, as proved by HPLC-MS analysis (Figure 4.10). After 3 hr of plasma treatment, the EEM signal was almost disappeared. This is partially due to the mineralization of the organic compounds (degree of mineralization of 20%, Figure 4.5(c)) and partially due to the breakdown of the molecules in the solution.

While the center of the main signal of propranolol is located at the emission wavelength of 350 nm, this value for fluoxetine and ibuprofen fluorescence signal is 290 nm. This can be explained based on the structure of the above-mentioned compounds. The initial structure of ibuprofen, fluoxetine and propranolol are shown in Figure 4.8, Figure 4.9 and Figure 4.10, respectively. The most notable difference between the structures of these molecules is in the arrangement of their aromatic rings. Ibuprofen contains only one aromatic ring. On the other hand, both fluoxetine and propranolol are comprised of two aromatic rings. The only difference in the structure of fluoxetine and propranolol is that in a propranolol molecule, the two rings are fused together in the form of naphthalene structure. In a fluoxetine molecule, the two rings are separated, located at the center and one end of the molecule. As mentioned before, the aromatic rings are the most important feature of molecules with significant fluorescence [188]. Normally, a rudimentary explanation of the fluorescence emission process is given by the simple case of the particle in the box concept in quantum physics. Although the detailed calculations is not the scope of this work, it only suffices to mention that based on the concept of the particle in the box, the energy required to excite the particle is inversely related to the size of the box [191]. Now, assuming that the particle in this case is an electron and the box is the size of the π -electron cloud, one can conclude that in a propranolol molecule, the size of the π -electron cloud is larger compared to the case of ibuprofen and fluoxetine, due to the attachment of the two rings. As a result, the energy required to excite electrons from the π -electron cloud of a propranolol molecules is lower than the excitation energy required for ibuprofen and fluoxetine molecules. This means that the fluorescence emission from propranolol molecules can be expected to occur at longer emission wavelengths.

Finally, as shown by Figure 4.17, the EEM signal decreased as the treatment time increased. Similar to the case of fluoxetine, the lack of an initial increase in the signal is due to the absence of oxygenated by-products, proved by HPLC-MS analysis (Figure 4.10). After 3 hr of plasma treatment, the EEM signal was almost disappeared. This is partially due to the mineralization of the organic compounds (degree of mineralization of 20%, Figure 4.5(c)) and partially due to the breakdown of the molecules in the solution.

4.8. Presence of ozone in the aqueous phase

As mentioned in the degradation pathway of ampicillin, ibuprofen and propranolol (sections 4.6.1, 4.6.2 and 4.6.4, respectively), one of the oxidation pathways for organic molecules is through the action of ozone molecules. This pathway can change the structure of the organic molecules in various ways, as discussed in the corresponding sections. As a result, in this section, the presence of ozone in the aqueous phase is investigated by means of Indigo method. The fundamental mechanism of the reaction of indigo dye with ozone molecules was proposed by Bader et al. [185], as described in section 4.3.3.4.

Figure 4.18(a) shows the change in the concentration of the detected ozone in one cycle of the plasma treatment process (15 min of the treatment stage followed by 15 min of the post treatment stage). The experiments were done in the absence and presence of ampicillin in the solution. In both cases, the concentration of ozone in the solution increased during the treatment stage. This is understandable since ozone is continuously created in the plasma in the gas phase and subsequently injected into the water.

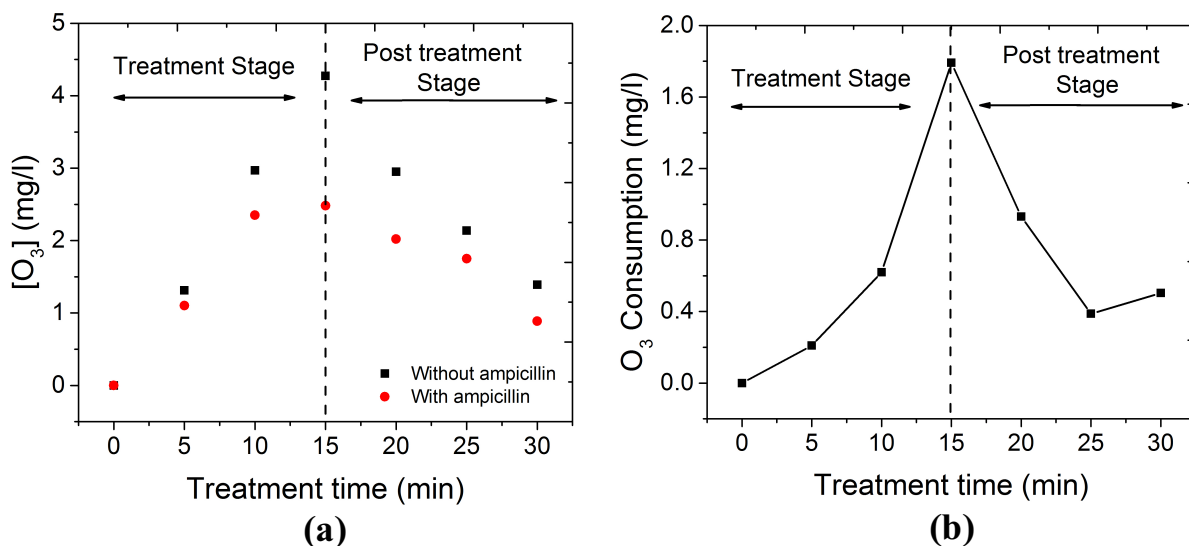


Figure 4.18. (a) The presence of ozone in the aqueous phase was investigated using the Indigo method [185]. The measurements were done for one cycle of the plasma treatment process, i.e. 15 min of treatment followed by 15 min of post treatment. The change in the absorbance of the indigo dye was converted into the concentration of ozone by means of a previously obtained calibration curve (Figure 4.2). The concentration of ozone was measured in the presence (100 mg/l) and also absence of ampicillin in the solution. In both cases, the concentration of ozone in the solution increased during the treatment stage. This is understandable since during this stage (i.e. presence of plasma), ozone is created continuously in the gas phase and introduced to the solution from the gas/liquid interface. On the other hand, the concentration of ozone declined during the post treatment stage. In this stage, since plasma is not present, the continuous production of ozone in the gas phase does not occur. As a result, the change in the concentration of ozone is controlled by ozone decomposition processes such as direct reaction of ozone and water molecules [152]. In the presence of ampicillin in the solution as a model pharmaceutical contaminant, lower concentrations of ozone were measured. This shows that ampicillin molecules compete with indigo dye molecules to consume ozone. The difference between the concentration of ozone measured in the presence and absence of ampicillin can show the amount of ozone consumed by ampicillin molecules, as shown in (b).

In the post treatment stage, the concentration of ozone decreases possibly due to its limited lifetime in the aqueous phase and its subsequent dissociation [152,154]. When ampicillin is present in the solution, it creates a competition with indigo molecules to consume ozone. As a result, the difference between the concentration of ozone in the presence and absence of ampicillin can be used to the first approximation to calculate the ozone consumption by ampicillin [121]. Figure 4.18(b) shows the concentration of ozone consumed by ampicillin and

its by-products during one cycle of the plasma treatment process. The ozone consumption increased during the treatment stage, possibly due to the increasing concentration of ozone created in the plasma. The decline in the ozone consumption during the post treatment stage can be attributed to the decreasing concentration of both ozone and organic molecules present in the aqueous phase.

Chapter 5: Conclusions and future directions³

A novel technique for the generation of AC driven, single electrode plasma is proposed. Non-thermal plasma is produced in air at atmospheric pressure, utilizing our helical resonator structure. Benefiting from the single electrode nature of the method, the application of this technique in various hypothetical situations was shown. In these scenarios, plasma can be generated in the air for pollution removal or it can be applied directly to the surface of water, ceramic tile, soil or other media for effective decontamination. Using the Floating Electrode Streamer Corona Discharge (FESCD) method proposed here, the removal of contamination (methylene blue) from water was further investigated. Moreover, the effect of process parameters such as the air gap distance, input voltage and plasma injection time on the efficiency of methylene blue removal was studied. The correlations between the studied parameters and the fundamental physiochemical processes such as the Townsend ionization (electron avalanche) and ozone concentration were reached. It is shown that using optimized parameters (an air gap distance of 2 mm, input voltage of 83 V and plasma injection period of 15 min), one could not only achieve optimum removal% and energy yield (0.02 g/kWh), but also created agents with a long lifetime in the solution. These agents continued the degradation process for up to an hour after the removal of the plasma from the surface in the post treatment stage. Moreover, the application of the helical resonator for plasma generation could offer many advantages that would possibly overcome the current limitations of non-thermal plasma techniques for real life applications. These advantages include the generation of plasma using a single electrode, simplifying the treatment apparatus, the ability of effective treatment using a simple AC

³ Parts of this section have been published in the journal of Environmental Science: Water Research & Technology, 2017, 3, 156-168.

waveform, lower driving electronic power consumption due to the amplifying nature of the helical resonator and high electrical energy efficiency.

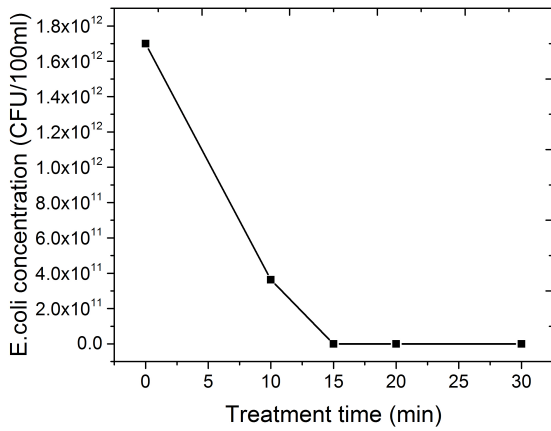
In the second part of this work, the effect of solution characteristics, such as the concentration of Cl^- in the solution, the role of various ionic species, the initial pH of the solution, and the initial concentration of MB, on treatment efficiency was investigated. The results indicate that at an optimum concentration of Cl^- (50 mg/l), the contaminant removal percentage is at its maximum (85%). Moreover, although the presence of Cl^- decreases the removal percentage during the treatment stage, it significantly enhances the removal percentage in the post treatment stage. It was hypothesized that this phenomenon is due to the formation of singlet oxygen ($^1\text{O}_2$) through a series of reactions mediated by Cl-based compounds. This hypothesis was analytically confirmed by HPLC-MS analysis and through the formation of sulfones and sulfinic acids in only treated solutions containing Cl^- . While scavengers such as phosphate and carbonate can deteriorate the efficiency of the decontamination significantly, the presence of sulfate ions resulted in almost equal contributions from the treatment and post treatment stage. This was attributed to the generation of sulfate radical anions during the treatment stage and peroxodisulfate ions during the post treatment stage. The initial pH of the solution proved to play an important role in both treatment and post treatment stages. While maximum removal% during the treatment stage was obtained for initial acidic conditions, the role of treatment and post treatment stages was almost equal in solutions with initial near neutral pH values. This was attributed to the sensitivity of the involved fundamental Cl-based chemical reactions to the initial pH of the solution. The results presented in this study shed light on possible effects of solution characteristics on the behavior of plasma-based water treatment processes.

Finally, the floating electrode streamer corona discharge (FESCD) system was used to degrade pharmaceutical drugs ampicillin, ibuprofen, fluoxetine and propranolol in tap water. After treatment of the solutions for 3 hr, 100% of ampicillin, 90% of ibuprofen, 99% of fluoxetine and 99% of propranolol were degraded. The energy yield for degradation of ampicillin, ibuprofen and propranolol was calculated to be in the range of 0.12-0.13 g/kWh. TOC analysis of the solutions revealed that although removal% of ibuprofen was the lowest, high mineralization was obtained in the case of ibuprofen containing solutions (56% for ibuprofen). The highest degree of mineralization was obtained in the case of fluoxetine containing solutions (60%). Degradation by-products detected by HPLC-MS indicated that for ampicillin and ibuprofen, the major degradation pathways include oxidation by hydroxyl radicals and ozone molecules. The direct effect of the oxygenation was only observed in the EEM signals of ampicillin where the initial increase in the fluorescence intensity was attributed to the addition of oxygen atoms to organic molecules. In the case of ibuprofen, this oxygenation occurred at the expense of losing the cyclic structure. Hence, the fluorescence intensity did not increase. Further compatibility between the HPLC-MS and EEM results could be seen where the decline in the fluorescence intensity in all four contaminants was attributed to the breakdown of the organic molecules. This study shows that with few modifications to the design of the decontamination reactor, real life applications of a plasma treatment system based on FESCD method is possible. Moreover, with further improvements, EEM analysis can be used as a powerful tool for following the degradation of pharmaceutical compounds in complex water matrices.

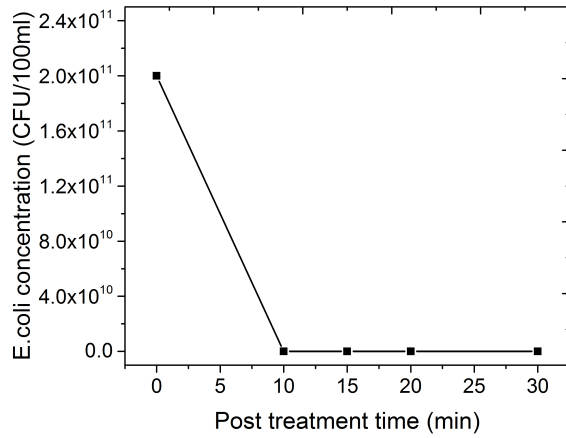
Two major future directions can be suggested. The first direction is to use further modeling and analysis to transform EEM analysis to a powerful tool for tracking the degradation of organic contaminants. The observations made during the EEM analysis of ibuprofen and fluoxetine

solutions where new fluorescence features were formed during the treatment are proof of this direction.

The second future direction is related to the application of the FESCD system for other applications. As suggested in Chapter 3, due to the single electrode nature of the FESCD method, many other applications can be proposed. One of these applications is disinfection of water and surfaces contaminated with pathogens. To demonstrate the capability of the FESCD system for this application, we performed preliminary experiments. In these experiments, tap water was spiked with a high concentration of *E. coli* (ATCC 25922 strain). In one experimental configuration, the contaminated water (100 ml) was treated with plasma for various periods of time (0, 10, 15, 20 and 30 min). The input voltage and the air gap distance were fixed at 80 V and 2 mm, respectively. This configuration is used to evaluate the efficiency of the direct plasma disinfection of water. In the second configuration, 100 ml of tap water was first treated for 15 min. After 15 min of plasma treatment, plasma was turned off and an aliquot of the bacteria solution was added to the water. Afterwards, the treated water sample spiked by the bacteria was kept under the fume hood for various time periods (10, 15, 20 and 30 min). In both experimental configurations, after the desired time periods were reached, water samples were vacuum filtered and standard plating and counting methods were used. Figure 5.1 shows the results obtained from both experiments. In both configurations, the FESCD system can effectively disinfect contaminated water.



(a)



(b)

Figure 5.1. The FESCD system was used to assess the pathogen disinfection capability of the method. (a) Water samples contaminated by *E. coli* were treated directly with plasma. (b) Water samples were first treated by plasma and then spiked by bacterial. In this configuration, the efficiency of the post treatment stage can be evaluated.

References

- [1] B. Halling-Sorensen, B. Halling-Sorensen, S.N. Nielsen, S.N. Nielsen, P.F. Lanzky, P.F. Lanzky, et al., Occurrence, fate and effects of pharmaceuticals substance in the environment - A review, *Chemosphere*. 36 (1998) 357–393.
doi:[http://dx.doi.org/10.1016/S0045-6535\(97\)00354-8](http://dx.doi.org/10.1016/S0045-6535(97)00354-8).
- [2] S.K. Khetan, T.J. Collins, Human Pharmaceuticals in the Aquatic Environment: A Challenge to Green Chemistry, *Chem. Rev.* 107 (2007) 2319–2364.
doi:10.1080/09593332208618186.
- [3] I. Panorel, S. Preis, I. Kornev, H. Hatakka, M. Louhi-Kultanen, Oxidation of aqueous pharmaceuticals by pulsed corona discharge., *Environ. Technol.* 34 (2013) 923–30.
doi:10.1080/09593330.2012.722691.
- [4] G. a. Loraine, M.E. Pettigrove, Seasonal variations in concentrations of pharmaceuticals and personal care products in drinking water and reclaimed wastewater in Southern California, *Environ. Sci. Technol.* 40 (2006) 687–695. doi:10.1021/es051380x.
- [5] V. Homem, L. Santos, Degradation and removal methods of antibiotics from aqueous matrices - A review, *J. Environ. Manage.* 92 (2011) 2304–2347.
doi:10.1016/j.jenvman.2011.05.023.
- [6] S. Mompelat, B. Le Bot, O. Thomas, Occurrence and fate of pharmaceutical products and by-products, from resource to drinking water, *Environ. Int.* 35 (2009) 803–814.
doi:10.1016/j.envint.2008.10.008.
- [7] M. Magureanu, N.B. Mandache, V.I. Parvulescu, Degradation of pharmaceutical compounds in water by non-thermal plasma treatment., *Water Res.* 81 (2015) 124–136.
doi:10.1016/j.watres.2015.05.037.
- [8] M.J. Stueic, K. Wayne, M.W. Collins, W. Paschal, L.J. Lorenz, L.A. Spangle, et al., Aqueous Acidic Degradation of the Carbacephalosporin Loracarbef, *J. Pharm. Sci.* 82 (1993) 1010–1017.
- [9] M.G. Lee, W.L. Chiou, Evaluation of potential causes for the incomplete bioavailability of furosemide: Gastric first-pass metabolism, *J. Pharmacokinet. Biopharm.* 11 (1983) 623–640. doi:10.1007/BF01059061.
- [10] A. Katsnelson, Vegetables grown with treated wastewater boost human exposure to pharmaceutical contaminants, 2016.
- [11] NEWS RELEASE More than 40 tonnes of B.C. medications safely disposed of each year, Vancouver, 2009. <http://www.metrovancouver.org/media-room/media->

releases/MediaReleases/2009-03-20-MediaRelease.pdf.

- [12] B. Kasprzyk-Hordern, R.M. Dinsdale, A.J. Guwy, The occurrence of pharmaceuticals, personal care products, endocrine disruptors and illicit drugs in surface water in South Wales, UK, *Water Res.* 42 (2008) 3498–3518. doi:10.1016/j.watres.2008.04.026.
- [13] X. Van Doorslaer, J. Dewulf, H. Van Langenhove, K. Demeestere, Fluoroquinolone antibiotics: An emerging class of environmental micropollutants, *Sci. Total Environ.* 500–501 (2014) 250–269. doi:10.1016/j.scitotenv.2014.08.075.
- [14] E.N. Evgenidou, I.K. Konstantinou, D.A. Lambropoulou, Occurrence and removal of transformation products of PPCPs and illicit drugs in wastewaters: A review, *Sci. Total Environ.* 505 (2015) 905–926. doi:10.1016/j.scitotenv.2014.10.021.
- [15] R. López-Serna, M. Petrović, D. Barceló, Occurrence and distribution of multi-class pharmaceuticals and their active metabolites and transformation products in the Ebro River basin (NE Spain), *Sci. Total Environ.* 440 (2012) 280–289. doi:10.1016/j.scitotenv.2012.06.027.
- [16] Y. Luo, W. Guo, H.H. Ngo, L.D. Nghiem, F.I. Hai, J. Zhang, et al., A review on the occurrence of micropollutants in the aquatic environment and their fate and removal during wastewater treatment, *Sci. Total Environ.* 473–474 (2014) 619–641. doi:10.1016/j.scitotenv.2013.12.065.
- [17] J.F. Henriques, A.R. Almeida, T. Andrade, O. Koba, O. Golovko, A.M.V.M. Soares, et al., Effects of the lipid regulator drug gemfibrozil: A toxicological and behavioral perspective, *Aquat. Toxicol.* 170 (2016) 355–364. doi:10.1016/j.aquatox.2015.09.017.
- [18] M. Petrović, B. Škrbić, J. Živančev, L. Ferrando-Climent, D. Barcelo, Determination of 81 pharmaceutical drugs by high performance liquid chromatography coupled to mass spectrometry with hybrid triple quadrupole-linear ion trap in different types of water in Serbia, *Sci. Total Environ.* 468–469 (2014) 415–428. doi:10.1016/j.scitotenv.2013.08.079.
- [19] C. Postigo, D. Barceló, Synthetic organic compounds and their transformation products in groundwater: Occurrence, fate and mitigation, *Sci. Total Environ.* 503–504 (2015) 32–47. doi:10.1016/j.scitotenv.2014.06.019.
- [20] L.H.M.L.M. Santos, A.N. Araújo, A. Fachini, A. Pena, C. Delerue-Matos, M.C.B.S.M. Montenegro, Ecotoxicological aspects related to the presence of pharmaceuticals in the aquatic environment, *J. Hazard. Mater.* 175 (2010) 45–95. doi:10.1016/j.jhazmat.2009.10.100.
- [21] D. Hummel, D. Löffler, G. Fink, T.A. Ternes, Simultaneous determination of psychoactive drugs and their metabolites in aqueous matrices by liquid chromatography

- mass spectrometry, *Environ. Sci. Technol.* 40 (2006) 7321–7328. doi:10.1021/es061740w.
- [22] L. Martin-Diaz, S. Franzellitti, S. Buratti, P. Valbonesi, A. Capuzzo, E. Fabbri, Effects of environmental concentrations of the antiepileptic drug carbamazepine on biomarkers and cAMP-mediated cell signaling in the mussel *Mytilus galloprovincialis*, *Aquat. Toxicol.* 94 (2009) 177–185. doi:10.1016/j.aquatox.2009.06.015.
- [23] M. Rabiet, A. Togola, F. Brissaud, J.L. Seidel, H. Budzinski, F. Elbaz-Poulichet, Consequences of treated water recycling as regards pharmaceuticals and drugs in surface and ground waters of a medium-sized mediterranean catchment, *Environ. Sci. Technol.* 40 (2006) 5282–5288. doi:10.1021/es060528p.
- [24] A. Marchlewicz, U. Guzik, D. Wojcieszńska, Over-the-Counter Monocyclic Non-Steroid Anti-Inflammatory Drugs in Environment—Sources, Risks, Biodegradation, *Water, Air, Soil Pollut.* 226 (2015) 355. doi:10.1007/s11270-015-2622-0.
- [25] M. Gorga, S. Insa, M. Petrovic, D. Barceló, Occurrence and spatial distribution of EDCs and related compounds in waters and sediments of Iberian rivers, *Sci. Total Environ.* 503–504 (2015) 69–86. doi:10.1016/j.scitotenv.2014.06.037.
- [26] M. Himmelsbach, W. Buchberger, C.W. Klampfl, Determination of antidepressants in surface and waste water samples by capillary electrophoresis with electrospray ionization mass spectrometric detection after preconcentration using off-line solid-phase extraction, *Electrophoresis.* 27 (2006) 1220–1226. doi:10.1002/elps.200500693.
- [27] A.T. Ford, P.P. Fong, The effects of antidepressants appear to be rapid and at environmentally relevant concentrations, *Environ. Toxicol. Chem.* 35 (2016) 794–798. doi:10.1002/etc.3087.
- [28] World Health Organization (WHO), Pharmaceuticals in drinking water:public health and environment water, sanitation, hygiene and health,Geneva,WHO/HSE/WSH/11.05, (2011). doi:10.1331/JAPhA.2010.09186.
- [29] M. Hijosa-Valsero, R. Molina, H. Schikora, M. Müller, J.M. Bayona, Removal of priority pollutants from water by means of dielectric barrier discharge atmospheric plasma, *J. Hazard. Mater.* 262 (2013) 664–673. doi:10.1016/j.jhazmat.2013.09.022.
- [30] R. Andreozzi, V. Caprio, A. Insola, R. Marotta, Advanced oxidation processes (AOP) for water purification and recovery, *Catal. Today.* 53 (1999) 51–59. doi:10.1016/S0920-5861(99)00102-9.
- [31] J.R. Bolton, K.G. Bircher, W. Tumas, C.A. Tolman, Figures-of-merit for the technical development and application of advanced oxidation technologies for both electric- and solar-driven systems (IUPAC Technical Report), *Pure Appl. Chem.* 73 (2001) 627–637.

doi:10.1351/pac200173040627.

- [32] M. Muruganandham, R.P.S. Suri, S. Jafari, M. Sillanpaa, G.-J. Lee, J.J. Wu, et al., Recent Developments in Homogeneous Advanced Oxidation Processes for Water and Wastewater Treatment, *Int. J. Photoenergy*. 2014 (2014) 1–22. doi:10.1155/2014/821674.
- [33] I.H. Kim, H. Tanaka, T. Iwasaki, T. Takubo, T. Morioka, Y. Kato, Classification of the degradability of 30 pharmaceuticals in water with ozone, UV and H₂O₂, *Water Sci. Technol.* 57 (2008) 195–200. doi:10.2166/wst.2008.808.
- [34] I. Kim, N. Yamashita, H. Tanaka, Performance of UV and UV/H₂O₂ processes for the removal of pharmaceuticals detected in secondary effluent of a sewage treatment plant in Japan, *J. Hazard. Mater.* 166 (2009) 1134–1140. doi:10.1016/j.jhazmat.2008.12.020.
- [35] R. Andreozzi, V. Caprio, R. Marotta, A. Radovnikovic, Ozonation and H₂O₂/UV treatment of clofibric acid in water: A kinetic investigation, *J. Hazard. Mater.* 103 (2003) 233–246. doi:10.1016/j.jhazmat.2003.07.001.
- [36] I. Arslan-Alaton, S. Dogruel, Pre-treatment of penicillin formulation effluent by advanced oxidation processes, *J. Hazard. Mater.* 112 (2004) 105–113. doi:10.1016/j.jhazmat.2004.04.009.
- [37] H. Shemer, Y.K. Kunukcu, K.G. Linden, Degradation of the pharmaceutical Metronidazole via UV, Fenton and photo-Fenton processes, *Chemosphere*. 63 (2006) 269–276. doi:10.1016/j.chemosphere.2005.07.029.
- [38] V.J. Pereira, K.G. Linden, H.S. Weinberg, Evaluation of UV irradiation for photolytic and oxidative degradation of pharmaceutical compounds in water, *Water Res.* 41 (2007) 4413–4423. doi:10.1016/j.watres.2007.05.056.
- [39] E.J. Rosenfeldt, P.J. Chen, S. Kullman, K.G. Linden, Destruction of estrogenic activity in water using UV advanced oxidation, *Sci. Total Environ.* 377 (2007) 105–113. doi:10.1016/j.scitotenv.2007.01.096.
- [40] R. Maciel, G.L. Sant’Anna, M. Dezotti, Phenol removal from high salinity effluents using Fenton’s reagent and photo-Fenton reactions, *Chemosphere*. 57 (2004) 711–719. doi:10.1016/j.chemosphere.2004.07.032.
- [41] R. Nithyanandam, R. Saravanane, Treatment of Pharmaceutical Sludge by Fenton Oxidation Process, *Int. J. Chem. Eng. Appl.* 4 (2013) 359–364. doi:10.7763/IJCEA.2013.V4.325.
- [42] D.R. Grymonpré, A.K. Sharma, W.C. Finney, B.R. Locke, The role of Fenton’s reaction in aqueous phase pulsed streamer corona reactors, *Chem. Eng. J.* 82 (2001) 189–207. doi:10.1016/S1385-8947(00)00345-4.

- [43] M.I. Badawy, M.Y. Ghaly, T.A. Gad-Allah, Advanced oxidation processes for the removal of organophosphorus pesticides from wastewater, *Desalination*. 194 (2006) 166–175. doi:10.1016/j.desal.2005.09.027.
- [44] M. Ravina, L. Campanella, J. Kiwi, Accelerated mineralization of the drug Diclofenac via Fenton reactions in a concentric photo-reactor, *Water Res.* 36 (2002) 3553–3560. doi:10.1016/S0043-1354(02)00075-1.
- [45] L.A. Pérez-Estrada, S. Malato, W. Gernjak, A. Agüera, E.M. Thurman, I. Ferrer, et al., Photo-fenton degradation of diclofenac: Identification of main intermediates and degradation pathway, *Environ. Sci. Technol.* 39 (2005) 8300–8306. doi:10.1021/es050794n.
- [46] O. González, C. Sans, S. Esplugas, Sulfamethoxazole abatement by photo-Fenton. Toxicity, inhibition and biodegradability assessment of intermediates, *J. Hazard. Mater.* 146 (2007) 459–464. doi:10.1016/j.jhazmat.2007.04.055.
- [47] J. Barek, J. Cvacka, J. Zima, M. De Meo, M. Laget, J. Michelon, et al., Chemical Degradation of Wastes of Antineoplastic Agents Amsacrine , Azathioprine , Asparaginase and Thiotepa, *Ann. Occup. Hyg.* 42 (1998) 259–266.
- [48] M. Boroski, A.C. Rodrigues, J.C. Garcia, L.C. Sampaio, J. Nozaki, N. Hioka, Combined electrocoagulation and TiO₂ photoassisted treatment applied to wastewater effluents from pharmaceutical and cosmetic industries, *J. Hazard. Mater.* 162 (2009) 448–454. doi:10.1016/j.jhazmat.2008.05.062.
- [49] P. Mojir Shaibani, K. Prashanthi, A. Sohrabi, T. Thundat, Photocatalytic BiFeO₃ nanofibrous mats for effective water treatment, *J. Nanotechnol.* 2013 (2013). doi:10.1155/2013/939531.
- [50] D. He, Y. Sun, L. Xin, J. Feng, Aqueous tetracycline degradation by non-thermal plasma combined with nano-TiO₂, *Chem. Eng. J.* 258 (2014) 18–25. doi:10.1016/j.cej.2014.07.089.
- [51] F. Méndez-Arriaga, S. Esplugas, J. Giménez, Photocatalytic degradation of non-steroidal anti-inflammatory drugs with TiO₂ and simulated solar irradiation, *Water Res.* 42 (2008) 585–594. doi:10.1016/j.watres.2007.08.002.
- [52] C. Reyes, J. Fernández, J. Freer, M.A. Mondaca, C. Zaror, S. Malato, et al., Degradation and inactivation of tetracycline by TiO₂ photocatalysis, *J. Photochem. Photobiol. A Chem.* 184 (2006) 141–146. doi:10.1016/j.jphotochem.2006.04.007.
- [53] T. Nakashima, Y. Ohko, Y. Kubota, A. Fujishima, Photocatalytic decomposition of estrogens in aquatic environment by reciprocating immersion of TiO₂-modified

- polytetrafluoroethylene mesh sheets, *J. Photochem. Photobiol. A Chem.* 160 (2003) 115–120. doi:10.1016/S1010-6030(03)00229-6.
- [54] S. Rafqah, P. Wong-Wah-Chung, S. Nelieu, J. Einhorn, M. Sarakha, Phototransformation of triclosan in the presence of TiO₂ in aqueous suspension: Mechanistic approach, *Appl. Catal. B Environ.* 66 (2006) 119–125. doi:10.1016/j.apcatb.2006.03.004.
- [55] V. Augugliaro, E. García-López, V. Loddo, S. Malato-Rodríguez, I. Maldonado, G. Marci, et al., Degradation of lincomycin in aqueous medium: Coupling of solar photocatalysis and membrane separation, *Sol. Energy.* 79 (2005) 402–408. doi:10.1016/j.solener.2005.02.020.
- [56] S. Kaniou, K. Pitarakis, I. Barlagianni, I. Poulios, Photocatalytic oxidation of sulfamethazine, *Chemosphere.* 60 (2005) 372–380. doi:10.1016/j.chemosphere.2004.11.069.
- [57] G. Chen, Electrochemical technologies in wastewater treatment, *Sep. Purif. Technol.* 38 (2004) 11–41. doi:10.1016/j.seppur.2003.10.006.
- [58] C. a Martínez-Huitile, S. Ferro, Electrochemical oxidation of organic pollutants for the wastewater treatment: direct and indirect processes., *Chem. Soc. Rev.* 35 (2006) 1324–1340. doi:10.1039/b517632h.
- [59] C. Comninellis, A. Kapalka, S. Malato, S.A. Parsons, I. Poulios, D. Mantzavinos, Advanced oxidation processes for water treatment: advances and trends for R&D, *J. Chem. Technol. Biotechnol.* 83 (2008) 769–776. doi:10.1002/jctb.1873.
- [60] C. Comninellis, Electrocatalysis in the electrochemical conversion/combustion of organic pollutants for waste water treatment, *Electrochim. Acta.* 39 (1994) 1857–1862. doi:10.1016/0013-4686(94)85175-1.
- [61] F. Bonfatti, S. Ferro, F. Lavezzo, M. Malacarne, G. Lodi, A. De Battisti, Electrochemical incineration of glucose as a model organic substrate. I. Role of the electrode material, *J. Electrochem. Soc.* 146 (1999) 2175–2179. doi:10.1149/1.1391909.
- [62] B. Pauwels, S. Deconinck, W. Verstraete, Electrolytic removal of 17 α - ethinylestradiol (EE2) in water streams, *J. Chem. Technol. Biotechnol.* 81 (2006) 1338–1343. doi:10.1002/jctb.
- [63] J. Hirose, F. Kondo, T. Nakano, T. Kobayashi, N. Hiro, Y. Ando, et al., Inactivation of antineoplastics in clinical wastewater by electrolysis, *Chemosphere.* 60 (2005) 1018–1024. doi:10.1016/j.chemosphere.2005.01.024.
- [64] I. Sirés, F. Centellas, J.A. Garrido, R.M. Rodríguez, C. Arias, P.L. Cabot, et al., Mineralization of clofibric acid by electrochemical advanced oxidation processes using a

- boron-doped diamond anode and Fe²⁺ and UVA light as catalysts, *Appl. Catal. B Environ.* 72 (2007) 373–381. doi:10.1016/j.apcatb.2006.12.002.
- [65] M. Murugananthan, S. Yoshihara, T. Rakuma, N. Uehara, T. Shirakashi, Electrochemical degradation of 17 β -estradiol (E2) at boron-doped diamond (Si/BDD) thin film electrode, *Electrochim. Acta.* 52 (2007) 3242–3249. doi:10.1016/j.electacta.2006.09.073.
- [66] A.A.J. Torriero, C.E. Tonn, L. Sereno, J. Raba, Electrooxidation mechanism of non-steroidal anti-inflammatory drug piroxicam at glassy carbon electrode, *J. Electroanal. Chem.* 588 (2006) 218–225. doi:10.1016/j.jelechem.2005.12.023.
- [67] B. Kasprzyk-Hordern, M. Ziółek, J. Nawrocki, Catalytic ozonation and methods of enhancing molecular ozone reactions in water treatment, *Appl. Catal. B Environ.* 46 (2003) 639–669. doi:10.1016/S0926-3373(03)00326-6.
- [68] B. Langlais, D.A. Reckhow, D.R. Brink, *Ozone in Water Treatment: Application and Engineering*, Lewis Publishers, Chelsea, Michigan, USA, 1991.
- [69] W.J. Masschelein, *Unit Processes in Drinking Water Treatment*, Marcel Dekker, New York, 1992.
- [70] B. Sun, M. Sato, J. Sid Clements, Optical study of active species produced by a pulsed streamer corona discharge in water, *J. Electrostat.* 39 (1997) 189–202. doi:10.1016/S0304-3886(97)00002-8.
- [71] G. Li, J. He, D. Wang, P. Meng, M. Zeng, Optimization and interpretation of O₃ and O₃/H₂O₂ oxidation processes to pretreat hydrocortisone pharmaceutical wastewater., *Environ. Technol.* 36 (2015) 1026–34. doi:10.1080/09593330.2014.971885.
- [72] S. Mozia, M. Janus, P. Brożek, S. Bering, K. Tarnowski, J. Mazur, et al., A system coupling hybrid biological method with UV/O₃ oxidation and membrane separation for treatment and reuse of industrial laundry wastewater, *Environ. Sci. Pollut. Res.* (2016) 1–11. doi:10.1007/s11356-016-7111-5.
- [73] E.U. Cokgor, I.A. Alaton, O. Karahan, S. Dogruel, D. Orhon, Biological treatability of raw and ozonated penicillin formulation effluent, *J. Hazard. Mater.* 116 (2004) 159–166. doi:10.1016/j.jhazmat.2004.08.011.
- [74] Z. Qiang, C. Adams, R. Surampalli, Determination of Ozonation Rate Constants for Lincomycin and Spectinomycin, *Ozone Sci. Eng.* 26 (2004) 525–537. doi:10.1080/01919510490885334.
- [75] M.O. Buffle, J. Schumacher, E. Salhi, M. Jekel, U. von Gunten, Measurement of the initial phase of ozone decomposition in water and wastewater by means of a continuous quench-flow system: Application to disinfection and pharmaceutical oxidation, *Water*

- Res. 40 (2006) 1884–1894. doi:10.1016/j.watres.2006.02.026.
- [76] W. Hua, E.R. Bennett, R.J. Letcher, Ozone treatment and the depletion of detectable pharmaceuticals and atrazine herbicide in drinking water sourced from the upper Detroit River, Ontario, Canada, *Water Res.* 40 (2006) 2259–2266. doi:10.1016/j.watres.2006.04.033.
- [77] N. Vieno, T. Tuhkanen, L. Kronberg, Removal of pharmaceuticals in drinking water treatment: effect of chemical coagulation., *Environ. Technol.* 27 (2006) 183–192. doi:10.1080/09593332708618632.
- [78] A.M. Vandenbroucke, R. Morent, N. De Geyter, C. Leys, Non-thermal plasmas for non-catalytic and catalytic VOC abatement, *J. Hazard. Mater.* 195 (2011) 30–54. doi:10.1016/j.jhazmat.2011.08.060.
- [79] F. Abdelmalek, M.R. Ghezzar, M. Belhadj, A. Addou, J.L. Brisset, Bleaching and degradation of textile dyes by nonthermal plasma process at atmospheric pressure, *Ind. Eng. Chem. Res.* 45 (2006) 23–29. doi:10.1021/ie050058s.
- [80] H.-H. Kim, Nonthermal Plasma Processing for Air-Pollution Control: A Historical Review, Current Issues, and Future Prospects, *Plasma Process. Polym.* 1 (2004) 91–110. doi:10.1002/ppap.200400028.
- [81] P. Lukes, B.R. Locke, Plasmachemical oxidation processes in a hybrid gas–liquid electrical discharge reactor, *J. Phys. D Appl. Phys.* 38 (2005) 4074–4081. doi:10.1021/ie0491342.
- [82] P. Bruggeman, C. Leys, Non-thermal plasmas in and in contact with liquids, *J. Phys. D. Appl. Phys.* 42 (2009) 53001. doi:10.1088/0022-3727/42/5/053001.
- [83] J.S. Chang, P.A. Lawless, T. Yamamoto, Corona Discharge Processes, *IEEE Trans. Plasma Sci.* 19 (1991) 1152–1166. doi:10.1109/27.125038.
- [84] P. Lukes, M. Clupek, V. Babicky, V. Janda, P. Sunka, Generation of ozone by pulsed corona discharge over water surface in hybrid gas–liquid electrical discharge reactor, *J. Phys. D. Appl. Phys.* 38 (2005) 409–416. doi:10.1088/0022-3727/38/3/010.
- [85] R.P. Joshi, S.M. Thagard, Streamer-like electrical discharges in water: Part II. environmental applications, *Plasma Chem. Plasma Process.* 33 (2013) 17–49. doi:10.1007/s11090-013-9436-x.
- [86] J. Zeng, B. Yang, X. Wang, Z. Li, X. Zhang, L. Lei, Degradation of pharmaceutical contaminant ibuprofen in aqueous solution by cylindrical wetted-wall corona discharge, *Chem. Eng. J.* 267 (2015) 282–288. doi:10.1016/j.cej.2015.01.030.

- [87] S.-P. Rong, Y.-B. Sun, Z.-H. Zhao, Degradation of sulfadiazine antibiotics by water falling film dielectric barrier discharge, *Chinese Chem. Lett.* 25 (2014) 187–192.
- [88] M. Magureanu, D. Piroi, N.B. Mandache, V. David, A. Medvedovici, V.I. Parvulescu, Degradation of pharmaceutical compound pentoxifylline in water by non-thermal plasma treatment, *Water Res.* 44 (2010) 3445–3453. doi:10.1016/j.watres.2010.03.020.
- [89] M. Magureanu, D. Dobrin, N.B. Mandache, C. Bradu, A. Medvedovici, V.I. Parvulescu, The mechanism of plasma destruction of enalapril and related metabolites in water, *Plasma Process. Polym.* 10 (2013) 459–468. doi:10.1002/ppap.201200146.
- [90] M. Magureanu, D. Piroi, N.B. Mandache, V. David, A. Medvedovici, C. Bradu, et al., Degradation of antibiotics in water by non-thermal plasma treatment, *Water Res.* 45 (2011) 3407–3416. doi:10.1016/j.watres.2011.03.057.
- [91] B.R. Locke, M. Sato, P. Sunka, M.R. Hoffmann, J.-S. Chang, Electrohydraulic Discharge and Nonthermal Plasma for Water Treatment, *Ind. Eng. Chem. Res.* 45 (2006) 882–905. doi:10.1021/ie050981u.
- [92] P. Lukes, B.R. Locke, Degradation of substituted phenols in a hybrid gas-liquid electrical discharge reactor, *Ind. Eng. Chem. Res.* 44 (2005) 2921–2930. doi:10.1021/ie0491342.
- [93] M. Sahni, B.R. Locke, Quantification of Hydroxyl Radicals Produced in Aqueous Phase Pulsed Electrical Discharge Reactors, *Ind. Eng. Chem. Res.* 45 (2006) 5819–5825. doi:10.1021/ie0601504.
- [94] J. Brisset, D. Moussa, A. Doubla, E. Hnatiuc, B. Hnatiuc, G. Kamgang Youbi, et al., Chemical Reactivity of Discharges and Temporal Post-Discharges in Plasma Treatment of Aqueous Media: Examples of Gliding Discharge Treated Solutions, *Ind. Eng. Chem. Res.* 47 (2008) 5761–5781. doi:10.1021/ie701759y.
- [95] A.M. Howatson, *An introduction to gas discharge*, 2nd ed., Pergamon Press, Great Britain, 1967.
- [96] Primer on “gas discharge,” (n.d.). <http://electric-cosmos.org/PrimerAboutGD.pdf>. (accessed October 3, 2016).
- [97] A. Fridman, A. Chirokov, A. Gutsol, Non-thermal atmospheric pressure discharges, *J. Phys. D. Appl. Phys.* 38 (2005) R1–R24. doi:10.1088/0022-3727/38/2/R01.
- [98] L.B. Loeb, *Basic Processes of Gaseous Electronics*, University of California Press, Berkeley, CA, 1960.
- [99] J.M. Meek, J.D. Craggs, *Electrical Breakdown of Gases*, Wiley, New York, 1978.

- [100] P. Lukes, E. Dolezalova, I. Sisrova, M. Clupek, Aqueous-phase chemistry and bactericidal effects from an air discharge plasma in contact with water: evidence for the formation of peroxyxynitrite through a pseudo-second-order post-discharge reaction of H₂O₂ and HNO₂, *Plasma Sources Sci. Technol.* 23 (2014) 15019. doi:10.1088/0963-0252/23/1/015019.
- [101] G. Kamgang-Youbi, J.-M. Herry, M.-N. Bellon-Fontaine, J.-L. Brisset, A. Doubla, M. Naïtali, Evidence of temporal postdischarge decontamination of bacteria by gliding electric discharges: application to *Hafnia alvei*, *Appl. Environ. Microbiol.* 73 (2007) 4791–4796. doi:10.1128/AEM.00120-07.
- [102] D. Moussa, a Doubla, G. Kamgang-Youbi, J.L. Brisset, Postdischarge Long Life Reactive Intermediates Involved in the Plasma Chemical Degradation of an Azoic Dye, *IEEE Trans. Plasma Sci.* 35 (2007) 444–453. doi:10.1109/TPS.2007.892578.
- [103] N. Shainsky, D. Dobrynin, U. Ercan, S.G. Joshi, H. Ji, A. Brooks, et al., Plasma Acid: Water Treated by Dielectric Barrier Discharge, *Plasma Process. Polym.* 9 (2012) doi: 10.1002/ppap.201100084. doi:10.1002/ppap.201100084.
- [104] P. Lukes, A.T. Appleton, B.R. Locke, Hydrogen Peroxide and Ozone Formation in Hybrid Gas–Liquid Electrical Discharge Reactors, *IEEE Trans. Ind. Appl.* 40 (2004) 60–67. doi:10.1109/TIA.2003.821799.
- [105] M.A. Tarr, Chemical degradation methods for wastes and pollutants: environmental and industrial applications, M. Dekker, New York, 2003.
- [106] a Fridman, a Chirokov, a Gutsol, TOPICAL REVIEW: Non-thermal atmospheric pressure discharges, *J. Phys. D.* 38 (2005) 1. doi:10.1088/0022-3727/38/2/R01.
- [107] U. Kogelschatz, *Process Technologies for Water Treatment*, Plenum, New York, 1988.
- [108] M. Magureanu, D. Piroi, N.B. Mandache, V. David, a. Medvedovici, C. Bradu, et al., Degradation of antibiotics in water by non-thermal plasma treatment, *Water Res.* 45 (2011) 3407–3416. doi:10.1016/j.watres.2011.03.057.
- [109] Y. Liu, S. Mei, D. Iya-Sou, S. Cavadias, S. Ognier, Carbamazepine removal from water by dielectric barrier discharge: Comparison of ex situ and in situ discharge on water, *Chem. Eng. Process. Process Intensif.* 56 (2012) 10–18. doi:10.1016/j.cep.2012.03.003.
- [110] H. Krause, B. Schweiger, E. Prinz, J. Kim, U. Steinfeld, Degradation of persistent pharmaceuticals in aqueous solutions by a positive dielectric barrier discharge treatment, *J. Electrostat.* 69 (2011) 333–338. doi:10.1016/j.elstat.2011.04.011.
- [111] G. Fridman, M. Peddinghaus, H. Ayan, A. Fridman, M. Balasubramanian, A. Gutsol, et al., 2006_Blood Coagulation and Living Tissue Sterilization by Floating-Electrode Dielectric Barrier Discharge in Air .pdf, (2006) 425–442. doi:10.1007/s11090-006-9024-

4.

- [112] G. Fridman, A. Shereshevsky, M.M. Jost, A.D. Brooks, A. Fridman, A. Gutsol, et al., Floating electrode dielectric barrier discharge plasma in air promoting apoptotic behavior in Melanoma skin cancer cell lines, *Plasma Chem. Plasma Process.* 27 (2007) 163–176. doi:10.1007/s11090-007-9048-4.
- [113] H.-F.J. and A. Arben Kojtari¹, Utku K Ercan², Josh Smith¹, Gary Friedman³, Richard B Sensenig², Somdev Tyagi⁴, Suresh G Joshi^{2*}, D. Brooks^{2*}, Chemistry for Antimicrobial Properties of Water Treated With Non- Equilibrium Plasma, *Nanomedicine Biother. Discov.* 4 (2013) 1–5. doi:http://dx.doi.org/10.4172/2155-983X.1000120.
- [114] A. Czernichowski, A Gliding discharge reactor for H₂S valorization or destruction, in: *Non-Thermal Plasma Tech. Pollut. Control*, 34th ed., NATO ASI Series, 1993: pp. 371–387.
- [115] S. Krishna, A. Maslani, T. Izdebski, M. Horakova, S. Klementova, P. Spatenka, Degradation of Verapamil hydrochloride in water by gliding arc discharge, *Chemosphere.* 152 (2016) 47–54. doi:10.1016/j.chemosphere.2016.02.083.
- [116] K.-F. Shang, Y. Wu, J. Li, G.-F. Li, D. Li, N.-H. Wang, Reduction of NO_x/SO₂ by Wire-plate Type Pulsed Discharge Reactor with Pulsed Corona Radical Shower, *Plasma Chem. Plasma Process.* 26 (2006) 443–454. doi:10.1007/s11090-006-9026-2.
- [117] J. Jarrige, P. Vervisch, Decomposition of three volatile organic compounds by nanosecond pulsed corona discharge: Study of by-product formation and influence of high voltage pulse parameters, *J. Appl. Phys.* 99 (2006) 113303/1-113303/10. doi:10.1063/1.2202700.
- [118] D. Dobrynin, G. Fridman, G. Friedman, A. Fridman, Physical and biological mechanisms of direct plasma interaction with living tissue, *New J. Phys.* 11 (2009) 115020. doi:10.1088/1367-2630/11/11/115020.
- [119] N. Sano, T. Kawashima, J. Fujikawa, T. Fujimoto, T. Kitai, T. Kanki, et al., Decomposition of Organic Compounds in Water by Direct Contact of Gas Corona Discharge: Influence of Discharge Conditions, *Ind. Eng. Chem. Res.* 41 (2002) 5906–5911. doi:10.1021/ie0203328.
- [120] a. Abou-Ghazala, S. Katsuki, K.H. Schoenbach, F.C. Dobbs, K.R. Moreira, Bacterial decontamination of water by means of pulsed-corona discharges, *IEEE Trans. Plasma Sci.* 30 (2002) 1449–1453. doi:10.1109/TPS.2002.804193.
- [121] D. Dobrin, C. Bradu, M. Magureanu, N.B. Mandache, V.I. Parvulescu, Degradation of diclofenac in water using a pulsed corona discharge, *Chem. Eng. J.* 234 (2013) 389–396. doi:10.1016/j.cej.2013.08.114.

- [122] D. Dobrin, M. Magureanu, C. Bradu, N.B. Mandache, P. Ionita, V.I. Parvulescu, Degradation of methylparaben in water by corona plasma coupled with ozonation, *Environ. Sci. Pollut. Res.* (2014) 12190–12197. doi:10.1007/s11356-014-2964-y.
- [123] A.T. Sugiarto, S. Ito, T. Ohshima, M. Sato, J.D. Skalny, Oxidative decoloration of dyes by pulsed discharge plasma in water, *J. Electrostat.* 58 (2003) 135–145. doi:10.1016/S0304-3886(02)00203-6.
- [124] M. Sato, T. Tokutake, T. Ohshima, A.T. Sugiarto, Aqueous phenol decomposition by pulsed discharges on the water surface, *IEEE Trans. Ind. Appl.* 44 (2008) 1397–1402. doi:10.1109/IAS.2005.1518870.
- [125] H. Wang, X. Chen, Kinetic analysis and energy efficiency of phenol degradation in a plasma-photocatalysis system., *J. Hazard. Mater.* 186 (2011) 1888–1892. doi:10.1016/j.jhazmat.2010.12.088.
- [126] N. Koprivanac, H. Kušić, D. Vujević, I. Peternel, B.R. Locke, Influence of iron on degradation of organic dyes in corona, *J. Hazard. Mater.* 117 (2005) 113–119. doi:10.1016/j.jhazmat.2004.03.023.
- [127] C.W. Van Neste, J.E. Hawk, A. Phani, J. a. J. Backs, R. Hull, T. Abraham, et al., Single-contact transmission for the quasi-wireless delivery of power over large surfaces, *Wirel. Power Transf.* 1 (2014) 75–82. doi:10.1017/wpt.2014.9.
- [128] H.W. Lee, S.H. Nam, A.A.H. Mohamed, G.C. Kim, J.K. Lee, Atmospheric pressure plasma jet composed of three electrodes: Application to tooth bleaching, *Plasma Process. Polym.* 7 (2010) 274–280. doi:10.1002/ppap.200900083.
- [129] P. Lukes, B.R. Locke, Degradation of Substituted Phenols in a Hybrid Gas–Liquid Electrical Discharge Reactor, *Ind. Eng. Chem. Res.* 44 (2005) 2921–2930. doi:10.1021/ie0491342.
- [130] L. Yu, X. Tu, X. Li, Y. Wang, Y. Chi, J. Yan, Destruction of acenaphthene, fluorene, anthracene and pyrene by a dc gliding arc plasma reactor, *J. Hazard. Mater.* 180 (2010) 449–455. doi:10.1016/j.jhazmat.2010.04.051.
- [131] L.G. Devi, C. Munikrishnappa, B. Nagaraj, K.E. Rajashekhar, Effect of chloride and sulfate ions on the advanced photo Fenton and modified photo Fenton degradation process of Alizarin Red S, *J. Mol. Catal. A Chem.* 374–375 (2013) 125–131. doi:10.1016/j.molcata.2013.03.023.
- [132] L. Wang, Aqueous organic dye discoloration induced by contact glow discharge electrolysis, *J. Hazard. Mater.* 171 (2009) 577–581. doi:10.1016/j.jhazmat.2009.06.037.
- [133] J.M. Aubry, Search for singlet oxygen in the decomposition of hydrogen peroxide by

- mineral compounds in aqueous solutions, *J. Am. Chem. Soc.* 107 (1985) 5844–5849.
doi:10.1021/ja00307a002.
- [134] X. Jin, X. Wang, J. Yue, Y. Cai, H. Zhang, The effect of electrolyte constituents on contact glow discharge electrolysis, *Electrochim. Acta.* 56 (2010) 925–928.
doi:10.1016/j.electacta.2010.09.079.
- [135] S.N. Ramjaun, R. Yuan, Z. Wang, J. Liu, Degradation of reactive dyes by contact glow discharge electrolysis in the presence of Cl⁻ ions: Kinetics and AOX formation, *Electrochim. Acta.* 58 (2011) 364–371. doi:10.1016/j.electacta.2011.09.052.
- [136] X. Jin, Q. Xia, H. Zhang, X. Wang, The role of electrolyte constituents and metal ions on dye discoloration with contact glow discharge electrolysis, *IEEE Trans. Plasma Sci.* 39 (2011) 3218–3221. doi:10.1109/TPS.2011.2166166.
- [137] L. Wang, X. Jiang, Y. Liu, Degradation of bisphenol A and formation of hydrogen peroxide induced by glow discharge plasma in aqueous solutions, *J. Hazard. Mater.* 154 (2008) 1106–1114. doi:10.1016/j.jhazmat.2007.11.016.
- [138] K. Mopper, X. Zhou, Hydroxyl radical photoproduction in the sea and its potential impact on marine processes., *Science.* 250 (1990) 661–4. doi:10.1126/science.250.4981.661.
- [139] Y. Yang, J.J. Pignatello, J. Ma, W.A. Mitch, Comparison of halide impacts on the efficiency of contaminant degradation by sulfate and hydroxyl radical-based advanced oxidation processes (AOPs), *Environ. Sci. Technol.* 48 (2014) 2344–2351.
doi:10.1021/es404118q.
- [140] P.K. Malik, S.K. Saha, Oxidation of direct dyes with hydrogen peroxide using ferrous ion as catalyst, *Sep. Purif. Technol.* 31 (2003) 241–250. doi:10.1016/S1383-5866(02)00200-9.
- [141] R. Yuan, S.N. Ramjaun, Z. Wang, J. Liu, Concentration profiles of chlorine radicals and their significances in OH-induced dye degradation: Kinetic modeling and reaction pathways, *Chem. Eng. J.* 209 (2012) 38–45. doi:10.1016/j.cej.2012.07.127.
- [142] P. Caregnato, J.A. Rosso, J.M. Soler, A. Arques, D.O. Mártire, M.C. Gonzalez, Chloride anion effect on the advanced oxidation processes of methidathion and dimethoate: Role of Cl₂⁻ radical, *Water Res.* 47 (2013) 351–362. doi:10.1016/j.watres.2012.10.018.
- [143] J.E. Grebel, J.J. Pignatello, W.A. Mitch, Effect of Halide Ions and Carbonates on Organic Contaminant Degradation by Hydroxyl Radical-Based Advanced Oxidation Processes in Saline Waters, *Environ. Sci. Technol.* 44 (2010) 6822–6828. doi:10.1021/es1010225.
- [144] J.J. Pignatello, Dark and photoassisted iron(3⁺)-catalyzed degradation of chlorophenoxy herbicides by hydrogen peroxide, *Environ. Sci. Technol.* 26 (1992) 944–951.
doi:10.1021/es00029a012.

- [145] J.E.F. Moraes, F.H. Quina, C.A.O. Nascimento, D.N. Silva, O. Chiavone-Filho, Treatment of Saline Wastewater Contaminated with Hydrocarbons by the Photo-Fenton Process, *Environ. Sci. Technol.* 38 (2004) 1183–1187. doi:10.1021/es034217f.
- [146] J. Kiwi, A. Lopez, V. Nadtochenko, Mechanism and kinetics of the OH-radical intervention during Fenton oxidation in the presence of a significant amount of radical scavenger (Cl⁻), *Environ. Sci. Technol.* 34 (2000) 2162–2168. doi:10.1021/es991406i.
- [147] C. Liang, Z.S. Wang, N. Mohanty, Influences of carbonate and chloride ions on persulfate oxidation of trichloroethylene at 20C, *Sci. Total Environ.* 370 (2006) 271–277. doi:10.1016/j.scitotenv.2006.08.028.
- [148] M. Marković, M. Jović, D. Stanković, V. Kovačević, G. Roglić, G. Gojgić-Cvijović, et al., Application of non-thermal plasma reactor and Fenton reaction for degradation of ibuprofen., *Sci. Total Environ.* 505 (2015) 1148–55. doi:10.1016/j.scitotenv.2014.11.017.
- [149] L.K. Wan, J. Peng, M.Z. Lin, Y. Muroya, Y. Katsumura, H.Y. Fu, Hydroxyl radical, sulfate radical and nitrate radical reactivity towards crown ethers in aqueous solutions, *Radiat. Phys. Chem.* 81 (2012) 524–530. doi:10.1016/j.radphyschem.2012.01.025.
- [150] F. Huang, L. Chen, H. Wang, Z. Yan, Analysis of the degradation mechanism of methylene blue by atmospheric pressure dielectric barrier discharge plasma, *Chem. Eng. J.* 162 (2010) 250–256. doi:10.1016/j.cej.2010.05.041.
- [151] L.O. de B. Benetoli, B.M. Cadorin, V.Z. Baldissarelli, R. Geremias, I.G. de Souza, N.A. Debacher, Pyrite-enhanced methylene blue degradation in non-thermal plasma water treatment reactor., *J. Hazard. Mater.* 237–238 (2012) 55–62. doi:10.1016/j.jhazmat.2012.07.067.
- [152] J.L. Sotelo, F.J. Beltran, F.J. Benitez, J. Beltran-Heredia, Ozone decomposition in water: Kinetic study, *Ind. Eng. Chem. Res.* 26 (1987) 39–43. doi:10.1021/ie00061a008.
- [153] M.S. Elovitz, U. von Gunten, H.-P. Kaiser, Hydroxyl Radical/Ozone Ratios During Ozonation Processes. II. The Effect of Temperature, pH, Alkalinity, and DOM Properties, *Ozone Sci. Eng.* 22 (2000) 123–150. doi:10.1080/01919510008547216.
- [154] T. Batakliiev, V. Georgiev, M. Anachkov, S. Rakovsky, S. Rakovsky, Ozone decomposition, *Interdiscip. Toxicol.* 7 (2014) 47–59. doi:10.2478/intox-2014-0008.
- [155] O.R. Wulf, R.C. Tolman, The Thermal Decomposition Of Ozone, *Proc. Natl. Acad. Sci.* 13 (1927) 272–275.
- [156] N. Okafor, *Environmental Microbiology of Aquatic and Waste Systems*, Springer Netherlands, 2011. doi:10.1007/978-94-007-1460-1.

- [157] L.W.T. Solutions, Ozone decomposition, 2013 (2011).
<http://www.lenntech.com/library/ozone/decomposition/ozone-decomposition.htm>.
- [158] B. Elvers, S. Hawkins, G. Schulz, Ullmann's Encyclopedia of Industrial Chemistry, 5th ed., VCH, Verlagsgesellschaft, 1991. doi:10.1002/star.19910430213.
- [159] P. Olszewski, J.F. Li, D.X. Liu, J.L. Walsh, Optimizing the electrical excitation of an atmospheric pressure plasma advanced oxidation process, *J. Hazard. Mater.* 279 (2014) 60–66. doi:10.1016/j.jhazmat.2014.06.059.
- [160] A. Gomes, E. Fernandes, J.L.F.C. Lima, Fluorescence probes used for detection of reactive oxygen species, *J. Biochem. Biophys. Methods.* 65 (2005) 45–80. doi:10.1016/j.jbbm.2005.10.003.
- [161] J.G. Mohanty, J.S. Jaffe, E.S. Schulman, D.G. Raible, A highly sensitive fluorescent micro-assay of H₂O₂ release from activated human leukocytes using a dihydroxyphenoxazine derivative, *J. Immunol. Methods.* 202 (1997) 133–141.
- [162] E. Albitar, S. Alfaro, M.A. Valenzuela, Photosensitized oxidation of 9,10-dimethylanthracene with singlet oxygen by using a safranin O/silica composite under visible light, *Photochem. Photobiol. Sci.* 14 (2015) 597–602. doi:10.1039/C4PP00261J.
- [163] M.C. DeRosa, R.J. Crutchley, Photosensitized singlet oxygen and its applications, *Coord. Chem. Rev.* 233–234 (2002) 351–371. doi:10.1016/S0010-8545(02)00034-6.
- [164] I. Kruk, *Environmental Toxicology and Chemistry of Oxygen Species*, Springer, 1998. doi:10.1007/978-3-540-49571-0.
- [165] K.S. Kim, C.S. Yang, Y.S. Mok, Degradation of veterinary antibiotics by dielectric barrier discharge plasma, *Chem. Eng. J.* 219 (2013) 19–27. doi:10.1016/j.cej.2012.12.079.
- [166] M. Halmann, *Photodegradation of water pollutants*, CRC press, New York, 1995.
- [167] R. Balachandran, M. Zhao, B. Dong, I. Brown, S. Raghavan, M. Keswani, Role of ammonia and carbonates in scavenging hydroxyl radicals generated during megasonic irradiation of wafer cleaning solutions, *Microelectron. Eng.* 130 (2014) 82–86. doi:10.1016/j.mee.2014.10.022.
- [168] L.S. Levitt, E.R. Malinowski, Mechanism of Organic Oxidation in Aqueous Solution. I. Kinetics of the Persulfate Oxidation of Isopropyl Alcohol, *J. Am. Chem. Soc.* 77 (1955) 4517–4521. doi:10.1021/ja01622a022.
- [169] G. V. Buxton, C.L. Greenstock, W.P. Helman, A.B. Ross, Critical Review of rate constants for reactions of hydrated electrons, hydrogen atoms and hydroxyl radicals ($\cdot\text{OH}/\cdot\text{O}^-$ in Aqueous Solution, *J. Phys. Chem. Ref. Data.* 17 (1988) 513–886.

doi:10.1063/1.555805.

- [170] A.T. Sugiarto, T. Ohshima, M. Sato, Advanced oxidation processes using pulsed streamer corona discharge in water, *Thin Solid Films*. 407 (2002) 174. doi:10.1016/S0040-6090(02)00036-6.
- [171] X. Wen, M. Wang, Z. Ding, G. Liu, Decoloration of Azo Dye Sunset Yellow by a Coaxial Insulated-Rod-to-Cylinder Underwater Streamer Discharge System, *Plasma Sci. Technol.* 14 (2012) 293–296. doi:10.1088/1009-0630/14/4/05.
- [172] S.B. Gupta, H. Bluhm, The potential of pulsed underwater streamer discharges as a disinfection technique, *IEEE Trans. Plasma Sci.* 36 (2008) 1621–1632. doi:10.1109/TPS.2008.2001231.
- [173] T. Kosjek, E. Heath, A. Krbavčič, Determination of non-steroidal anti-inflammatory drug (NSAIDs) residues in water samples, *Environ. Int.* 31 (2005) 679–685. doi:10.1016/j.envint.2004.12.001.
- [174] M. Klavarioti, D. Mantzavinos, D. Kassinos, Removal of residual pharmaceuticals from aqueous systems by advanced oxidation processes, *Environ. Int.* 35 (2009) 402–417. doi:10.1016/j.envint.2008.07.009.
- [175] R. Wise, Antimicrobial resistance: priorities for action., *J. Antimicrob. Chemother.* 49 (2002) 585–586. doi:10.1093/jac/49.4.585.
- [176] K. Kümmerer, Antibiotics in the aquatic environment - A review - Part I, *Chemosphere*. 75 (2009) 417–434. doi:10.1016/j.chemosphere.2008.11.086.
- [177] S.M. Mitchell, J.L. Ullman, A.L. Teel, R.J. Watts, PH and temperature effects on the hydrolysis of three ??-lactam antibiotics: Ampicillin, cefalotin and cefoxitin, *Sci. Total Environ.* 466–467 (2014) 547–555. doi:10.1016/j.scitotenv.2013.06.027.
- [178] C.W. Knapp, J. Dolfing, P.A.I. Ehlert, D.W. Graham, Evidence of increasing antibiotic resistance gene abundances in archived soils since 1940, *Environ. Sci. Technol.* 44 (2010) 580–587. doi:10.1021/es901221x.
- [179] R.L. Myers, *The 100 Most Important Chemical Compounds – A Reference Guide*, Greenwood, Westport, 2007.
- [180] P. Wehrwein, Astounding increase in antidepressant use by Americans Title, *Harvard Heal. Blog.* (2011). <http://www.health.harvard.edu/blog/astounding-increase-in-antidepressant-use-by-americans-201110203624> (accessed October 14, 2016).
- [181] “Prozac nation” claim as antidepressant use soarstle, *NHS Choices.* (2013).

- [182] R.B. Bringolf, R.M. Heltsley, T.J. Newton, C.B. Eads, S.J. Fraley, D. Shea, et al., Environmental occurrence and reproductive effects of the pharmaceutical fluoxetine in native freshwater mussels, *Environ. Toxicol. Chem.* 29 (2010) 1311–1318. doi:10.1002/etc.157.
- [183] Who, Analyzing and controlling pharmaceutical expenditures, *Manag. Access to Med. Heal. Technol.* (2012) 33. <http://apps.who.int/medicinedocs/documents/s19617en/s19617en.pdf>.
- [184] D.M. Jarvie, *Total Organic Carbon (TOC) Analysis*, (2014).
- [185] H. Bader, J. Hoigné, Determination of ozone in water by the indigo method, *Water Res.* 15 (1981) 449–456. doi:10.1016/0043-1354(81)90054-3.
- [186] M. Li, *Organic Chemistry of Drug Degradation*, Royal Society of Chemistry, Ringoes, New Jersey, 2012.
- [187] W. Waters, A. Rollin, C. Bardwell, J. Schneider, T. Aanerud, Oxidation of Secondary Alcohols with Ozone, *J. Org. Chem.* 41 (1976) 889–891.
- [188] J. Weiss, Fluorescence of Organic Molecules, *Nature.* 152 (1943) 176–178.
- [189] S.F. McGarry, A. Baker, Organic acid fluorescence: Applications to speleothem palaeoenvironmental reconstruction, *Quat. Sci. Rev.* 19 (2000) 1087–1101. doi:10.1016/S0277-3791(99)00087-6.
- [190] W. Chen, P. Westerhoff, J.A. Leenheer, K. Booksh, Fluorescence Excitation-Emission Matrix Regional Integration to Quantify Spectra for Dissolved Organic Matter, *Environ. Sci. Technol.* 37 (2003) 5701–5710. doi:10.1021/es034354c.
- [191] M. Sauer, J. Hofkens, J. Enderlein, *Basic Principles of Fluorescence Spectroscopy*, in: *Handb. Fluoresc. Spectrosc. Imaging*, WILEY-VCH Verlag GmbH & Co. KGaA, Weinheim, 2011: pp. 1–30. http://www.wiley-vch.de/books/sample/3527316698_c01.pdf <http://doi.wiley.com/10.1002/9783527633500.ch1> <http://www.ncbi.nlm.nih.gov/pubmed/7633532>.